Source Apportionment of Fine and Ultrafine Particles in California

REPORT TO THE CALIFORNIA AIR RESOURCES BOARD

Project # 01-306

Prepared by:

Dr. Michael J. Kleeman[1]
Michael A. Robert[1]
Sarah G. Riddle[2]
Chris A. Jakober[3]

[1]Department of Civil and Environmental Engineering
[2]Department of Chemistry
[3] Agriculture and Environmental Chemistry Graduate Group
University of California, Davis
One Shields Avenue, Davis, CA, 95616

Dr. Michael Hannigan

Department of Mechanical Engineering
University of Colorado, Boulder

August 2007

DISCLAIMER

The statements and conclusions in this report are those of the contractor and not necessarily those of the California Air Resources Board. The mention of commercial products, their source, or their use in connection with material reported herein is not to be construed as actual or implied endorsement of such products.

This report was prepared by the University of California at Davis as an account of work partially sponsored by the Coordinating Research Council (CRC). Neither the CRC, members of the CRC, the University of California at Davis nor any person acting on their behalf: (1) makes any warranty, express or implied, with respect to the use of any information, apparatus, method, or process disclosed in this report, or (2) assumes any liabilities with respect to use, or damages resulting form the use or inability to use, any information, apparatus, method, or process disclosed in this report.

ACKNOWLEDGEMENTS

The authors would like to thank the staff of the California Air Resources Board Haagen-Smit Laboratory for their assistance with gasoline vehicle emissions sample collection. The authors would like to thank the staff at the WVU transportable HDDV dynamometer facility in Riverside, CA for their assistance in vehicle testing. The authors would like to thank Dr. Arey and Dr. Atkinson at the University of California, Riverside for use of their laboratory space during the HDDV testing. The authors would like to thank Dr. Kimberly Prather, David Sodeman, and Stephen Toner of the University of California, San Diego for their assistance with sample collection. The authors would like to thank Dr. James Schauer at the University of Wisconsin, Madison, for help with quantification standards. The authors would like to thank Karen Magliano (ARB Planning Technical Support Division) for help during the California Regional Particulate Air Quality Study (CRPAQS) and Jorn Herner (ARB Research Division) and Dan Chang (University of California, Davis) for samples collected at Bakersfield and Sacramento. Finally, the authors would like to thank Dr. Nehzat Motallebi at the California Air Resources Board (Research Division) for help with project coordination.

This research was partially supported by the Coordinating Research Council under contract #E-55/59-1.5a, the National Science Foundation's Nanophases in the Environment, Agriculture, and Technology – Integrative Graduate Education, Research, and Training (NEAT-IGERT) initiative award number DGE-9972741, and the United States Environmental Protection Agency Science to Achieve Results Program under contract # R832414-010.

This Report was submitted in fulfillment of Project # 01-306 "Source Apportionment of Fine and Ultrafine Particles in California" by the University of California at Davis under the partial sponsorship of the California Air Resources Board. Work was completed as of March 31, 2007.

TABLE OF CONTENTS

LIST OF FIGURES

LIST OF TABLES

ABSTRACT

Source profiles for particles smaller than 0.1 μm in diameter (PM0.1) were measured from light-duty gasoline-powered vehicles, heavy-duty diesel vehicles, pine wood combustion, oak wood combustion, eucalyptus wood combustion, rice straw combustion, and meat cooking. The high-resolution size-resolved measurements revealed that tailpipe emissions of particles from gasoline- and diesel-powered vehicles contain separate contributions from lubricating oil and fuel that can be resolved using different tracer compounds. Measurements in a roadside environment demonstrated that the majority of the roadway PM0.1 mass was derived from gasoline fuel and diesel fuel with smaller contributions from lubricating oil. Measurements at Sacramento, Modesto, and Bakersfield during the California Regional Particulate Air Quality Study (CRPAQS) showed that the majority of the PM0.1 mass was composed of organic carbon with smaller amounts of elemental carbon. Wood combustion and meat cooking account for the majority of the PM0.1 organic carbon and therefore the majority of the PM0.1 mass. Gasoline fuel, diesel fuel, and lubricating oil accounted for the majority of the PM0.1 elemental carbon, which constitutes a smaller fraction of the PM0.1 mass but may be equally important for health effects.

EXECUTIVE SUMMARY

Background: Atmospheric Particulate Matter (PM) is associated with increased human mortality and morbidity in many epidemiological studies. It has been postulated that ultrafine particles (Dp < 0.1 μm) (PM0.1) are more pathogenic and are thus a likely candidate for some observed correlation between fine PM and adverse health. The composition and source origin of ultrafine particles must be determined to fully investigate their relationship with human health.

Methods: Ultrafine (Dp<0.1 μm; PM0.1) source profiles were measured for the particulate matter emissions from heavy duty diesel vehicles, light duty gasoline vehicles, biomass combustion sources (pine, oak, eucalyptus, rice straw) and meat cooking. Samples collected on cascade impactors were solvent-extracted and then analyzed using gas chromatography followed by mass spectrometry (GC-MS). Extensive quality assurance checks were conducted to verify the accuracy of each measurement and the suitability of each compound for ultrafine source apportionment calculations.

Results: Levoglucosan and cholesterol were found to be suitable tracers for biomass combustion and meat cooking in all size fractions between 0.056 – 1.8 μm particle diameter. Two hopanes (17α(H)-21β(H)-29-norhopane and 17α(H)-21β(H)-hopane) and two steranes (αββ-20R-stigmastane and αββ-20S-stigmastane) were found to be good surrogates for lubricating oil contributions to PM0.1 concentrations for both gasoline and diesel vehicles. Heavy polycyclic aromatic hydrocarbons (PAHs) (benzo[ghi]perylene and coronene) were found to be good surrogates for gasoline fuel contributions to PM0.1. Light PAHs (fluoranthene and pyrene) were used to estimate diesel fuel source contributions to ambient particulate matter during sources tests and in the roadside environment but these compounds can only serve as approximate tracers and they must be used with great care. Diesel fuel contributions to PM0.1 in the ambient environment were calculated using the residual fraction of EC as a tracer.

The contributions from lubricating oil and fuel to EC and OC emissions could be explained using source profiles that employed hopanes and steranes as tracers for lubricating oil and PAHs as tracers for fuel. Tailpipe particulate matter emissions from gasoline- and diesel-powered vehicles had significant contributions from both lubricating oil and fuel that varied as a function of vehicle type, emissions control technology, and driving cycle. Fuel-rich conditions encountered under cold-start gasoline or high load diesel cycles promoted elemental carbon (EC) emissions derived from gasoline fuel and diesel fuel, respectively. Smoking gasoline vehicles emitted large amounts of organic carbon (OC) derived from lubricating oil, but also large amounts of organic carbon derived from gasoline fuel. Idling diesel engines also emitted large amounts of fuel-derived organic carbon that was not present under higher loads.

Size-resolved particulate matter samples were collected upwind and downwind of the Interstate 5 (I5) freeway in San Diego during July 21-27, 2004 and processed using the same analytical techniques that were applied to the source profiles. The size distributions

of hopanes, steranes, heavy PAHs, and light PAHs measured in the roadside environment were unimodal with a peak between 0.1 – 0.18 μm particle diameter and a tail extending into the ultrafine size fraction (Dp<0.1 μm). These size distributions were very similar to those emitted from heavy duty diesel and light duty gasoline vehicles during chassis dynamometer tests. Source apportionment calculations using size-resolved source profiles showed that the majority of the PM0.1 mass released from the freeway was produced by gasoline fuel and diesel fuel, with relatively minor contributions from lubricating oil.

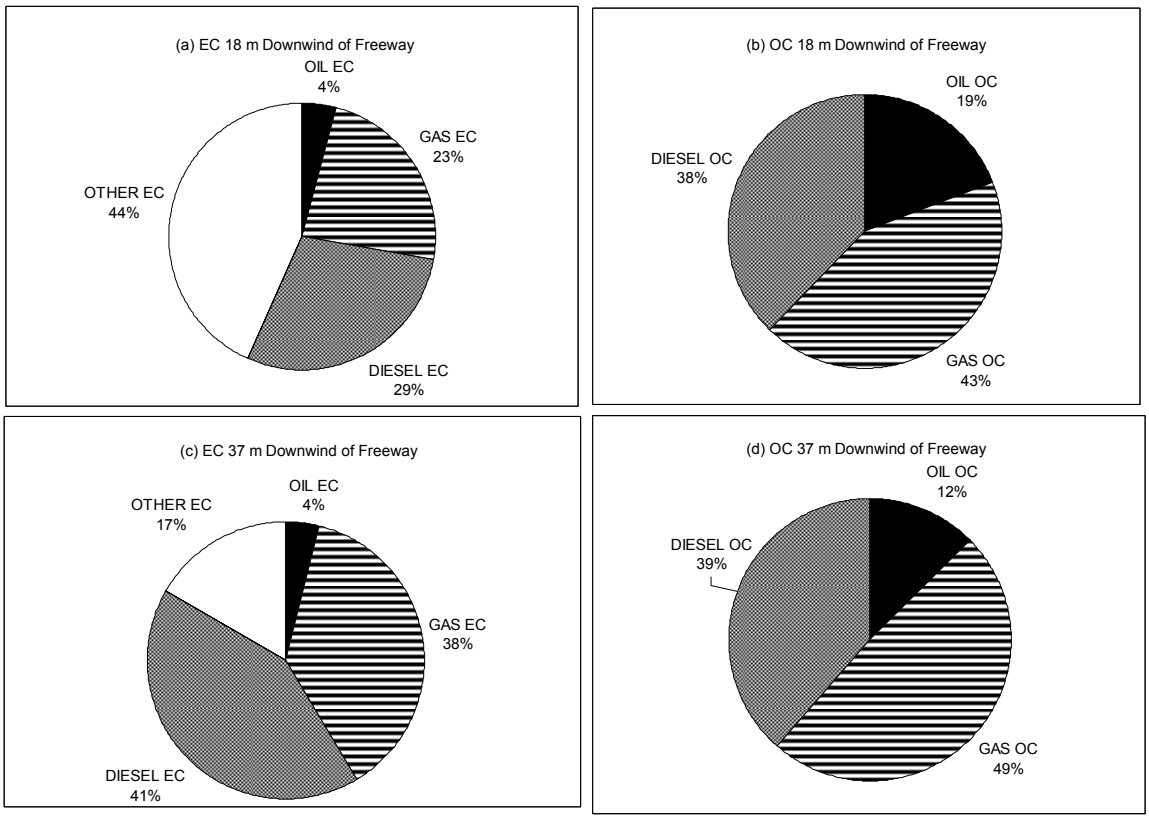

Figure ES-1: Calculated source contributions to elemental carbon (EC) and organic compounds (OC) in the PM0.1 size fraction 18 m downwind of the freeway (panels a, b) and 37 m downwind of the freeway (panels c, d). Oil EC and OC includes contributions from all vehicle types. Gas EC and OC refer to contributions derived from gasoline fuel only. Diesel EC and OC refer to contributions derived from diesel fuel only.

Size-resolved samples of airborne particulate matter collected at Sacramento, Modesto, and Bakersfield during the California Regional Particulate Air Quality Study (CRPAQS) were extracted with organic solvents and analyzed for detailed organic compounds using GC-MS. Organic and elemental carbon accounted for virtually all of the mass in the PM0.1 size fraction. PM0.1 elemental carbon concentrations ranged from 0.03 μg m^{-3} during the daytime to 0.18 μg m^{-3} during the nighttime. Source apportionment calculations reveal that gasoline fuel, diesel fuel, and lubricating oil accounted for the majority of the PM0.1 elemental carbon concentrations, with relatively minor contributions from biomass combustion and meat cooking. PM0.1 organic carbon concentrations were higher than elemental carbon concentrations, ranging from 0.2 μg m^{-}

^{3} during the daytime to 0.8 µg m^{-3} during the nighttime. Wood combustion and meat cooking were found to be the two largest sources of ultrafine organic carbon, with smaller contributions from diesel fuel, gasoline fuel, and lubricating oil.

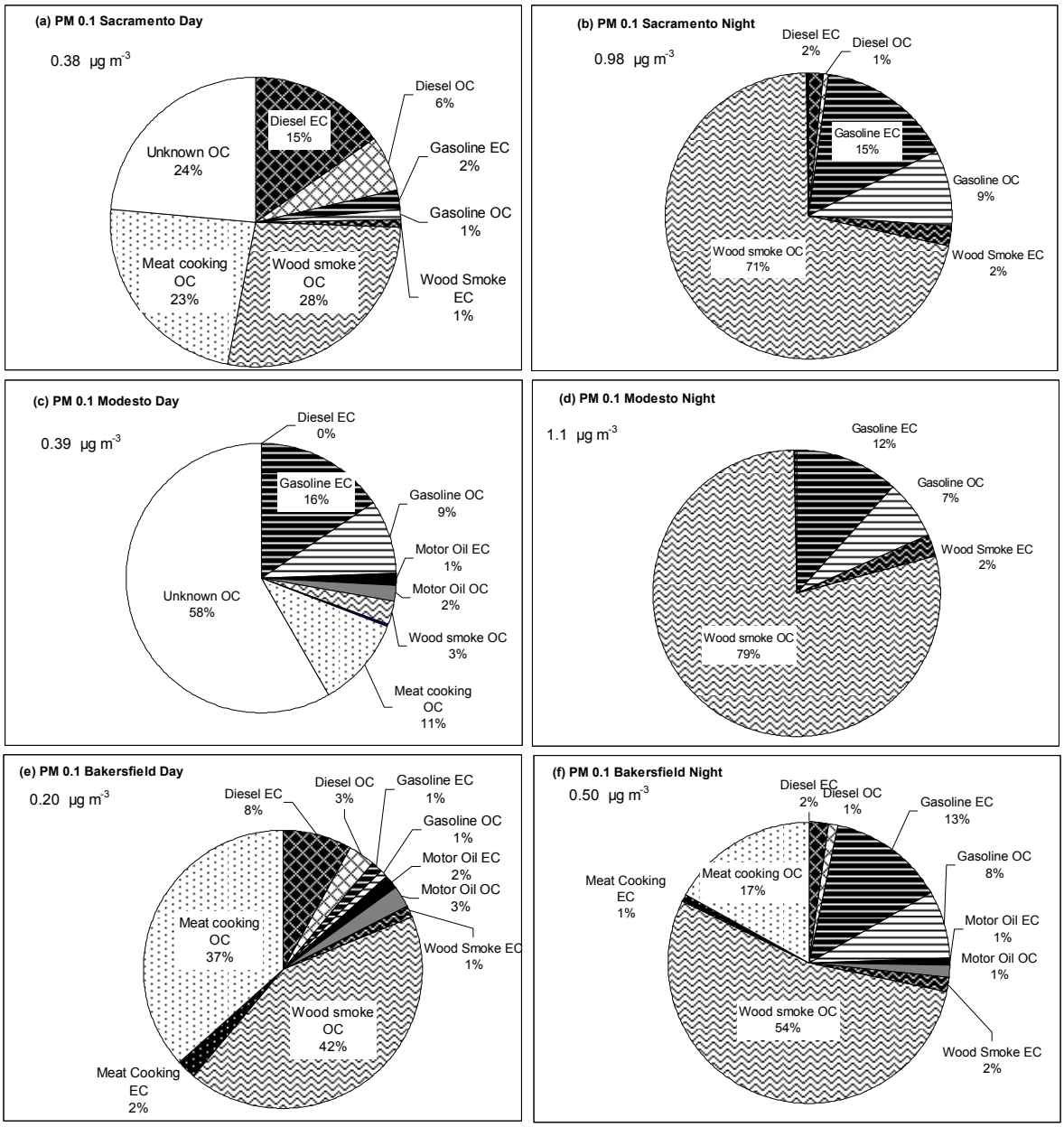

Figure ES-2: Predicted source contributions to PM0.1 concentrations at Sacramento during 7 sampling days between December 15-27, 2000 and Modesto and Bakersfield on 11 sampling days between December 15, 2000 – January 7, 2001. Daytime measurements were made between 10am – 6pm, while nighttime measurements were made between 8pm – 8am each day.

The PM0.1 source apportionment methodology used to produce the results in Figures ES-1 and ES-2 is consistent with (but not identical to) molecular marker Chemical Mass Balance (CMB) methods employed in previousPM2.5 source apportionment studies. The majority of the source apportionment information is carried by a set of "core" trace

organic compounds that are specific to individual sources. Diesel and gasoline vehicles account for the majority of the PM0.1 mass in the roadside environment and the source apportionment methology can identify these contributions when they are present. The ambient sampling locations at Sacramento, Modesto, and Bakersfield were not located in the immediate roadside environment. The PM0.1 concentrations measured at these locations reflect the mix of sources that were close to the monitors during the cold stagnant conditions experienced during the study. The dominance of wood combustion in the PM0.1 size range results from the large levoglucosan concentrations measured during the sampling event. The significant meat cooking contributions result from the relatively high cholesterol concentrations measured at all sampling locations.

Conclusions: PM0.1 concentrations in the roadside environment adjacent to a busy freeway were dominated by contributions from gasoline fuel and diesel fuel with smaller contributions from lubricating oil. PM0.1 mass at residential and light commercial locations in Sacramento, Modesto, and Bakersfield were dominated by wood combustion and meat cooking during a winter stagnation event. These findings reflect the proximity of the sampling locations to each source type. Future inhalation exposure studies may wish to target wood combustion and meat cooking sources as potential causes of adverse health effects in central California cities during cold winter stagnation events.

Future Work: The PM0.1 source apportionment methodology developed in the current study should be applied to receptor sites in a large urban city such as Los Angeles to determine if gasoline and diesel vehicles are the dominant source of PM0.1 mass at residential and light commercial locations within a broader region that has high traffic density.

1 INTRODUCTION

1.1 Motivation

Atmospheric Particulate Matter (PM) has been found to be associated with increased human mortality and morbidity in many epidemiological studies [1]. Recent studies have suggested an even stronger association between the fine fraction of PM (aerodynamic diameter < 2.5 μm) and morbidity/mortality *[1-3]*. It has been postulated that ultrafine particles (aerodynamic diameter < 0.1 μm; PM0.1) may be reposnsible for some of the observed adverse health effects *[4-9]*. There is some evidence to support the hypothesis that ultrafine PM can localize in the mitochondria of epithelial cells where they induce major structural damage *[10]*. The composition and source origin of ultrafine particles must be determined to fully investigate their relationship with observed human health effects.

Statistical source apportionment techniques can provide valuable insight about the contribution that different sources make to airborne particle concentrations. Information of this type plays a vital role in the design of emissions control programs to reduce airborne particle concentrations. A need exists in California to use source apportionment techniques to understand current contributions to airborne fine and ultrafine particle concentrations and to better understand how sources contribute to the features of PM2.5 that are suspected to cause adverse health effects.

The research described in this final report quantifies source contributions to fine and ultrafine particle mass in California using molecular marker source profiles. This information provides scientists and regulators with a starting point from which they can determine how to best protect the public from particulate air pollution.

1.2 Research Objectives

The overall objective of this project was to perform a source apportionment of airborne fine and ultrafine particulate matter (PM) in California. A new ultrafine particle source library was developed from previously collected biomass source samples and newly collected samples of PM emitted from light duty gasoline-powered motor vehicles and heavy duty diesel trucks. This information was combined with ambient ultrafine particle samples to identify major sources and unexplained concentrations of airborne ultrafine particles during the California Regional Particulate Air Quality Study (CRPAQS). This work was organized as twelve (12) separate objectives as described below.

1.2.1 Size and Composition Distribution of PM Emitted from Heavy-Duty Diesel Vehicles

PM emissions from Heavy Duty Diesel Vehicles (HDDVs) were sampled using a transportable chassis dynamometer combined with a dilution sampling system. Four HDDVs were tested using partial or full California HHDDT driving cycles with a simulated inertial weight of either 56,000 lbs or 66,000 lbs. The exhaust from each

vehicle was collected using cascade impactors, filter-based samplers, and real-time analyzers. Particulate matter filters were then analyzed for carbonaceous and ionic species content using Thermal Optical Transmittance (TOT) and Ion Chromatography (IC), respectively. Test-averaged ultrafine and fine PM emission rates are reported as are reconstructed size-resolved mass distributions and temporal analyses on finer time scales.

Note: Material in this chapter has been submitted for publication in the Journal of the Air and Waste Management Association and should be referenced in future studies as "M. A. Robert, C. A. Jakober and M. J. Kleeman. (2007) Size and Composition Distributions of Particulate Matter Emissions 2. Heavy Duty Diesel Vehicles. Journal of the Air and Waste Management Association, submitted for publication."

1.2.2 Size and Composition Distribution of PM Emitted from Light Duty Gasoline-powered Vehicles

PM emissions from Light Duty Gasoline Vehicles (LDGVs) were sampled using a chassis dynamometer combined with a dilution sampling system. Emissions were measured from 30 LDGVs divided into 7 categories based on emissions control technology. The exhaust from each vehicle was collected using cascade impactors, filter-based samplers, and real-time analyzers. Particulate matter filters were then analyzed for carbonaceous and ionic species content using Thermal Optical Transmittance (TOT) and Ion Chromatography (IC), respectively. Test-averaged ultrafine and fine PM emission rates are reported as are reconstructed size-resolved mass distributions and temporal analyses on finer time scales.

Note: Material in this chapter has been submitted for publication in the Journal of the Air and Waste Management Association and should be referenced in future studies as "M. A. Robert, C. A. Jakober, S. VanBergen, and M. J. Kleeman. (2007) Size and Compostion Distributions of Particulate Matter Emissions 1. Light Duty Gasoline Vehicles. Journal of the Air and Waste Management Association, submitted for publication."

1.2.3 Size Distribution of Trace Organic Species Emitted from Heavy-Duty Diesel Vehicles

Size-resolved samples of PM emitted from Heavy-Duty Diesel Vehicles (HDDVs) were extracted using organic solvents and analyzed for trace organic compounds using a gas chromatograph coupled with ion trap mass spectrometry (GC-ITMS). The analysis focused on hopanes, steranes, and PAHs that may prove to be useful tracers for source apportionment studies. Compounds that passed quality control checks were identified and concentrations in the PM1.8 and PM0.1 size fractions are reported.

Note: Material in this chapter has been published in Environmental Science and Technology and should be referenced in future studies as "Riddle, S. G.; Robert, M. A.; Jakober, C. A.; Hannigan, M. P.; Kleeman, M. J. (2007) Size Distribution of Trace Organic Species Emitted from Heavy-Duty Diesel Vehicles. Environ. Sci. Technol., 41(6); 1962-1969."

1.2.4 Size Distribution of Trace Organic Species Emitted From Light-Duty Gasoline Vehicles

Size-resolved samples of particulate matter emitted from Light Duty Gasoline Vehicles (LDGVs) were extracted using organic solvents and analyzed for trace organic compounds using a gas chromatograph coupled with ion trap mass spectrometry (GC-ITMS). The analysis focused on hopanes, steranes, and PAHs that may prove to be useful tracers for source apportionment studies. Compounds that passed quality control checks were identified and concentrations in the PM1.8 and PM0.1 size fractions are reported.

Note: Material in this chapter has been submitted for publication in Environmental Science and Technology and should be referenced in future studies as "Riddle, S. G.; Robert, M. A.; Jakober, C. A.; Hannigan, M. P.; Kleeman, M. J. (2007) Size Distribution of Trace Organic Species Emitted from Light Duty Gasoline Vehicles. Environ. Sci. Technol., submitted for publication"

1.2.5 Metals Content of Gasoline, Diesel Fuel, and Lubricating Oil

The elemental composition of gasoline, diesel fuel, and lubricating oil samples collected from a fleet of in-use light duty gasoline and heavy duty diesel vehicles was analyzed using inductively-coupled plasma – mass spectrometry (ICP-MS). The goal of the analysis was to identify the source of tailpipe elemental emissions from these same vehicles during chassis dynamometer studies. Elements that passed quality control checks were identified and concentrations in the PM1.8 and PM0.1 size fractions are reported.

1.2.6 Size Distributions of Metals Emitted from Light Duty Gasoline-Powered Motor Vehicles and Heavy Duty Diesel Trucks

Tailpipe metal emissions from light duty gasoline vehicles and heavy duty diesel vehicles operated under transient driving cycles were measured using a dilution sampling system combined with cascade impactors. The goal of the analysis was to identify the source of elemental concentrations in a roadside environment. Elements that passed quality control checks were identified and concentrations in the PM1.8 and PM0.1 size fractions are reported.

1.2.7 Size and Composition Distributions of Particulate Matter Emissions from a Busy California Freeway

Particle size and composition distributions were measured at 1 site upwind and 2 sites downwind of the I-5 freeway in San Diego, CA. The goal of this study was to observe the tailpipe signatures of light duty gasoline vehicles and heavy duty diesel vehicles in the roadside environment. Comparisons between chassis dynamometer measurements and roadside measurements were made for all monitored species.

1.2.8 Separating Lubricating Oil vs. Fuel Contributions to Particulate Matter Emissions from Light Duty Gasoline and Heavy Duty Diesel Vehicles

Size-resolved samples of particulate hopanes, steranes, and PAHs were used as independent variables in a multiple regression analysis to identify lubricating oil and fuel contributions to elemental and organic carbon emissions from light duty gasoline vehicles and heavy duty diesel vehicles during transient chassis dynamometer tests. The amount of total carbon associated with motor oil is relatively constant, but the distribution between EC and OC depends on the driving cycle and the engine technology. Fuel contributions to emitted PM were larger than oil contributions for all vehicles tested except gasoline vehicles emitting visible smoke. The majority of the fuel carbon was emitted as elemental carbon for vehicles operating under fuel-rich conditions (high load diesel and cold-start gasoline) and organic carbon under leaner conditions.

Note: Material in this chapter is scheduled for future submission to Environmental Science and Technology and should be referenced in future studies as "Kleeman, M.J., Riddle, S. G.; Robert, M. A.; Jakober, C. A. (2007) Separating Lubricating Oil vs. Fuel Contriibutions to Particulate Matter Emissions from Light Duty Gasoline and Heavy Duty Diesel Vehicles. Environ. Sci. Technol., in preparation"

1.2.9 Source Contributions to Fine and Ultrafine Particulate Matter in a Roadside Environment

Size-resolved samples of airborne PM were collected upwind and downwind of the Interstate 5 freeway in San Diego, California, over a 1 week period. Samples were analyzed for chemical composition using the same methods applied to source profiles. The size distribution of organic tracer compounds measured in the roadside environment was very similar to the size distributions measured from gasoline and diesel vehicles during chassis dynamometer tests. Source apportionment calculations revealed that the majority of the ultrafine particle mass in the roadside environment was associated with gasoline fuel and diesel fuel with relative minor contributions from lubricating oil.

Note: Material in this chapter is scheduled for future submission to Environmental Science and Technology and should be referenced as "Riddle, S. G.; Robert, M. A.; Jakober, C. A.; Hannigan, M. P.; Kleeman, M. J. (2007) Source Contributions to Fine and Ultrafine Particulate Matter in a Roadside Environment. Environ. Sci. Technol., in preparation"

1.2.10 Size Distribution of Trace Organic Species Emitted from Biomass Combustion

Size-resolved samples of particulate matter emissions from meat cooking, pine, oak, eucalyptus, and rice straw combustion were collected using cascade impactors and analyzed for trace organic compounds using GC-MS. Cholesterol and levoglucosan were found to have relatively uniform concentrations relative to total carbon emissions in each particle size fraction emitted from meat cooking and wood combustion, respectively. Emissions rates of these compounds in the ultrafine size fraction are reported.

Note: Material in this chapter is scheduled for future submission to Environmental Science and Technology and should be referenced in future studies as "Kleeman, M. J., Robert, M. A.; Riddle, S. G.; Fine, P.M.; Hays, M.D.; Schauer, J.J.; Hannigan, M. P.; (2007) Size Distribution of Trace Organic Species Emitted from Biomass Combustion. Environ. Sci. Technol., in preparation"

1.2.11 Source Contributions to Ultrafine and Fine Particulate Matter During a Severe Winter Pollution Event (CRPAQS)

Size-resolved samples of airborne particulate matter collected at Sacramento, Modesto, and Bakersfield during the California Regional Particulate Air Quality Study were analyzed for organic compounds using GC-MS. The size-distribution of cholesterol, levoglucosan, hopanes+steranes, and heavy PAHs were generally different emphasizing the fact that these compounds are emitted as a source-oriented external mixture. Source apportionment calculations were carried out to identify contributions to both fine and ultrafine particle mass during daytime and nighttime sampling periods.

Note: Material in this chapter is scheduled for future submission to Environmental Science and Technology and should be referenced in future studies as "Kleeman, M. J., Robert, M. A.; Riddle, S. G.; Jakober, C.; Fine, P.M.; Hays, M.D.; Schauer, J.J.; Hannigan, M. P.; (2007) Source Contributions to Fine and Ultrafine Particulate Matter During the California Regional Particulate Air Quality Study. Environ. Sci. Technol., in preparation"

1.2.12 Source Apportionment of Fine PM During the Vehicle-Oriented Trajectory Study (SCOS97)

Fine PM samples collected during the vehicle-oriented trajectory study were analyzed for organic carbon, elemental carbon, organic molecules, and trace elements. Self-consistent source profiles were collected for a variety of sources and the Chemical Mass Balance model was applied to identify source contributions to the results. The study was limited by the quality of the ambient measurements, but a simplified CMB approach was able to quantify vehicle contributions to EC and OC concentrations.

2 SIZE AND COMPOSITION DISTRIBUTION OF PM EMITTED FROM HEAVY-DUTY DIESEL VEHICLES

2.1 Introduction

The characterization of particulate matter (PM) size and composition distributions emitted from in-use diesel vehicles operated under real-world conditions is essential in order to help quantify the environmental impact of these particles. Diesel PM emissions have been found to be associated with adverse health effects including increased human mortality and morbidity *[2, 9, 11]*. Many carcinogenic and mutagenic compounds have been measured in diesel particulate matter *[12-16]*, and it has been designated as a Toxic Air Contaminant by the state of California *[17]* and as a mobile source air toxic by the U.S. Environmental Protection Agency *[18]*. Diesel engines are believed to be the major source of elemental carbon (EC) in both urban environments *[19]* and in the global atmosphere *[20]*. The optical properties of diesel PM have been shown to reduce regional visibility *[21]* as well to directly affect the radiative balance of the atmosphere *[22]*. In all cases, the environmental impact of the diesel exhaust particles is directly influenced by their size and composition.

Diesel engine technology and diesel fuel formulation have evolved over the past decades to reduce air pollution emissions. It is important to characterize the size and composition distribution of particles emitted from contemporary diesel engines and to compare these measurements to older engines to quantify our progress on air pollution problems. Heavy duty diesel vehicles are of special interest because these vehicles comprise only a small fraction of the total vehicles on the road but they contribute significantly to on-road mobile source primary PM emissions *[23]*. A common method to measure emissions from a vehicle is to operate it on a chassis dynamometer while collecting the emitted particles on filters that can then be analyzed for chemical composition. Heavy Duty Diesel Vehicles (HDDVs) with a gross vehicle weight greater than 30,000 lbs are too large to test on most chassis dynamometers under realistic driving cycles and so simplified cycles are often used. While these simplified tests provide valuable information *[24-26]*, they do not fully reveal all the emissions trends that can occur during dynamic driving cycles. Likewise, tunnel studies *[27-30]* do not fully capture the range of heavy duty diesel vehicle driving cycles and direct engine dynamometer measurements *[31, 32]* do not fully represent emissions from complete vehicles. Attempts to measure emissions from on-road vehicles using real-time instruments *[33, 34]* study the most realistic vehicle emissions, but real-time measurement techniques are still under development and so they currently provide an incomplete characterization of particle size and chemical composition. There is no perfect method to characterize emissions from heavy duty diesel vehicles, and so a combined weight of evidence approach must be continued for the present term.

The purpose of this chapter is to report the size and composition distributions of PM released from contemporary HDDVs measured using a chassis dynamometer / dilution sampling system that employs filter-based samplers, cascade impactors, and

Scanning Mobility Particle Size (SMPS) measurements. The chassis dynamometer used in this study was able to simulate realistic dynamic vehicle driving cycles and inertial loads. The data set includes a range of different vehicle types and emission control technologies. In the present study, particle size and composition distributions in six size fractions between 0.056 - 1.8 μm particle diameters are reported in addition to bulk $PM_{1.8}$ data. Ultrafine PM is defined as particles with aerodynamic diameter between 56 – 100 nm (as collected by stage 10 of a MOUDI operated at the recommended flow rate of 30 L min^{-1}) and fine PM is defined as particles with aerodynamic diameter less than 1.8 μm ($PM_{1.8}$) (as collected by RAAS filter sample using AIHL-design cyclone separators *[35]* operated at 30 L min^{-1}). These are useful functional definitions because very little of the PM mass collected in this study had aerodynamic particle diameters below 56 nm or above 1.8 μm. Vehicle emissions characteristics as a function of time for different vehicles and driving cycles are also presented.

2.2 Methodology

PM emissions were captured from the exhaust systems of vehicles as they were driven through various driving cycles on chassis dynamometers. The emissions were diluted in two stages before sampling (Figure 2-1). A constant volume sampling system was used for primary exhaust dilution. The actual primary dilution rate changed as a function of time during each test. Secondary dilution was used to achieve total dilution factors that are comparable to those experienced by real-world vehicles and to avoid condensation of water in sampling lines. A constant flow rate of exhaust (after primary dilution) was drawn into the Stack Dilution Tunnel (SDT), described by Hildemann et al. *[36]* through a heated inlet line, cyclone manifold, and calibrated sample venturi. The size cut of the cyclone manifold was greater than 1.8 μm particle diameter. Secondary dilution air was passed through a pre-filter, High Efficiency Particulate Air (HEPA) filter, and 1.5 ft^3 of activated carbon to remove ambient PM and gas-phase organic species. Following secondary dilution and turbulent mixing in the SDT, the sample stream was aged for approximately 60 seconds in a Residence Time Chamber (RTC).

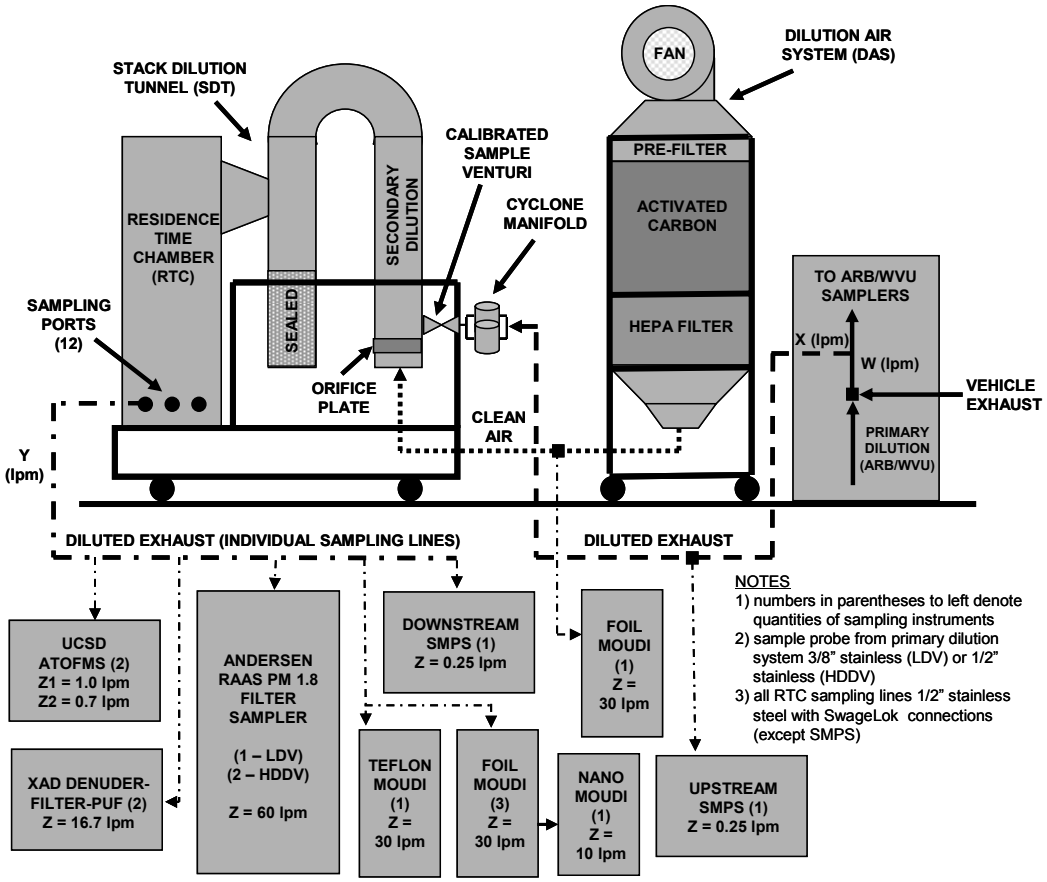

Figure 2-1: Dilution sampling system used to collect size-resolved particulate matter samples from heavy duty diesel vehicles.

A variety of PM sampling equipment was employed for all chassis dynamometer tests (Table 2-1). Bulk $PM_{1.8}$ was collected using Andersen Reference Ambient Air Samplers (RAASs) (Andersen Instruments, Smyrna, GA). Size-resolved PM was collected using Micro Orifice Uniform Deposit Impactors (MOUDIs) (MSP Corporation, Shoreview, MN), in six size fractions between 41 nm and 1.6 μm in aerodynamic diameter. A nano-MOUDI (MSP Corporation, Shoreview, MN) was used to collect three PM size fractions below ~40 nm in aerodynamic diameter. Scanning Mobility Particle Sizers (SMPSs) (TSI Incorporated, Shoreview, MN) sampled time resolved PM distributions from 18 nm to 687 nm both upstream of the SDT and downstream of the RTC.

PM emissions from HDDVs were collected using the equipment described in Table 2-1 at the West Virginia University (WVU) transportable dynamometer facility at a grocery distribution center in Riverside, CA in June and July of 2003. Four HDDVs were tested (Table 2-2) spanning a wide range in vehicle age and engine technology; all vehicles tested had stock exhaust systems with no additional emissions reduction technologies installed. The chassis dynamometer used in the tests employed a combination of fly wheels and electrical motors to simulate inertial loads of either 56,000 or 66,000 pounds. All vehicles were tested using partial or full California Air Resources Board (CARB) Heavy Heavy-Duty Diesel Truck (HHDDT) cycles consisting of five

modes – an idle mode, a creep mode, a transient mode, a low speed cruise, and a high speed cruise *[37]*. Table 2-3 presents details on the HHDDT driving cycle.

Table 2-1: Sampling equipment information used during emissions testing.

instrument	manufacturer	qty	flow rate (lpm)	lower size (µm)	upper size (µm)	collection media information type	collection media information specifications	analysis type
$PM_{1.8}$ BULK FILTER SAMPLER (RAAS)	ANDERSEN INSTRUMENTS	1 (LDGV)	60[a]	---	1.80	QUARTZ 47mm	Pallflex 2500QAT-UP	OC/EC, trace organics
						TEFLON 47mm	Pall Teflo 2.0 um	ions, metals
		2 (HDDV)	120[a]			NYLON 47mm[b]	Pall Nylasorb 1.0 um	ions
						GLASS 47mm[c]	Pall Type A/E	ions
MOUDI MODEL 110	MSP CORPORATION	4	30	0.41	1.60	ALUMINUM 47mm[d]	MSP Corporation	OC/EC, trace organics
						QUARTZ 37mm	Pallflex 2500QAT-UP	OC/EC
		1	30	0.41	1.60	TEFLON 47mm	Pall Teflo 2.0 um	ions, metals
						TEFLON 37mm	Pall Zeflour 2.0 um	ions, metals
NANO-MOUDI	MSP CORPORATION	1	10[e]	0.01	0.41	ALUMINUM 47mm[d]	MSP Corporation	OC/EC, trace organics
						QUARTZ 47mm	Pallflex 2500QAT-UP	OC/EC
SMPS	TSI INCORPORATED	2	0.25	0.02	0.62	---	----	temporal PM size distributions
XAD DENUDER-						Polystyrene Resin	URG-2000-30B8	
FILTER-	UCD	2	16.7	---	1.80	QUARTZ 47mm	Pall Tissuquartz 3.0 um	trace polar organics
PUF[f]						Polyurethane Foam	URG-2000-30PC	
ATOFMS[f]	UCSD	1	1.0	0.30	2.50	----	----	single particle analyses
UF-ATOFMS[f]	UCSD	1	0.7[g]	0.05	0.30			

[a] 6 legs at 10 lpm per leg; [b] treated with sodium carbonate; [c] treated with oxalic acid; [d] baked 48 hours at 550°C prior to use; [e] NANO-MOUDI instrument is downstream of a foil
MOUDI and its flow rate does not contribute to the total flowrate; [f] details to be reported separately; [g] total flow rate is 28 lpm when considering upstream UCSD MOUDI

Table 2-2 Summary of heavy duty diesel vehicles tested.

model year	make	mileage (miles)	load weight (lbs)	engine information type	year	# cyl	disp (liters)	hp (bhp)
1999	Freightliner	138,553	56,000	Detroit Diesel Series 60	1998	6	12.7	500
1998	Kenworth	587,244	56,000 66,000	Cummins N14-460E+	1997	6	14.0	460
1992	Volvo	595,242	56,000	Caterpillar 3406B	1991	6	14.6	280
1985	Freightliner	988,726	56,000	Caterpillar 3406	1984	6	14.6	310

Table 2-3: HHDDT driving cycle summary.

phase / mode	avg speed (mph)	max speed (mph)	distance (miles)	time per mode (sec)
IDLE[a]	0.0	0.0	0.00	1799
CREEP[a]	1.8	8.2	0.50	1012
TRANSIENT[a]	15.3	47.5	2.60	687
LOW-SPEED CRUISE[a]	39.9	59.3	23.00	2082
HIGH SPEED CRUISE	50.3	67.2	10.50	759

[a] PHASE / MODE FOLLOWED BY 10 MINUTES WITH VEHICLE OFF

The diesel fuel used to power HDDVs was 'tank fuel' (the fuel in the tank when the vehicle was procured for testing), and was assumed to be California diesel fuel. Most diesel fuels in California are alternative formulations which means that even though the nominal fuel specification calls for 10% aromatic content and no more than 500 ppm sulfur, the actual aromatic content tends to be approximately 19-20% (or higher) and the sulfur content ~150-200 ppm [38].

Table 2-4 summarizes the complete HDDV sample set, which consists of two background samples and six vehicle/class samples. Most HDDV samples were collected from individual vehicles driven through a full 5-mode HHDDT test; one HDDV sample was collected from a single vehicle operated under six idle and six creep modes of the HHDDT cycle. Particulate matter samples were collected after two stages of dilution. The primary dilution system mixed the hot exhaust with ambient air that was pre-filtered to remove particles. Primary dilution ratios averaged over the entire test cycle were typically 18-20 with the exception of one sample that used the idle/creep driving cycle where the primary dilution ratio was 112.5. Secondary dilution was used to increase the overall dilution factor to more realistic values. Secondary dilution ratios averaged over the entire test cycle were 5-10, yielding overall dilution rates of 129-584. Real-world dilution ratios experienced in a roadside environment in the initial period after exhaust is released to the atmosphere can reach as high as 1000. The dilution ratios used in the current test were a compromise between the desire to simulate real-world conditions and the need to collect sufficient quantities of particulate matter for chemical analysis.

Dilution ratio data was used during background subtraction as part of the emissions factor calculations. Concentrations measured during tunnel blank tests were multiplied by the ratio of the (actual test primary dilution factor) / (tunnel blank primary dilution factor) and subtracted from the actual test concentration. This method assumes that the majority of the background signal is associated with the primary dilution air since measurements taken from secondary dilution air found no contamination from this portion of the sampling system. The behavior of PM size distributions below 40nm are a strong function of dilution conditions [39] and so the size distributions of PM with aerodynamic diameters smaller than 50 nm are not reported in the current study because they may not be representative of real-world conditions.

Table 2-4: Heavy duty diesel vehicle sample collection summary.

sample ID	vehicle type	driving cycle	# of vehicles	# of cycles	total miles	total min	dilution ratio information primary	secondary	total
HDDV-0	PRE-BLANK	n/a	n/a	n/a	n/a	187	1.0	10.0	10.0
HDDV-1	FREIGHTLINER (1999)	IDLE/CREEP	1	6	3.2	282	112.5	5.2	583.6
HDDV-2	FREIGHTLINER (1999)	56k 5-MODE	1	1	36.7	109	17.8	9.4	166.8
HDDV-3	KENWORTH (1998)	56k 5-MODE	1	1	36.6	109	17.1	7.5	128.6
HDDV-4	KENWORTH (1998)	66k 5-MODE	1	1	36.5	109	19.6	9.7	189.7
HDDV-5	VOLVO (1992)	56k 5-MODE[a]	1	1	35.8	109	18.0	9.1	163.9
HDDV-6	FREIGHTLINER (1985)	56k 5-MODE	1	1	36.1	109	19.0	8.9	169.8
HDDV-7	POST-BLANK	n/a	n/a	n/a	n/a	152	1.0	10.0	10.0

[a] MAX SPEED 56-60 MPH DUE TO ENGINE GOVERNOR

Particulate matter samples were collected using Reference Ambient Air Quality Samplers (RAAS) (Andersen Instruments, Smyra GA) and Micro Orifice Uniform Deposit Impactors (MOUDIs) (MSP Corporation, Shoreview MN). Sample collection media included Teflon filters (Teflo R2PJ047, Pall Corp.), quartz fiber filters (QAO47, Pall Corp.) and foil substrates (MSP Corp.). Continuous measurements of particle size distributions were made using a Scanning Mobility Particle Sizer (SMPS) (TSI Incorporated, Shoreview MN). Samples were analyzed using the methodology described by Robert et al. [40]. Particulate matter mass was measured using a Cahn 28 microbalance. The concentration of organic and elemental carbon was measured with a Carbon Aerosol Analysis Lab Instrument (Sunset Laboratories, Tigard, OR) employing the NIOSH 5040 protocol *[41]* as described by Birch and Cary *[42]*. A multiplier of 1.4 was used to convert OC to OM *[43]*. Water-soluble ions were measured using an ion chromatograph (DX-600 workstation, Dionex Corporation, Sunnyvale, CA).

2.3 Results

2.3.1 Data Reduction and Quality Assurance

Protocols for sample handling and analyses are reported by Robert et al. [40] and so only a brief summary is included here. Size-resolved PM mass distributions were constructed based on the sum of elemental carbon (EC) and organic matter (OM, which is OC * 1.4) measured on MOUDI stages. The maximum of three collocated MOUDI measurements in each size fraction was used to represent the most accurate size distribution data under the assumption that particle bounce was the dominant collection artifact and that particles that bounce off an upper stage will be collected by the MOUDI afterfilter *[44]*. Using this approach, 64% of the reconstructed MOUDI stage masses fell within the respective gravimetric data error bounds (±1 standard deviation); 81% fell within ±2 standard deviations.

Table 2-5 shows the results from a linear regression analysis between co-located $PM_{1.8}$ RAAS and summed MOUDI ($PM_{1.8}$) samples. The linear correlation coefficients for the maximum summed MOUDI mass, EC, and OM and corresponding RAAS measurements are 0.86, 0.83, and 0.80, with corresponding R^2 values ranging from 0.83 – 0.98. The agreement between collocated MOUDI and filter-based measurements is similarly strong for sodium, ammonium, magnesium, calcium, and sulfate with R^2 ranging between 0.87 – 0.97 and correlation slope ranging between 0.74 – 1.18. Reconstructed mass measurements created by summing the measured chemical species can be more accurate than gravimetric mass measurements because the uncertainty in the chemical analysis is much smaller than the uncertainty in the gravimetric measurements. The agreement between collocated MOUDI and filter-based reconstructed mass measurements is excellent with R^2 equal to 0.97 and slope equal to 0.82. The strong agreement between collocated MOUDI measurements and RAAS filter samples improves confidence in the precision of the measurements.

Table 2-5: Linear regression analyses for co-located PM1.8 heavy duty diesel samples.

Sample #1	Sample #2	slope	R^2
Sum of Teflon MOUDI Gravimetric	RAAS Gravimetric	0.71	0.99
Sum of Average Foil MOUDI Gravimetric	RAAS Gravimetric	0.65	0.98
Sum of MOUDI Maxima Gravimetric	RAAS Gravimetric	0.86	0.98
Sum Average Foil MOUDI EC	RAAS EC	0.67	0.88
Sum of Maximum Foil MOUDI EC	RAAS EC	0.83	0.83
Sum of Average Foil MOUDI OM	RAAS OM	0.66	0.97
Sum of Maximum Foil MOUDI OM	RAAS OM	0.80	0.97
Sum of MOUDI Teflon Sodium	Average RAAS Sodium	1.07	0.97
Sum of MOUDI Teflon Ammonium	Average RAAS Ammonium	0.81	0.98
Sum of MOUDI Teflon Magnesium	Average RAAS Magnesium	1.18	0.87
Sum of MOUDI Teflon Calcium	Average RAAS Calcium	1.07	0.94
Sum of MOUDI Teflon Sulfate	Average RAAS Sulfate	0.74	0.97
Sum of Reconstructed MOUDI Mass	Reconstructed RAAS Mass	0.82	0.97
MOUDI Reconstructed Mass	MOUDI Gravimetric Total	1.01	0.92
RAAS Reconstructed Mass	RAAS Gravimetric	0.99	0.99

The accuracy of the particle size distribution measurements made by the SMPS during this study was checked in two independent tests. Particle size distributions measured by the SMPS downstream of the secondary dilution air system were compared to upstream SMPS measurements. The ratio of the upstream and downstream measurements was approximately constant for all particles sizes above 50 nm and equal to the theoretical dilution factor calculated using measured flow rates. Furthermore, an independent set of downstream SMPS measurements was taken by Toner et al. [45]. The average ratio of these spatially co-located (but temporally shifted) downstream SMPS measurements above 50 nm is 1.49 ± 0.20. The offset between these SMPS measurements may have been caused by a flow rate calibration problem. The downstream SMPS used in the current study was calibrated immediately before use.

The precision of the size and composition measurements reported in the current study was evaluated by comparing the results from similar or identical tests. The idle and creep test (HDDV-1) was based on a sequence of six repetitions of the idle + creep driving modes. The average relative standard deviation of SMPS measurements across all particle sizes above 50 nm was 26% and 20% for the idle and creep modes, respectively. Tests HDDV-2-3 and HDDV-2-4 used the same vehicle driven through the same HHDDT cycle. The only difference between the two tests is the simulated inertial load – 56,000 lbs for the former and 66,000 lbs for the latter (an 18% increase). The particle size and composition distributions measured during both of these tests were very similar, increasing confidence in the precision of the results.

Particle size data below 40 nm are not presented in the current study because it has been shown that PM size distributions below this size are a strong function of dilution air temperature and relative humidity *[39]*. These parameters were monitored but not controlled in the current study and therefore the resulting particulate data in this size range may not be representative of real-world conditions.

2.3.2 Emissions Comparisons

Figure 2-2 compares ultrafine and fine PM emissions from HDDVs across three categories in units of mg/km. Emissions across four HDDVs tested with full 5-mode HHDDT driving cycles and 56,000 lb inertial loads are compared in the category presented in Figure 2-2. Fine and ultrafine PM emissions rates for HDDVs ranged from 183 – 581 mg/km and 24 – 72 mg/km, respectively. Ultrafine and fine PM emissions rates for HDDVs were almost an order of magnitude higher than PM emissions rates for light-duty gasoline vehicles as reported by Robert et al. [40]. When total ultrafine and fine PM emission magnitudes were normalized to the newest vehicle tested, they ranged from a factor of 0.7 to 2.9. A similar comparison between old and new gasoline-powered vehicles yielded emission rate ratios of 576 and 187 for fine and ultrafine particles, respectively [40].

Both PM0.1 and PM1.8 emissions were well correlated with vehicle production age and engine production date ($R2 = 0.952$ and 0.960 for PM0.1 and PM1.8 in both cases and as observed by Toner et al. [45]) but are not well correlated with vehicle/engine mileage ($R2 = 0.508$ and 0.525 for PM0.1 and PM1.8). These data indicate that emissions are most likely a function of engine technology and to a lesser extent engine use history.

Emissions released during an idle/creep test and a full 5-mode HHDDT test for the same vehicle with a 56,000 lb inertial load are compared in the second category presented in Figure 2-2. The emissions (in units of mg/km) from the idle and creep modes were much higher than those from the 5-mode HHDDT cycle because a much shorter distance was traveled during the idle and creep modes, a finding in agreement with previous studies [37, 46].

Emissions from the same vehicle tested with 56,000 and 66,000 inertial loads using the 5-mode HHDDT driving cycle are compared in the third category presented in Figure 2-2. Although Yanowitz et al. [47] reported an increase in particulate carbon emissions with increasing power output for two of three HDDVs tested, there was little difference in the PM emissions rate between 56,000 lb and 66,000 lb simulated loads in the present study; total ultrafine PM mass decreased 6% and total fine PM mass decreased 5% for the 66,000 lb test. The subtle nature of these changes relative to previous findings [47] may be due to the small increase in inertial weight (18%) or the transient driving cycles used in the current study. The speciation of the carbonaceous emissions was affected by the load condition. Ultrafine PM EC increased 22% and fine PM EC decreased 2% when load increased from 56,000 lb to 66,000 lb; ultrafine PM OM decreased 38% and fine PM OM decreased 7% when load increased from 56,000 lb to 66,000 lb. Overall, the higher load condition appears to reduce the OM emissions that coat the non-volatile EC particles, shifting the remaining EC to smaller sizes.

All of the HDDVs tested in the current study had higher ultrafine and fine PM EC emissions than PM OM emissions when tested using the full 5-mode HHDDT cycle. The average EC/OM ratio for all vehicles tested was 2.72 for ultrafine PM and 1.63 for fine PM. The EC/OM ratios were reversed for the idle and creep mode test. Average EC/OM ratios were 0.57 for ultrafine PM and 0.34 for fine PM under these driving conditions. This difference is consistent with observations by Fraser et al. [46]. For indirect injection engines with standard fuel, Alander et al. [48] reported PM2.0 EC/OM ratios between 0.64 and 1.61, with the differences attributed to changes in vehicle speed and/or power output. Ratios for indirect injection engines with reformulated fuel varied from 1.06 to 2.63, and ratios for direct injection engines with reformulated fuel ranged from 2.86 to 6.25. Numerous researchers have used the ratio of EC to OM measured in the atmosphere to estimate the amount of secondary organic aerosol formation and the contribution of diesel engines to ambient PM concentrations. The fundamental variability between EC/OM ratios generated by light-duty gasoline vehicles versus HDDVs and between HDDVs operated under different conditions illustrates the large amount of uncertainty that can enter into these types of calculations.

Table 2-6 presents ultrafine PM, fine PM, EC, OM, and gaseous compound emission rates for the HDDV sample set. Whereas fine PM emission rates have been previously reported for heavy-duty gasoline vehicles, fewer studies have reported ultrafine PM emission rates and this is the first study found to specifically report ultrafine PM emission rates for heavy heavy-duty diesel vehicles operated on chassis dynamometers using the HHDDT driving cycle. Linear regressions of PM versus gaseous species emissions in Table 2-6 across the vehicles tested indicate no significant correlations when the idle/creep test is excluded. However, PM emission rates are strongly correlated with each gaseous species emission rate across all samples when the idle/creep test is included.

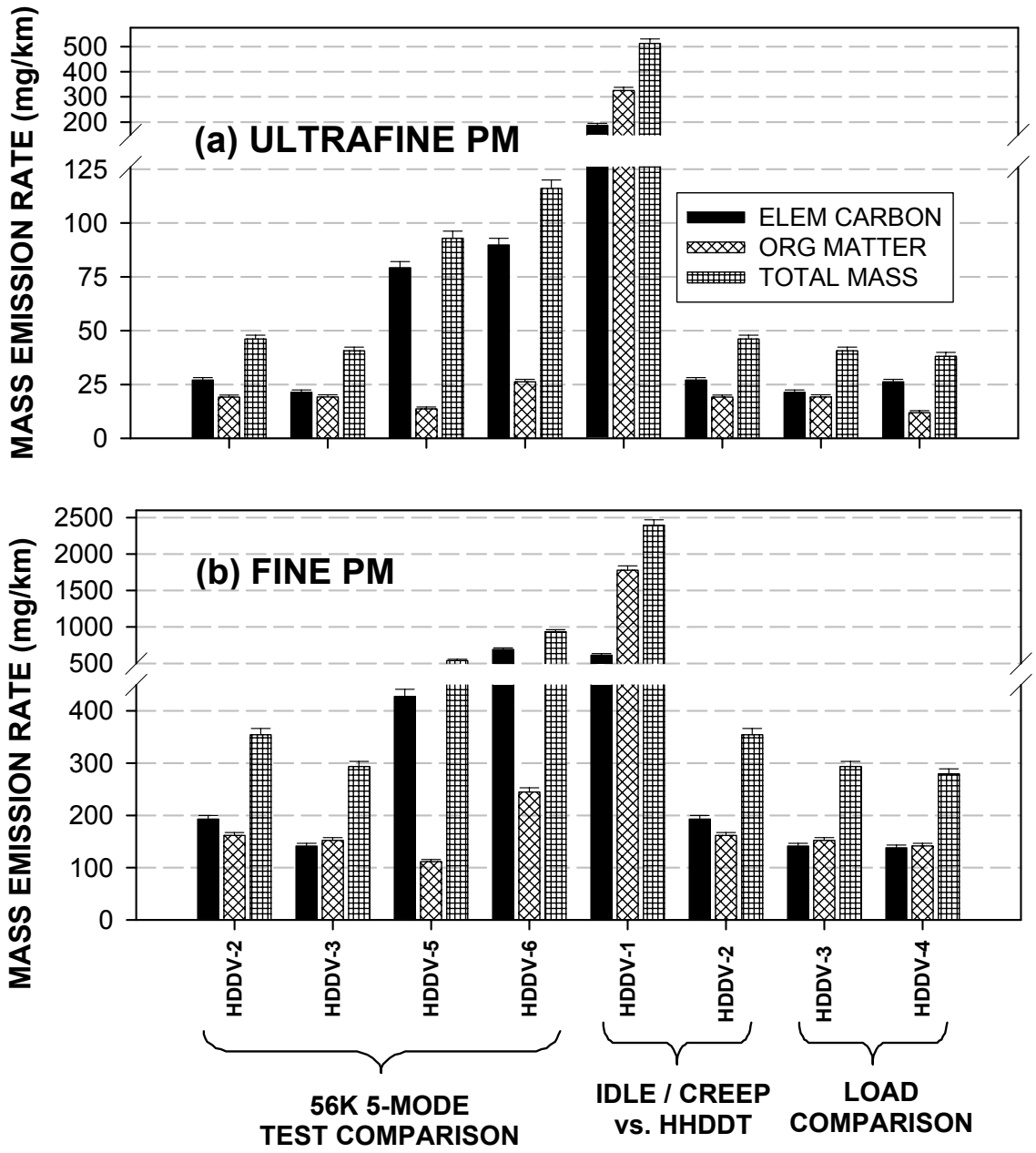

Figure 2-2: Heavy Duty Diesel Vehicle (HDDV) ultrafine and fine particulate matter (PM) emissions for 56,000 lb (56k) and 66,000 lb (66k) inertial loads.

Table 2-6: HDDV PM and select gas-phase emission rates.

	Robert et al. (2006)		Coordinating Research Council (2005)			
vehicle test	**PM0.1** (mg/km)	**PM1.8** (mg/km)	**CO** (g/km)	**CO2** (g/km)	**NO_X** (g/km)	**FIDHC** (g/km)
HDDV-1	318.3	1486.2	44.6	5416	133.4	3.95
HDDV-2	28.7	220.4	4.2	1182	21.3	0.18
HDDV-3	25.3	182.5	1.5	1182	18.7	0.91
HDDV-4	23.7	173.9	1.6	1085	16.5	0.73
HDDV-5	57.7	334.9	2.1	1009	7.1	0.50
HDDV-6	72.1	580.6	4.0	1047	17.4	0.71

Several other chassis dynamometer studies have reported fine PM emission rates comparable to those reported in Table 2-6. Two studies in particular have reported PM emission rates from HDDVs using the HHDDT cycle. Cocker et al. *[49]* reported PM mass emission rates from a 2000 model year HDDV ranging from 81 mg/km in the cruise mode to 588 mg/km in the creep mode. Shah et al. *[37]* reported an eleven-vehicle fleet (1996-2000) averaged PM emission rate ranging from 134 mg/km in the cruise mode to 635 mg/km in the creep mode. Direct comparison of these results to the results from this study is difficult due to the fact that this study reports PM mass emission rates across the entire HHDDT cycle versus each inter-cycle mode. The average fine PM emission rate in this study, excluding the idle/creep sample, is 299 mg/km. The distance-weighted average of the results reported by Cocker et al. *[49]* is 164 mg/km and by Shah et al. *[37]* is 257 mg/km. The idle/creep PM emission rate reported in this study is 1486 mg/km, compared to 940 mg/km by Cocker et al. *[49]* and 1016 mg/km (range 479-1734 mg/km) reported by Shah et al. *[37]* for the creep-only mode.

2.3.3 Size and Composition Distributions

Figure 2-3 shows the size and composition of PM released during six HDDV tests measured using MOUDIs and analyzed using thermal-optical EC/OC measurements as described in section 2.2. The peak in the PM mass distribution for all tests occurred between 100 - 180 nm. The full 5-mode HHDDT driving cycle tests were dominated by EC, while the idle/creep sample had a markedly larger percentage of OM emissions. This finding agrees with results reported from co-located Aerosol Time-of-Flight Mass Spectrometer (ATOFMS) measurements made by Toner et al. *[45]* and it is also consistent with an independent set of diesel engine emissions measurements made by Fraser et al. *[46]* where it was found that older vehicles have a higher ratio of EC/OM at all particle sizes. The 56,000 lb and 66,000 lb inertial load tests conducted with the same vehicle appeared to result in the same approximate size and composition distribution with a slight increase in ultrafine emissions at the higher loads. The EC and OM maxima in all HDDV samples fell within 100 nm and 180 nm, which correspond to the maxima in the corresponding reconstructed mass distributions.

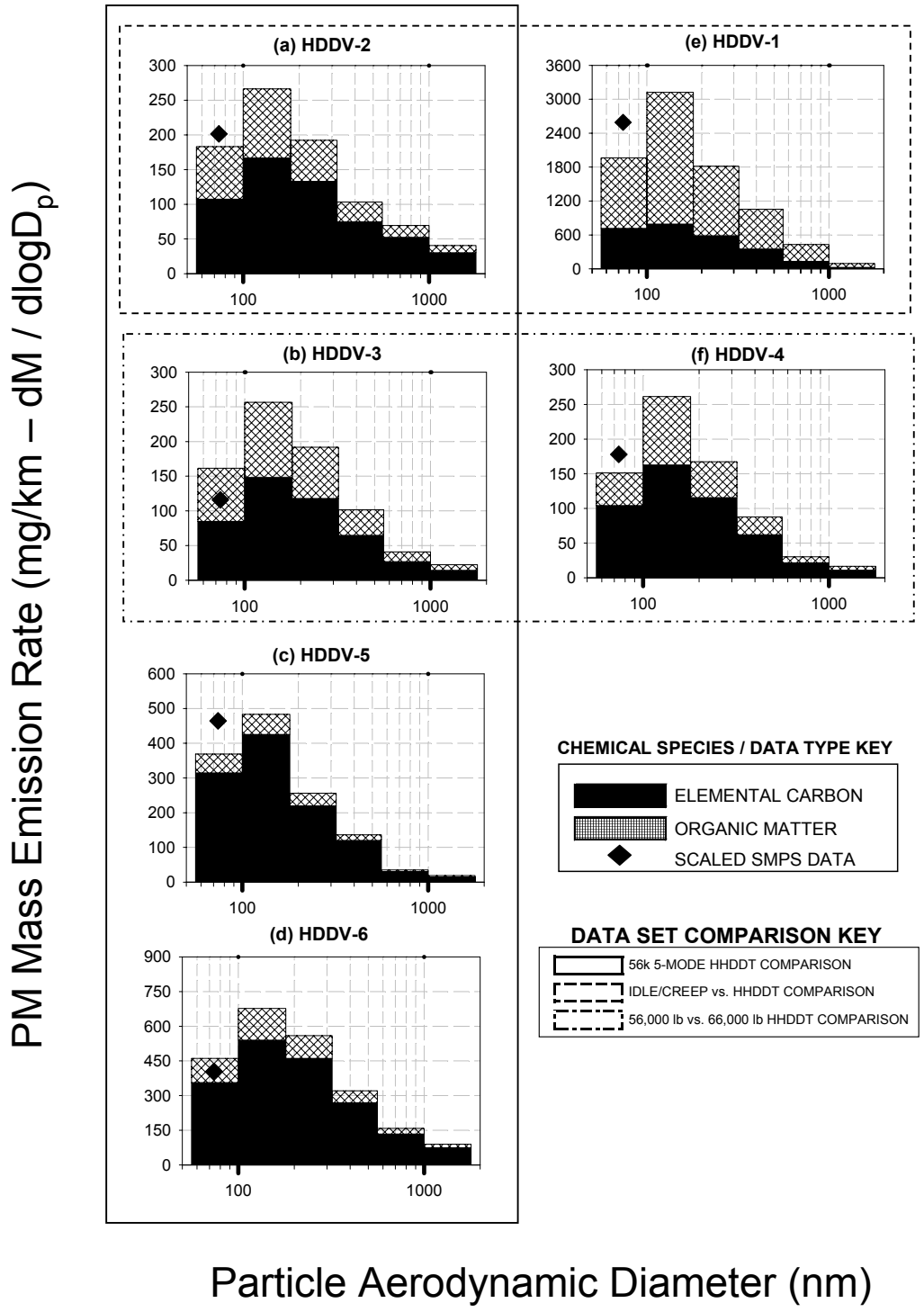

Figure 2-3: Normalized size and composition distributions of particulate matter (PM) emitted from heavy duty diesel vehicles (HDDVs).

Figure 2-4 shows the size and composition distribution of sodium, ammonium, magnesium, calcium, and sulfate released from the six HDDV samples. Error bars presented are the Method Detection Limits (MDLs) based on analytical uncertainty of the ion chromatography (IC) method utilized, defined as three times the standard deviation of seven measurements of the lowest detectable standard for each ionic species over a three-day period. The total PM0.1 and PM1.8 emissions rates are included in each panel, along with a comparison between the sum of MOUDI impactor samples and a collocated RAAS filter sample. Missing panels indicate that the measured size distribution did not pass quality control checks summarized in Section 2.3.1. Missing size distributions were typically below the IC minimum detection limits and/or did not sum to yield a PM1.8 concentration that was consistent with a co-located filter measurement. Due to short distance traveled during the idle/creep test, the ionic species mass emission rates (ng/km) in this sample were higher than all of the other samples. Calcium was the most abundant ion detected in the emissions. Calcium emitted from the oldest vehicles tested (HDDV-5,6) had size distributions that peaked in the ultrafine range, while calcium emitted from newer vehicles (HDDV-2,3) peaked at larger sizes. Calcium is commonly added to lubricating oil to reduce the buildup of acidity. Calcium has been observed previously in ambient ultrafine particles *[44]*. The ammonium size distributions also generally peaked at smaller particle sizes, but no consistent pattern was observed for the remaining ionic species distributions. Ultrafine PM emissions rates for sodium, ammonium, magnesium, calcium, and sulfate, ranged from 3 - 9 ng/km, 5 - 14 ng/km, 4 - 54 ng/km, 4 - 81 ng/km, and 1 - 8 ng/km, respectively.

2.3.4 Particle Morphology and SMPS Scaling Factors

PM material densities were estimated using the size-resolved composition information shown in Figure 2-2 and assuming a density of 2.0 g/cc for EC and 1.4 g/cc for organic matter *[50]*. Resulting average PM material densities ranged from 1.59 g/cc to 1.91 g/cc, values that bracket a recent estimate of diesel PM density of 1.78 g/cc by Park et al. *[51]*. Material density was the lowest for the idle/creep sample because it was dominated by OM; the average material density excluding this test was 1.83 ± 0.06 g/cc.

Figure 2-3 presents scaled SMPS particle mass distributions superimposed on the reconstructed MOUDI mass distributions in the ultrafine PM range. SMPS measurements were scaled to accurately represent the respective mass distributions because the SMPS and the MOUDI classify particle size based on differing properties [40]. Whereas the SMPS measures particle number as a function of electrical mobility diameter, the MOUDI measures particle size as a function of aerodynamic diameter.

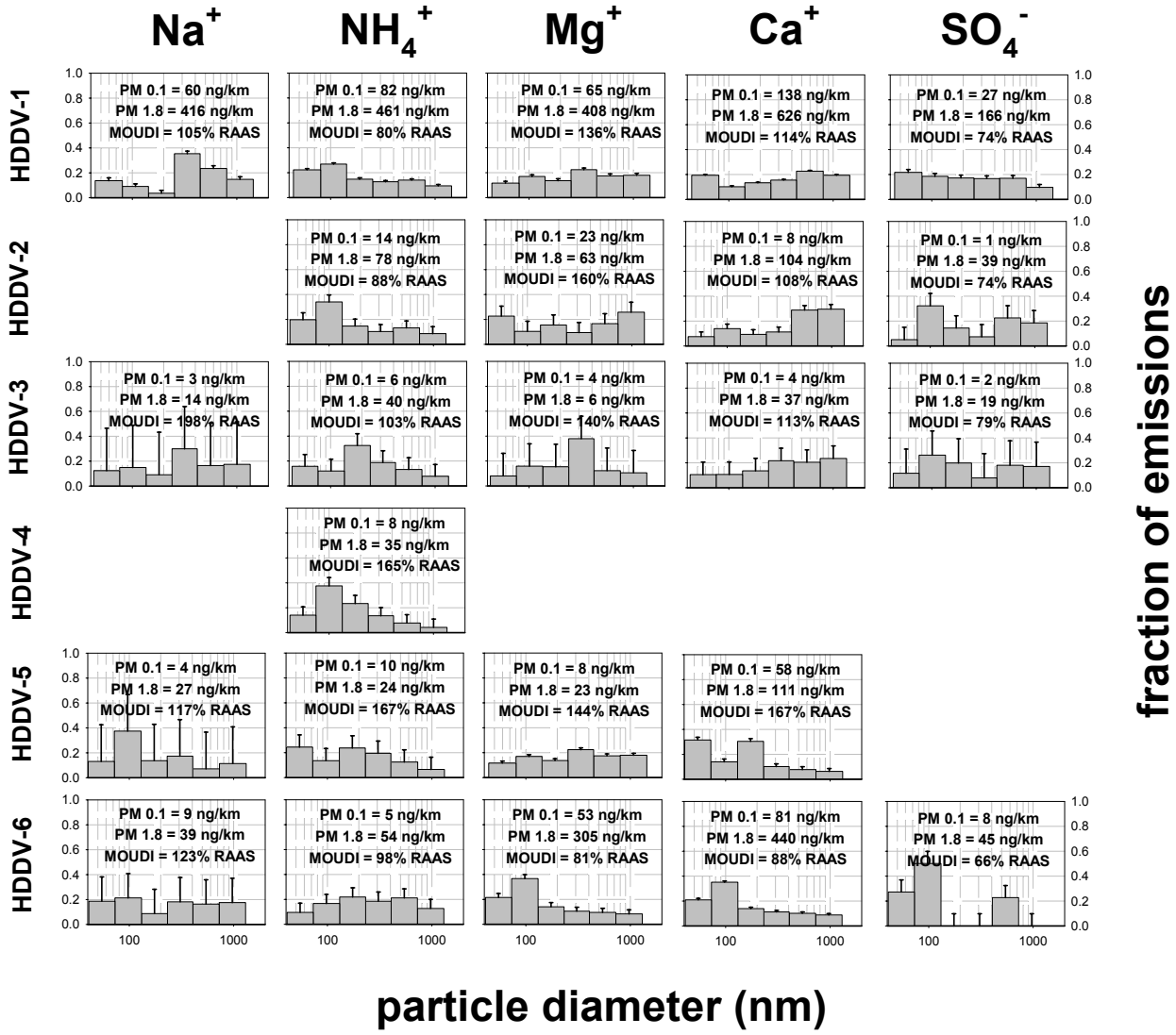

Figure 2-4: Normalized size distributions of water-soluble ions contained in particulate matter (PM) emitted from heavy duty diesel vehicles (HDDVs).

Particle aerodynamic equivalent diameter is related to particle mobility diameter and particle effective density by the equation:

$$\rho_{eff} d_{me}^2 C_{me} = \rho_o d_{ae}^2 C_{ae} \qquad [1]$$

where d_{me} is the mobility diameter, ρ_{eff} is the PM effective density (a function of mobility diameter), ρ_o is the unit density (1 g/cc), d_{ae} is the aerodynamic equivalent diameter, and C is the Cunningham Slip Correction Factor *[52]*. Effective densities for diesel PM are usually measured with particle electrical classifiers and impactors in series *[31, 53-56]*. Since experimental data for the effective density as a function of mobility diameter was not measured in this study (all measurements in parallel), four parameter logistic functions were fit to the effective density versus mobility diameter data measured by Park

et al. *[31]*. Separate curve fits were generated for an idling diesel engine and for a diesel engine under load (R^2 = 0.994 and 0.995 respectively) so that they could be applied correspondingly to the one idle/creep and five load samples in this study. These effective density relationships were used to iteratively solve Equation [1] to convert SMPS size cuts based on mobility diameter to aerodynamic diameter. Because the raw SMPS data assumed a material density of 1 g/cc, these same effective density relationships were also used to convert the SMPS particle volume to particle mass on a size-resolved basis. The particle effective density relationships derived from previous measurements *[31]* perform well in the current study for particles with diameter less than 100 nm, with the MOUDI stage 10 mass in good agreement with scaled SMPS data from 56-100 nm on a mg/km basis (slope 0.77 with R^2 = 0.995; slope 0.98 with R^2 = 0.838 excluding the idle/creep sample). The particle effective density derived in previous studies for diameters larger than 100 nm are 2 – 5 times greater than the apparent effective density of the particles measured in the current study (data not shown in Figure 2-3). Confidence in the MOUDI measurements from this study is enforced by the good agreement between the reconstructed summed MOUDI mass and the Andersen Reference Ambient Air Sampler (RAAS) measurements (82% as indicated in Table 2-5). Confidence in the SMPS data from this study is likewise enforced by agreement between SMPS measurements taken both upstream and downstream of the secondary dilution system (accounting for the effects of dilution ratio) and also the agreement between co-located SMPS measurements. The data consistency suggests that observations of low effective particle density are credible and thus an area for future investigation. The low effective particle densities observed in the current study at aerodynamic diameters above 100 nm may be caused by the multiple vehicle chassis dynamometer tests that employed transient driving cycles with dilution air at temperatures of ~40^{o}C. This contrasts with previous studies that measured effective densities in a laboratory setting with serial SMPS and impactor measurements of a single diesel engine using an engine dynamometer under steady-state conditions *[31]*.

2.3.5 Emissions Versus Time

Figure 2-5 shows $PM_{0.1}$ emissions as a function of time (mode) for five HDDV tests using the full 5-mode HHDDT cycle in units of mg, mg/km, and mg/liter of fuel consumed. HDDV fuel consumption is calculated as the average of instantaneous (per second) CO_2 emissions data assuming 2.77 kg of gaseous CO_2 emissions per liter of diesel fuel consumed *[57]*. The majority of the PM mass (mg) was emitted during the transient and cruise modes. On a mass per kilometer basis, the highest emissions occurred during the creep mode, generally followed by the transient, low-speed cruise, and high-speed cruise modes (there was no data for the idle cycle as it had no associated distance traveled). On a mass per liter of fuel consumed basis, the transient mode dominated emissions in all samples. This is due to the combination of high mass emission and relatively high fuel consumption rates associated with the accelerations during the transient mode.

Uncertainty bars in Figure 2-5 represent one standard deviation of the magnitudes of the four individual 75 second SMPS scans that comprise the respective five minute

average; each of these four data points represent the averaged cumulative mass distribution for either $PM_{0.1}$ or $PM_{0.56}$ for the vehicle tested. It follows that large error bars, such as those present in the transient and cruise modes, are indicative of highly variable mass emission rates during those driving cycle modes.

2.3.6 Size Distributions Versus Driving Cycle Mode

Figure 2-6 illustrates the size distribution of particle mass emissions associated with different vehicles during the idle mode (Figure 2-6a) and creep mode (Figure 2-6b), and the transient and cruise modes (Figure 2-6c) based on scaled SMPS data. The older vehicles generally had higher particulate matter emissions rates than the newer vehicles during these modes. The peak in the particle mass distribution for the newest vehicle occurred at approximately 70 nm during both the idle and creep modes. The peak in the particle mass distribution associated with older vehicles occurred at diameters larger than 100 nm during the idle and creep modes. Similar trends in particle size distributions were not apparent during other modes of the HHDDT tests. Toner et al. *[45]* observed that the newest vehicle in this study was the highest emitter of PM on a particle number basis. Other studies of diesel emissions have observed that the vehicle with the lowest fine PM mass emissions emitted the greatest number of ultrafine particles *[58, 59]*. In some cases this has been attributed to changes in fuel characteristics or to engine after-treatment effects *[59, 60]*.

2.4 Conclusions

Chassis dynamometer test measurements of PM emissions from four HDDVs using the idle/creep and full HHDDT driving cycles revealed several important PM emissions trends. Ultrafine and fine PM emission rates (ug/km) increased with vehicle age as expected. The majority of the particulate matter was carbonaceous material. PM emissions using the HHDDT driving cycle were dominated by EC, with the idle/creep test was dominated by OM, results which are consistent with several other similar studies. The peak in the PM mass distributions occurred between 72 - 135 nm for all vehicles. Increasing the simulated inertial weight of the test vehicle from 56,000 lb to 66,000 lb resulted in a slight decrease for both the $PM_{0.1}$ and $PM_{1.8}$ mass emissions rates due to a reduction of OM. Fine PM EC emission rates were approximately constant at higher loads, but the EC size distribution was shifted to smaller particle diameter as the OM coating was removed. The most abundant ionic species detected was calcium with lesser amounts of magnesium, sodium ammonium ion, and sulfate.

The driving mode with the highest PM emission rates depended on the units used in the comparison. In units of mg, high PM emissions were associated with the transient and cruise modes of the HHDDT driving cycle. In units of mg/km, the highest PM emissions were observed during the creep mode. In units of mg/liter, the highest PM emissions occurred during the transient mode. The newest vehicle tested was not the highest overall emitter during the overall 5-mode driving cycle, but it had the highest ultrafine PM emission rate during the idle mode of any vehicle tested.

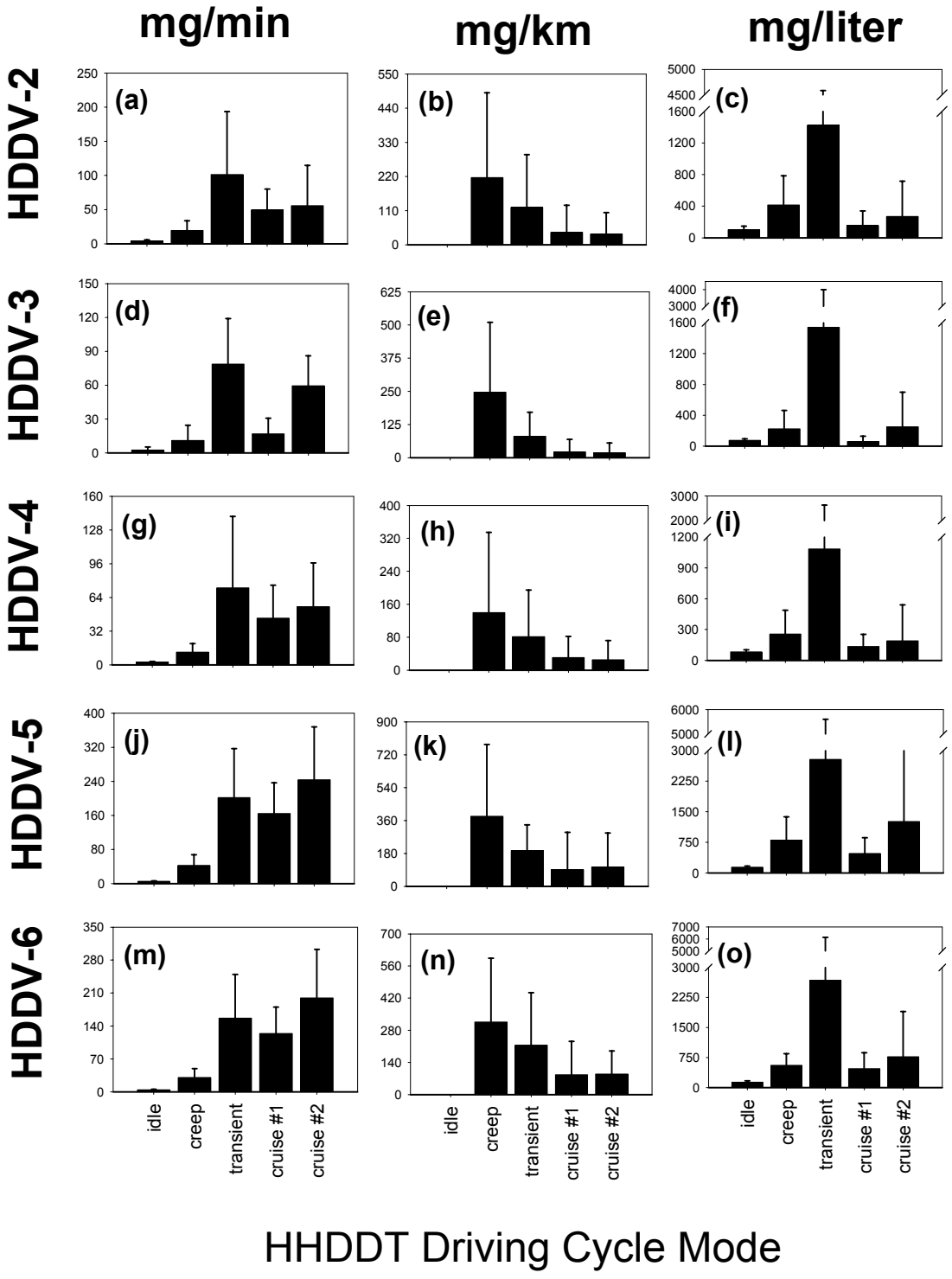

Figure 2-5: PM0.1 emissions as a function of time for different HDDVs.

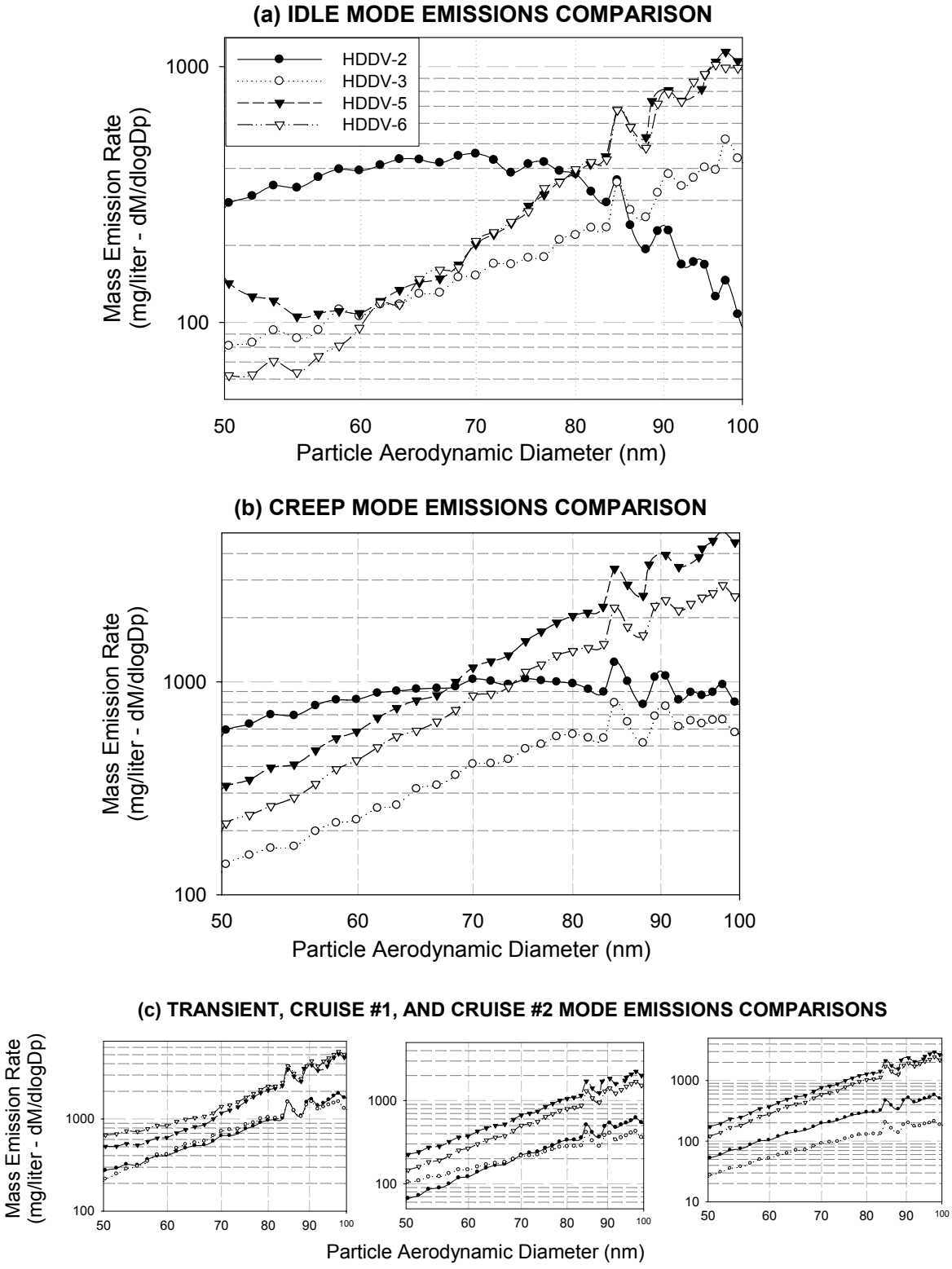

Figure 2-6: Particle size distributions for HDDVs operating Particle size distributions for HDDVs operating under idle conditions (panel a), creep conditions (panel b), and transient conditions (panel c).

3 SIZE AND COMPOSITION DISTRIBUTION OF PM EMITTED FROM LIGHT DUTY GASOLINE-POWERED VEHICLES

3.1 Introduction

Atmospheric Particulate Matter (PM) has been found to be associated with increased human mortality and morbidity in many epidemiological studies *[1]*. Recent studies have suggested an even stronger association between the fine fraction of PM (aerodynamic diameter < 2.5 μm) and morbidity/mortality *[1-3]*. It has been postulated that ultrafine particles (aerodynamic diameter < 0.1 μm) may be responsible for some of the observed adverse health effects *[4-9]*. There is some evidence to support the hypothesis that ultrafine PM can localize in the mitochondria of epithelial cells where they induce major structural damage *[10]*. The composition and source origin of ultrafine particles must be determined to fully investigate their relationship with human health.

Preliminary studies indicate that combustion processes are the dominant source of ultrafine particles in the urban atmosphere *[61]*. In many urban areas, transportation is the leading source of particulate combustion emissions *[58, 61]*. Due to the introduction of new vehicle technologies such as Low Emission Vehicles (LEVs) in the 1990s, the mix of the on-road light-duty gasoline vehicle fleet has changed significantly in the United States. A need exists to measure the size and composition distribution of PM emitted from present-day transportation sources to help quantify the contribution that these sources make to ambient fine and ultrafine PM concentrations.

The purpose of this chapter is to report the size and composition distributions of PM released from contemporary gasoline-powered light-duty vehicles (LDGVs) measured using a chassis dynamometer / dilution sampling system that employs filter-based samplers, cascade impactors, and Scanning Mobility Particle Size (SMPS) measurements. Ultrafine PM is defined as particles with aerodynamic diameter between 56 – 100 nm (as collected by stage 10 of a Micro Orifice Uniform Deposit Impactor) and fine PM is defined as particles with aerodynamic diameter less than 1.8 μm ($PM_{1.8}$) (as collected by a Reference Ambient Air Sampler filter sample). These are useful functional definitions because very little of the PM mass collected in this study had aerodynamic particle diameters below 56 nm or above 1.8 μm ($PM_{1.8}$ is functionally equivalent to $PM_{2.5}$ in the current study). The data set includes different vehicle types and emission control technologies operated under multiple driving cycles. In the present study, particle size and composition distributions in six size fractions between 0.056 - 1.8 μm particle aerodynamic diameter are reported in addition to bulk $PM_{1.8}$ data. Vehicle emissions characteristics as a function of time for different technology types and driving cycles are also presented.

3.2 Experimental Methods

PM emissions from LDGVs were collected at the California Air Resources Board (CARB) Haagen-Smit Laboratory (HSL) in El Monte, CA during August and September of 2002. LDGVs were tested using a chassis dynamometer and the diluted exhaust was characterized using numerous instruments operated by multiple research groups. LDGV emissions of gas-phase hydrocarbons (HC), CO, CO_2, CH_4, NO, and NO_x, as well as alcohols, aldehydes, sulfates, non-methane organic gases (NMOG), and non-methane hydrocarbons (NMHC) were measured by researchers at CARB. Sodeman et al. *[62]* characterized PM emissions using Aerosol Time of Flight Mass Spectrometers (ATOFMS). UCD researchers collected gas-phase emissions and bulk $PM_{1.8}$ samples using annular denuders upstream of filter substrates and polyurethane foam (PUF) plugs. University of California, Davis (UCD) researchers also collected $PM_{1.8}$ and size-resolved samples using filter-based samplers, Micro-Orifice Uniform Deposit Impactors (MOUDIs), and Scanning Mobility Particle Sizers (SMPSs). PM data from the bulk, size-resolved, and time-resolved emission samples are reported.

3.2.1 Vehicle Test Fleet

Test vehicles were selected to represent the on-road vehicle fleet as best possible, taking into consideration aspects such as vehicle weight, emissions control technology, mileage, and manufacturer. Thirty LDGVs were tested (Table 3-1). LDGVs were grouped into five categories based on emissions control technology: Low Emission Vehicles (LEVs), Three Way Catalyst (TWC) vehicles, Oxidation Catalyst (OCAT) vehicles, Non-catalyst (NCAT) vehicles, and vehicles observed to emit blue smoke (SMOKERs). Within these categories, vehicles could be further classified as passenger cars (PCs) or Light-Duty Trucks (LDTs)/Sport Utility Vehicles (SUVs). Separate PM samples were collected for each LDGV category in order to obtain enough mass for chemical analyses.

The gasoline used to power the LDGVs was purchased at retail stations throughout Los Angeles, CA. Only two vehicles required additional fuel to complete their chassis dynamometer cycles; they were re-fueled at two different retail gasoline stations near the testing facility. Fuel was assumed to be California reformulated gasoline, containing $\leq$ 35 ppm sulfur. Maricq et al. *[63]* found no appreciable difference in fine PM emissions from a passenger car on a chassis dynamometer using the FTP cycle between this base fuel (35 ppm sulfur) and laboratory variants containing 350 and 600 ppm sulfur. Since it is possible that the fuel sulfur content could influence sulfuric aerosol formation and the sulfur content of the fuel is unknown, data below 56 nm is not reported in this study. Fuel and oil samples were collected from each vehicle and their composition is reported in Chapter 6.

Table 3-1: Summary of light duty gasoline-powered vehicles tested.

category[a]	year	make	model	mileage	engine information	fuel delivery technology[b]
LEV PC	1996	Honda	Civic	77,703	4 cylinder	SFI
LEV PC	1998	Honda	Accord	97,811	4 cylinder	SFI
LEV PC	1999	Toyota	Camry LE	43,160	6 cylinder	SFI
LEV PC	1999	Nissan	Sentra GXE	52,630	4 cylinder	SFI
LEV PC	2002	Chevrolet	Monte Carlo	20,230	6 cylinder	FI
LEV LDT/SUV	1998	Ford	Explorer	82,513	8 cylinder / 302	SFI
LEV LDT/SUV	2000	Jeep	Grand Cherokee	31,751	6 cylinder	SFI
LEV LDT/SUV	2000	Toyota	Tacoma	51,554	6 cylinder	SFI
LEV LDT/SUV	2002	Nissan	Pathfinder	8,169	6 cylinder	SFI
LEV LDT/SUV	2003	Chevrolet	Silverado	1,264	8 cylinder / 292	SFI
TWC PC	1988	Chrysler	Plymouth Horizon	32,097	4 cylinder	EPFI
TWC PC	1988	Honda	Civic DX	174,163	4 cylinder	EPFI
TWC PC	1991	Toyota	Camry	95,532	4 cylinder	MPFI
TWC PC	1991	Ford	Taurus	136,983	6 cylinder	MPFI
TWC PC	1994	Honda	Acura	104,441	4 cylinder	SFI
TWC PC	1998	Ford	Mustang	10,697	6 cylinder	SFI
TWC PC	1999	Cadillac	Sedan DeVille	35,320	8 cylinder / 280	FI
TWC LDT/SUV	1987	Suzuki	Samurai	57,124	4 cylinder	Carbureted – 2 BBL
TWC LDT/SUV	1989	Toyota	SR5 Pick up	59,231	6 cylinder	FI
TWC LDT/SUV	1989	Chrysler	Caravan LE	207,104	6 cylinder	EPFI
TWC LDT/SUV	1995	Chevrolet	Suburban	91,618	8 cylinder/ 350	TBFI
TWC LDT/SUV	1996	Nissan	Frontier Pick-up	55,940	4 cylinder	SFI
TWC LDT/SUV	1997	Ford	Expedition XLT	78,173	8 cylinder / 280	SFI
OCAT PC	1977	Mercedes	280 E	118,119	6 cylinder	FI
OCAT PC	1979	Toyota	Corolla	8,661	4 cylinder	Carbureted – 2 BBL
OCAT PC	1980	Honda	Accord	88,642	4 cylinder	Carbureted – 3 BBL
NCAT PC	1953	Chevrolet	Bel-Air	96,176	6 cylinder	Carbureted – 1BBL
NCAT PC	1965	Ford	Mustang	55,280	8 cylinder / 289	Carbureted – 4 BBL
SMOKER	1968	Ford	Cougar	63,622	8 cylinder / 302	Carbureted – 4 BBL
SMOKER	1993	Chevrolet	S-10 Blazer	162,750	6 cylinder	FI

[a] LEV = LOW EMISSION VEHCILE, PC = PASSENGER CAR, LDT = LIGHT-DUTY TRUCK, TWC = THREE-WAY CATALYST, OCAT = OXIDATION CATALYST, NCAT = NON-CATALYST, SMOKER = VEHICLE EMITTING VISIBLE SMOKE

[b] FI = FUEL INJECTED, MPFI = MULTI-PORT FUEL INJECTED, EPFI = ELECTRONIC PORT FUEL INJECTION, TBFI = THROTTLE BODY INJECTED, SFI = SEQUENTIAL FUEL INJECTED, 1 BBL = ONE BARREL, 2 BBL = TWO BARREL, 3 BBL = THREE BARREL, 4 BBL = FOUR BARREL

LDGVs were tested using three different driving cycles: the Federal Test Procedure (FTP), the Unified Cycle (UC), and the Correction Cycle (CC) *[62]*. The FTP cycle has moderate transient sections with the lowest top speed of all three cycles. The UC cycle has the highest acceleration and greatest speed of all the cycles tested. The CC cycle has a higher average speed section than the FTP cycle with some transient driving [64]. Table 3-2 presents details on each of these driving cycles, and their individual driving traces are provided in each panel of Figure 3-5.

Table 3-2: Driving cycle summary for light duty gasoline vehicles.

driving cycle	phase / mode	avg speed (kph)	max speed (kph)	distance (km)	time per mode (sec)
FTP	1[a]	41.2	91.2	5.78	505
FTP	2[b]	25.7	55.2	6.29	869
FTP	3	41.2	91.2	5.78	505
UC	1[a]	22.8	66.1	1.45	300
UC	2[b]	43.9	108.1	14.32	1135
UC	3	22.8	66.1	1.45	300
CC	1	88.3	115.2	33.63	1370
CC	2	36.8	90.4	8.37	821

[a] COLD START; [b] PHASE / MODE FOLLOWED BY 10 MINUTES WITH VEHICLE OFF

Table 3-3 summarizes the complete LDGV sample set, which consists of two background samples and ten vehicle/class samples. As few as two and as many as 40 total driving cycles were composited onto each LDGV emissions sample in order to ensure that enough PM mass was collected to support chemical analyses. All composited sample sets are integer multiples of the number of vehicles in that test set; i.e. 40 LEV cycles represent four independent cycles from ten separate vehicles. Total LDGV test sample times ranged from a minimum of 58 minutes for the vehicles with the highest emission rates (SMOKERS) to a maximum of 1253 minutes for the vehicles with the lowest emission rates (LEVs). The relative emission rates of LDGVs within a category (combined into a single test) were estimated from real-time SMPS measurements and measured dilution ratios.

The breadth and depth of the cumulative sample set provide several inter-comparisons which were investigated. Emissions released during full FTP cycles were compared between LEVs, TWC PCs, OCAT PCs, NCAT PCs, and SMOKERS. Emissions released from partial FTP cycles were compared between these classes and TWC LDT/SUVs. Emissions released from partial FTP, UC, and CC cycles were compared across the same set of TWC LDT/SUV vehicles.

Table 3-3: Summary of light duty gasoline-powered vehicle tests.

sample ID	vehicle type	driving cycle	# of vehicles	# of cycles	total km	total min	dilution ratio information		
							primary	secondary	total
LDGV-0	PRE-BLANK	n/a	n/a	n/a	n/a	175.0	1.0	8.9	8.9
LDGV-1	LEV PC/LDT/SUV	FTP	10	40	713.8	1252.7	16.9	7.5	127.3
LDGV-2	TWC PC	FTP	6	12	214.1	375.8	18.2	6.9	125.7
LDGV-3	TWC PC	UC	6[a]	6	103.3	173.5	14.5	3.9	55.8
LDGV-4	TWC HONDA	UC	1	2	34.4	57.8	20.5	3.7	75.1
LDGV-5	TWC LDT/SUV	Ucb	5	5	78.9	144.6	12.9	3.7	47.3
LDGV-6	TWC LDT/SUV	CC	5	5	210.1	182.6	10.1	3.8	37.9
LDGV-7	TWC LDT/SUV	FTP[b]	5	5	60.4	156.6	18.2	3.7	66.9
LDGV-8	OCAT PC	FTP	3	3	53.5	94.0	14.8	26.5	392.5
LDGV-9	NCAT PC	FTP	2	2	35.7	62.6	11.6	11.2	129.3
LDGV-10	SMOKERS	FTP	2	2	35.7	62.6	11.1	11.2	124.2
LDGV-11	POST-BLANK	n/a	n/a	n/a	n/a	178.0	1.0	12.4	12.4

[a] TWC PC 1998 HONDA CIVIC NOT INCLUDED, [b] FIRST TWO PHASES OF DRIVING CYCLE ONLY

3.2.2 Sampling Methodology

PM emissions were captured from the exhaust systems of vehicles as they were driven through various driving cycles on chassis dynamometers. The emissions were diluted in two stages before sampling (Figure 2-1). A constant volume sampling system was used for primary exhaust dilution. The actual primary dilution rate changed as a function of time during each test, but average values ranged from 10 to 21. Secondary dilution was used to approach total dilution factors that are comparable to those experienced by real-world vehicles and to avoid condensation of water in sampling lines. Average secondary dilution ratios ranged from 4 to 27 and thus total dilution ratios ranged from 9 to 393. A constant flow rate of exhaust (after primary dilution) was drawn into the Stack Dilution Tunnel (SDT), described by Hildeman et al. *[36]* through a heated inlet line, cyclone manifold, and calibrated sample venturi. Secondary dilution air was passed through a pre-filter, HEPA filter, and 1.5 ft^3 of activated carbon to remove ambient PM and gas-phase organic species. Following secondary dilution and turbulent mixing in the SDT, the sample stream was aged for approximately 60 seconds in a ~0.10 m^3 Residence Time Chamber (RTC).

Dry bulb temperature measurements at the output of the RTC ranged from 22°C to 28°C, and wet bulb temperatures ranged from 21°C to 25°C. The minimum relative humidity measured during the LDGV sampling campaign was 70% and the maximum was 97%; the range (max - min) for each test varied from 3% to 22% with an average of 11%. Bukowieki et al. *[39]* showed that the behavior of PM size distributions below 40 nm in vehicle exhaust is a strong function of dilution air temperature and relative humidity. In the present study temperature and relative humidity of dilution air were monitored but not controlled. As a result, the size distributions of PM with aerodynamic diameters smaller

than 40 nm are not reported in the current study because they may not be representative of real-world conditions.

A variety of PM sampling equipment was employed for all chassis dynamometer tests (Table 2-1). Bulk $PM_{1.8}$ was collected using Andersen Reference Ambient Air Samplers (RAASs) (Andersen Instruments, Smyrna, GA). Size-resolved PM was collected using Micro Orifice Uniform Deposit Impactors (MOUDIs) (Model 110, MSP Corporation, Shoreview, MN), in six size fractions between 56 nm and 1.8 μm in aerodynamic diameter. A nano-MOUDI (MSP Corporation, Shoreview, MN) was used to collect three PM size fractions below ~40 nm in aerodynamic diameter. Three MOUDIs were loaded with foil substrates used to measure carbonaceous species while one MOUDI was loaded with Teflon substrates to measure elemental composition and water-soluble ions. Scanning Mobility Particle Sizers (SMPSs) (SMPS Model 3080, DMA Model 3081, CPC Model 3025A, TSI Incorporated, Shoreview MN) sampled time resolved PM distributions from 18 nm to 687 nm mobility diameter both upstream of the SDT and downstream of the RTC.

3.2.3 Data Reduction and Quality Assurance

All samples were sealed in Petri dishes with Teflon tape and stored in laboratory freezers (-16 °C) after collection. All Teflon and aluminum media were weighed before and after sample collection using a Cahn 28 microbalance in a constant temperature (20-25 °C) and relative humidity (30-40 %) controlled environment.

The mass of organic carbon (OC) and elemental carbon (EC) was determined for each quartz and aluminum substrate using thermal optical transmittance (TOT) method (Carbon Aerosol Analysis Lab Instrument, Sunset Laboratories, Tigard, OR) employing the NIOSH 5040 protocol *[41]* as described by Birch and Cary *[42]*. The amount of pyrolyzed EC on each stage was determined using information about the relative amount of pyrolyzed EC measured on co-located quartz filters as described by Herner et al. *[65]*. OC measurements were converted to organic matter (OM) using a multiplier of 1.4 *[43]*. This value was chosen as it yielded estimates of particle material density (1.42 g/cc – 1.82 g/cc) in agreement with previous laboratory estimates (1.50 g/cc – 1.80 g/cc) of soot particles comprised of differing combinations of black carbon (BC), polycyclic aromatic hydrocarbons (PAHs), and aliphatic hydrocarbons *[66]*.

Each stage of the MOUDI loaded with Teflon substrates and RAAS Teflon filters was analyzed for anions (chloride, nitrate, phosphate, sulfate) and cations (sodium, ammonium, potassium, magnesium, calcium) using ion chromatography (DX-600 workstation, Dionex Corporation, Sunnyvale, CA). Ionic speciation data are presented only when certain quality assurance metrics were met. These included good agreement between co-located RAAS measurements, the sum of MOUDI stage data falling with a factor of two (50% - 200%) of the averaged RAAS measurements, continuous size distributions, and data present above the ion chromatography analytical Method Detection Limit (MDL).

Total PM and species mass emissions (μg) were determined using the equation:

total mass = [mass on substrate * (W/X) * (Y/Z)] – [background mass * (DR_{BG}/DR_S)] [1]

where W = primary (diluted) exhaust flow rate, X = SDT sample venturi flow rate, Y = secondary (diluted) exhaust flow rate, and Z = sampling instrument flow rate (see Table 3-4). After converting mass (μg) to sampled concentration (μg/m^3 of air), background subtraction was employed based on the dilution ratio used during the background test (DR_{BG}) and the dilution ratio actually used during sample collection (DR_S). This approach assumes that the majority of the background signal was due to PM in the primary dilution air.

Size-resolved PM mass distributions were constructed based on the sum of EC and OM because the carbon analysis method was more accurate than gravimetric methods (± 10 μg / filter gravimetric and ± ~2.0 μg/filter carbon, also see intercept data in Table 3-5) and because ionic species contributed a negligible amount of mass to the to the PM composition (< 2%) and was based on a single measurement per test. 54% of the reconstructed MOUDI stage masses fell within the respective gravimetric data error bounds (±1 standard deviation); 79% fell within ±2 standard deviations. Three MOUDIs loaded with foil substrates were used for each carbonaceous size distribution measurement. The average level of agreement between co-located MOUDI stages across all LDGV sample sets was ±35% relative to their respective averages. Non-ideal behavior primarily results from particles bouncing off impactor surfaces rather than adhering to them *[67]*. In the current study, MOUDI impactor stages were not coated with an anti-bounce agent because this coating would interfere with future trace organics analyses. Combustion particles emitted from vehicles are partially derived from lubricating oil reducing (but not eliminating) their tendency to bounce. Previous experiments have shown that particles bouncing off upper stages of the MOUDI tend to also bounce off subsequent stages and are finally collected by the instrument's afterfilter *[44]*. The most accurate measure of the true particle size distribution from co-located MOUDI samplers therefore is obtained from the maximum recorded value on each set of collected stages (not the average value).

Table 3-5 shows the results from a linear regression analysis between co-located $PM_{1.8}$ RAAS and MOUDI samples (summed MOUDI stage measurements effectively yield $PM_{1.8}$) with and without the outlying SMOKER data point. In all cases, the sum of maximum MOUDI mass, OM, and EC measurements shows better agreement with corresponding RAAS measurements than the average MOUDI mass, OM, and EC. Maximum summed MOUDI mass, EC, and OM and corresponding RAAS measurements have linear correlation slopes equal to 0.93, 0.81, and 0.64 without the SMOKER data (0.97, 0.90, and 0.70 with the SMOKER data). Corresponding R^2 values ranged from 0.90 – 1.00. The strong agreement between maximum MOUDI measurements and RAAS filter samples is a necessary check to build confidence in the size-resolved samples. Co-located MOUDI stage maxima were thus used for reconstructed PM mass distributions throughout the current study. Differences in regression statistics with and

without the SMOKER data indicate the impact that such outliers could have in a skewed distribution of vehicle emissions data.

The reduced OC concentrations on MOUDI samples relative to RAAS samples suggest that some semi-volatile material may have been lost during sample collection. This hypothesis was investigated in a series of laboratory experiments. A combination of semi-volatile compounds known to be present in vehicle exhaust were spiked on both clean foil substrates and quartz filters that were then installed in a MOUDI and RAAS filter-based sampler, respectively. These instruments were operated at their nominal flow rates (30 L min^{-1} MOUDI; 10 L min^{-1} RAAS channel) with upstream HEPA filters so that all incoming air was free of particles. A series of multiple clean quartz filters were installed downstream of each instrument to detect any semi-volatile material that volatilized during a simulated sample times ranging from 1-3 hrs. OM mass measurements were made after sample collection using the TOT carbon analysis method described above for all foil substrates and quartz filters. Semi-volatile compounds volatilized from both MOUDI foil substrates and RAAS quartz filters under the conditions studied. A fraction of this semi-volatile material was collected on the downstream quartz backup filters. The loss of semi-volatile compounds was smaller for quartz filters than from foil substrates, likely because quartz filters have larger surface area and the flow rate through the RAAS quartz filters was smaller than the flow rate through the MOUDI. This volatilization artifact explains the differences between the MOUDI and RAAS OM concentrations reported in the current study, while non-volatile species such as EC show better agreement.

Table 3-4: Linear regression analysis for co-located PM1.8 samples collected from LDGVs.

		excluding LGDV-10			including LGDV-10		
Sample #1	**Sample #2**	**slope**	**intercept (ug/km)**	**R^2**	**slope**	**intercept (ug/km)**	**R^2**
Sum of Teflon MOUDI Gravimetric	RAAS Gravimetric	0.67	-386.3	0.98	0.87	-3245.7	1.00
Sum of Average Foil MOUDI Gravimetric	RAAS Gravimetric	0.58	-1656.0	0.87	0.78	-4359.6	1.00
Sum of MOUDI Maxima Gravimetric	RAAS Gravimetric	0.93	-749.8	0.99	0.97	-1378.1	1.00
Sum Average Foil MOUDI EC	RAAS EC	0.60	33.0	0.88	0.81	-452.8	0.94
Sum of Maximum Foil MOUDI EC	RAAS EC	0.81	384.2	0.90	0.90	173.3	0.96
Sum of Average Foil MOUDI OM	RAAS OM	0.48	-122.4	0.98	0.59	-934.7	1.00
Sum of Maximum Foil MOUDI OM	RAAS OM	0.64	213.0	0.94	0.70	-229.9	1.00
Sum of MOUDI Teflon Ammonium	Average RAAS Ammonium	0.99	0.4	1.00	1.22	-4.0	1.00
Sum of MOUDI Teflon Calcium	Average RAAS Calcium	1.35	-0.3	0.74	1.36	-0.3	1.00
Sum of MOUDI Teflon Sulfate	Average RAAS Sulfate	1.16	0.0	1.00	NR[a]	NR[a]	NR[a]
Sum of Reconstructed MOUDI Mass	Reconstructed RAAS Mass	0.59	3377.1	0.72	0.70	2207.9	1.00
MOUDI Reconstructed Mass	MOUDI Gravimetric Total	1.31	-447.6	0.94	1.31	-354.5	1.00
RAAS Reconstructed Mass	RAAS Gravimetric	1.01	444.4	0.99	0.95	1413.3	1.00

[a] NOT REPORTED

SMPS data were obtained for each individual vehicle. Upstream and downstream SMPS scans were initialized simultaneously at the time when the vehicle was first started. Resultant data were averaged for all vehicles and across five-minute periods (four 75-sec scans), with sample sizes ranging from n = 2 for NCATs to n = 40 for LEVs, to account for data variability (i.e. transients) and to produce a test average indicative of temporal emissions. These size-resolved test averages were compared to MOUDI size distributions after mobility to aerodynamic diameter conversion, resulting in good agreement between instruments for the ultrafine PM fraction.

The CARB Hagen-Smit Laboratory analyzed the gaseous phase concentrations of CO, CO_2, CH_4, and NO_x of the dilute vehicle exhaust following sample collection and storage in 9.8 cubic feet capacity baked Tedlar bags. A HORIBA model FMA – 220 Flame Ionization Magneto-Pneumatic Analyzer quantified the total hydrocarbons, HORIBA models AIA – 210 and AIA – 220 Infrared Analyzers quantified carbon monoxide and carbon dioxide, a HORIBA model GFA – 220 Methane Analyzer quantified the methane, and a HORIBA model CLA – 220 Chemiluminescent Analyzer quantified the NO_x in the exhaust sample *[68]*.

3.3 Results

3.3.1 Emissions Comparisons

Emissions comparisons were generated for ultrafine PM (MOUDI stage 10, with size cuts ranging within 56 nm to 100 nm) and fine PM (Andersen RAAS $PM_{1.8}$) by dividing total reconstructed mass per sample by the total number of miles driven per sample. Figure 3-1 shows a comparison of ultrafine (panel a) and fine PM (panel b) emissions in μg/km units across three categories. The first category compares emissions across five LDGV classes – LEVs, TWC PCs, OCATs, NCATs, and SMOKERs – tested with full FTP cycles. The SMOKER vehicles were the highest ultrafine and fine PM emitters, followed by the OCATs, NCATs, TWC PCs, and LEVs. As shown in Figure 3-2, based on ultrafine PM emissions normalized to LEVs, one SMOKER vehicle is equivalent to 187 LEVs, one OCAT to 49 LEVs, one NCAT to 41 LEVs, and one TWC PC to 2.4 LEVs. The same calculation for fine PM emissions resulted in ratios of 576, 43, 21, and 2.5 for SMOKERS, OCATs, NCATs, and SMOKERS relative to LEVs, respectively. The lower PM emission rates of newer vehicles are expected due to improvements in vehicle emissions control technologies and the degradations of older vehicle maintenance with time.

The second category in Figure 3-1 illustrates the difference between full FTP and UC driving cycles for TWC PCs – the results show that the UC cycle produced higher emissions than the FTP cycle. The third category in Figure 3-1 compares partial FTP, UC, and CC cycles for TWC LDTs/SUVs – results show that the UC cycle had the highest ultrafine and fine emissions, followed by the CC and the FTP cycles. As shown in Figure 3-2b, the ratio of the UC to FTP emissions for TWC PCs is 4.1 for ultrafine PM and 1.5 for fine PM. The ratio of TWC LDT/SUVs UC to FTP emissions is 21.1 for ultrafine PM and 8.3 for fine PM, and for CC to FTP emissions is 3.8 for ultrafine PM and 2.5 for fine PM. These data show that the FTP cycle resulted in the lowest overall

ultrafine and fine PM emissions of all the cycles tested, a result consistent with previous studies *[69]*. Agencies considering of the use of the FTP cycle during routine monitoring and inspection programs should thus recognize the possibility of underestimating PM emissions inventories for transportation sources. Additional quantification of this possible underestimation, based on regional driving patterns and vehicle fleet and fuel characteristics, is recommended for future research.

Panel (c) of Figure 3-1 illustrates the EC/OM ratios for ultrafine and fine PM across the same vehicle class / driving cycle comparisons in panels (a) and (b). The average EC/OM ratio for ultrafine PM (based on MOUDI stage 10 data) was 0.60 across all LDGV tests. On an ultrafine PM emission basis, the lowest emitting vehicle class (LEV) was dominated by EC while the highest emitting vehicle class (SMOKER) was dominated by OM; the ultrafine LEV EC/OM ratio was also significantly higher than that for TWC PCs, OCATs, and NCATs. This finding confirms the correlation between newer emissions reduction technology and higher ultrafine PM EC fractions *[58, 70]*. On an ultrafine PM basis, the lowest emitting driving cycle (FTP) had the highest percentage of EC, followed by the CC and UC cycles. These findings indicate the EC/OM ratio of LDGV ultrafine PM emissions is not only a function of emissions control technology (vehicle class) and vehicle maintenance (i.e. SMOKER class), but also driving patterns/cycles.

The average EC/OM ratio for fine PM (based on RAAS $PM_{1.8}$ data) was 0.32 across all LDGV tests. The trend observed in EC/OM ratios for fine PM was identical to the trend observed for ultrafine PM, with the lowest emitting vehicle class (LEV) emitting particles with the largest EC/OM ratio and the highest emitting vehicle class (SMOKER) dominated by OM. The fine LEV EC/OM ratio was also higher than that for TWC PCs, OCATs, and NCATs. Fine particles emitted from TWC PCs driven through the FTP cycle had a similar EC/OM ratio as did particles released from the same TWC PCs driven through the UC cycle. Fine particles released from TWC LDTs/SUVs driven through the CC had a significantly higher EC fraction than particles emitted from the same TWC LDTs/SUVs driven through the UC or the FTP cycle. These results suggest that the EC/OM ratio of fine PM emissions is a strong function of vehicle technology with smaller effects related to the vehicle driving cycle.

The decrease in EC/OM ratio with increasing vehicle age may be at least partially explained by the lean fuel mixtures of OCATs, NCATs, and SMOKERs as indicated by their high NOx emissions relative to LEVs and TWCs (Table 3-6). Vehicle operation at lean mixtures reduces EC formation potential *[71]*. This trend could also be reflective of higher emissions of OM due to fuel and oil in older vehicle that is emitted exclusive of the combustion process (i.e. leaking o-rings, gaskets, etc.).

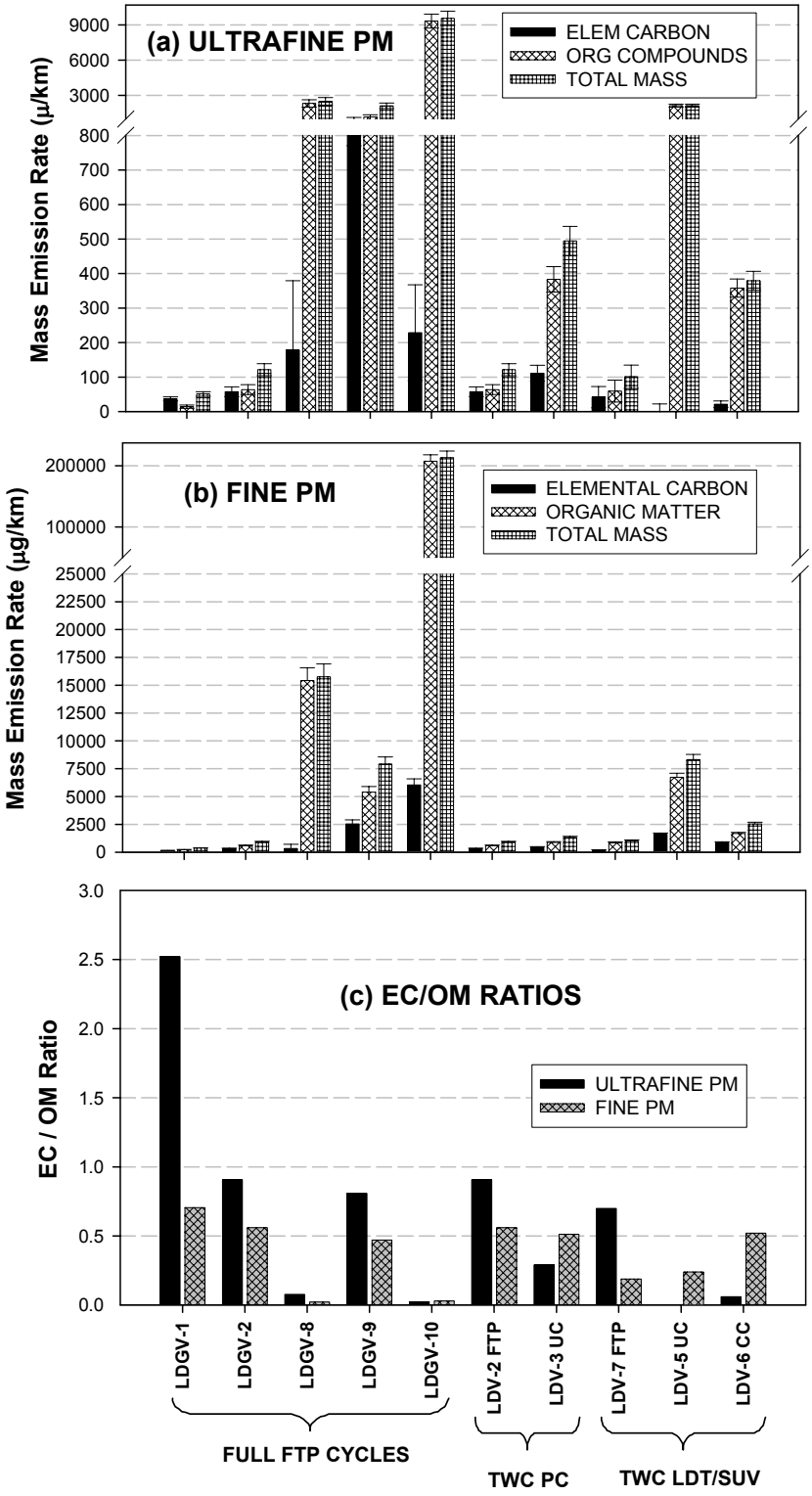

Figure 3-1: Light-Duty Gasoline Vehicle (LDGV) (a) ultrafine particulate matter (PM) emission rates, (b) fine PM emission rates, and (c) elemental carbon to organic matter (EC/OM) ratios. Error bars in panels (a) and (b) indicate analytical measurement uncertainty.

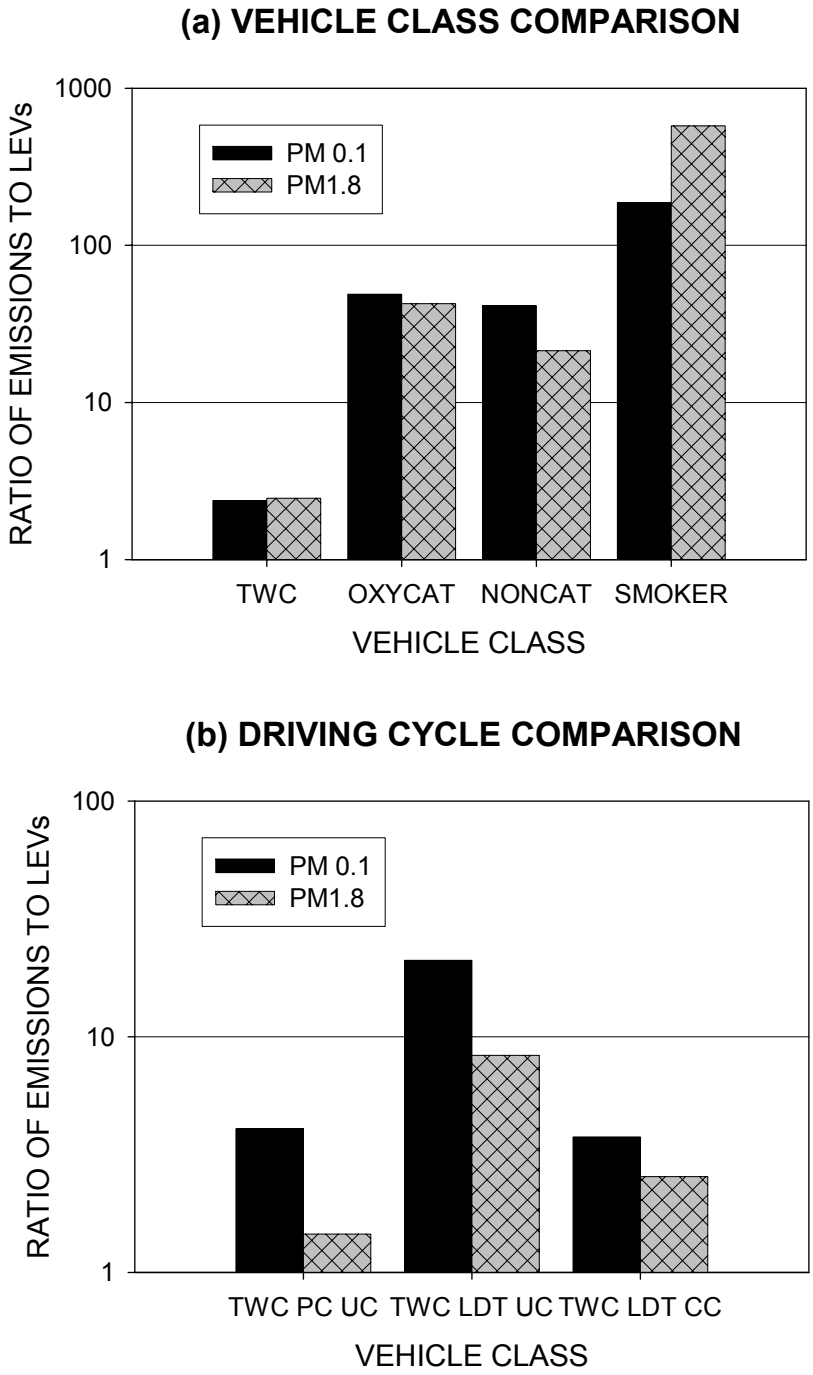

Figure 3-2: Light-Duty Gasoline Vehicle (LDGV) PM0.1 and PM1.8 emissions (a) normalized to Low Emission Vehicles (LEVs) across vehicle class using full FTP driving cycles, and (b) normalized to the FTP driving cycle using the UC driving cycle for TWC PCs and the UC and CC driving cycles for TWC LDT/SUVs.

Table 3-6 presents ultrafine PM, fine PM, EC, OM, and gaseous compound emission rates for the LDGV sample sets. Whereas PM_{10} emission rates have been previously reported for light-duty gasoline vehicles, fewer studies have reported fine PM emission

rates and this is the first study found to specifically report ultrafine PM emission rates. Several chassis dynamometer studies report PM emission rates comparable to those reported in Table 3-6. Chase et al. *[72]* reported fine PM emission rates for newer gasoline vehicles (1994-1998) using California Phase 2 reformulated gasoline and using the FTP cycle. Fine PM emission rates for cars with low mileage ranged from 0.11 mg/km - 0.53 mg/km; for cars with higher mileage emission rates ranged from 0.20 mg/km – 1.43 mg/km. Durbin et al. *[73]* reported PM_{10} emission rates for 129 gasoline vehicles stratified by model year ranging from 1.6 mg/km for the newest vehicles (1991-1997) to 30.6 mg/km for older vehicles (1981-1985). Cadle et al. *[70]* measured summertime PM FTP emission rates for gasoline vehicles ranging from 2.0 mg/km for newer vehicles (1991-1996) to 64 mg/km for older vehicles (1971-1980) with an emission rate for smoking vehicles of 219 mg/km. Durbin et al. *[74]* also measured the PM emission rates of 23 smoking vehicles recruited in the South Coast Air Quality Management District to range from 40 mg/km to 1452 mg/km with an average of 249 mg/km. Schauer et al. *[75]* measured fine PM emission rates from nine catalyst-equipped gasoline vehicles ranging from 0.8 mg/km – 36.4 mg/km, and from two noncatalyst-equipped gasoline vehicles from 200 mg/km – 985 mg/km. In comparison, the average fine PM emission rate in this study for LEVs (1996-2002) was 0.37 mg/km, for TWC vehicles (1991-1997) was 0.9 mg/km, for OCAT vehicles (1977-1980) was 15.8 mg/km, for NCAT (1953-1965) vehicles was 7.9 mg/km, and for SMOKER vehicles was 213 mg/km. The lack of agreement between NCAT/older vehicle data is likely due to the few number of vehicles (n=2) tested in this study, and possibly due to vehicle maintenance / condition within these vehicle classes. Linear regressions of PM versus gaseous species emissions in Table 3-6 across vehicle technology class and across driving cycle within the same vehicle class indicate no significant correlations within these contexts.

Table 3-5: LDGV PM and select gas-phase emission rates.

	Present Study				CARB (2003)			
vehicle class - driving cycle	**PM0.1** (µg/km)	**PM1.8** (µg/km)	**CH4** (g/km)	**CO** (g/km)	**CO2** (g/km)	**NO_X** (g/km)	**NMOG** (g/km)	**NMHC** (g/km)
LEV - FTP	51.2	370.5	0.010	0.982	246.438	0.103	0.039	0.048
TWC - FTP	121.4	910.0	0.021	2.345	222.486	0.290	0.125	0.067
OC - FTP	2501.7	15766.8	0.081	7.137	266.319	1.625	0.912	1.107
NC - FTP	2115.0	7925.8	0.451	67.411	234.257	1.036	6.194	6.171
SMOKER - FTP	9564.5	213354.5	0.307	37.855	261.187	0.855	20.248	19.957
TWC PC - UC	494.4	1322.7	0.025	3.800	243.332	0.378	NR[a]	0.172
TWC LDT/SUV - FTP	101.0	999.7	0.031	4.606	244.488	0.303	NR[a]	0.187
TWC LDT/SUV - UC	2131.1	8326.6	0.042	8.055	283.110	0.671	NR[a]	0.309
TWC LDT/SUV - CC	379.1	2547.0	0.021	2.604	206.229	0.628	NR[a]	0.089

[a] NOT REPORTED

3.3.2 Size and Composition Distributions

Figure 3-3 shows the size and composition distribution of PM released from nine LDGV categories. The peak in the PM mass distributions occurred between 100 - 180 nm for all vehicles except for the SMOKER class. The peak in the SMOKER PM mass distribution occurred between 180 – 320 nm. The size range of the maxima in the EC distributions for each LDGV class was consistent with the size range of the maxima of the reconstructed mass distributions as shown in Figure 3-3. For all FTP cycles, the maxima of the OM distributions were also aligned with the respective maxima of the reconstructed mass distributions. However, for two of the three alternative driving cycles (LDGV-3 and LDGV-6), the OM maxima fell between 56 – 100 nm, versus 100 – 180 nm for their reconstructed mass distributions. For the third alternate driving cycle sample (LDGV-5) the OM mass distribution was shifted toward the 56 - 100 nm size range, although the OM mass peak remained between 100 nm - 180 nm. These findings show that alternate driving cycles produce higher fractions of ultrafine PM OM than does the FTP cycle.

Across full FTP cycles (panels (a) through (e)), newer vehicle classes had higher percentages of EC across all particle sizes than older vehicles. With the exception of NCATs, the maxima in the percentage of EC in the reconstructed mass distributions shifted to larger sizes with increasing vehicle age. These results are indicative of increased OM emissions in older vehicles coating smaller particles and shifting OM size distributions to larger diameters.

Across driving cycle comparisons (panels (b) and (f); (g) (h) and (i)), EC/OM ratios peak between 100 – 180 nm aerodynamic diameter for FTP cycles but are shifted to larger diameters for the UC and CC cycles. EC/OM ratios peak between 180 – 320 nm aerodynamic diameters for the UC cycle and 320 – 560 nm for the CC cycle, the latter of which also has the highest peak value. The aggressive nature of the CC cycle, specifically a sustained high speed, may increase engine/combustion temperatures, preserving an EC distribution while burning off semi-volatile OM species.

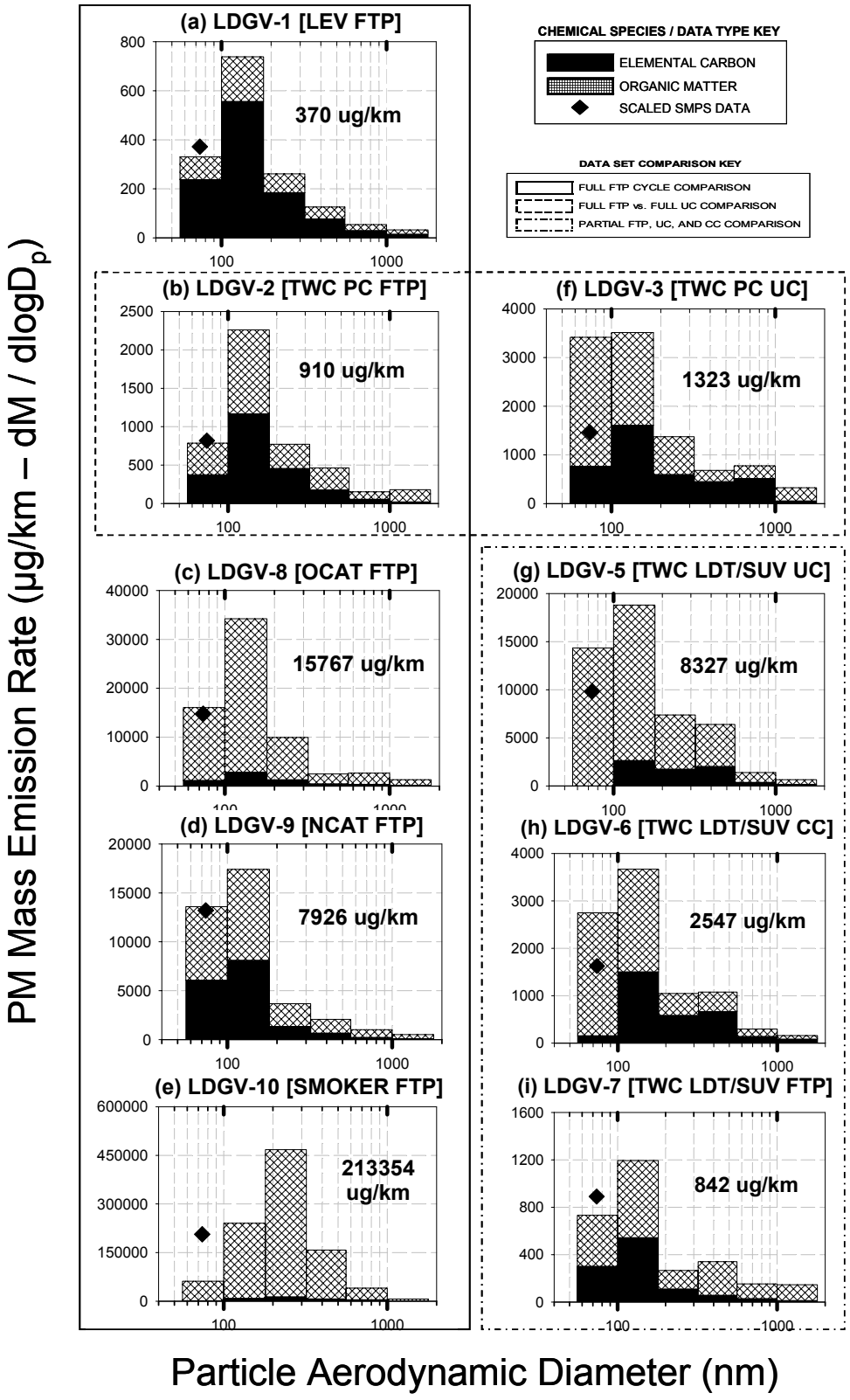

Figure 3-3: Normalized size and composition distributions of particulate matter (PM) emitted from Light-Duty Gasoline Vehicles (LDGVs).

3.3.3 Particle Morphology and SMPS Scaling Factors

PM material densities were estimated using the size-resolved composition information shown in Figure 3-3 and assuming a density of 2.0 g/cc for EC and 1.4 g/cc for organic matter *[50]*. Resulting average PM material densities ranged from 1.42 g/cc to 1.82 g/cc. These values are comparable to recent estimates of laboratory-generated soot particles by Slowik et al. *[66]*. In that study, the material density of soot PM with a composition of 90% black carbon (BC), 5% PAHs, and 5% aliphatic hydrocarbons was 1.80 g/cc; in contrast the LEV material density (highest % of EC~BC in this study) was 1.82 g/cc. Slowik et al. *[66]* reported a material density of soot PM with a composition of 45% BC, 50%, PAHs, and 5% aliphatic hydrocarbons of 1.50 g/cc; in contrast the SMOKER material density (lowest % of EC~BC in this study) was 1.42 g/cc.

Figure 3-3 shows the mass of ultrafine particles measured by the SMPS superimposed on the reconstructed MOUDI mass distributions in the ultrafine PM range. Because the SMPS and the MOUDI classify particle size based on differing properties, SMPS measurements were scaled to accurately represent the respective mass distributions as described in Chapter 2. Briefly, the effective density relationship for LDGVs measured by Maricq et al. *[76]* was used to convert SMPS electrical mobility diameter to aerodynamic equivalent diameter following the method described by Park et al. *[31, 76]*. This effective density relationship was also used to convert the SMPS particle volume distribution to a particle mass distribution since the raw SMPS data assumed a material density of 1 g/cc. Use of the particle effective density relationship derived from previous measurements *[31, 76]* results in MOUDI stage 10 mass in agreement with scaled SMPS data from 56-100 nm on a ug/km basis with a slope of 1.10 and R^2 = 0.929 without SMOKER data (slope of 0.31 and R^2 = 0.881 including SMOKER data). Thus ultrafine SMPS data may be used as a strong indicator of ultrafine PM emissions for qualitative trend analyses. SMPS data are not reported above 100 nm as the agreement with MOUDI measurements is not as strong in this size range.

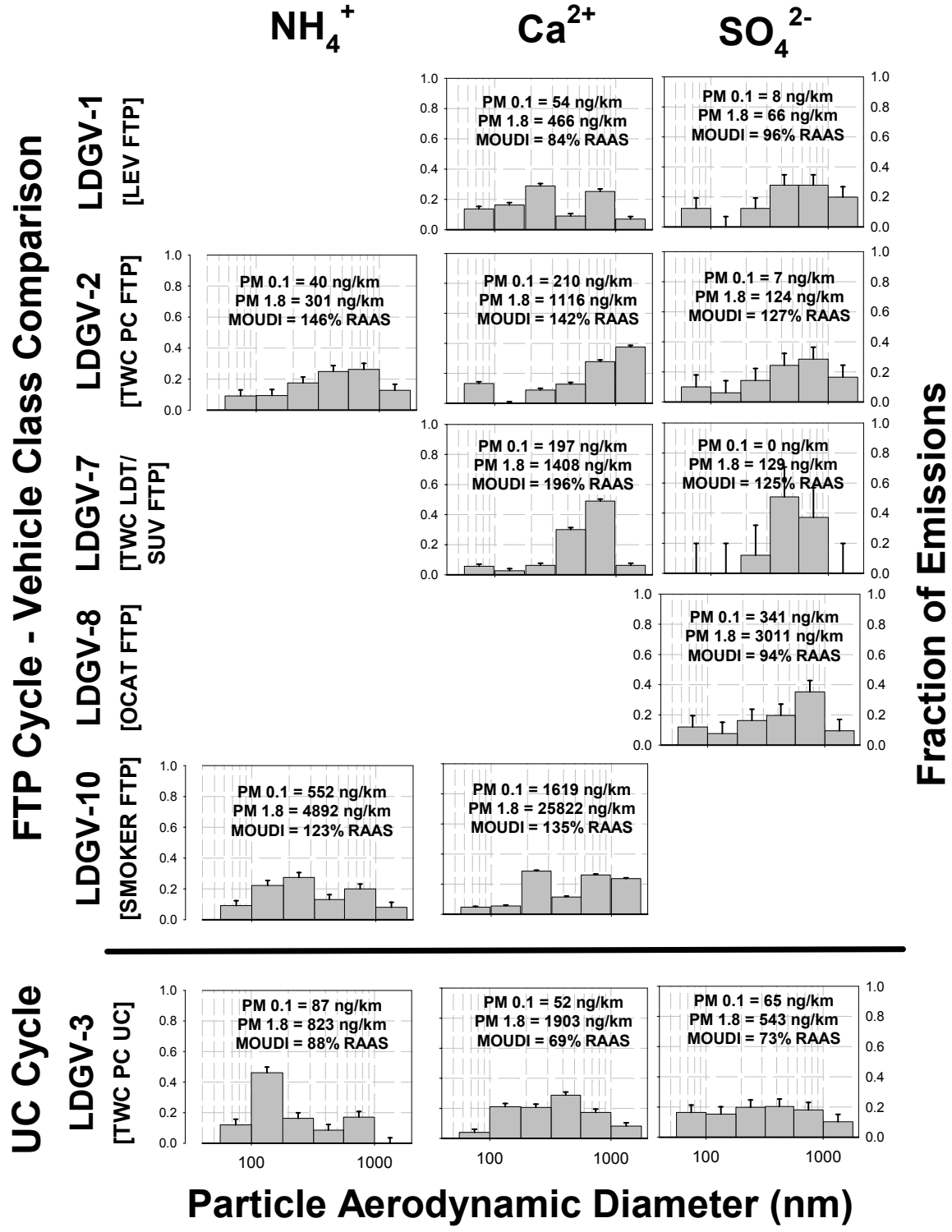

Figure 3-4 Normalized size distributions of water –soluble ions contained in particulate matter (PM) emitted from Light-Duty Gasoline Vehicles (LDGVs).

3.3.4 Ionic Species Distributions

Figure 3-4 shows the size and composition distribution of ammonium, calcium, and sulfate released from six LDGV categories. Sulfate may be produced by trace amounts of sulfur in the gasoline used to power the motor vehicles. Calcium is commonly added to lubricating oil to reduce the accumulation of acidity. Ammonium ion may have been introduced into the exhaust as gas-phase ammonia during primary dilution and then partitioned to the particle phase. Other water-soluble ions including chloride, nitrate, phosphate, sodium, potassium and magnesium were not detected at levels significantly above method detection limits. Ultrafine PM ammonium emission rates ranged from 40 ng/km to 552 ng/km and $PM_{1.8}$ ammonium emission rates ranged from 301 ng/km to 4892 ng/km. Ultrafine PM calcium emission rates ranged from 54 ng/km to 1619 ng/km and $PM_{1.8}$ calcium emission rates ranged from 466 ng/km to 25822 ng/km. Ultrafine PM sulfate emission rates ranged from 0 ng/km to 341 ng/km and $PM_{1.8}$ sulfate emission rates ranged from 66 ng/km to 4483 ng/km. The sulfate size distributions generally peaked at larger particle sizes, with no apparent pattern observed for the ammonium and calcium distributions. Error bars presented are the Method Detection Limits (MDLs) based on analytical uncertainty of the ion chromatography method utilized, defined as three times the standard deviation of seven measurements of the lowest detectable standard for each ionic species over a three-day period.

3.3.5 Cumulative Emissions Versus Time

Figure 3-5 panels (a) through (f) show LDGV ultrafine emissions as a function of time for seven LDGV classes tested with FTP cycles in units of μg/km, based on the scaled ultrafine PM SMPS data shown in Figure 3-3. A driving cycle period including a vehicle cold start is indicated by a plus sign (‘+’), and including a vehicle warm start by a minus sign (‘-‘). Mass per kilometer measurements are based on three-minute rolling averages of the instantaneous speed data.

For LEVs, TWCs, and OCATs (panels (a) through (d)), emissions were dominated by the period immediately after the vehicle was cold-started (‘+’). TWC LDT/SUVs emitted roughly twice the amount of ultrafine PM per km than TWC PCs across the entire driving trace. The NCAT and SMOKER temporal emissions are more correlated with the cold start (‘+’), as well as vehicle accelerations throughout the cycle and the FTP Phase III warm start (‘-‘). This result indicates that the NCAT and SMOKER vehicles were likely not as well maintained as the newer vehicle classes.

Figure 3-5 panels (g) through (k) show LDGV ultrafine emissions as a function of time for three different driving cycles using TWC PCs and TWC LDTs/SUVs. With respect to TWC PCs (panels (g) and (h)), whereas the FTP cycle emissions are dominated by the cold start, the UC cycle emissions are more evenly distributed versus time. This result affirms the impact of hard accelerations, present later in the UC cycle, on vehicle emissions. With respect to TWC LDT/SUVs, three driving cycles were compared (panels (i) through (k)). FTP emissions were evenly distributed across the partial cycle in the absence of a cold start, at magnitudes less than the TWC PC cold start but above

remaining TWC PC levels. This is an additional example of LDT/SUV emissions exceeding PC emissions within the same vehicle class. TWC/LDT UC emissions were much higher than corresponding FTP and CC emissions even in the absence of a cold start, re-affirming the impact of hard accelerations and implicating vehicle maintenance / response under these conditions. TWC LDT/SUV CC data show higher emission rates in the acceleration portion of the driving cycle than during constant high-speed cruise. Collectively, these results indicate that, for the vehicles tested, hard accelerations contribute to emissions to a greater degree than the presence of a warm or cold start, especially for older vehicles and to a lesser extent LDT/SUVs. This may help explain why FTP emission rates are the lowest reported among the three driving cycles.

The observation that LDT/SUVs emit more PM per km than PCs is not explained by vehicle age (LEV LDT/SUVs are newer than the LEV PCs, TWC LDT/SUVs are of similar age to TWC PCs). However, LDT/SUV engines are on average slightly larger than PCs and their curb weights are heavier, a combination resulting in lower fuel efficiency. This fact coupled with the different response of the LDT/SUVs versus PCs to the same driving cycle (i.e. maintenance and/or combustion stoichiometry during accelerations) may be responsible for these differences. Maricq also concluded that transient particle measurements from spark ignition vehicles coincide with periods of relatively heavy acceleration *[77]*, data which is not correlated with engine displacement or mileage. While this latter conclusion can not be drawn in the present study due to vehicle compositing within tests, it suggests that SUV/LDTs may have fuel injection, spark timing, and air-to-fuel ratios during accelerations that result in greater PM formation during acceleration events *[77, 78]*.

Error bars in Figures 3-5 represent one standard deviation of the magnitudes of the four individual 75 second SMPS scans that comprise the respective five minute average; each of these four data points represent the averaged cumulative mass distribution for ultrafine PM for the vehicle class tested. As such the error bars shown in Figure 3-5 are indicators of the temporal variability of mass emissions across a five minute scan, not indicators of between-vehicle variability. It follows that large error bars, such as those present in the FTP initial cold start region, are indicative of a highly variable mass emission rates during those time periods. Analyses of raw SMPS data confirms that the majority of emissions in cold start tests are emitted in the first two minutes and drop sharply thereafter, confirming this assertion. Throughout Figure 3-5 large error bars are consistently associated with cold starts, warm starts, and hard accelerations.

Temporal emissions in Figure 3-5 were also generated based on mass emission rates of ug/min and ug/liter. LDGV fuel consumption was calculated based on driving cycle phase-averaged gaseous CO_2 emissions data, assuming 2.28 kg of gaseous CO_2 emissions per liter of gasoline consumed *[57]*. The results from these alternate analyses show the same trends and variability between different vehicle classes as did emissions expressed in μg/km units and thus are not reported.

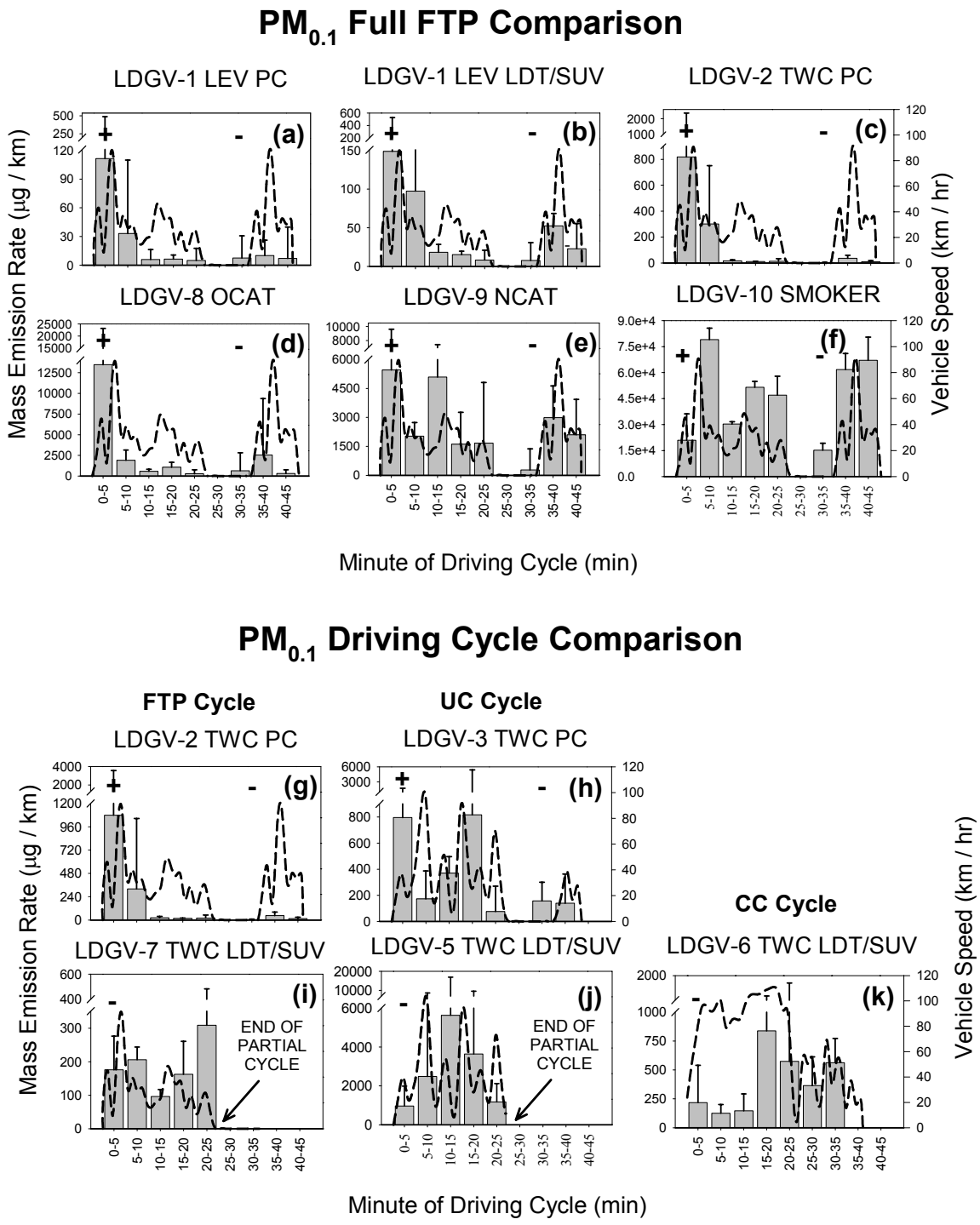

Figure 3-5: Ultrafine PM emissions as a function of time for (a) different Light-Duty Gasoline Vehicle (LDGV) classes and (b) different LDGV driving cycles. ['+' = cold start; '-' = warm start].

3.4 Conclusions

This study provides ultrafine and fine PM emission rates and compositional information for traditional classes of vehicle technologies (TWCs, OCATs, NCATs, and SMOKERs) as well as for Low Emission Vehicles (LEVs). Although LEV PM emissions are considerably lower than older vehicle classes they are the most ubiquitous class of gasoline-powered vehicles in California *[68]*. Separation of test vehicles into these technology classes provides a measure of PM emissions reduction over the last several decades and a basis for fleet emissions within California and the United States. The vehicles recruited were chosen to represent a realistic sampling of those currently in use. However, due to the variability of vehicle mileage, maintenance, fuels, and sample size, the resultant data should be used accordingly when building an ultrafine emissions inventory database for LDGVs.

Chassis dynamometer testing of five LGDV PM emissions technology classes using the FTP, UC, and CC driving cycles revealed several important PM emissions trends. Although ultrafine and fine PM emission rates (ug/km) decreased with newer vehicle technologies, the ratio of EC/OM increased in both the ultrafine and fine PM ranges for newer vehicle classes. The FTP cycle was found to yield the lowest PM emission rates of the three driving cycles investigated. The peak in the PM mass distributions occurred between 100 - 180 nm for all vehicles except for the SMOKER class which occurred between 180 – 320 nm. Ionic species comprised a negligible amount of total PM emissions.

Temporal analyses revealed that high ultrafine PM emission events are associated with vehicle cold starts, warm starts, and hard accelerations. This behavior is consistent when mass emission rates are expressed in ug, ug/km, and ug/L units. Light duty trucks and sport utility vehicles were observed to emit nearly twice the amount of ultrafine and fine PM as LEV passenger cars, partially due to fuel efficiency but also due to operating characteristics during accelerations. The ultrafine emissions from newer vehicles are dominated by cold-start conditions, whereas in older vehicles ultrafine PM emissions are more uniform throughout the driving cycle. Since older vehicles can disproportionately impact the distribution of local fleet emissions, this result could have an impact on their contribution to local and regional ambient PM loads.

4 SIZE DISTRIBUTION OF TRACE ORGANIC SPECIES EMITTED FROM HEAVY-DUTY DIESEL VEHICLES

4.1 Introduction

Motor vehicle exhaust from diesel-powered engines is a major source of fine airborne particulate matter in urban environments [79-81]. Previous size distribution measurements of diesel vehicle exhaust aerosol indicate that these particles are at least partially in the ultrafine size range (Dp < 100 nm) that can penetrate deep into the lung [61, 82]. Recent evidence suggests that ultrafine particle concentrations can cause adverse health effects [2, 10, 83-85]. It is essential to determine the composition of diesel particles as a function of their size to better understand their potential health effects and to calculate their contribution to the overall ultrafine particle concentration in the atmosphere. Polycyclic aromatic hydrocarbons (PAHs), hopanes, and steranes are of particular interest when studying diesel ultrafine particles. PAHs have been shown to be both carcinogenic and mutagenic in epidemiological studies [86-88]. Hopanes and steranes can act as chemical "fingerprints" for statistical source apportionment calculations [79, 89].

Previous studies have quantified PAH, hopane, and sterane concentrations in the fine size range (Dp < 2.5 μm) that are emitted from medium-duty and heavy duty diesel vehicles [13, 82, 90-92] tested under a variety of load conditions. Other studies have measured the size distribution of PAHs emitted from diesel engines tested under simplified engine dynamometer tests, chassis dynamometer tests, or tunnel studies [33, 90]. No study has been published to date that describes the size-resolved emissions of PAHs, hopanes, and steranes from on-road heavy duty diesel vehicles (HDDVs) tested under realistic conditions.

The purpose of this study is to describe the size distribution of PAH, hopane, and sterane concentrations contained in airborne particles released from on-road HDDVs tested using a dilution sampling system. All vehicles were operated under realistic driving cycles and dilution conditions were adjusted to achieve a balance between sample collection times and the need to simulate the high dilution rates that are experienced in the atmosphere. Potential tracers for ultrafine source apportionment studies are identified and source apportionment profiles are presented for 6 vehicle tests.

4.2 Methods

4.2.1 Sample Collection

On-road heavy duty diesel vehicles (HDDVs) release the majority of the diesel particulate matter in urban areas within the United States. HDDVs typically have 300-600 HP engines and the loaded vehicle weight ranges from 55,000-65,000 lbs. Measuring HDDV emissions under realistic conditions poses unique challenges. Engine dynamometers can not simulate the load experienced by an engine operating in an actual

vehicle. Chassis dynamometers are generally not designed to operate at such large inertial loads. The dilution tunnels used with engine and chassis dynamometers may not completely capture the dynamics of the dilution experienced by diesel particulate matter in the real world. Tunnel studies have similar dilution artifacts and vehicles in the tunnel tend to operate at a single load condition that does not capture the full driving cycle. Chase experiments must separately quantify the diesel engine exhaust from the background aerosol. This process requires real-time instruments with relatively fast response time. Several such instruments are currently under development, but each of them requires traditional measurements to make the real-time measurements quantitative. A perfect method for the characterization of diesel engine emissions under real-world conditions does not currently exist. A weight of science approach is required using each of the techniques described above in the most realistic manner possible.

In the current study, samples of particulate matter were collected from 4 heavy duty diesel vehicles using a chassis dynamometer combined with a dilution sampling system combined with Micro Orifice Uniform Deposit Impactors (MOUDIs) (MSP Corporation, Shoreview, MN) and Reference Ambient Air Samplers (RAAS) (Andersen Instruments, Smyra GA). Table 4-1 summarizes the 6 tests that were conducted in the present study. The basic driving cycle used for all tests was the California Air Resources Board (CARB) Heavy Heavy Duty Diesel Test (HHDDT) as summarized in Table 2-3. The chassis dynamometer used in these tests was one of the few such systems in the United States that is capable of testing diesel vehicles under such realistic conditions. Test # HDDV-1 focused on the first two modes (idle and creep) while all other tests used the full 5 modes of the HHDDT. Test # HDDV-4 used an inertial weight of 66,000 lbs while all other tests used an inertial weight of 56,000 lbs. The truck used in test # HDDV-5 had an engine governor that limited the maximum speed to 60 miles hr^{-1}.

Multiple legs of a RAAS sampler loaded with quartz filters were used in parallel to collect PM1.8 samples of diesel particulate during each of the tests described in Table 2-1. The sample flow rate for each filter was 10 L min^{-1}. Each filter was baked at 550 ºC for 48 hrs prior to sample collection to reduce background contamination. Each filter was stored in a Petri dish lined with aluminum foil that had also been baked for 48 hrs prior to use. Petri dishes were sealed with Teflon tape and stored in a freezer at -18^{o}C until samples were ready for analysis. Three MOUDIs loaded with aluminum foil substrates were used in parallel to collect diesel particulate matter to obtain enough mass for size-resolved GC-MS analysis. The sample flow rate through the MOUDIs was 30 L min^{-1}. Each aluminum substrate was handled with the same protocol as quartz filters described above. Aluminum substrates were weighed after sample collection to determine mass accumulation.

4.2.2 Sample Extraction and Analysis for Organic Compounds

Aluminum substrates from three MOUDI impactors were composited by size for each test and extracted as one sample. Quartz filter PM 1.8 samples were extracted individually. Sampling substrates were spiked with an isotopically labeled sterane (ααα-20R-cholesatne-d_4) and two isotopically labeled PAHs (chrysene-d_{12} and

dibenz[ah]anthracene-d_{14}) then allowed to dry. Substrates were then placed into screw-cap centrifuge tubes for organic solvent extraction. Each tube is filled with ~15 mL of dichloromethane is then capped and sealed with Teflon tape. The tubes were then suspended in an ultrasonic cleaning bath and sonicated for 15 minutes. Following sonication, the tubes were centrifuged for 10 minutes at 3500 rpm to settle any suspended solids. Using baked Pasteur pipettes each extract was transferred into a graduated centrifuge tube. The sonication extraction procedure was then repeated and both the first and second extractions were combined. Extracts were then reduced in volume under Nitrogen evaporation to a final volume of 200 μL.

The organic chemical speciation data collected for this project was obtained on a Varian 3400 gas chromatograph (GC) coupled with a Varian 2000 ion-trap mass spectrometer (ITMS). The instrument was operated in electron ionization (EI) mode. This technique will be referred to as GC-ITMS from this point forward. Additionally, data files were processed using Varian Saturn GC-MS Workstation software version 5.51 with chromatographic peak integrations being performed manually.

The separation of the analytes is performed on an Agilent J&W DB-XLBMSD capillary GC column (30m x 0.25mm i.d. x 0.25 μm film thickness). The stationary phase for this particular column consists of a 5% phenyl/95% methyl substituted polysiloxane. Grade 5 helium is the carrier gas utilized for the analyses at a linear velocity of 37 cm s^{-1}. The gas was additionally purified using a VICI Helium purifier cartridge (Supelco, Bellfonte, PA)

Samples are injected using a cool-on-column technique rather than typical vapor injections. Samples volumes of 20 μL are introduced into the injection port containing a liner with an approximately 1/8" plug of glass wool. The injection port is initially at a temperature of 35^{o}C, roughly 5 ^{o}C below the solvent boiling temperature. The initial temperature is held for 5 minutes before the injection port temperature is ramped to 300 ^{o}C at a rate of 100 ^{o}C min^{-1}. The split vent remains off for the first five minutes of the injector temperature program. The introduction of samples in this manner allows us to use larger injection volumes than would be possible with a hot injector, which becomes limited by the solvent expansion volume in relation to the volume of the injection port liner.

The GC column oven is held at an initial temperature of 35 ^{o}C for the first five minutes of the analysis. This allows for cryo-focusing of the analytes on the head of the column as they vaporize out of the injection port. After five minutes the column oven is ramped to 330 ^{o}C at a rate of 5 ^{o}C min^{-1}. The column is held at this temperature for ten minutes, which leads to a total analysis time of 74 minutes per injection.

Operating conditions of the mass spectrometer are as follows: The ion trap oven, manifold and transfer line are held at 250, 80 and 270 ^{o}C respectively. EI analyses are performed with an emission current of 10 μA, a target ion count of 2000 and a maximum ionization time of 25000 μsec. These operating parameters are those recommended by the manufacturer with slight modification. The GC_ITMS was operated in electron

impact (EI) ionization mass spectrometry/selected ion monitoring (SIM) mode. For PAHs the parent ion masses were scanned for. Hopanes and steranes were monitored by scanning for their predominant fragment ions, m/z =191 and m/z=217/218 respectively.

Multiple point calibration curves, typically 5 or 6 points, are analyzed preceding and following each set of sample extracts. These calibration solutions range in concentration from 5 to 7000 pg uL^{-1}. Calibration solutions are analyzed in order from the least to most concentrated solution to minimize any potential carryover between analyses. Following the last calibration point a solvent blank is injected to ensure no analyte carryover had occurred.

Calibration curves for the purpose of sample quantification are generated for analytes observed in the sample extracts using the instrument response for both the pre and post calibration curve. The formula utilized to generate the response curves is as follows:

$$(\text{Peak Area})_{\text{analyte}}/[\text{Conc.}]_{\text{analyte}} = \text{Response Factor} \times (\text{Peak Area})_{\text{IS}}/[\text{Conc.}]_{\text{IS}}$$

This equation can be rearranged in multiple ways to generate appropriate calibration curves for accurate analyte quantification using the internal standardization method. Chemical species were identified by a match in the relative retention time and mass spectra of the analyte compared to that of an authentic standard. When no authentic standard was available, analytes were identified by their mass spectrum and comparison of relative retention times to those in the literature. Limits of detection and limits of quantification are given in Table 4-2.

4.2.3 Quality Assurance

Figure 4-1 shows the agreement between collocated MOUDI and RAAS measurements for 28 organic compounds of interest in the present study. Panels (a-k) illustrate agreement for hopanes and steranes that are useful tracers for lubricating oil. Panels (l-bb) illustrate agreement for polycyclic aromatic hydrocarbons (PAHs) that contribute to the toxicity of diesel particulate matter. The RAAS filter masses shown in Figure 4-1 have been multiplied by a factor of 3 to adjust for the flow rate difference between RAAS (10 L min^{-1}) and MOUDI (30 L min^{-1}) samplers. The error bars in Figure 4-1 reflect the analytical uncertainty of the GC-MS analysis.

Table 4-1: GC-MS limits of Quantification and Detection during heavy duty diesel measurements.

Compound	LOQ (pg/μL)[a]	LOD (pg/μL)[b]
Hopanes		
17α(H)-21β(H)-29-norhpane	6.2	1.8
18α(H)-29-norneohopane[c]	6.2	1.8
17α(H)-21β(H)-hopane	4.8	1.4
22S-17α(H)-21β(H)-30 homohopane[c]	4.8	1.4
22R-17α(H)-21β(H)-30 homohopane[c]	4.8	1.4
Steranes		
20R,13β(H)-17α(H)-diacholestane[c]	9.7	2.9
20S,13β(H)-17α(H)-diacholestane[c]	9.7	2.9
ααα-20S-stigmastane [c]	5.3	1.6
αββ-20R-stigmastane	5.3	1.6
αββ-20S-stigmastane [c]	5.3	1.6
ααα-20R-stigmastane [c]	5.3	1.6
PAHs		
Phenanthrene	0.94	0.28
Anthracene	3.6	1.1
A-methylphenanthrene[c]	5.3	1.6
B-methylphenanthrene[c]	5.3	1.6
C-methylphenanthrene[c]	5.3	1.6
D-methylphenanthrene[c]	5.3	1.6
Fluoranthene	0.26	0.08
Pyrene	0.22	0.06
benzo[ghi]fluoranthene	1.0	0.30
Chrysene	0.32	0.10
benzo[b]fluoranthene	0.46	0.14
benzo[k]fluoranthene	0.44	0.12
benzo[e]pyrene	1.2	0.36
benzo[a]pyrene	0.26	0.08
indeno[1,2,3-cd]pyrene	0.62	0.18
benzo[ghi]perylene	0.76	0.22
Coronene	2.2	0.66

[a] Limit of quantification determined using a signal:noise ratio of 10:1, [b] Limit of detection determined using a signal:noise ratio of 3:1, [c]no pure standard available LOQ and LOD estimated using a standard compound of the same class with the closest retention time

The solid line shown in each panel of Figure 4-1 is a linear regression analysis between the MOUDI and adjusted RAAS measurements for each organic compound. The dashed line shown in each panel of Figure 4-1 is a linear regression analysis between MOUDI and adjusted RAAS measurements for the average value of organic carbon measured using thermal optical carbon analysis [93]. The MOUDIs collect less organic carbon than the RAAS filter samplers because of greater volatilization losses associated with the higher flow rates in the MOUDI. The amount of organic carbon collected by the MOUDIs during the 6 HDV tests was approximately 65% of the organic carbon collected by RAAS filter samplers. The individual organic compounds shown in Figure 4-1 generally have MOUDI losses that are equal or greater than the volatilization of organic carbon. Table 4-2 lists the regression slope and correlation coefficients for each organic

compound and for the maximum and average values of organic carbon measured by MOUDI vs. RAAS filter sampler.

Table 4-2: Comparison of co-located MOUDI and filter measurements of heavy duty diesel particulate matter.

Compound	MW	Slope	R^2
Hopanes			
17α(H)-21β(H)-29-norhpane	398	0.5515	0.8828
18α(H)-29-norneohopane[1]	398	-0.1328	0.2757
17α(H)-21β(H)-hopane	412	0.4596	0.6728
22S-17α(H)-21β(H)-30 homohopane[1]	426	0.2788	0.3482
22R-17α(H)-21β(H)-30 homohopane[1]	426	0.3541	0.2500
Steranes			
20R,13β(H)-17α(H)-diacholestane[1]	372	0.1188	0.1218
20S,13β(H)-17α(H)-diacholestane[1]	372	0.1905	0.2807
ααα-20S-stigmastane [1]	400	0.3151	0.4800
αββ-20R-stigmastane	400	0.4809	0.9487
αββ-20S-stigmastane [1]	400	0.3830	0.7113
ααα-20R-stigmastane [1]	400	0.2034	0.4294
PAHs			
Phenanthrene	178	0.5528	0.9657
Anthracene	178	0.8578	1.0000
A-methylphenanthrene	192	0.4424	0.9396
B-methylphenanthrene	192	0.4685	0.9173
C-methylphenanthrene	192	0.4471	0.9602
D-methylphenanthrene	192	0.4512	0.9169
Fluoranthene	202	0.4325	0.9060
Pyrene	202	0.4094	0.8844
benzo[ghi]fluoranthene	226	0.7132	0.9435
Chrysene	228	0.4732	0.8796
benzo[b]fluoranthene	252	0.3729	0.8403
benzo[k]fluoranthene	252	0.4466	0.7125
benzo[e]pyrene	252	0.2600	0.4450
benzo[a]pyrene	252	0.5261	0.9033
indeno[1,2,3-cd]pyrene	276	0.5082	1.000
benzo[ghi]perylene	276	0.8596	0.8831
Coronene	300	0.2577	1.000
Organic Carbon			
organic carbon (average)		0.6609	0.9715
organic carbon (maximum)		0.7804	0.9740

[1] Analyte identification based on comparisons to relative retention times to those in the literature.

Consistency between MOUDI and filter measurements is a necessary check to build confidence in the accuracy of the size distribution measurements. Hopanes 17α(H)-21β(H)-29-norhopane (Figure 4-1 a) and 17α(H)-21β(H)-hopane (Figure 4-1 c) appear to exhibit the most consistent behavior between MOUDI and filter measurements as demonstrated by correlation slopes = 0.5515-0.4596 and correlation coefficients R^2 = 0.8828- 0.6728. Likewise, steranes αββ-20R-stigmastane (panel i) and αββ-20S-stigmastane (panel j) exhibit the most consistent behavior between MOUDI and filter measurements with correlation slopes = 0.4809 - 0.3830 and correlation coefficients R^2 = 0.9487- 0.7113. These four species appear to have the greatest promise as size-resolved tracers for diesel particulate matter. The majority of the PAH species appear to behave

consistently when collected with MOUDI and filter samplers although some species are present at concentrations that are below the analytical uncertainty.

4.3 Results and Discussion

4.3.1 Observed Size Distribution Patterns

Size distributions for lubricating oil tracers and PAHs are presented in Figures 4-2 and 3 respectively. The solid line represents the measured value normalized to total analyte mass while the dashed lines illustrate the analytical uncertainty (sample collection uncertainty is not shown)**.** Figure 4-2 Row 1 shows the normalized size distribution of lubricating oil tracer compounds emitted from a 1999 Freightliner HDDV operated using the idle and creep portions of the HHDDT. All of the hopanes emitted during the idle and creep modes had a mass distribution peak between 0.18-0.32 μm aerodynamic particle diameter. The size distributions of the two most promising tracer hopanes are consistent with the size distribution of one of the promising tracer steranes (αββ-20R-stigmastane). The size distribution of the other promising tracer sterane (αββ-20S-stigmastane) is discontinuous with zero mass detected between 0.18-0.32 μm aerodynamic particle diameter. Based on these size distributions 15-20% of the most suitable tracer mass appears to be contained in the smallest size fraction (0.056 – 0.10 μm aerodynamic particle diameter) during idle and creep operation.

Figure 4-2 Row 2 shows the normalized size distribution of hopanes and steranes emitted from a 1999 Freightliner HDDV operated using the full 5-mode HHDDT with a simulated inertial weight of 56,000 lbs. A comparison of Row 9 and Row 2 illustrates the behavior of the same vehicle operated under idle+creep modes vs. the full 5-mode HDDT cycle. The hopanes emitted during the HHDDT have a normalized size distribution that peaks between 0.10-0.18 μm aerodynamic particle diameter as do the size distributions for the two primary steranes measured. Based on the results shown in Figure 4-2 Row 2, the fraction of the tracer mass contained in particles with aerodynamic diameter between 0.056-0.10 μm is approximately 25-30%.

Figure 4-2 Row 3 shows that the normalized hopane size distribution emitted by the 1998 Kenworth HDDV operated using the full 5-mode HHDDT with an inertial weight of 56,000 lbs peaks between 0.10-0.18 μm aerodynamic particle diameter. The two most promising steranes exhibit a peak in their normalized size distributions similar to the hopanes. The fraction of the tracer mass contained in particles with aerodynamic diameter between 0.056-0.10 μm is approximately 10-30% of the total tracer mass collected.

Figure 4-2 Row 4 presents the size distributions for the hopanes and steranes for the 1998 Kenworth HDDV operated using the full 5-mode HHDDT with an inertial weight of 66,000 lbs. A comparison of Row 3 and Row 4 illustrates the behavior of the same vehicles tested using the 5-mode HHDDT using different inertial weights. Shifts to smaller sizes are observed for the hopanes and steranes under higher loads. The peak in the normalized size distribution of the lubricating oil tracers occurs in the ultrafine size

fraction, 0.056 – 0.01 μm aerodynamic particle diameter, under a simulated inertial load of 66,000 lbs. The increased load produced approximately twice as much tracer mass (20-45%) in the ultrafine size fraction (see Figure 4-2 Row 3 vs. Row 4).

Trends in size distributions for the 1992 Volvo HDDV operated using the full 5-mode HHDDT with an inertial weight of 56,000 pounds are shown in Figure 4-2 Row 5. Size distributions were obtained for both hopanes. The peak in the distribution for these analytes occurred between 0.10-0.18 μm aerodynamic particle diameter with varying amounts in the other size fractions. Discontinuous size distributions were observed for both steranes. No other analytes in any sample exhibited this normalized size distribution pattern and the reason for the variation in this sample is unknown.

Normalized size distributions for trace organic species emitted from the 1985 Freightliner HDDV operated using the full 5-mode HHDDT with an inertial weight of 56,000 lbs are shown in Figure 4-2 Row 6. Lubricating oil tracers identified in this test had size distributions that peaked between 0.10 – 0.18 μm aerodynamic particle diameter, with a second smaller mode observed for hopanes between 0.56-1.0 μm aerodynamic particle diameter. Approximately 10 - 20 % of the observed tracer mass is contained in particles between 0.056-0.10 μm is aerodynamic diameter.

Rows 1-4 of Figure 4-2 generally illustrates that increasing load causes the size distribution of the trace compounds emitted from HDDVs produced after 1998 to decrease from ~0.32 μm aerodynamic diameter to < 0.10 μm aerodynamic diameter. Rows 5 and 6 of Figure 4-2 generally illustrate that the size distribution of tracer compounds emitted from older technology vehicles becomes more bimodal. This latter trend may be related to the control technology or it may be caused by the general wear on the older vehicles. The construction of fleet-average emissions factors for tracer compounds in different size fractions will need to consider vehicle age and driving mode in order to accurately represent the emissions profiles.

Figure 4-3 illustrates the normalized size distributions of light 3 and 4 ring polycyclic aromatic hydrocarbons (PAHs) emitted from HDDVs in a format that is analogous to Figure 4-2. The first row of Figure 4-3 shows that light PAHs emitted from a 1999 Freightliner HDDV operated using the idle and creep portions of the HHDDT peaked between 0.10-0.32 μm aerodynamic particle diameter. Rows 2-6 of Figure 4-3 illustrate that PAH emissions from all 5-mode HHDDT driving cycle test peaked between 0.10-0.18 μm aerodynamic particle diameter. The only exception to this trend was that size distributions of light PAHs emitted from the 1998 Kenworth HDDV were somewhat variable (Figure 4-3 Row 3). Four ring PAHs fluoranthene and pyrene exhibited a peak in their normalized size distribution between 0.18 – 0.56 μm aerodynamic particle diameter, but also had a significant portion of their mass between 0.10-0.18 μm aerodynamic particle diameter. Benzo[ghi]fluoranthene emitted from the 1998 Kenworth HDDV peaked between 0.18 – 0.56 μm aerodynamic particle diameter.

The mix of PAHs emitted from HDDVs in the current study was sensitive to vehicle load conditions and control technology. Figure 4-4 shows the size distribution of

five and six ring nonvolatile PAHs including benzo[b]fluoranthene, benzo[k]fluoranthene benzo[e]pyrene, benzo[a]pyrene, benzo[ghi]perylene, and coronene that were detected in the idle and creep emissions. These larger PAHs were detected in much smaller amounts in the other driving cycles thus discontinuous size distributions were observed. These heavy PAH compounds exhibit the same general size distribution pattern as the hopanes and the light PAHs with the exception of coronene (Figure 4-4 Row 2) which was only observed in particles larger than 0.32 μm aerodynamic particle diameter. Coronene has been identified as a potential tracer for gasoline-powered vehicles [79, 94]. The presence of coronene in the exhaust of diesel engines operated under idle and creep conditions suggests that this compound is not a unique tracer for gasoline engine exhaust. The oldest vehicle tested (1985) had much higher emissions of PAHs than any other vehicle considered in the present study. Anthracene (not shown) was detected in the emissions from the 1985 vehicle with a slightly higher concentration in the ultrafine size fraction.

4.3.2 Source Profiles

Ratios of analyte mass (μg) to total organic carbon mass (g) for the PM 1.8 and the PM 0.1 size fractions are shown in Tables 4-3 and 4-4 respectively. Total organic and elemental carbon was measured from a subsection of each sample using a thermal-optical measurement technique as discussed in Section 2. The relative analyte/OC concentrations can be used as source profiles to calculate contributions to particulate matter mass in the PM1.8 and PM0.1 size fractions. A comparison of Tables 4-3 and 4-4 reveals several important trends. The relative abundance of the lubricating oil tracers in both the fine and ultrafine size fractions is a function of load condition. Columns 2 and 4 in Tables 4-3 and 4-4 compare the relative abundance of tracers emitted from the same vehicle tested under idle+creep and HDDT driving cycles with an inertial weight of 56,000 lbs. Columns 6 and 8 of Tables 4-3 and 4-4 compare the relative abundance of tracers emitted from the same vehicle tested under the HDDT driving cycle with an inertial weight of 56,000 lbs and 66,000 lbs. In both cases, the increased load condition results in a reduction of the tracer mass in the PM1.8 size fraction and an increase in the tracer mass in the PM0.1 size fraction. The decrease of hopanes and steranes in the fine particle fraction at higher loads matches trends observed in previous studies [95]. Part of this reduction may be related to increased combustion temperatures at higher loads causing thermal destruction of the tracers. Higher engine loads also decrease the effective density of the diesel exhaust particles [31] causing a greater fraction of the residual tracers to shift to the ultrafine size range collected by the MOUDIs.

A comparison of columns 4, 6, 9, and 11 in Tables 4-3 and 4-4 illustrates that the relative abundance of lubricating oil tracers in the PM1.8 and PM0.1 size fractions is not a strong function of vehicle age when the vehicles were tested with the HHDDT and 56,000 lbs inertial weight. Steranes in the ultrafine size range were generally not detected in the two oldest vehicles that were tested (1992 and 1985). Hopane and sterane emissions increase with the oil consumption rate (related to vehicle age and maintenance) and decrease with higher engine load (exhaust temperature) [31]. In the present study, the oldest vehicle (1985) had the highest emission rates of hopanes and steranes during the basecase 56,000lb HHDDT test. The second oldest vehicle (1992) also had the

lowest rated engine horsepower, putting it under higher relative load during the basecase test. As a result, the second oldest vehicle had the lowest emissions rates of hopanes and steranes in the current study.

The relative abundances of PAHs in the PM0.1 and PM1.8 size fractions emitted from the oldest vehicle tested (1985 HDV) were significantly higher than for any other vehicle tested. Tests with greater loads generally produced emissions with a greater relative abundance of light PAHs but with reduced concentrations of heavy PAHs. Some heavy PAHs were only observed during the idle and creep test.

4.3.3 Comparison to Previous Measurements

The current study is the first to examine the size distribution of particulate trace organic species emitted from on-road heavy duty diesel vehicles operated under realistic dynamic driving cycles. Comparisons to previous measurements made using simpler test conditions can help to illustrate common trends in the data as well as emphasize new trends identified in the current tests due to the more realistic test conditions.

Zielinska et al. [90] measured the size distribution of PAHs emitted from military diesel vehicles operated under steady-state load conditions. Most of the four to six ring nonvolatile PAHs detected in the current study were also observed in that previous work. Zielinska et al. found that the emitted PAH size distribution was a function of engine load condition. Likewise, the results of the current study suggest that the peak in the PAH size distribution shifted to larger sizes for the idle-creep load condition vs. the full 5-mode HHDDT test.

Figure 4-4 shows a comparison of the emission factors (μg/km) measured in the current study with those of Rogge et. al. (1993) [13]. The top panel of Figure 4-4 shows that the emission rates of lubricating oil tracers measured in the current study are much lower (2-12 times) than those measured by Rogge. The oldest vehicle tested in the current study (1985 HDV) generally had the highest tracer emissions rates, suggesting that newer vehicles burn less lubricating oil. The center and bottom panel of Figure 4-4 compare emissions rates of light PAHs and heavy PAHs, respectively. The PAH emission rates for all vehicles examined in this study bracket those measured by Rogge. The PAH emissions rates for the 1992 Volvo and the 1985 Freightliner are two to four times higher than the emissions rate measured by Rogge et.al. For the newer vehicles, PAH emission rates were ⅔ to ½ of those reported by Rogge et. al. These results suggest that newer, lower mileage heavy duty trucks emit less PAHs per kilometer than older vehicles.

Figures 4-5 and 4-6 show that emission factors (μg analyte / kg of fuel burned) of three lubricating oil tracers measured in the current study fall in the range of values reported by other investigators in both the fine [13, 14, 90] and ultrafine (PM0.18) [96] size fractions. Concentrations for heavy PAHs measured in this study also show strong agreement with previous measurements made using dilution systems [90] but were

significantly lower than roadside measurements [96] for most analytes other than coronene in both the fine and ultrafine size fractions.

4.4 Conclusions

Comparison between the mass of each trace organic compound collected by the MOUDI impactors and by the collocated filter samples shows a reasonable agreement for most analytes. All PAHs have size distributions that pass internal consistency QA/QC checks as shown in Table 4-2. Lubricating oil tracers 17α(H)-21β(H)-29-norhopane, 17α(H)-21β(H)-hopane, αββ-20R-stigmastane, and αββ-20S-stigmastane were identified as the four most self-consistent size-resolved PM emissions tracers. These tracers have approximately 10-20% of their mass in the ultrafine size fraction during both the idle+creep test and during the full 5-mode HHDDT cycle with 56,000 lbs inertial weight. This fraction increases to 20-45% for the higher load test with an inertial load of 66,000 lbs.

Noticeable trends in the size distributions are observed for both the lubricating oil tracers and the PAHs as a function of driving cycle. In the idle creep sample, both classes of compounds peak between 0.18-0.32 μm aerodynamic particle diameter. The PAH size distributions peak between 0.1-0.18 μm aerodynamic particle diameter for all 5-mode tests at either 56,000 lbs or 66,000 lbs. The hopane and sterane size distributions also peak between 0.080-0.143 during the 5-mode HHDDT test with 56,000 lbs inertial weight. The peak in the hopane and sterane size distributions shifts to 0.56 – 0.1 during the 66,000 lb inertial test.

Source profiles constructed using the relative abundance of trace organic compounds to total organic carbon mass are functions of vehicle age and load condition in both the fine and ultrafine size fractions. Increasing load conditions reduce the relative abundance of lubricating oil tracers in the PM1.8 size fraction but increase the relative abundance of these tracers in the PM0.1 size fraction. The relative abundances of PAHs in the PM0.1 and PM1.8 size fractions emitted from the oldest vehicle tested (1985 HDV) were significantly higher than for any other vehicle tested. The relative abundance of PAHs in the ultrafine size fraction is generally 2-3 times larger than in the PM1.8 size fraction. Tests with greater loads generally produced emissions with a greater relative abundance of light PAHs but with reduced concentrations of heavy PAHs. Some heavy PAHs were only observed during the idle and creep test.

Table 4-3: Ratio of analyte mass (µg) to organic carbon mass (g) for the RAAS filter measurements for organic compounds emitted from HDDVs in the PM1.8 size fraction. Uncertainty values represent analytical uncertainty.

Compound	1999 Frtlnr Idle/Creep		1999 Frtlnr 56K		1998 Knwrth 56K		1998 Knwrth 66K		1992 Volvo 56K		1985 Frtlnr 56K	
Hopanes	ratio	error	ratio	error	ratio	error	ratio	error	ratio	error	ratio	error
17α(H)-21β(H)-29-norhpane	348.4	34.4	171.5	17.0	285.0	32.7	163.1	19.7	144.9	18.5	177.0	16.0
17α(H)-21β(H)-hopane	186.2	18.4	122.3	12.2	278.5	31.9	196.6	24.7	234.3	29.7	197.7	18.2
Steranes												
αββ-20R-stigmastane	101.7	10.1	78.5	7.8	133.3	15.3	81.7	11.3	65.2	8.3	171.8	15.7
αββ-20S-stigmastane [1]	83.3	8.2	61.5	6.1	112.9	13.0	25.3	6.7	101.1	12.8	118.4	11.1
PAHs												
phenanthrene	9.2	2.9	96.6	12.5	125.1	18.0	31.4	9.3	73.8	12.4	422.7	47.8
anthracene	ND		ND		ND		ND		ND		24.5	6.0
A-methylphenanthrene	9.7	14.9	60.0	25.7	70.5	29.1	165.8	62.5	40.6	34.7	375.6	50.8
B-methylphenanthrene	12.1	14.9	141.0	29.7	142.8	33.5	205.4	64.5	103.2	37.1	493.8	61.9
C-methylphenanthrene	ND		51.6	25.5	68.2	29.0	114.5	60.6	66.9	35.4	275.5	42.4
D-methylphenanthrene	ND		41.8	25.2	57.5	28.6	82.8	59.8	56.3	35.1	201.9	37.2
fluoranthene	22.3	3.7	115.6	14.5	91.5	13.4	71.6	13.1	305.9	44.3	458.9	51.8
pyrene	48.1	7.2	250.8	30.8	282.1	39.5	156.9	24.3	684.8	98.6	781.5	88.0
benzo[ghi]fluoranthene	13.1	2.7	15.5	4.1	56.2	8.8	41.8	7.3	79.5	12.6	106.0	12.3
chrysene	5.0	2.9	ND		24.2	6.3	30.9	12.1	20.5	7.2	37.3	7.3
benzo[b]fluoranthene	11.9	8.0	ND		25.1	15.0	51.9	56.1	23.5	18.5	62.3	29.6
benzo[k]fluoranthene	4.3	1.7	ND		4.4	3.1	4.3	28.0	ND		6.0	14.6
benzo[e]pyrene	10.4	3.4	ND		18.4	6.5	15.4	8.6	31.6	8.7	41.8	6.5
benzo[a]pyrene	8.4	4.0	ND		18.7	7.6	2.1	9.5	ND		13.4	5.2
indeno[1,2,3-cd]pyrene	8.5	7.4	ND		ND		ND		ND		ND	
benzo[ghi]perylene	36.7	5.8	ND		20.7	8.3	12.6	23.6	ND		ND	
coronene	16.2	3.0	ND		ND		ND		ND		ND	

[1] Analyte identification based on comparisons to relative retention times to those in the literature.

[2] ND = not detected

Table 4-4: Ratio of analyte mass (µg) to organic carbon mass (g) for the MOUDI measurements for organic compounds emitted from HDDVs in the PM0.1 size fraction. Uncertainty values represent analytical uncertainty.

Compound	Frtlnr Idle/Creep		Frtlnr 56K		Knwrth 56K		Knwrth 66K		Volvo 56K		Frtlnr 56K	
Hopanes	ratio	error	ratio	error	ratio	error	ratio	error	ratio	error	ratio	error
17α(H)-21β(H)-29-norhpane	149.6	9.0	138.9	9.0	104.6	6.7	560.4	48.7	189.6	14.1	93.1	6.6
17α(H)-21β(H)-hopane	127.0	7.7	125.2	8.2	111.1	7.1	649.8	57.2	184.6	13.8	124.9	9.5
Steranes												
αββ-20R-stigmastane	42.0	2.5	66.6	4.3	41.5	2.7	195.0	18.4	ND		ND	
αββ-20S-stigmastane [1]	37.9	2.3	47.8	3.1	29.5	1.9	155.4	15.2	ND		ND	
PAHs												
phenanthrene	19.9	2.8	105.2	10.7	27.8	5.0	61.5	12.6	125.4	13.9	235.6	22.4
anthracene	ND		ND		ND		ND		ND		79.2	9.8
A-methylphenanthrene	ND		110.1	24.4	20.4	23.2	ND		90.6	31.5	288.7	42.6
B-methylphenanthrene	ND		155.2	26.4	29.5	23.2	ND		191.0	35.4	364.9	46.9
C-methylphenanthrene	ND		65.9	23.1	11.7	23.1	ND		115.0	32.2	205.7	38.8
D-methylphenanthrene	ND		60.2	23.0	9.3	23.1	ND		90.5	31.5	148.4	36.8
fluoranthene	6.2	1.9	163.5	15.7	29.4	4.6	62.5	12.8	379.2	38.4	355.4	33.2
pyrene	10.1	3.0	361.1	34.2	74.5	9.1	200.8	26.1	950.8	95.5	559.2	52.0
benzo[ghi]fluoranthene	2.8	1.7	16.2	3.6	34.4	4.7	49.4	7.8	80.5	9.3	94.9	9.3
chrysene	2.3	2.2	ND		18.3	4.8	27.3	14.8	19.4	6.1	33.0	7.4
benzo[b]fluoranthene	5.5	6.1	ND		17.7	12.4	36.9	72.0	ND		51.9	33.2
benzo[k]fluoranthene	1.7	1.3	ND		ND		ND		ND		ND	
benzo[e]pyrene	5.6	2.5	ND		6.4	5.0	26.6	11.2	ND		ND	
benzo[a]pyrene	4.3	3.0	ND		5.8	5.9	ND		ND		ND	
indeno[1,2,3-cd]pyrene	2.4	5.7	ND		ND		ND		ND		ND	
benzo[ghi]perylene	12.4	3.4	ND		ND		ND		ND		ND	
coronene	ND		ND		ND		ND		ND		ND	

[1] Analyte identification based on comparisons to relative retention times to those in the literature.

[2] ND = not detected

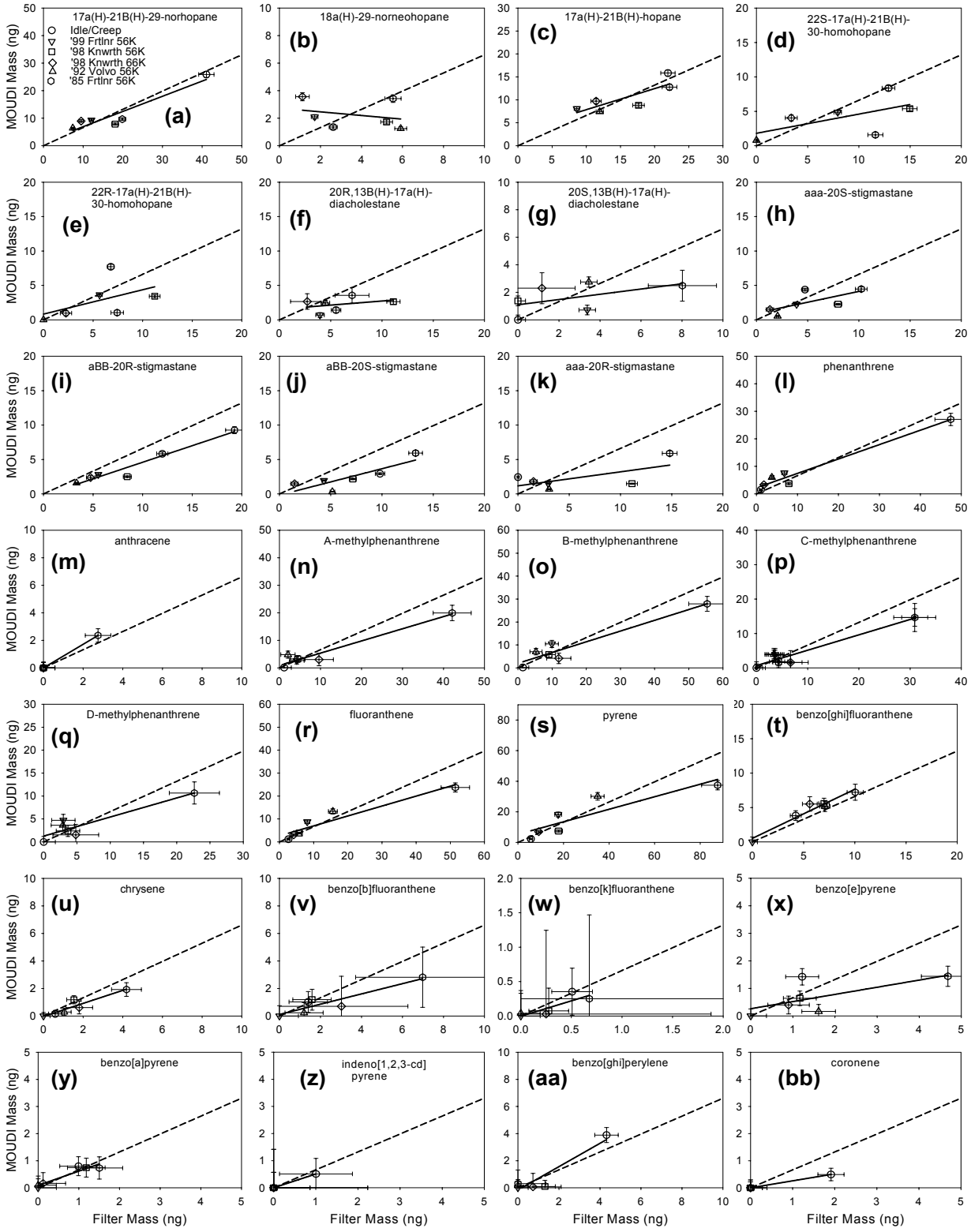

Figure 4-1: Comparison between collocated MOUDI and RAAS filter measurements for organic compounds emitted from HDVs in the PM1.8 size fraction. Uncertainty bars represent analytical uncertainty. The dashed line represents agreement between MOUDI and filter measurement.

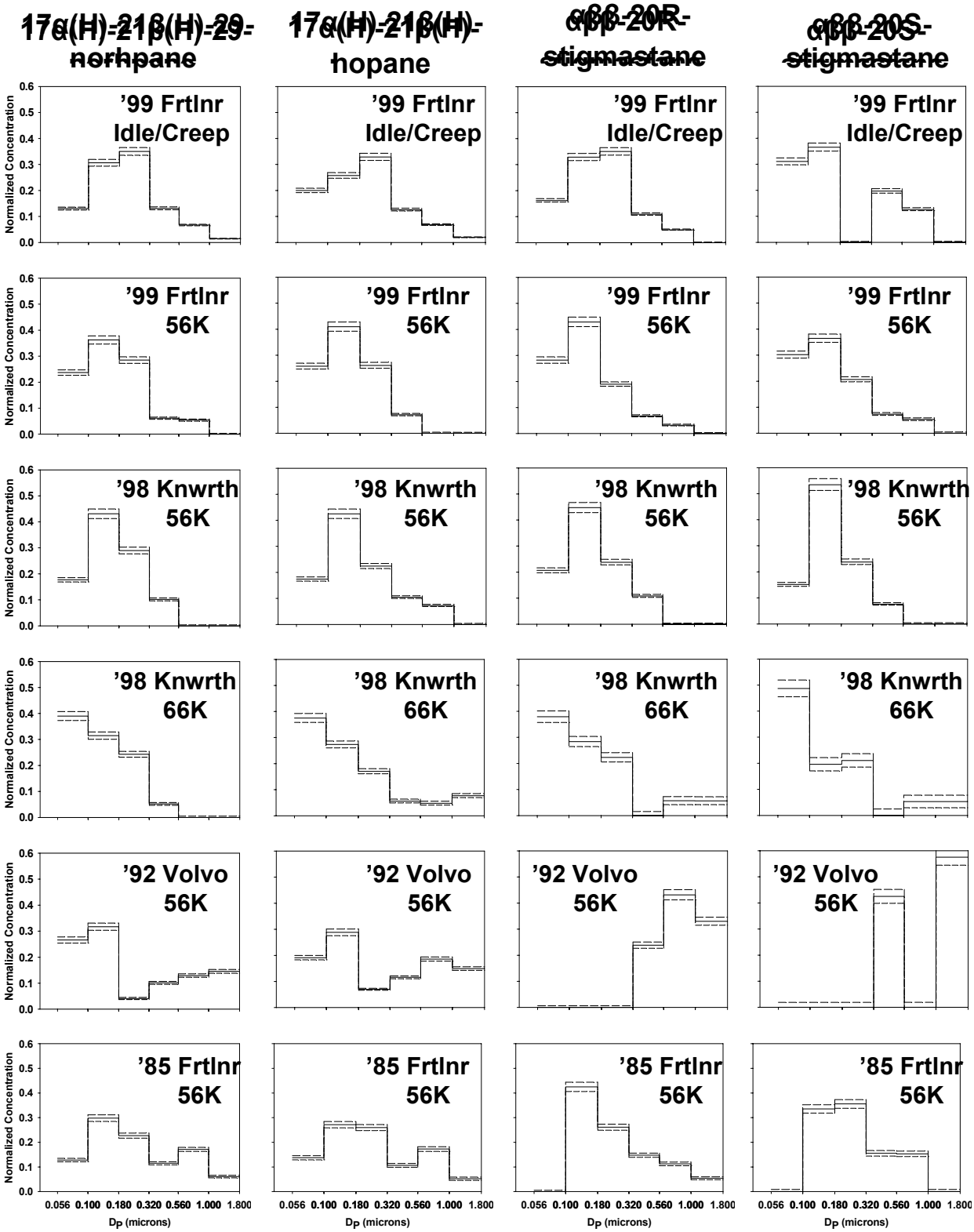

Figure 4-2: Normalized size distribution of lubricating oil organic compounds emitted from all HDDVs examined. Size distributions were normalized to total analyte mass for each analyte observed on the MOUDI substrates. The solid line represents the measured value while the dashed lines illustrate the analytical uncertainty.

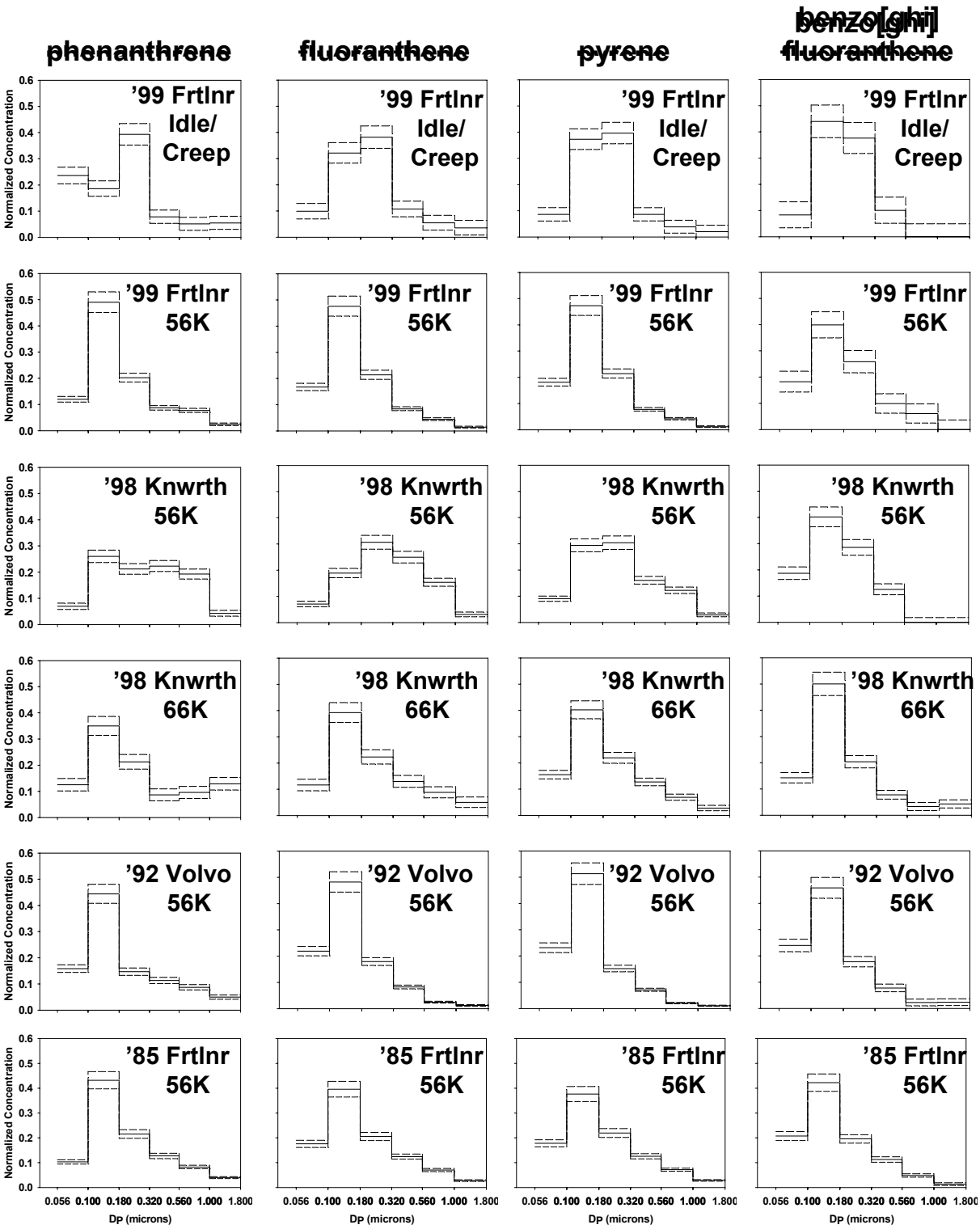

Figure 4-3: Normalized size distribution of four light PAH compounds emitted from all HDDVs examined. Size distributions were normalized to total analyte mass for each analyte observed on the MOUDI substrates. The solid line represents the measured value while the dashed lines illustrate the analytical uncertainty.

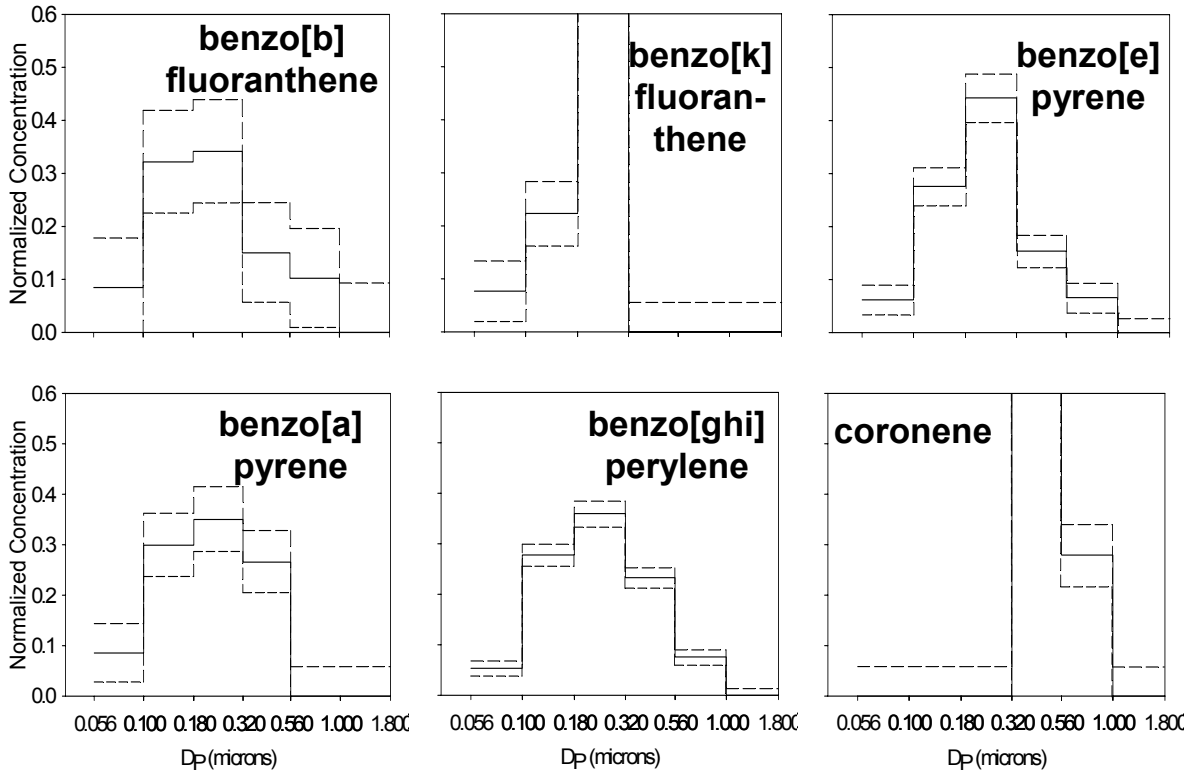

Figure 4-4: Normalized size distributions for heavy PAH compounds emitted from the 1999 Freightliner operated under idle and creep conditions. Size distributions were normalized to total analyte mass for each analyte observed on the MOUDI substrates. The solid line represents the measured value while the dashed lines illustrate the analytical uncertainty.

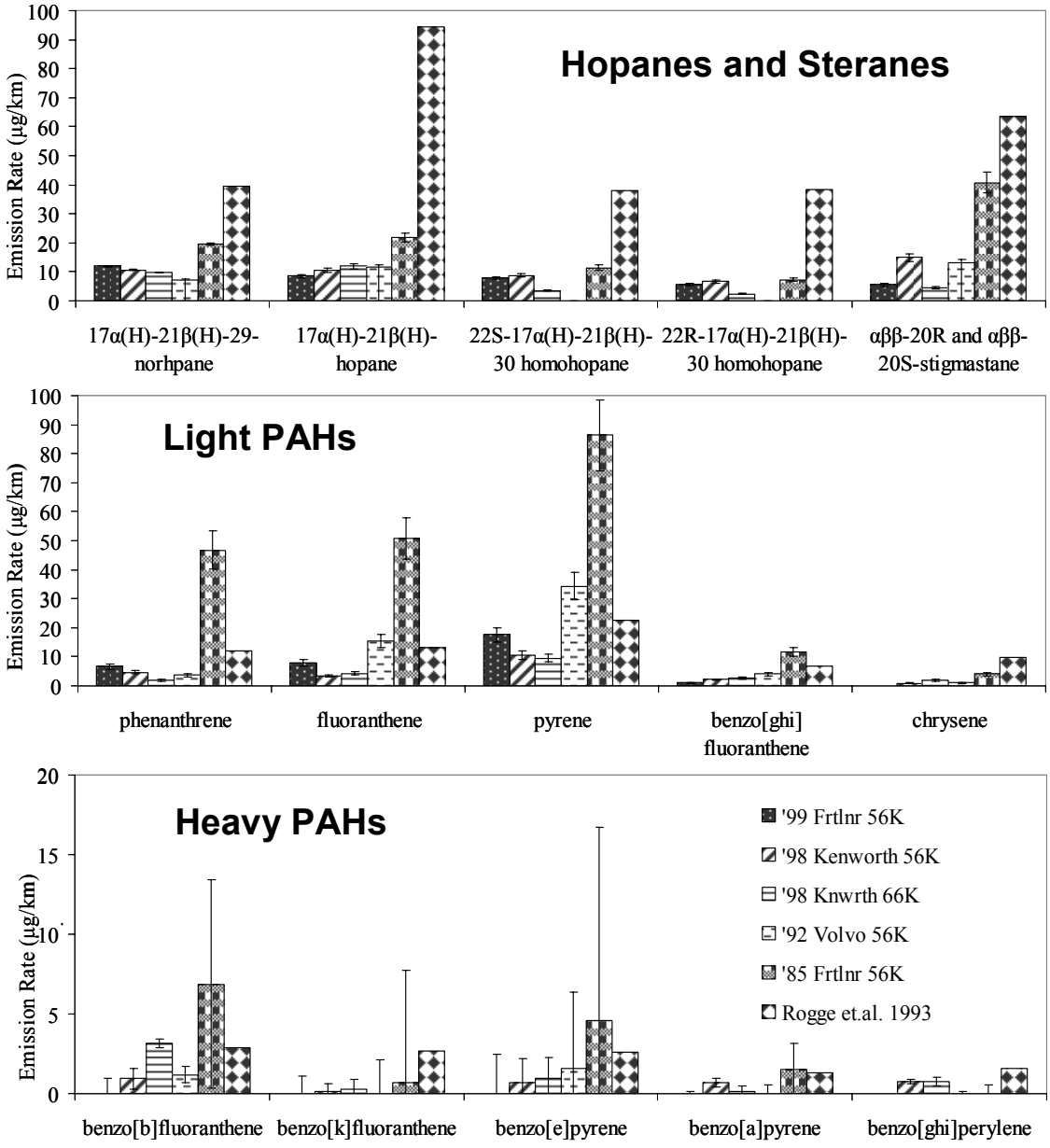

Figure 4-5: Comparison of PM 1.8 emission factors (µg/km) with those of Rogge et.al. 1993.

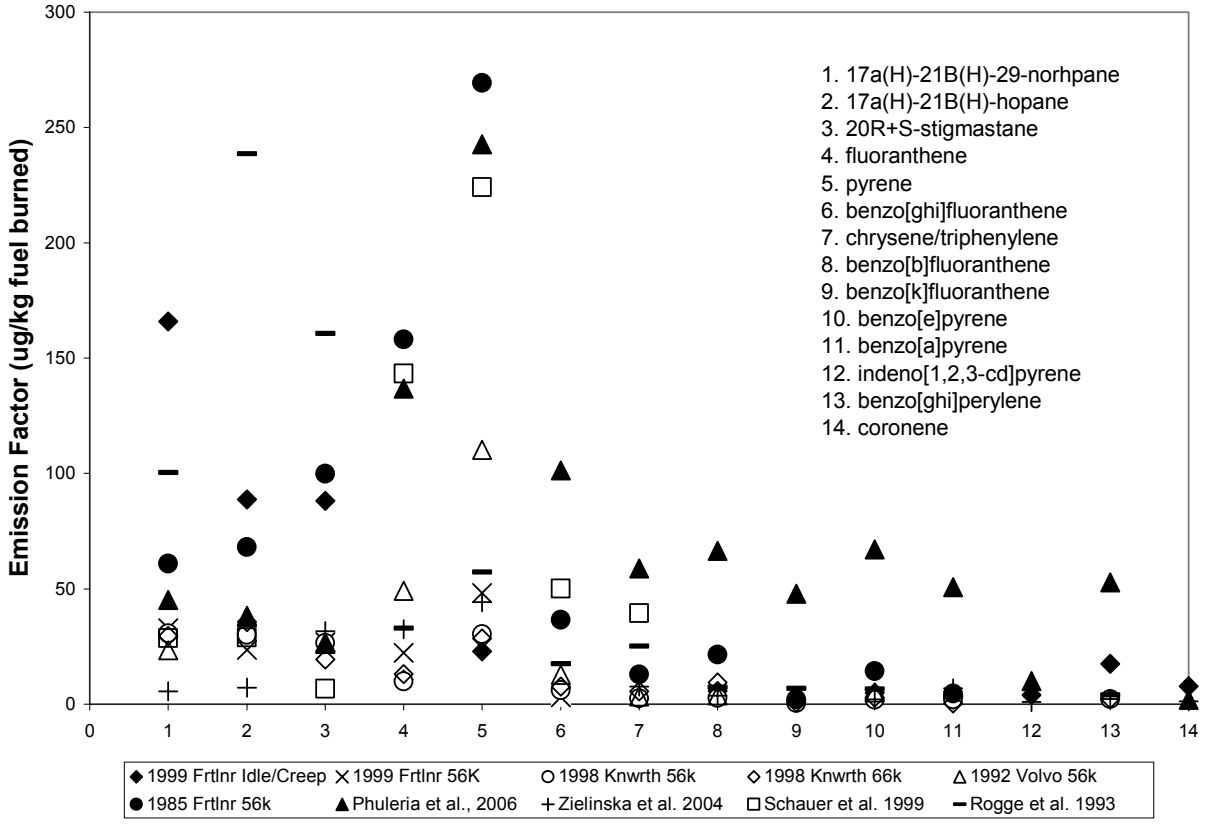

Figure 4-6: Comparison of PM1.8 emission factors (µg analyte / kg fuel burned) measured in the current study with those of Phuleria et al. (2006), Zielinska et al. (2004), Schauer et al. (1999), and Rogge et al. (1993).

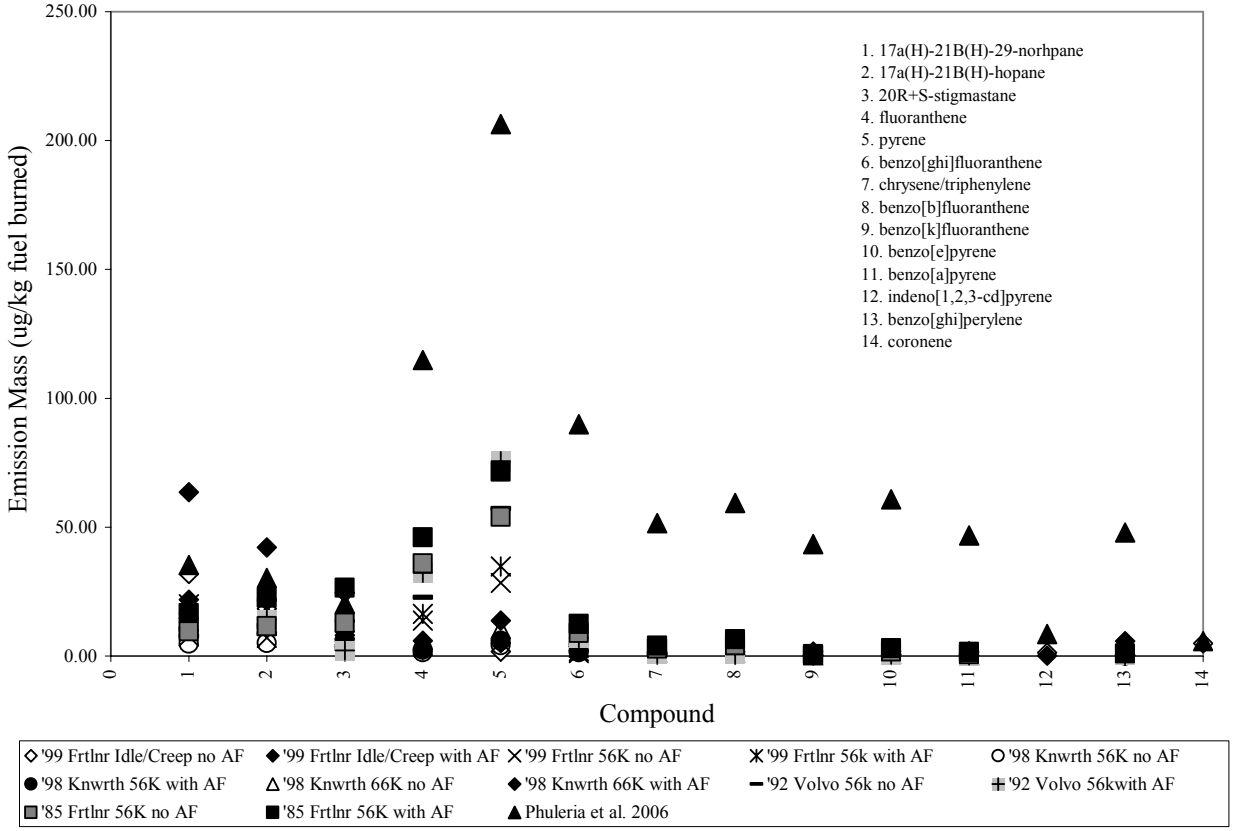

Figure 4-7: PM0.18 emissions factors measured in the current study with and without the MOUDI after filter (AF). Note that PM0.18 is not the definition of ultrafine particles used in the current study (PM0.1). Results measured by Phuleria et al. 2006 are shown for comparison. PAH trends are similar to those shown in Figure 4-6.

5 SIZE DISTRIBUTION OF TRACE ORGANIC SPECIES EMITTED FROM LIGHT-DUTY GASOLINE VEHICLES

5.1 Introduction

Many studies have identified adverse health effects associated with high levels of fine (Dp < 2.5 μm) airborne particulate matter [2, 85]. Particles in the ultrafine size range (Dp < 0.1 μm) have been linked to pulmonary and cardiovascular health concerns [5, 10, 83-85]. Light-duty gasoline vehicles (LDGVs) are a major source of fine particulate matter in highly populated areas [80, 97, 98] with a significant portion of this particle mass in the ultrafine size range [61, 82]. A recent study identified emissions from gasoline-powered motor vehicles as highly toxic to human lung tissue [99]. The ability to recognize the health effects of size-resolved airborne particles emitted from gasoline-powered motor vehicles is limited by our ability to identify these particles in the atmosphere. A size-resolved chemical "fingerprint" or source profile is needed to quantify gasoline exhaust particle concentrations under realistic conditions.

Several investigators have quantified PAH, hopane, and sterane concentrations in the fine size range (Dp < 2.5 μm) that are emitted from LDGVs [13, 28, 75, 100]. These compounds were studied because they are useful for the construction of source profiles. Hopanes and steranes are uniquely associated with lubricating oil [79, 89] and heavy PAHs such as coronene have been suggested as tracers for gasoline exhaust [19, 94]. Certain PAHs have been shown to be both carcinogenic and mutagenic in epidemiological studies, thus assessment of the size distribution of these compounds is vital to assess their potential health implications [86-88]. One study has reported the concentration of PAHs, hopanes and steranes in particles smaller than 0.18 μm diameter adjacent to a roadway [101]. There is no study to date which simultaneously determines the size distributions of these compounds from in-use LDGVs in the fine and ultrafine size fractions as a function of driving cycle.

The purpose of this study is to report the size distributions of 28 particle-phase hopane, sterane, and PAH compounds contained in tailpipe emissions from 5 categories of light duty gasoline-powered vehicles spanning a range of engine types, emissions control technologies, and driving cycles. Measurements are reported for 6 size fractions between 0.056 – 1.8 μm particle aerodynamic diameter. Potential tracers for ultrafine source apportionment studies are identified and ultrafine source profiles are presented.

5.2 Methods

5.2.1 Sample Collection

Size resolved and bulk PM 1.8 particulate matter emissions from LDGVs were collected at the California Air Resources Board (CARB) Haagen-Smit Laboratory (HSL) in El Monte, CA during August and September of 2002 using a chassis dynamometer

combined with a dilution sampling system as discussed in Chapter 3. Bulk PM1.8 was collected using Andersen Reference Ambient Air Samplers (RAASs) (Andersen Instruments, Smyrna, GA). Size-resolved PM was collected using three Micro Orifice Uniform Deposit Impactors (MOUDIs) (MSP Corporation, Shoreview, MN), in six size fractions between 0.056 - 1.8 μm in aerodynamic diameter. Twenty-eight test LDGVs were grouped into five categories based on emissions control technology: Low Emission Vehicles (LEVs), Three Way Catalyst (TWC) vehicles, Oxidation Catalyst (OCAT) vehicles, Non-catalyst (NCAT) vehicles, and visibly smoking vehicles (SMOKERs). Within these categories, vehicles could be further classified as passenger cars (PCs) or Light-Duty Trucks (LDTs)/Sport Utility Vehicles (SUVs). Tables 3-1, 3-2, and 3-3 provide information about the vehicle test matrix with more details provided in chapter 3. Composite PM samples were collected for each LDGV category in order to obtain enough mass for chemical analyses. LDGVs were tested using three different driving cycles: the Federal Test Procedure (FTP), the Unified Cycle (UC), and the Correction Cycle (CC) [62]. The FTP cycle has moderate transient sections with the lowest top speed of all three cycles. The UC cycle has the highest acceleration and greatest speed of all the cycles tested. The CC cycle has a higher average speed section than the FTP cycle with some transient driving [102].

5.2.2 Sample Extraction and Analysis for Organic Compounds

Extraction and analysis methods were identical to those employed during previous analysis of diesel engine exhaust described in Chapter 4 [103] and so only a brief summary is provided here. Samples were spiked with anisotopically labeled sterane and two labeled PAHs and then sonicated twice in 15 mL of dichloromethane. Extracts were combined and then concentrated to 50 μL via nitrogen evaporation (heavily loaded samples were only reduced in volume to 200 μL). Analysis was performed using an Agilent J&W DB-XLBMSD capillary gas chromatograph column followed by a Varian gas chromatograph-ion trap mass spectrometer (GC-ITMS). Analytes were identified by comparison to authentic standards or by comparison of relative retention times and mass spectra to those in the literature [104]. The instrument analysis program was identical to that described in Chapter 4. Limits of detection and limits of quantification are given in Table 5-1.

Table 5-1: Limits of Quantification and Detection for Trace Organic Compounds Measured in Particulate Matter Emitted from Light Duty Gasoline-Powered Vehicles.

Compound		
Hopanes	LOQ (pg/μL)[a]	LOD (pg/μL)[b]
18α(H)-21β(H)-22, 29, 30-trisnorhpane[c]	6.2	1.8
17α(H)-21β(H)-22, 29, 30-trisnorhpane[c]	6.2	1.8
17α(H)-21β(H)-29-norhpane	6.2	1.8
18α(H)-29-norneohopane[c]	4.8	1.4
17α(H)-21β(H)-hopane	4.8	1.4
22S-17α(H)-21β(H)-30-homohopane[c]	4.8	1.4
22R-17α(H)-21β(H)-30-homohopane[c]	4.8	1.4
22S-17α(H)-21β(H)-30-bishomohopane[c]	4.8	1.4
22R-17α(H)-21β(H)-30-bishomohopane[c]	4.8	1.4
Steranes		
20R,13β(H)-17α(H)-diacholestane[c]	9.7	2.9
20S,13β(H)-17α(H)-diacholestane[c]	9.7	2.9
ααα-20S-stigmastane [c]	5.3	1.6
αββ-20R-stigmastane	5.3	1.6
αββ-20S-stigmastane [c]	5.3	1.6
PAHs		
benzo[b]fluoranthene	0.46	0.14
benzo[k]fluoranthene	0.44	0.12
benzo[e]pyrene	1.2	0.36
benzo[a]pyrene	0.26	0.08
perylene	0.47	0.14
indeno[1,2,3-cd]pyrene	0.62	0.18
benzo[ghi]perylene	0.76	0.22
indeno[1,2,3-cd]fluoranthene[c]	0.62	0.18
dibenzo[def,mno]chrysene[c]	0.76	0.22
dibenzo[a,c + a,h]anthracene	1.4	0.42
benzo[b]chrysene[c]	1.4	0.42
coronene	2.2	0.66
MW 302 isomers group 1[c]	2.4	0.73
MW 302 isomers group 2[c]	2.4	0.73

[a] Limit of quantification determined using a signal:noise ratio of 10:1, [b] Limit of detection determined using a signal:noise ratio of 3:1, [c]no pure standard available LOQ and LOD estimated using a standard compound of the same class with the closest retention time

5.3 Results and Discussion

5.3.1 Quality Assurance Checks

Figure 5-1 illustrates agreement between co-located MOUDI and filter measurements in the current study as a quality assurance check on the size distribution measurements. Panels (a-n) illustrate agreement for hopanes and steranes that are useful tracers for lubricating oil. Panels (o-bb) illustrate agreement for non-volatile polycyclic aromatic hydrocarbons (PAHs). The error bars in Figure 5-1 reflect the analytical uncertainty of the GC-MS analysis.

In Figure 5-1, the solid line shown in each panel is a linear regression analysis between the MOUDI and sampling flow rate adjusted RAAS measurements for each organic compound. The dashed line shown in each panel is a linear regression analysis between MOUDI and adjusted RAAS measurements for the average value of organic carbon measured using thermal optical carbon analysis [93]. The relative losses of the individual organic compounds from the MOUDI are generally slightly larger than the volatilization of organic carbon. The regression slopes and correlation coefficients for each organic compound measured by MOUDI vs. RAAS filter sampler are given in Table 5-2.

Table 5-2: Linear regression statistics for co-located MOUDI vs. filter measurements of particulate matter emitted from light duty gasoline vehicles.

Compound		
Hopanes	**slope**	**R^2**
18α(H)-21β(H)-22, 29, 30-trisnorhpane[1]	0.6911	0.9438
17α(H)-21β(H)-22, 29, 30-trisnorhpane[1]	0.9847	0.9641
17α(H)-21β(H)-29-norhpane	0.9202	0.9773
18α(H)-29-norneohopane[1]	0.5725	0.7479
17α(H)-21β(H)-hopane	0.7526	0.9589
22S-17α(H)-21β(H)-30-homohopane[1]	0.8912	0.7718
22R-17α(H)-21β(H)-30-homohopane[1]	0.9827	0.9812
22S-17α(H)-21β(H)-30-bishomohopane[1]	0.9630	0.9673
22R-17α(H)-21β(H)-30-bishomohopane[1]	0.6041	0.6931
Steranes		
20R,13β(H)-17α(H)-diacholestane[1]	0.4725	0.8837
20S,13β(H)-17α(H)-diacholestane[1]	0.3598	0.5943
ααα-20S-stigmastane[1]	0.6537	0.8472
αββ-20R-stigmastane	0.8057	0.8353
αββ-20S-stigmastane[1]	1.281	0.9402
PAHs		
benzo[b]fluoranthene	0.5643	0.9766
benzo[k]fluoranthene	0.3082	0.8018
benzo[e]pyrene	0.8682	0.9936
benzo[a]pyrene	1.042	0.9965
perylene	1.030	0.9846
indeno[1,2,3-cd]pyrene	0.5644	0.9639
benzo[ghi]perylene	0.6628	0.9983
indeno[1,2,3-cd]fluoranthene[1]	0.8327	0.9865
dibenzo[def,mno]chrysene[1]	0.8904	0.9904
dibenzo[a,c + a,h]anthracene	0.4596	0.2518
benzo[b]chrysene[1]	0.5292	0.9886
coronene	0.6804	0.9950
MW 302 isomers group 1[1]	0.7059	0.9738
MW 302 isomers group 2[1]	0.6319	0.9607
[1] Analyte identification based on comparisons to relative retention times to those in the literature.		

Consistency between MOUDI and filter measurements is a necessary check to build confidence in the accuracy of the size distribution measurements. Most PAH species identified in this study behave consistently when collected with MOUDI and

filter samplers. Five of the PAHs identified (compounds o, p, t, x, and y) exhibit less consistent behavior than the other PAHs quantified in this study; while the exact cause of the discrepancies for these compounds is unknown it may be due in part to the low concentrations measured that are near the limit of detection for the method used. Hopanes 17α(H)-21β(H)-29-norhopane (Figure 5-1 c) and 17α(H)-21β(H)-hopane (Figure 5-1 e) appear to exhibit the most consistent behavior between MOUDI and filter measurements as demonstrated by correlation slopes = 0.75-0.92 and correlation coefficients R^2 = 0.98- 0.96, and these compounds are also observed in most samples. Hopanes 22R-17α(H)-21β(H)-30-homohopane (panel g) and 22S-17α(H)-21β(H)-30-bishomohopane (panel h) also exhibit strong agreement between filter and MOUDI measurements but were not observed in all vehicle classes tested thus are not a good candidate for a size-resolved motor vehicle particulate matter tracer. Other observed hopanes show reasonable agreement between the two measurements with slopes ranging from 0.5725 to 0.8912. Steranes αββ-20R-stigmastane (panel m) and αββ-20S-stigmastane (panel n) exhibit the most consistent behavior between MOUDI and filter measurements with correlation slopes = 0.81 – 1.28 and correlation coefficients R^2 = 0.84- 0.94. Four other steranes measured (panels j, k, and l) do not show such a strong agreement between sampling techniques with slopes of 0.47, 0.36, and 0.65 and correlation coefficients less than 0.9. Lubricating oil tracers, 17α(H)-21β(H)-29-norhopane (Figure 5-1 c), 17α(H)-21β(H)-hopane (Figure 5-1 e), αββ-20R-stigmastane (panel m) and αββ-20S-stigmastane (panel n) appear to have the greatest promise as size-resolved tracers for vehicular particulate matter. These same four hopanes and steranes were identified in a study of diesel exhaust particle size distributions [103] suggesting that they are general tracers for size-resolved lubricating oil particles emitted from motor vehicles.

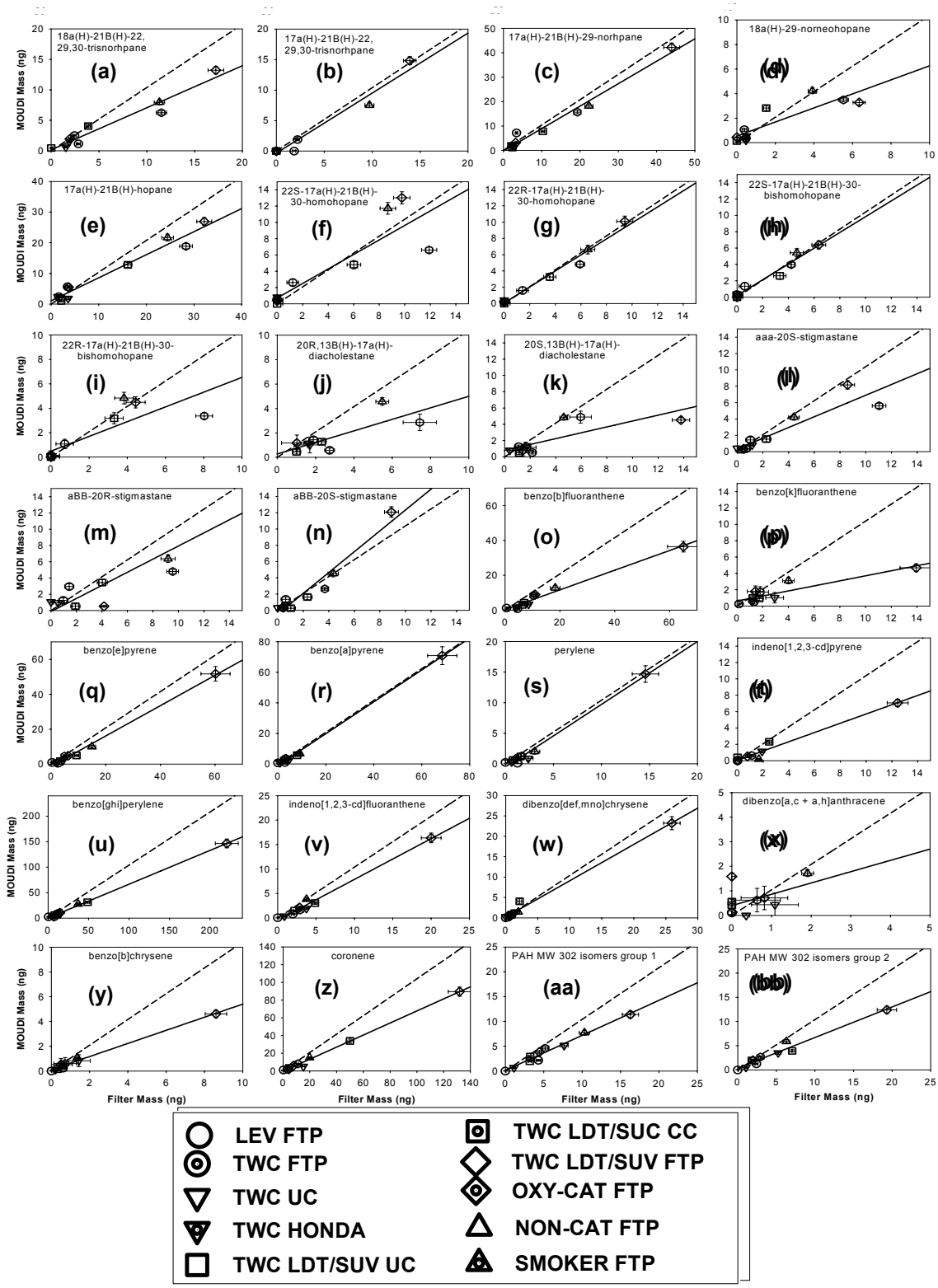

Figure 5-1: Comparison between the mass collected by the MOUDI sampler with the PM1.8 filter mass. All MOUDI values include the after-filter.

5.3.2 Observed Size Distribution Patterns

Normalized size distributions for hopanes, steranes, and PAHs can be calculated by dividing the mass in each size fraction by the total mass summed across all size fractions. The normalized size distributions of the most self-consistent particle-phase hopanes, steranes, and PAHs observed in the current study had similar shapes. The average normalized size distributions of lubricating oil tracers (hopanes and steranes) and PAHs are shown in Figures 5-2 and 5-3, respectively. Uncertainty bars shown in Figures 5-2 and 5-3 are one standard deviation of the individual compound values used to calculate the average within each size fraction.

Figure 5-2 (a-e) shows the relative size distribution of hopanes and steranes emitted from the different vehicle classes operated under the FTP driving cycle. The variation of the hopane and sterane size distributions shown in Figure 5-2 (a-e) is caused by differences in engine characteristics and emissions control technology. All vehicle classes exhibit a mode in the hopane and sterane size distribution between 0.1-0.18 μm (or 0.18-0.32 μm for SMOKERS). Vehicles equipped with three way catalysts (including LEVs and TWCs) have much lower PM1.8 hopane and sterane emissions rates compared to other technology classes and a significant fraction of the hopanes and steranes were found in particles with diameter > 0.32 μm. Continuous measurements during each test show that the majority of the PM emitted from LEV and TWC vehicles was released during the "cold-start" portion of the FTP driving cycle when the catalyst was not active [40]. It is therefore not surprising that NCAT vehicles (Figure 5-2d) also have a significant fraction of hopanes and steranes contained in particles larger than 0.32 μm even though measurements show that NCAT emissions were much larger and occurred more uniformly throughout the test [40]. Once the catalyst reaches operating temperature it appears to remove hopanes and steranes contained in particles larger than 0.32 μm. This point is emphasized in Figure 5-2 (i) that shows emissions from TWC vehicles operated under the first two modes of the FTP driving cycle under "warm-start" conditions. The fraction of hopanes and steranes in particles with diameter greater than 0.32 μm emitted by TWC "warm-start" vehicles (1i) is greatly reduced relative to TWC tests that were dominated by cold-start emissions (1 a,b).

Figure 5-2c shows that hopane and sterane emissions from OCAT vehicles are dominated by a single mode between 0.1 – 0.18 μm particle diameter. It is expected that OCAT vehicles also emit hopanes and steranes in size fractions larger than 0.32 μm diameter before the catalyst reaches operating temperature, but continuous measurements indicate that the OCAT vehicles emitted significant amounts of PM throughout the entire test, not just during the cold start [40]. Table 3-6 shows that total PM1.8 emissions from OCAT vehicles were an order of magnitude larger than emissions from TWC vehicles. The OCAT vehicles tested in the current study had an average model year of 1979 while the average model year of TWC vehicles ranged from 1992 – 2000. Engine technology improvements over time and newer engine condition reduce emissions from the newer vehicles.

Figure 5-2e shows that hopane and sterane emissions from SMOKER vehicles are dominated by a single mode between 0.1 – 0.56 μm. Table 3-6 shows that emissions rates from SMOKER vehicles were an order of magnitude larger than OCAT vehicles and two orders of magnitude larger than TWC vehicles. One of the two SMOKER vehicles tested in the current study was equipped with a catalyst while the other was not. Continuous measurements show that the non-catalyst equipped SMOKER vehicle dominated the emissions [40]. The fact that SMOKER hopane and sterane size distributions had a single mode instead of the more typical bimodal distribution for vehicles operating without a catalyst suggests that the formation mechanism for the lubricating oil particles in the SMOKER exhaust was atypical, as might be expected for a vehicle emitted visible smoke.

Figures 5-2 (g-i) illustrate the effect of operating cycle on the size distribution of particulate hopane and steranes emitted from TWC LDT/SUVs. Both the Unified Cycle (1g) and the Correction Cycle (1h) have higher average speed and sharper accelerations than the first two modes of the FTP (1i). All tests involved "warm-start" operation where the catalyst was close to operating temperature at the beginning of the test. The fraction of hopane and sterane emissions in the 0.056-0.1 μm size fraction increases from ~0.05 at lower FTP loads (1i) to ~0.3 at the higher UC and CC loads (1g,h). This trend qualitatively matches the behavior of hopane and sterane size distributions emitted from diesel vehicles under different load conditions [103]. Park et al. [31] showed that the effective density of diesel exhaust particles decreases as engine load increases. This reduces the apparent aerodynamic diameter of the exhaust particles, causing a greater fraction of the hopanes and steranes to appear in the ultrafine size fraction. The trends shown in Figure 5-2 (g-i) suggest that similar behavior occurs for particles emitted from gasoline engines.

Figure 5-3 (a-e) shows relative size distribution of heavy PAHs emitted from the different vehicle classes operated under the FTP driving cycle. Vehicle emission control technology had much less of an impact on PAH size distributions than it did on hopane and sterane size distributions (compare Figure 5-2a-e to Figure 5-3a-e). All PAHs with reasonable error bounds exhibited size distributions that peak between 0.10-0.18 μm (SMOKER emissions peak between 0.1-0.32 μm). Approximately 70 – 90% of the PAH mass is contained in the dominant size fraction. The ultrafine fraction contains ~10% of the observed PAH mass (~1% for SMOKERs). The SMOKER exhaust PAHs are shifted to larger sizes likely through condensational growth processes. Figure 5-3 (g-i) illustrates the effect of driving cycle on heavy PAH size distributions. The UC and CC driving cycles increase the fraction of heavy PAHs in the ultrafine size range by a factor of approximately 2 in a manner consistent with hopane and sterane trends. The geometric standard deviation for PAH size distributions emitted from all vehicle classes was generally smaller than the corresponding hopane and sterane size distribution.

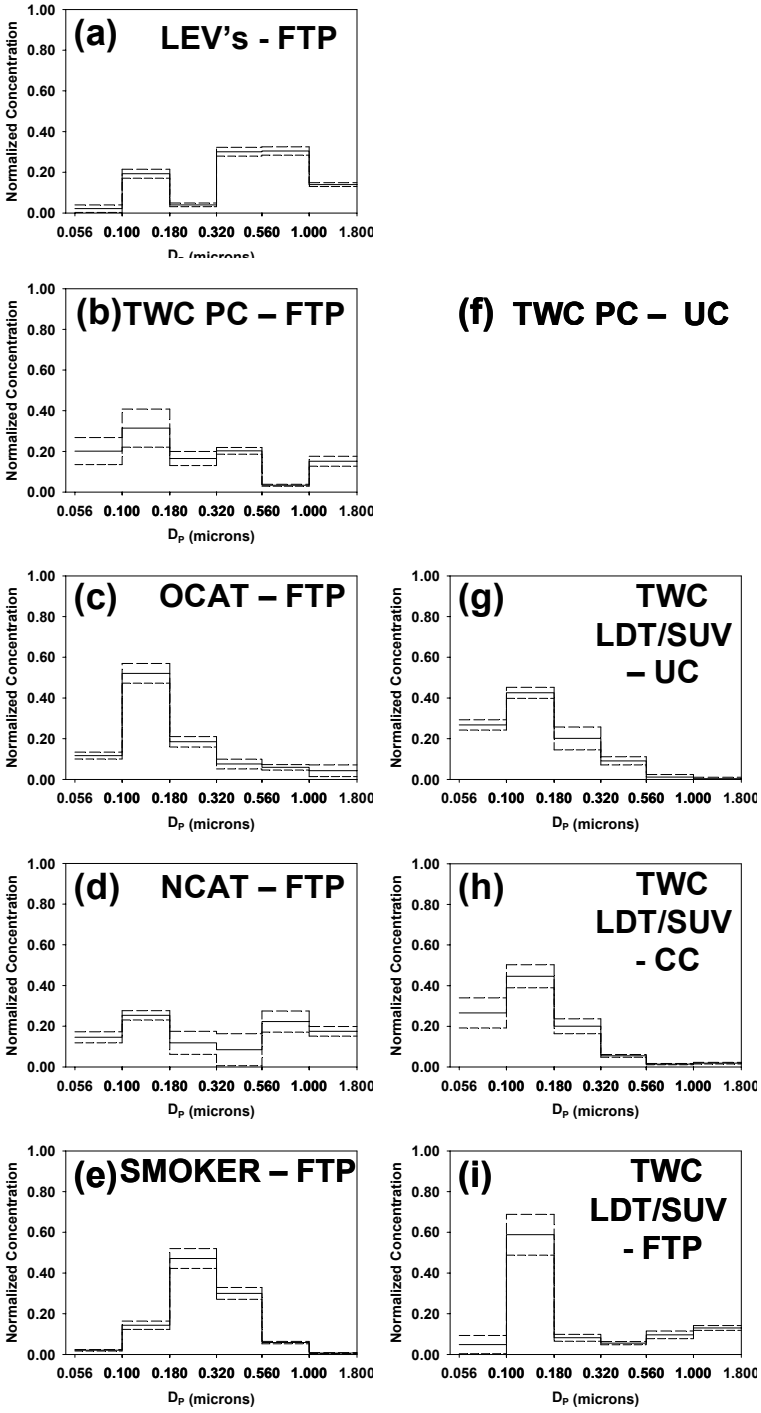

Figure 5-2: Average size distributions for 17α(H)-21β(H)-29-norhpane, 17α(H)-21β(H)-hopane, αββ-20R-stigmastane, and αββ-20S-stigmastane contained in particles larger than 0.056 µm particle aerodynamic diameter. Size distributions were normalized to total analyte mass observed on the MOUDI substrates. The solid line represents the average value while the dashed lines illustrate +/- one standard deviation about the mean. Panel (f) is below detection limit. Panel (i) excludes steranes.

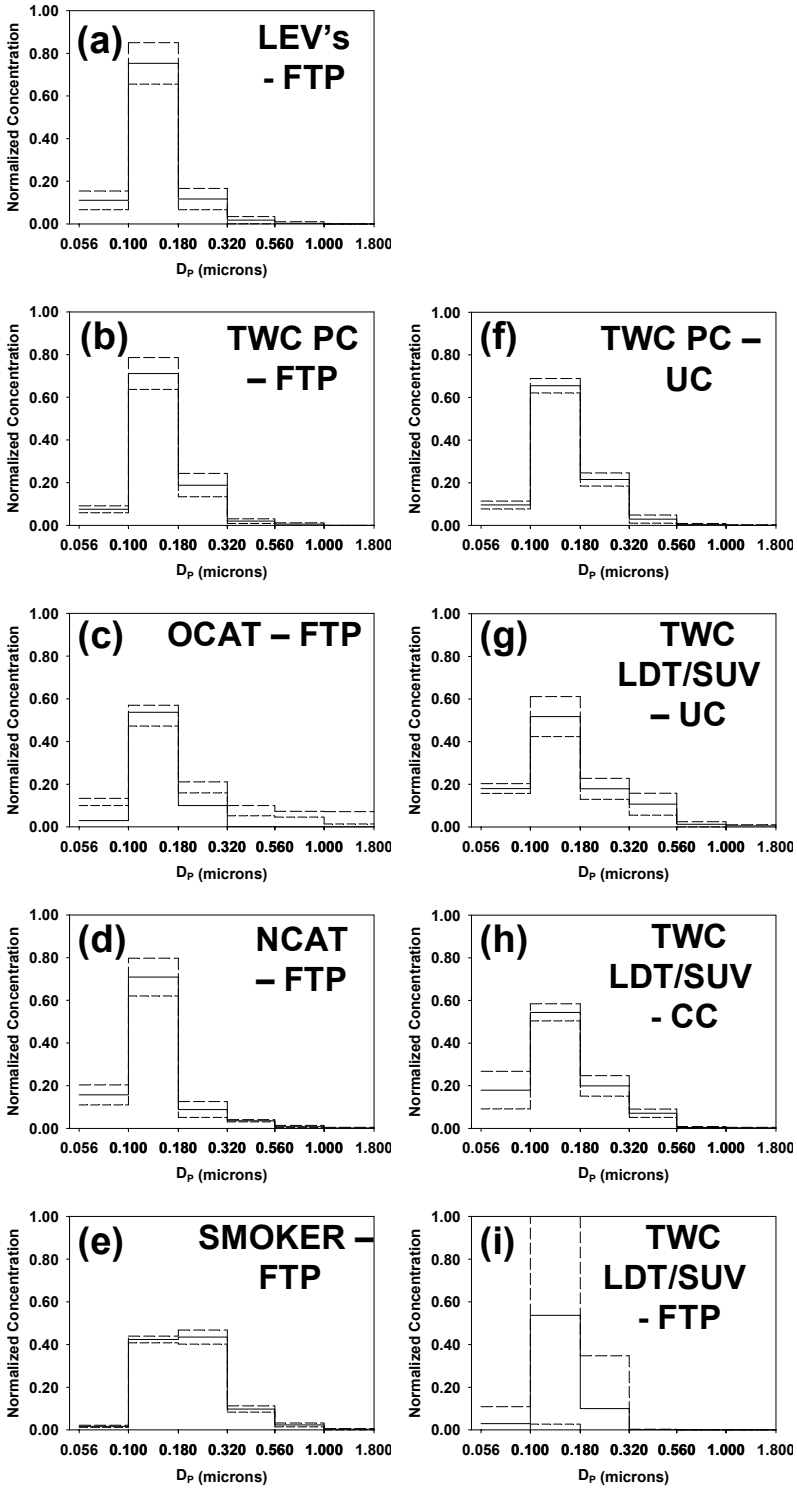

Figure 5-3: Average PAH normalized size distributions for benzo[e]pyrene, benzo[a]pyrene, perylene, benzo[ghi]perylene, indeno[1,2,3-cd]fluoranthene, dibenzo[def,mno]chrysene, coronene, and the molecular weight 302 isomers contained in particles larger than 0.056 µm particle aerodynamic diameter. Size distributions were normalized to total analyte mass observed on the MOUDI substrates. The solid line represents the average value while the dashed lines illustrate +/- one standard deviation about the mean.

Tailpipe emissions of particulate hopanes and steranes originate exclusively from lubricating oil. PAHs are present in the parent gasoline [105] and they can be formed in the combustion process from simpler organic compounds [106]. PAHs can also accumulate in lubricating oil over time [107]. The lack of similarity between the hopane and sterane size distributions (Figure 5-2) vs. PAH size distributions (Figure 5-3) suggests that PAH concentrations in the lubricating oil are small for the vehicles used in the current study.

5.3.3 Source Profiles

Profiles for source apportionment analysis can be constructed using the ratio of tracer mass to total organic mass in each size fraction of interest. Total organic mass concentrations for each test were measured by Robert el al. [40] using a thermal-optical technique [41, 42].

Ratios of analyte mass to total organic carbon mass (μg / g) emitted by different vehicle classes operated under the FTP driving cycle are shown in Tables 5-3 and 5-4 for the PM1.8 and the PM0.1 size fractions, respectively. Uncertainty estimates shown in Tables 5-3 and 5-4 were calculated as the standard deviation of the combined analytical uncertainty of the analyte mass measurement and organic carbon mass measurement. The relative concentration of hopanes and steranes emitted in the PM1.8 and PM0.1 size fractions were within 40% for all vehicle categories except for TWC PCs (factor of ~4 enhancement in PM0.1) and NON-CATs (factor of ~4 enhancement in PM1.8). TWC PCs exhibited an apparent enhancement in the relative concentration of hopanes and steranes in the PM0.1 size fraction due to a reduction in organic carbon mass.

The lower portions of Tables 5-3 and 5-4 show that the relative concentration of PAHs emitted in the PM1.8 and PM0.1 size fractions during the FTP driving cycle are generally a factor of ~2 larger than the relative concentrations in the PM0.1 size fraction for all vehicle categories except SMOKERs (no enhancement) and LEVs (slight enhancement of light PAHs, slight depletion of heavy PAHs). This may be caused by a shift of organic mass derived from motor oil to particles larger than 0.32 μm as suggested in Figures 5-2 (a,e), reducing the denominator used to calculate the PAH/OC ratio.

Tables 5-3 and 5-4 show that the highest relative concentrations of PAHs were emitted by the non-catalyst vehicles (2-5 times greater than the TWC vehicles). Two PAHs, benzo[ghi]perylene and coronene are a much higher percentage of the organic carbon then the other PAHs measured for all tests. These PAHs are found at significant concentrations in gasoline and have very stable structures capable of surviving the combustion process [108]. Coronene has been proposed as a tracer chemical for particulate matter generated by light-duty gasoline vehicles [79, 94].

Table 5-3: PM1.8 ratio of analyte mass to total organic carbon mass (µg / g) for Low Emission Vehicles (LEV), Three Way Catalyst Passenger Cars (TWC PC), Oxidation Catalyst cars (OXY-CAT), non-catalyst equipped vehicles (NON-CAT), and vehicles emitting visible smoke operated under the FTP driving cycle.

Compound	LEV		TWC PC		OXY-CAT		NON-CAT		SMOKERS	
Hopanes	ratio	error	ratio	error	ratio	error	ratio	error	ratio	error
17α(H)-21β(H)-29-norhopane	142	4	153	1	136	4	205	6	98	0.7
17α(H)-21β(H)-hopane	107	4	100	2	162	5	184	7	72	0.5
Steranes										
αββ-20R-stigmastane	64	3	ND[2]		25	2	165	6	35	0.3
αββ-20S-stigmastane[1]	28	3	45	1	ND[2]		89	4	20	0.2
PAHs										
benzo[e]pyrene	163	4	300	4	99	3	801	24	135	1
benzo[a]pyrene	191	6	346	4	39	3	692	21	154	2
Perylene	83	4	169	4	29	2	137	6	33	0.4
benzo[ghi]perylene	509	13	1050	8	318	10	4206	124	495	4
indeno[1,2,3-cd]fluoranthene[1]	130	3	265	2	40	1	419	12	45	0.4
dibenzo[def,mno]chrysene[1]	40	4	104	4	ND[2]		188	7	58	0.5
Coronene	238	6	1077	7	198	6	4309	127	296	3
MW 302 isomers[1]	222	6	457	4	50	2	442	13	40	0.3

[1] Analyte identification based on comparisons to relative retention times to those in the literature.
[2] ND = not detected

Table 5-4: PM 0.1 ratio of analyte mass to total organic carbon mass (µg / g) for Low Emission Vehicles (LEV), Three Way Catalyst Passenger Cars (TWC PC), Oxidation Catalyst cars (OXY-CAT), non-catalyst equipped vehicles (NON-CAT), and vehicles emitting visible smoke operated under the FTP driving cycle.

Compound	LEV		TWC PC		OXY-CAT		NON-CAT		SMOKERS	
Hopanes	ratio	error	ratio	error	ratio	error	ratio	error	ratio	error
17α(H)-21β(H)-29-norhopane	92	7	467	19	82	2	88	3	97	0.8
17α(H)-21β(H)-hopane	110	15	686	28	82	4	46	6	84	1
Steranes										
αββ-20R-stigmastane	50	11	244	10	40	3	33	4	34	0.6
αββ-20S-stigmastane[1]	ND[2]		91	4	23	3	16	4	37	0.6
PAHs										
benzo[e]pyrene	70	6	69	7	32	2	304	8	127	1
benzo[a]pyrene	151	20	142	7	20	5	230	9	142	2
Perylene	ND[2]		56	9	ND[2]		66	6	26	0.8
benzo[ghi]perylene	616	45	785	34	163	6	2242	58	412	4
indeno[1,2,3-cd]fluoranthene[1]	134	10	201	9	18	1	193	5	43	0.5
dibenzo[def,mno]chrysene[1]	95	17	100	12	ND[2]		29	7	30	1
Coronene	366	25	577	24	105	2	2350	60	273	3
MW 302 isomers[1]	328	24	368	15	29	1	205	6	33	0.4

[1] Analyte identification based on comparisons to relative retention times to those in the literature.
[2] ND = not detected

Tables 5-5 and 5-6 show the concentrations of organic compounds relative to total organic mass ($\mu g\ g^{-1}$) emitted by TWC vehicles operated under different driving cycles. PM0.1 hopanes and steranes emitted from the TWC PCs operated using the UC driving cycle failed quality control checks and are not reported. Table 5-5 shows that the relative concentration of hopanes and steranes in the PM1.8 size fraction was significantly enhanced during the UC driving cycle compared to the FTP cycle for TWC PCs. In contrast, Table 5-6 illustrates that the relative concentrations of hopanes and steranes are not enhanced in the PM1.8 emitted from TWC LDT/SUVs under the more strenuous UC and CC driving cycles compared to the FTP cycle. The different behavior may be caused by the use of "cold-starts" for the tests summarized in Table 5-5 and "warm-starts" for the tests summarized in Table 5-6.

Table 5-6 shows that the relative concentration of most hopanes and steranes in the PM0.1 size fraction decrease slightly under the more strenuous UC and CC driving cycles relative to the FTP. Figure 5-2 (g-i) illustrated that hopanes and steranes shift to smaller sizes under the heavier load conditions. The relative concentration of hopanes and steranes decreased under heavier load conditions because an even larger increase in organic matter occurred in the PM0.1 size fraction under the UC and CC driving cycles. Overall, the trends illustrated by variations in vehicle load conditions shown in Tables 5-5 and 5-6 reflect the fact that the PM1.8 concentration of organic matter decreases under heavier load conditions while the PM0.1 concentration of organic matter increases. A full discussion of organic matter emissions during the current tests is provided by Robert et al. [40].

The lower portions of Tables 5-5 and 5-6 illustrate the effect of driving cycles on the relative concentrations of PAHs emitted from TWC vehicles in the PM0.1 and PM1.8 size fractions. Table 5-5 shows that the relative concentration of PAHs in the PM0.1 size fraction decreases by an order of magnitude under the UC driving cycle vs. the FTP cycle. Figures 5-3 (b,f) illustrate that the size distribution of PAHs did not shift substantially between the FTP and UC driving cycle tests. The change in relative PAH concentrations are once again caused by an increase in the organic matter concentration in the PM0.1 size fraction during the UC test. Table 5-6 shows that similar trends cannot be detected during the TWC tests involving "warm-starts" because many of the PAHs were below the method detection limit due to light sample loadings.

Table 5-5: PM 0.1 and PM 1.8 ratio of analyte mass to total organic carbon mass (µg / g) for TWC-PC vehicles operated under FTP and UC driving cycles.

Compound	PM 0.1				PM 1.8			
	FTP		UC		FTP		UC	
Hopanes	ratio	error	ratio	error	ratio	error	ratio	error
17α(H)-21β(H)-29-norhopane	467	19	ND		153	1	753	16
17α(H)-21β(H)-hopane	686	28	ND		100	2	1177	25
Steranes								
αββ-20R-stigmastane	244	10	ND		ND		295	4
αββ-20S-stigmastane [1]	91	4	ND		45	1	170	7
PAHs								
benzo[e]pyrene	69	7	19	0.6	300	4	243	6
benzo[a]pyrene	142	7	24	2	346	4	188	6
perylene	56	9	7	2	169	4	58	4
benzo[ghi]perylene	785	34	111	2	1050	8	603	13
indeno[1,2,3-cd]fluoranthene[1]	201	9	28	0.5	265	2	160	4
dibenzo[def,mno]chrysene[1]	100	12	18	2	104	4	67	4
coronene	577	24	71	0.8	1077	7	325	7
MW 302 isomers[1]	368	15	45	0.6	457	4	185	4

[1] Analyte identification based on comparisons to relative retention times to those in the literature.
[2] ND = not detected

Table 5-6: PM 0.1 and PM 1.8 ratio of analyte mass to total organic carbon mass (µg / g) for LDT/SUV vehicles operated under FTP, UC, and CC driving cycles. All tests were "warm-starts". FTP test only included the first two modes of the standard FTP cycle.

Compound	PM 0.1						PM 1.8					
	FTP		UC		CC		FTP		UC		CC	
Hopanes	ratio	error	ratio	error	ratio	error	ratio	error	ratio	error	ratio	error
17α(H)-21β(H)-29-norhopane	136	13	282	2	240	2	430	37	269	3	325	4
17α(H)-21β(H)-hopane	630	58	273	2	336	3	430	37	294	3	477	5
Steranes												
αββ-20R-stigmastane	189	22	46	0.6	110	1	179	16	111	1	161	2
αββ-20S-stigmastane [1]	78	17	51	0.6	46	0.5	79	8	52	0.6	62	0.7
PAHs												
benzo[e]pyrene	38	7	116	1	48	1	39	4	180	2	83	1
benzo[a]pyrene	ND		32	1	32	0.7	ND		110	2	54	0.8
perylene	ND		21	0.7	18	1	ND		37	0.6	28	0.8
benzo[ghi]perylene	89	26	372	3	86	2	74	10	446	5	191	3
indeno[1,2,3-cd]fluoranthene[1]	17	6	60	0.4	20	0.5	ND		45	0.5	49	0.6
dibenzo[def,mno]chrysene[1]	ND		ND		6	2	ND		23	0.7	13	1
coronene	ND		242	2	101	1	33	3	239	3	185	2
MW 302 isomers[1]	ND		72	0.5	33	0.5	ND		100	1	69	1

[1] Analyte identification based on comparisons to relative retention times to those in the literature.
[2] ND = not detected

5.4 Conclusions

Size distributions for particulate hopanes+steranes and nonvolatile PAHs emitted from five classes of light-duty gasoline-powered vehicles were measured using the Federal Test Procedure (FTP), Unified Cycle (UC), and Correction Cycle (CC) driving cycles. 17α(H)-21β(H)-29-norhopane, 17α(H)-21β(H)-hopane, αββ-20R-stigmastane and αββ-20S-stigmastane were highly correlated and behaved consistently across sampling methods. Coronene and benzo[ghi]perylene were the most ubiquitous heavy PAHs detected in the vehicle exhaust.

Hopane+sterane distributions emitted from vehicles without an operating catalyst (including "cold-start" emissions) were bimodal with one mode between 0.1-0.18 μm and the second mode > 0.32μm diameter. Hopane+sterane emissions released from vehicles with an operating catalyst had a single mode between 0.1-0.18 μm diameter. Hopane+sterane emissions from visibly smoking vehicles had a single mode between 0.18-0.32 μm diameter. Heavy PAH size distributions for all vehicle classes consistently had a single mode between 0.10-0.18 μm particle diameter (0.1-0.32 μm diameter for smoking vehicles). The geometric standard deviations for PAH size distributions were generally smaller than the corresponding hopane+sterane distributions.

PAH, hopane and sterane emissions shifted to smaller sizes during the more aggressive UC and CC driving cycles relative to the FTP. The fraction of PAH, hopane and sterane emissions in the ultrafine (D_p<0.1 μm) range more than doubled during "warm-start" UC and CC cycles vs. the FTP cycle. The enhancement of ultrafine PAHs during "cold-start" UC driving cycles was less pronounced. Source-profiles constructed using (analyte mass) / (organic carbon (OC) mass) in the fine and ultrafine size fractions were approximately equal during all FTP tests except for enhanced ultrafine (hopane+sterane) / OC concentrations emitted from passenger cars equipped with three way catalysts. The PAH / OC concentrations in the ultrafine size fraction decreased by an order of magnitude under the UC vs. FTP driving cycle. These trends suggest that hopanes+steranes and heavy PAHs act as tracers for separate processes of particulate organic carbon formation.

6 ELEMENTAL COMPOSITION OF GASOLINE, DIESEL FUEL, AND LUBRICATING OIL FROM LIGHT-DUTY GASOLINE AND HEAVY-DUTY DIESEL VEHICLES

6.1 Introduction

Many studies have analyzed particulate matter (PM) emissions from motor vehicles and detected the presence of several transition metals and other elements *[24, 32, 63]*. The elemental composition of PM collected near roadways *[109]* and exposure to these freeway emissions *[110-112]* are of considerable interest. The elemental composition of motor vehicle PM has been utilized for source apportionment of ambient aerosols via numerical methods such as positive matrix factorization *[113, 114]*. However, few studies have investigated the elemental composition of in-situ motor vehicle fuels and oils. Knowledge of the elemental composition of these base combustion components is important for interpreting the composition of motor vehicle PM emissions and ultimately the contributions that these emissions make to ambient PM and human exposure.

This chapter reports the elemental composition of gasoline, diesel fuel, and lubricating oils sampled from in-use vehicles utilized in previous chassis dynamometer PM emissions studies. Elemental composition was determined by Inductively-coupled Plasma-Mass Spectrometry (ICP-MS) methodologies for these fluids either in their native (gasoline and diesel fuel) or diluted (lubricating oil) forms. Due to problems with sample introduction, sooting, system stability, and organic fragment interferences, ICP-MS has not traditionally been viewed as the most appropriate technique for the measurement of trace metals in organic matrices, especially those with low vapor pressures [115]. These obstacles have been overcome in the current study via the implementation of an intelligent and optimized system design, the use of a multi-mode octopole, the introduction of oxygen into the carrier gas, and a careful selection of system components, tuning parameters, and operating guidelines.

The elemental composition data from this study will enhance the interpretation of related research considering motor vehicle PM emission composition and ambient roadside PM measurements.

6.2 Methods

6.2.1 Sample Collection and Storage

Gasoline, diesel fuel, and motor oil samples were collected from vehicles studied during two separate chassis dynamometer experiments. Gasoline and motor oil from LDGVs were collected in the summer of 2002 at the California Air Resources Board (ARB) Haagen-Smit laboratory in El Monte, CA. Particulate matter emissions of 30 LDGV vehicles of various technology classes were collected using various driving cycles [40]. Diesel fuel and motor oil from HDDVs were collected in the summer of 2003 at the West Virginia University transportable dynamometer facility in Riverside, CA. The PM

emissions of four HDDVs were collected using partial or full driving cycles and under varying simulated inertial loads [93].

LDGV oil samples and HDDV diesel fuel samples were analyzed independently from each vehicle examined. However, LDGV gasoline samples were composited into seven samples prior to analysis and individual LDGV gasoline sample composition is not reported herein. The seven LDGV gasoline composite samples represent equal fractions (by volume) of the following vehicle categories: low emission vehicle (LEV) passenger cars (PCs) [n=5] and light duty trucks (LDTs) [n=5], three-way catalyst (TWC) PCs [n=6], TWC LDTs [n=5], oxidation catalyst vehicles (OCATs) [n=3], non-catalyst equipped vehicles (NCATs) [n=2], and vehicles visibly emitting blue smoke (SMOKERS) [n=2].

Gasoline and diesel fuel samples were stored in clear glass ~50 mL bottles (QPak), and oil samples were stored in amber ~20 mL vials at -18^{o}C until analysis. Because glass is known to contain several elements measured in this study *[116]*, a complementary laboratory experiment was performed to quantify metals leached from clear and amber glass vials using the ICP-MS methodology herein. A 30 mL volume of a 75% acetone : 25% 1 N HNO3 solution (m/m) was stored in three Corning vials, thee clear glass vials, and thee amber vials for 24 hours. All vials were placed on a shaker table for two hours during this period. Fluid extracts and applicable standards were analyzed with an Agilent 7500i ICP-MS using oxygen introduced into the carrier gas. Results of this analysis showed minimal concentration of elements of interest from clear glass; the concentrations were higher from the amber vials. However, since the motor oil samples in this study were diluted by factors of 200 to 250, no blank subtraction based on the leaching of elements from either clear or amber storage vessels was conducted.

6.2.2 ICP-MS Methodology

Sample analysis was carried out in this study using a conventionally configured Agilent 7500ce ICP-MS (Agilent, Palo Alto, CA). Gasoline, diesel fuel, and diluted motor oil samples – as well as associated rinses, blanks, and standards – were drawn from sample vials (50 mL Corning polypropylene, Fisher Scientific, Pittsburgh, PA) using a peristaltic pump at a flow rate of 0.4mL/min and nebulized using a Micromist nebulizer (AR35-01-FM005, Glass Expansion Inc., Pocasset, MA) with argon carrier gas at 0.61 L/min. The resultant fine mist passed through a cooled (-5^{o}C) double-pass spray chamber that removed larger droplets and spray condensation. Sample spray was mixed with pure oxygen (99.995%, Airgas, Sacramento, CA) using a 'tee' upstream of the quartz torch (1.5mm inner diameter)Glass Expansion) and then with argon at 16 L/min as the plasma gas. and energized it A radio frequency coil with 1550W of forward power sustained the plasma, evaporated the remaining solvent, decomposed the resulting aerosol, dissociated molecules and ionized the elements. The plasma was then drawn through nickel cones and positive ions extracted with a series of lenses into the vacuum chamber. The ionbeam passed through an octopole collision/reaction cell which was operated in three modes – one without gas flow, one with He gas flow, and one with H_2 gas flow.

Detection was achieved with a quadrupole mass spectrometer. ICP-MS Chemstation software (Agilent) was used to control the instrument and to provide count-per-second quantification of individual elemental species and isotopes.

6.2.3 Gasoline, Diesel Fuel, and Motor Oil Analyses

Diesel fuel and composite gasoline samples were analyzed without dilution. Due to the low viscosity and heavy sample loading of the motor oil, both LDGV and HDDV oil samples were diluted in PremiSolv ICP Solvent (Conostan, Ponca City, OK). LDGV oil samples were diluted by a factor of 200 and HDDV oil samples were diluted by a factor of 250.

Since no standardized laboratory grade gasoline or diesel fuel was available, the rinses, blanks, and standard matrix fluids for the gasoline and diesel fuel analyses were purchased commercially. The base gasoline used in this study was an ARCO 87 octane gasoline purchased in Woodland, CA. The base diesel fuel used in this study was a Chevron diesel fuel purchased in West Sacramento, CA. Both fuels were stored at room temperature in new Department of Transportation approved fuel containers until use in the laboratory. The base matrix for motor oil analyses was PremiSolv ICP solvent (Conostan), which is designed for use as a diluent in ICP analyses of metals in oil and other organic fluids and is completely miscible with motor oil, as well as with gasoline and diesel fuel in small amounts (< 10% v/v).

Laboratory calibration standards were made from a commercially available stock solution of an oil-based 23-element standard (Conostan) and a mixture of 12 commercially available single-element oil-based standards (Conostan). These stock solutions were diluted using the base gasoline, base diesel fuel, and PremiSolv. Although instrument response varied between sample matrices, as a qualitative assessment the elemental concentrations of the base gasoline and diesel fuel were investigated using the certified PremiSolv-based standards. Results indicated that the base gasoline and diesel fuels had negligible elemental composition concentrations compared to the samples of interest, and were thus suitable for base fluids in this experiment. Recovery experiments were also performed satisfactorily as part of this assessment and are inherent in the calculation of instrument and method detection limits. Seven-point calibration curves were run for each set of standards with standard concentrations ranging from 10 – 1000 ppb (ng/mL) for gasoline and diesel fuel analyses and 100 – 10000 ppb for motor oil analyses.

Three methods were employed in this study to analyze the gasoline, diesel fuel, and motor oil samples. Each method scanned the mass spectrum in a no-gas mode, a helium mode, and a hydrogen mode for a subset of elements as shown in Tables 6-2 and 6-3. The main difference in the three methods was the oxygen flow rate, which was balanced to prevent sooting due to incomplete combustion while also preventing oxidation of the ICP-MS sampling and/or skimmer cones. In addition, the He and H_2 were slightly different for the three types of samples. For gasoline: oxygen flow, He flow

and H_2 flow were 0.12 L/min, 5mL/min and 2.5mL/min respectively; for diesel fuel: 0.09 L/min, 5mL/min and 4.5mL/min and for motor oil: 0.04 L/min, 4.5mL/min and 4mL/min. The ICP-MS was tuned in each mode prior to sample analysis using a 100 ppb solution of the Spex2 a 23-element standard (vendor, location) to maximize instrument sensitivity while minimizing interfering signals. Sequences of dedicated rinses, blanks, standards, and successive rinses and blanks were employed prior to sample introduction with periodic dedicated rinses interspersed in the sample sequence. Analysis time for one sample was ~19 minutes, which includes rinsing of previous sample and uptake, plus stabilization and acquisition periods for each sample in all 3 modes.

Six replicate measurements were made for each count-per-second data point, with each element scanned for 0.1 second in no-gas mode and 0.5 second in He and H_2 modes. Raw data files were converted to count-per-second data using the FileView32 program (Agilent). Calibration curves were manually generated, reviewed for QA/QC (blank subtraction, slope, R^2) and applied to the raw count-per-second data as applicable. All elemental concentrations are reported in ppb units, corrected for dilution where applicable.

Sample sets were analyzed from cleanest to dirtiest; gasoline samples were first, followed by diesel fuel, and finally motor oil. The nebulizer and sample/skimmer cones were cleaned between sample sets, followed by several hours of throughput with base rinse fluid.

6.2.4 Expected Interferences and Mode/Isotope Choices for Data Reporting

Traditionally ICP-MS has not been considered as the most appropriate technique for the measurement of trace metals in organic matrices due to perceived problems with sample introduction, plasma stability, carbon deposition on the interface and lenses, and the formation of carbon-based interferences [115]. All but carbon-based interferences were resolved via careful choices concerning method development parameters along with the appropriate system components and operational guidelines.

The issue of carbon-based interferences is pertinent to this study and deserves further discussion. Based on knowledge of the sample matrices' chemical structures and compositions used in this study, and the interaction of these matrices with argon and oxygen, the following compounds could possibly interfere with the listed elements having similar mass-to-charge ratios: (a) the tail of ^{12}C with B, (b) C_2 and C_2H with Mg, (c) C_2H_3 and CHN with Al, (d) C_2H_4 and C_2H_5 with Si, (e) Ar with Ca, (f) ArC and ArCH with Cr, (g) ArOH with Fe, and (h) C_5 fragments with Ni, Cu, and Zn.

To minimize these potential interferences, many elements were analyzed in more than one ICP-MS analysis mode. Si, P, S, K, and Sc were all analyzed in the no-gas, He, and H_2 modes. B, Na, Mg, and Ca were analyzed in the no-gas and H_2 modes. Al, Ti, V, Cr, Mn, Fe, Co, Ni, Cu, Zn, As, Se, and Cd were analyzed in the no-gas and He modes. All remaining elements were analyzed solely in the no-gas mode. Additionally, multiple

isotopes (m/z ratios) of several elements were analyzed, specifically Mg, Si, Ca, Cr, Ni, Cu, Zn, and Se.

Analysis of multiple isotopes and use of multiple instrument modes yielded a matrix of quantitative results with respect to elemental concentrations. In the majority of cases, quantitative results across instrument modes and element isotopes were very similar and thus internally consistent and valid. As expected, there were some differences between modes and/or isotopes. However, the order of these differences was less than the variability across samples within the LDGV and HDDV data sets. Whereas the quantitative data rarely differed by more than a factor of two across instrument modes or isotopes, it commonly differed by orders of magnitude across individual vehicle samples. Given this fact and to maintain consistency throughout this study, all concentration data for an element across instrument modes and isotopes was averaged and compared to an MDL that was subjected to an identical mathematical transformation. For example, the data for Cu presented throughout this manuscript represents and average of the Cu concentration data for ^{63}Cu and ^{65}Cu in both the no-gas and He analysis modes, for a total of 4 measurements. Likewise, the single MDL for Cu reported herein is the average of the four MDLs for ^{63}Cu and ^{65}Cu in both the no-gas and He analysis modes.

6.2.5 Method Precision and Accuracy

Measures of the gasoline, diesel fuel, and motor oil methodologies' precision and accuracy were obtained via the calculation of method detection limits and the comparison of duplicate measurements.

Instrument detection limits (IDLs) were calculated using U.S. Environmental Protection Agency methodology (40 CFR 136) in which the IDL is equivalent to 3 times the standard deviation of a seven duplicate measurements run over three non-consecutive days. The samples used for this calculation are low-concentration standards. Thus the IDLs reflect methodological variability from each sample handling and analysis step in the laboratory including fluid transfer steps; cleanliness of vials, pipette tips, and other equipment that comes in contact with the samples; instrument cleanliness; tuning parameters and resultant instrument sensitivity and noise; and quantification effects. The IDLs are in essence based on a series of spiking and recovery experiments; more accurate recoveries results in lower the IDLs. The results of the individual recovery experiments are not presented herein.

MDLs for the gasoline and diesel fuel samples are the same as the IDLs since those samples were not diluted prior to processing. However, since the LDGV and HDDV oil samples were diluted by factors of 200 and 250 prior to analysis, the MDLs for those methods are 200 and 250 times their respective IDLs. IDL and MDL values for each method are presented below in Table 6-1.

Table 6-1: ICP-MS instrument and Method Detection Limits (ppb).

	IDL = MDL		IDL	MDL	
element	LDGV gasoline	HDDV diesel fuel	motor oil	LDGV oil	HDDV oil
B	15.8	32.7	74.4	14871	18589
Na	7.7	34.2	134.0	26801	33501
Mg	26.8	40.4	32.2	6449	8061
Al	15.6	43.3	6.9	1372	1715
Si	41.8	31.7	131.2	26246	32807
P	32.8	2.1	29.3	5866	7332
S	15.1	19.9	46.8	9359	11699
K	34.0	35.2	45.0	8990	11238
Ca	15.3	29.5	16.8	3370	4212
Sc	39.6	43.9	41.1	8211	10263
Ti	24.1	23.9	14.9	2984	3730
Cr	32.4	26.4	17.3	3460	4325
Mn	25.7	14.5	4.2	836	1046
Fe	24.8	24.3	8.2	1640	2050
Ni	37.7	43.1	11.3	2255	2819
Cu	24.9	13.3	2.5	495	619
Zn	38.8	31.8	2.7	531	664
Se	38.6	33.6	20.6	4129	5161
Sr	20.3	16.9	9.4	1876	2345
Mo	26.7	11.0	1.6	317	396
Ag	19.9	11.5	1.4	281	352
Cd	30.7	15.1	1.8	361	451
Sn	23.3	11.8	1.2	242	302
Sb	23.4	11.7	1.0	204	255
Ba	23.5	12.6	1.7	344	430
Pb	22.4	9.1	1.6	313	391

Method accuracy was assessed by comparing duplicate measurements as shown below in Figure 6-1. Panel (a) shows the agreement between elements above MDL for two fuel composites from the same set of five LEV LDTs. Panel (b) shows the agreement for data above MDL between two sets of LDGV oil samples, the first sampled after a dilution of 20X (x-axis) and the second after a dilution of 200X (y-axis). Panel (c) presents data analogous to panel (b) for the HDDV oil samples, the first data set diluted by a factor of 25X (x-axis) and the second by a factor of 250X (y-axis). The dotted line in each panel represents a 1:1 relationship. In each case the duplicate measurements agree well with very high R^2 values.

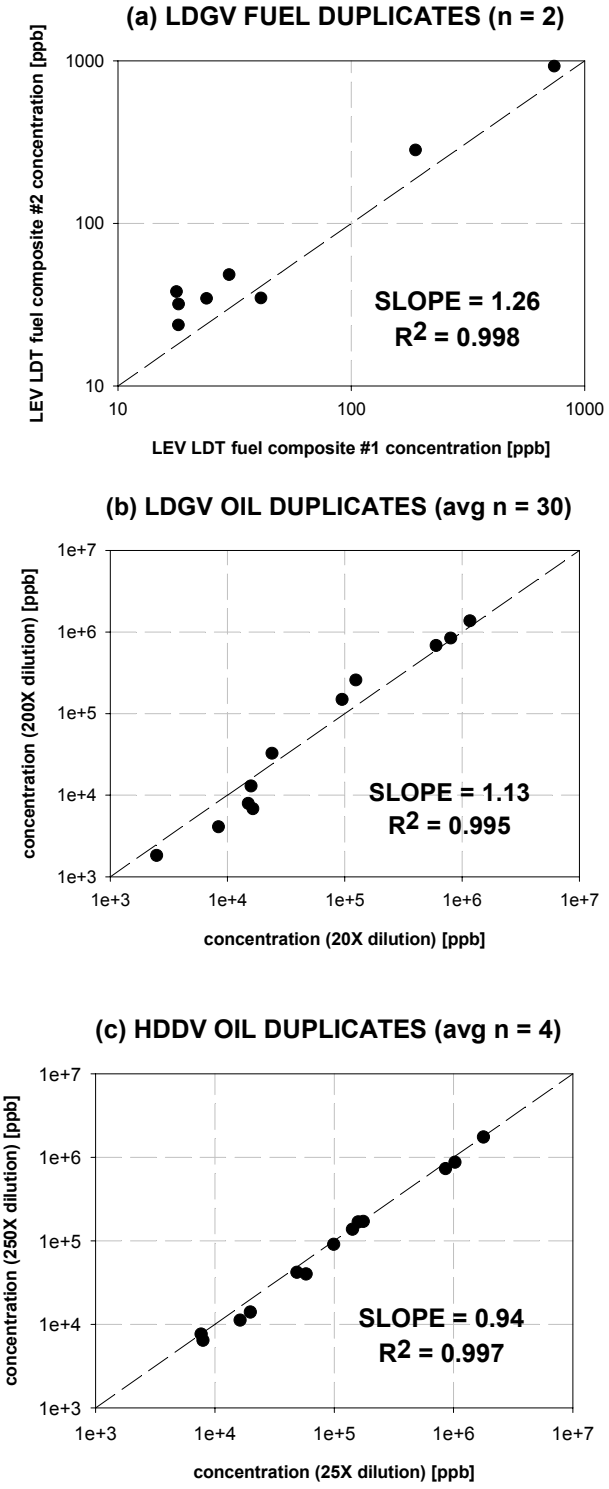

Figure 6-1: Comparison of duplicate fuel and oil measurements made using ICPMS.

6.3 Results and Discussion

6.3.1 Elemental Composition of Gasoline, Diesel Fuel, and Motor Oil.

Table 6-2 presents the elemental composition of LDGV gasoline and HDDV diesel fuel in units of ppb (ng element mass per gram of solution) for each sample set. Each column represents data from a single sample – composite gasoline samples for LDGVs and individual vehicles for HDDVs. Table 6-3 presents analogous data for motor oil collected from the same LDGVs and HDDVs. Data in the LDGV columns of Table 6-3 represent measurements from multiple motor oil samples (one per LDGV) averaged into the same composite scenarios as the gasoline samples in Table 6-2; data in the HDDV columns represent individual vehicles as in Table 6-2. Values above MDL in Tables 6-1 and 6-2 are shown in clear boxes while values below MDL are shown in gray boxes.

The most abundant elements observed in the LDGV gasoline was S (~1 ppm), followed by Si (473 ppb), Ni (61 ppb), Fe (40 ppb), and Cu (38 ppb), with all other element averages below MDLs. Two of the sample sets had concentrations of K above its MDL. Sulfur in gasoline originates from sulfur-containing compounds present in the base crude oil feedstock that were not completely removed during the refining process. The fact that S concentrations were virtually uniform in all the fuels at ~1ppm confirms that this element is not enhanced by the host vehicle. Sodium can be introduced into gasoline either from saltwater contamination of the crude oil feedstock or as part of the de-sulfurization process that includes a caustic wash step. Most of the remaining detected elements also likely originate from the refining process and the removal of sulfur from the gasoline. Silica, iron, nickel, and copper are all present in zeolites that can be used to remove sulfur from gasoline. Several gasoline samples also contained detectable amounts of potassium and scandium that may also originate from catalysts.

As reported in Table 6-2, elemental concentrations in HDDV diesel fuel were generally observed to be higher than in LDGV gasoline. Average S concentrations in the HDDV diesel fuel was ~16 ppm, reflecting the current trend of low S content in California diesel fuel. The next most abundant element averages were for Zn (7970 ppb), Ca (5522 ppb), P (2705 ppb), Si (1652 ppb), and Sr (1063 ppb). Ten other element averages were also above their MDLs. There was significantly more relative variability within the HDDV diesel fuel compositions than between the LDGV elemental compositions. Elements detected in the diesel fuel may have originated during the refining process, from diesel fuel additives, or from within the test vehicles. Many diesel fuel additive products are currently available including antigels, cetane boosters, de-icers, emissions reducers, fuel and tank cleaners, fuel savings additives, injector cleaners, microbial clean-ups, and water removal additives. Some of these additive packages are known to contain Sr and Fe. Others may originate from fuel oil compositions engineered to reduce particulate emissions – the antismoke properties of the salts of different metals including Ca, Ba, Mg, Fe, Ni, Mn, and Cu have been well established *[117]*. Fe, Mo, and Ni may originate from contact with steel and Cu from tubing or brass fittings. Ag could

be from solder; it has been increasingly phased in as Pb is phased out and produces very versatile and strong joints.

Table 6-3 presents the elemental composition from the LDGV and HDDV motor oil data sets. Concentrations of all elements are much higher than those of either LDGV gasoline or HDDV diesel fuel samples. This is somewhat expected since motor oil is re-circulated throughout an internal combustion engine typically over many thousands of miles, whereas fuel is consumed over the course of only several hundred miles of vehicle distance traveled.

Zn and P, two of the three most abundant elements observed in the motor oil samples, are the prime anti-wear additives in today's motor oils. These additives provide protection from metal-to-metal contact on surfaces and when oil pressure is too low to build up a protective film. Acid neutralizers are also commonly added to production motor oils. S was the most abundant element in the gasoline and diesel fuel samples. During the combustion process, this sulfur can combine with oxygen to form sulfur dioxide, or sulfuric acid. Sulfuric acid and other corrosive compounds can work their way past piston rings and into motor oil where it is circulated throughout the engine. To prevent these acids from destroying internal machined surfaces, anti-corrosion additives such as Mg, Ca, and B are often utilized. These three elements were also observed in high concentrations in the LDGV and HDDV motor oil data sets.

Figure 6-2 presents the range of LDGV gasoline (panel a) and motor oil (panel b) data measured in this study as a box and whisker plot illustrating (from bottom to top) the minimum observation, lower quartile, median, upper quartile, and maximum observations. MDLs for each element are shown as an asterix (*). Individual oil samples are shown in Figure 6-2b rather than mathematically compositing them as was done in Table 6-3. Figure 6-3 likewise presents the variability in the HDDV diesel fuel and motor oil samples. Due to the small number of samples (n=4), construction of a box plot was not possible. For each measurement, the average, and the MDL is therefore presented for every element.

Trends between the LGDV and HDDV data sets are consistent with Ca as the most abundant element (averaged concentration of 1370 LDGV and 1743 ppm HHDV), followed by Zn (842 ppm LDGV and 872 ppm HDDV), P (682 ppm LGDV and 732 ppm HDDV), S and K (257 ppm LDGV and 168 ppm HDDV, 228 ppm LDGV and 171 ppm HDDV). Several other elements were present in averaged concentrations above their MDLs, including, in decreasing order of HDDV abundance, Mg, Na, Fe, Sr, B, Mo, Pb, Ag, Si, Cu, and Ni. Two of the LDGV composited data sets also had Al levels above its MDL. As shown in Figures 6-2b and 6-3b, there is considerable variability between individual samples with the LDGV and HDDV data sets for most elements, with less relative variability among data points near or above MDLs. As with the gasoline and diesel fuel data sets, there is no apparent correlation between elemental concentrations and vehicle class (LDGVs) or individual vehicles (HDDVs). This observation implies that the variability in elemental composition is a function of a difference aspect of

differences between vehicles, such as the age of the oil (i.e. time elapsed since most recent oil change), vehicle maintenance, or differing operational practices.

Table 6-2: LDGV Gasoline and HDDV Diesel Fuel Elemental Composition (ppb).

	LDVs							HDDVs			
	LEVs		TWC		OCAT	NCAT	SMKR				
element	PCs	LDTs	PCs	LDTs				HDDV-1	HDDV-2	HDDV-3	HDDV-4
B	0.0	0.0	0.0	0.0	0.0	0.0	0.0	0.0	0.0	11.7	389.2
Na	48.4	39.1	51.9	98.9	45.3	108.4	76.1	1489.9	3018.2	4203.8	8179.0
Mg	0.0	0.0	0.0	0.0	0.0	0.0	0.0	0.0	0.0	34.6	2731.9
Al	0.0	0.0	0.0	0.0	0.0	0.0	0.0	0.0	0.0	0.0	12.1
Si	271.3	235.6	289.5	741.1	204.0	978.4	588.3	1903.5	1810.6	1718.3	1177.4
P	0.0	0.0	0.0	2.3	0.0	0.0	0.0	480.7	1229.4	1103.8	8007.6
S	953.6	834.0	890.5	1010.0	940.3	1214.5	1201.2	18794.1	19474.8	7173.9	18462.3
K	19.0	20.9	18.8	35.2	10.9	49.1	32.0	37.7	49.4	52.0	38.4
Ca	0.0	1.2	0.0	12.2	0.0	8.3	4.8	14.9	86.7	3465.0	18521.3
Sc	39.8	27.9	42.7	68.3	20.6	135.9	84.6	0.0	0.0	0.0	0.0
Ti	0.0	0.0	0.0	0.0	0.0	0.0	0.0	0.0	0.9	0.0	254.6
Cr	1.5	5.2	2.3	11.5	0.0	17.2	7.5	0.0	22.1	13.7	9.5
Mn	0.2	0.0	0.0	0.2	0.0	0.6	0.1	9.6	15.0	10.8	45.5
Fe	20.0	25.0	18.2	50.3	4.4	117.3	43.6	6.3	285.8	20.4	1187.6
Ni	46.5	29.2	58.9	50.2	61.2	97.4	80.9	200.6	191.7	0.0	0.0
Cu	53.3	37.9	44.5	55.0	29.0	31.0	14.5	14.3	8.9	11.0	383.9
Zn	1.2	1.2	1.2	31.3	3.8	35.0	4.2	30.5	153.2	4525.4	27170.7
Se	1.1	1.3	0.9	1.3	0.7	1.6	0.7	10.8	10.0	2.6	0.4
Sr	0.0	0.0	0.0	0.0	0.0	0.0	0.0	96.0	396.3	734.6	3026.9
Mo	0.0	0.0	0.0	0.0	0.0	0.0	0.0	2.3	4.1	255.6	46.6
Ag	0.0	0.0	0.0	0.0	0.0	0.0	0.0	0.3	0.4	0.0	8.1
Cd	0.0	0.0	0.0	0.0	0.0	0.0	0.0	0.0	0.0	0.0	8.5
Sn	0.0	0.0	0.0	0.0	0.0	0.0	0.0	1.2	6.9	0.1	13.6
Sb	0.0	0.0	0.0	0.0	0.0	0.0	0.0	0.0	0.1	0.0	3.0
Ba	0.0	0.0	0.0	0.0	0.0	0.0	0.0	0.0	13.8	14.5	92.1
Pb	0.0	0.0	0.0	0.0	0.0	1.2	0.0	40.1	33.8	35.9	791.0

Table 6-3: LDGV and HDDV Motor Oil Elemental Composition (ppb).

	LDVs							HDDVs			
	LEVs		TWC		OCAT	NCAT	SMKR				
element	PCs	LDTs	PCs	LDTs				HDDV-1	HDDV-2	HDDV-3	HDDV-4
B	16363	23786	10400	11486	88	8610	6507	18719	6153	5964	33414
Na	41869	45793	57575	59496	42203	34981	28664	0	184578	178783	0
Mg	156397	149631	84497	221772	191341	195804	41293	101478	78576	76447	293776
Al	3430	831	3459	2661	292	1611	461	0	2203	2276	105
Si	25474	26396	13783	13915	16643	12902	17707	8974	8900	8775	3509
P	725497	754731	625550	801465	549118	650696	665096	389762	915170	893407	723498
S	288017	300445	202668	265384	213995	236568	297730	110162	195603	192071	173654
K	19595	23866	61133	14081	13269	13166	14234	31855	320919	313427	14190
Ca	1495393	1638325	1378638	1449076	828990	1354176	1445108	970647	2327359	2334031	1341715
Sc	2917	4126	1744	2016	2871	1404	1618	593	274	356	418
Ti	1866	1938	1238	2024	1036	1345	2294	222	1586	1525	989
Cr	2931	910	2257	1832	117	48	551	0	4506	4392	0
Mn	1375	10	337	270	303	0	0	0	384	259	0
Fe	22543	5249	32606	19998	1954	6830	1304	8961	71114	71083	16701
Ni	7393	4169	4135	8358	5382	5849	4585	0	0	2723	6635
Cu	19564	5242	5191	5406	4196	13859	1759	0	12394	12261	980
Zn	864139	897422	753022	1026368	654452	851819	844605	492899	1042169	1034230	918425
Se	0	17	155	0	4	0	0	886	315	178	97
Sr	13361	9544	17611	27706	125976	0	34030	23375	55444	44430	36559
Mo	0	7017	5761	6128	698	0	28168	23935	15370	15114	1597
Ag	794	845	2786	1620	656	690	165	5723	11905	7768	5044
Cd	771	97	587	533	87	0	0	12	674	305	0
Sn	178	0	0	0	0	0	1777	0	512	574	0
Sb	0	70	0	0	0	0	2036	0	0	0	0
Ba	378	2032	0	130	763	0	0	0	30	0	0
Pb	3276	1536	4360	0	0	0	19487	7	22141	21822	715

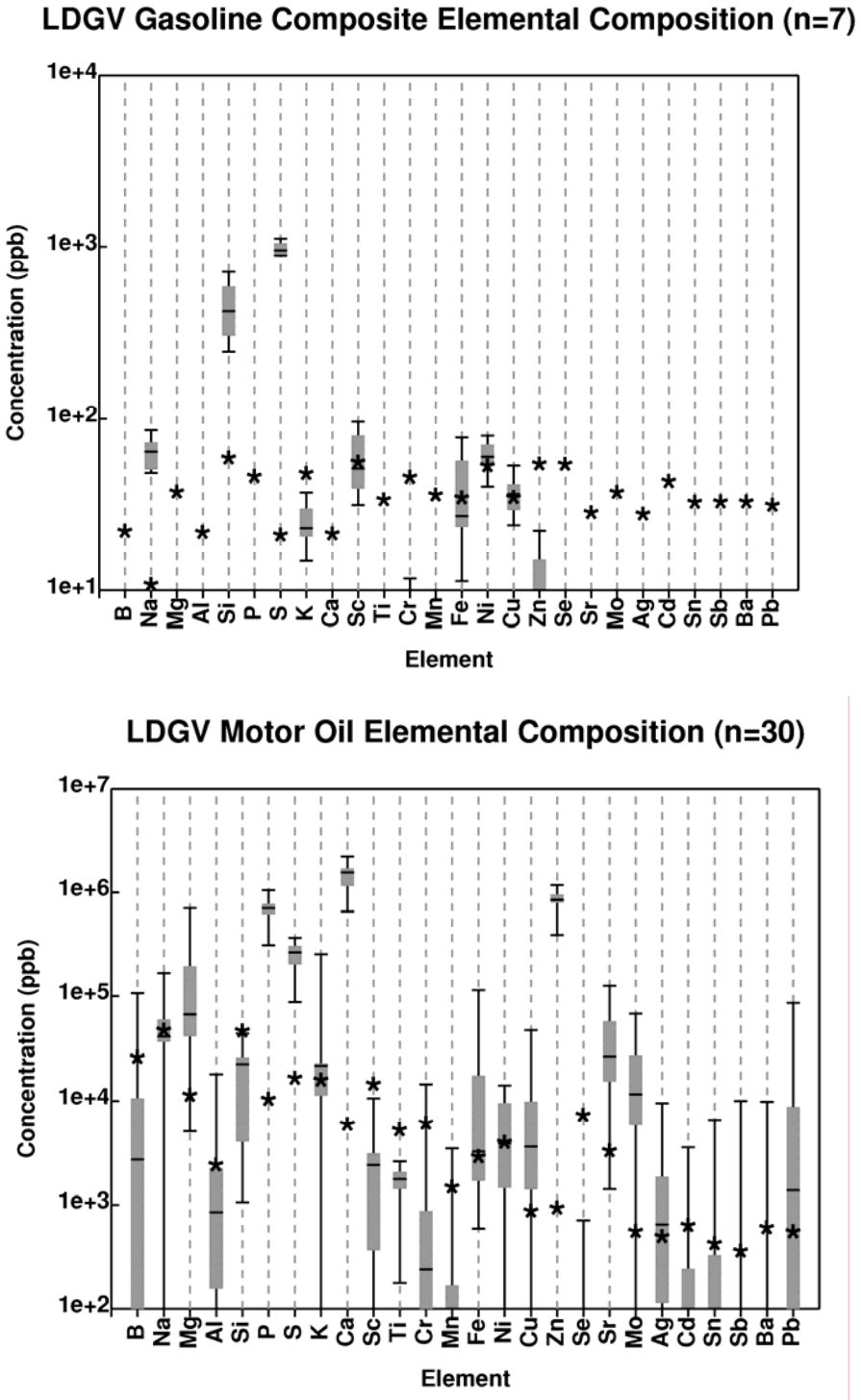

Figure 6-2: (a) LDGV gasoline composite elemental composition (ppb, n=7) and (b) LDGV motor oil elemental composition (ppb, n=30) measured using ICP-MS. Asterisks denote MDL values.

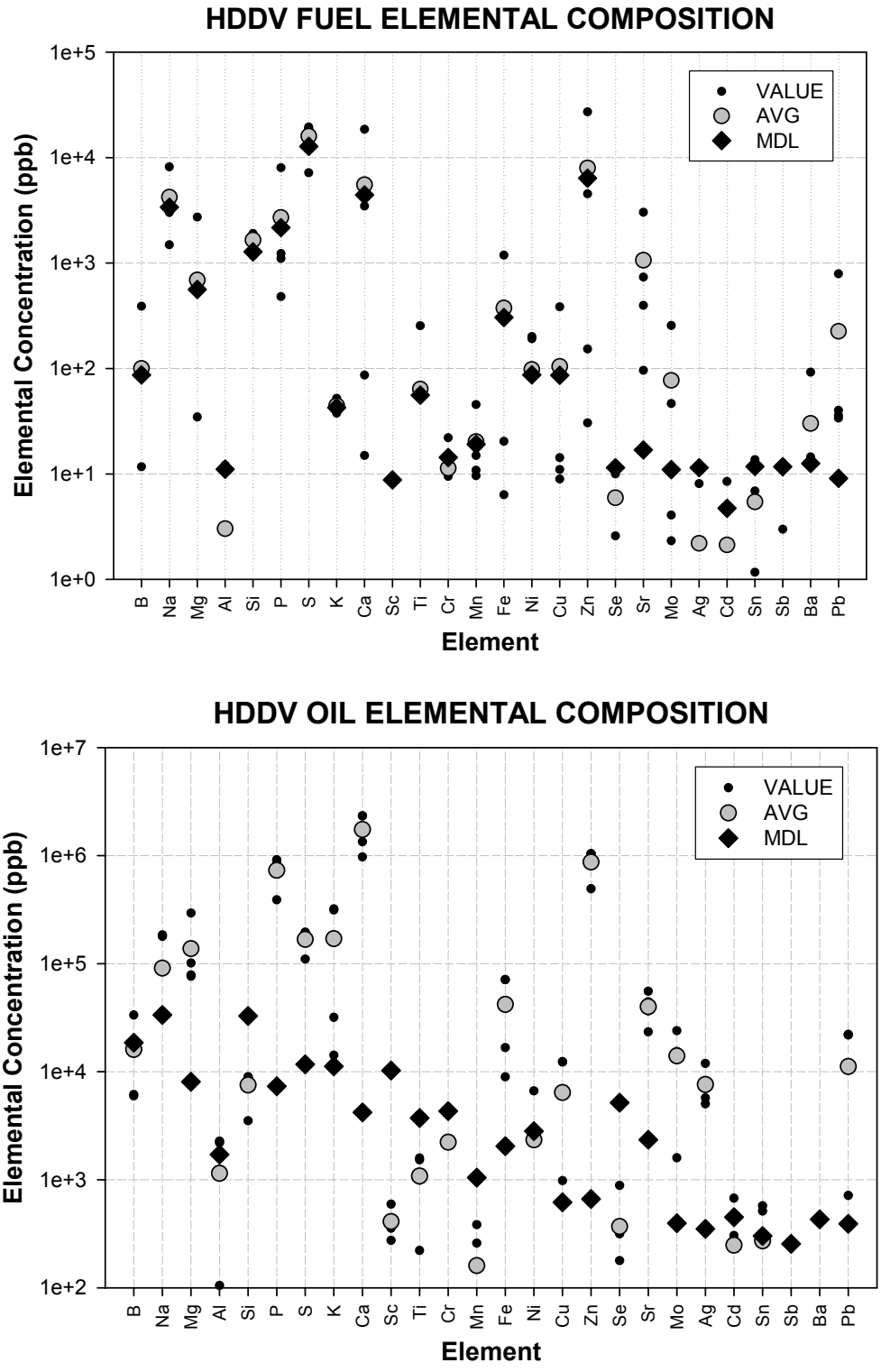

Figure 6-3: HDDV (a) Diesel Fuel and (b) Motor Oil elemental composition measured using ICP-MS.

6.3.2 Comparisons to Other Studies

Although several previous studies have quantified the elemental composition of particulate matter exhaust from gasoline and diesel vehicles *[24, 32, 63]*, very few have quantified the elemental composition of gasoline or diesel fuel, and virtually none have quantified the elemental composition of motor oil as sampled from in-use vehicles. Agilent Technologies, Inc. previously quantified the elemental composition of base gasoline fuel obtained directly from the gas station pump of a leading petroleum company [115]. This study was conducted in the UK and observed the most abundant metals to be Si (317 ppb), P (310 ppb), Pb (25 ppb), Zn (12 ppb), Mg (5 ppb), and Ca (4 ppb), with lesser amounts of Al, Ti, V, Cr, Mn, Fe, Ni, Cu, Mo, Cd, Ag, and Ba. In comparison, the most abundant metals observed for the average of all gasoline composites were S (1006 ppb), Si (473 ppb), Ni (61 ppb), Fe (40 ppb), Cu (38 ppb), and K (27 ppb). S and K were not reported in the Agilent study and there were similar concentrations observed between studies for Si, Ca, and Zn. The differences in the values between the studies can be attributed to many factors including (a) differences in fuel composition based on geographic location, (b) differences in new station fuel versus tank fuel from in-use LDGVs, and (c) the number of samples quantified. With respect to the last difference, in many cases the data reported in Agilent study are of similar scale of at least one of seven LDGV composite fuels analyzed in this study (notable exceptions are P, Ni, Cu, and Pb).

Wang et al. [118] quantified the metals content of both diesel fuel and exhaust for an in-use diesel engines in Taiwan. The most abundant metals reported in the diesel fuel were Si, Ca, Al, Fe, Mg, and Zn, and significant concentrations of all other metals in Table 6-3 except P, S, and K (which were not reported). The most abundant metals in diesel fuel from this study are S, Zn, Ca, P, Si, and Sr. Except for Zn and Sr, the concentrations reported by Wang et al. were much higher (generally 1-2 orders of magnitude) than reported in this study. These large differences are likely attributed to differences in California versus Taiwanese diesel fuel formulations. .

These two comparisons highlight the lack of studies in this area as well as the high degree of variability within data sets and between reported results. Many of these differences can be attributed to factors not associated with testing methodology, but as shown in the present study significant variability still exists within the same geographic region and based on the same available base fuels and oils. It is important that any emissions mitigation strategy recognize contributions from fuel and oil constituents to emissions and consider the high degree of potential contamination variability in fuels and oils following purchase but prior to combustion.

6.4 Conclusions

Gasoline, diesel fuel, and motor oil samples, obtained from light-duty gasoline and heavy-duty diesel vehicles, were analyzed for their elemental composition using Inductively Coupled Plasma – Mass Spectrometry. Elemental composition was determined using multiple instrument octopole modes and including the introduction of

oxygen in the carrier gas. The most abundant elements observed in gasoline from light-duty gasoline vehicles (LDGVs) were S, Si, Ni, Fe, and Cu; in diesel fuel from heavy-duty diesel vehicles (HDDVs) the most abundant elements were S, Zn, Ca, P, Si, and Sr. Trends between the LGDV and HDDV motor oil data sets are consistent with Ca as the most abundant element followed by Zn, P, S and K. The primary source of these elements in gasoline is expected to come from within the vehicles sampled whereas the primary source of elements in diesel fuel and motor oils is likely from additive packages.

7 ELEMENTAL COMPOSITION OF PARTICULATE MATTER EMISSIONS FROM LIGHT-DUTY GASOLINE AND HEAVY-DUTY DIESEL VEHICLES

7.1 Introduction

Previous research reported the carbonaceous and ionic content of ultrafine and fine particulate matter (PM) from Light-Duty Gasoline Vehicles (LDGVs) and Heavy Heavy-Duty Diesel Vehicles (HDDVs), concluding that these species constituted the bulk of fine PM emissions based on reconstructed mass distributions [40, 93]. Although the elemental composition of motor vehicle emissions, especially their trace metal content, is a relatively small amount of the total PM mass, it is of interest for several reasons. Stohs and Bagchi reported that metals play an important role in many toxicological mechanisms including redox cycling, the production of reactive oxygen species, fenton-like reactions, and the induction of the production of stress proteins *[119]*. Characterization of and exposure to these elemental components of motor vehicle PM, especially in the vicinity of roadways, has been an area of active research *[120, 121]*. The existence of trace metals in atmospheric droplets results in appreciable impacts on droplet chemistry including aqueous complexation reactions, redox reactions, and photochemical reactions.

This chapter reports the size-resolved elemental composition of PM emissions from LDGV and HDDV chassis dynamometer experiments. Previously collected PM emission samples were extracted and analyzed for their elemental composition using Inductively Coupled Plasma – Mass Spectrometry methodologies optimized for the analysis of motor vehicle PM. The resultant data reported as ultrafine (< 100 nm) and fine (< 1800 nm) emission factors (ng/km) and size-resolved and mass distributions, are compared to reported elemental compositions from gasoline, diesel fuel, and motor oil sampled from the same LDGVs and HDDVs [122], and will serve as the basis for the interpretation of related research characterizing the size and composition distributions of ambient PM sampled near a freeway.

7.2 Methods

7.2.1 Sample Collection and Storage

Particulate matter samples were collected from vehicles studied during two separate chassis dynamometer experiments as described in Chapters 2 and 3. Light-Duty Gasoline Vehicle (LDGV) PM samples were collected at the California Air Resources Board's Haagen-Smit laboratory in El Monte, CA in the summer of 2002. Heavy-Duty Diesel Vehicle (HDDV) PM samples were collected at the West Virginia University transportable dynamometer facility in Riverside, CA in the summer of 2003. Additional details of the 30 LDGV vehicles tested are reported in Chapter 3. Additional details of the 4 HDDVs tested using partial or full driving cycles and under varying simulated inertial loads are discussed in Chapter 2. LDGV and HDDV PM samples were collected on 47mm Teflon filters (Teflo R2PJ047, Pall Corp) in both studies and were stored at -16 °C for subsequent analyses.

7.2.2 ICP-MS Methodology

The sample analysis technique used in this study parallels that reported in Chapter 6 by Robert et al. [122]. In this method, extracted PM samples are analyzed using a conventionally configured Agilent 7500ce ICP-MS (Agilent, Palo Alto, CA). Using argon as a carrier gas at a flow rate of 0.67 – 0.70 L/min, a nebulized fine mist is passed through a cooled (-5C) double-pass spray chamber, mixed with pure oxygen (99.995%, Air Gas, Sacramento, CA) at a flow rate of 0.04 lpm, and then mixed with argon at 16 L/min as the plasma gas. The ICP-MS plasma is sustained with 1550W of forward power from an RF coil, which effectively ionizes the elements. Positive ions are extracted by a series of lenses and are steered through an octopole that was operating in three modes. In the first mode there is no gas flow within the octopole, in the second He flows through the octopole, and in the third H2 flows through the octopole. The use of these three modes minimizes interference from organic fragments in some cases. Ions of discrete mass-to-charge ratios were passed to a detector using a quadrupole and a count-per-second quantification was performed using Agilent's ChemStation software.

7.2.3 Instrument and Method Detection Limits

Instrument detection limits were calculated using U.S. Environmental Protection Agency methodology (40 CFR 136) in which the IDL is equivalent to 3 times the standard deviation of a seven duplicate measurements run over three non-consecutive days. This methodology is identical to the approach described in Chapter 6. Instrument Detection Limits (IDLs) per instrument mode and per every element isotope are presented in Table 7-1. Averaged MDL values for the elements presented in this study for each LDGV and HDDV data set are presented in Table 7-2.

Table 7-1: ICPMS instrument detection limits by mode and isotope.

	PM acetone MDLs (ppb)			
element // m/z	no gas	He mode	H2 mode	04/06 (He)
Li / 7	10			1
Be / 9	500			
B / 11	---		---	
Na / 23	10		33	14
Mg / 24	---		1821	11
Mg / 25	---		---	45
Al / 27	9	8		36
Si / 28	527	525	337	---
Si / 29	565	594	548	---
P / 31	471	438	540	---
S / 34	297	340	327	---
K / 39	3	3	5	7
Ca / 40			15	12
Ca / 43	4		16	28
Sc / 45	28	23	19	40
Ti / 47	645857	8249		45
V / 51	7	7		0
Cr / 52	7	7		1
Cr / 53	6	7		4
Mn / 55	7	7		0
Fe / 57	12	7		8
Co / 59	7	7		0
Ni / 60	7	7		11
Ni / 62	6	7		12
Cu / 63	8	8		0
Cu / 65	8	8		0
Zn / 66	9	8		1
Zn / 68	8	8		2
As / 75	7	7		1
Se / 77	9	7		6
Se / 78	7	6		0
Sr / 88	7			0
Y / 89	3			0
Zr / 90	50			0
Mo / 95	14864			0
Ag / 107	7			0
Cd / 111	7	7		0
Sn / 118	32			0
Sb / 121	9759			0
Ba / 137	7			0
La / 139	3			0
Pb / 208	7			1
Bi / 209	7			0

Table 7-2: ICPMS method detection limits for LDGV and HDDV data sets.

	LIGHT-DUTY GASOLINE VEHICLES (mg/km)									HEAVY-DUTY DIESEL VEHICLES (mg/km)					
MDLs	LDGV-2	LDGV-3	LDGV-4	LDGV-6	LDGV-7	LDGV-8	LDGV-9	LDGV-10	LDGV-11	HDDV-1	HDDV-2	HDDV-3	HDDV-4	HDDV-5	HDDV-6
	LEV	TWC PC	TWC PC	TWC LDT/SUV			OCAT	NCAT	SMKR	#1 I/C	#1 HHDDT	#2 HHDDT	#2 HHDDT	#3 HHDDT	#4 HHDDT
element	FTP	FTP	UC	UC	CC	FTP	FTP	FTP	FTP	56K	56K	56K	66K	56K	56K
Na	4.34E+00	1.25E+01	1.94E+01	2.45E+01	9.33E+00	3.19E+01	2.12E+02	1.41E+02	1.41E+02	2.84E+03	4.38E+02	2.59E+02	4.60E+02	4.34E+02	4.26E+02
Mg	7.51E+04	7.53E+04	7.54E+04	7.55E+04	7.52E+04	7.57E+04	7.96E+04	7.80E+04	7.80E+04	5.17E+03	7.97E+02	4.71E+02	8.36E+02	7.89E+02	7.74E+02
Al	1.83E+00	5.28E+00	8.19E+00	1.03E+01	3.95E+00	1.35E+01	8.96E+01	5.95E+01	5.95E+01	1.20E+03	1.85E+02	1.10E+02	1.94E+02	1.83E+02	1.80E+02
P	9.89E+01	2.85E+02	4.41E+02	5.58E+02	2.13E+02	7.27E+02	4.83E+03	3.21E+03	3.21E+03	6.48E+04	9.99E+03	5.91E+03	1.05E+04	9.89E+03	9.71E+03
S	6.58E+01	1.90E+02	2.94E+02	3.71E+02	1.42E+02	4.84E+02	3.22E+03	2.13E+03	2.13E+03	4.31E+04	6.65E+03	3.93E+03	6.98E+03	6.58E+03	6.46E+03
K	7.26E-01	2.09E+00	3.24E+00	4.10E+00	1.56E+00	5.34E+00	3.55E+01	2.35E+01	2.35E+01	4.76E+02	7.34E+01	4.34E+01	7.70E+01	7.26E+01	7.13E+01
Ca	2.36E+00	6.81E+00	1.05E+01	1.33E+01	5.08E+00	1.74E+01	1.15E+02	7.66E+01	7.66E+01	1.22E+03	1.88E+02	1.11E+02	1.97E+02	1.86E+02	1.82E+02
Cr	1.43E+00	4.11E+00	6.37E+00	8.05E+00	3.07E+00	1.05E+01	6.97E+01	4.63E+01	4.63E+01	8.19E+02	1.26E+02	7.47E+01	1.32E+02	1.25E+02	1.23E+02
Mn	1.51E+00	4.35E+00	6.74E+00	8.52E+00	3.25E+00	1.11E+01	7.37E+01	4.89E+01	4.89E+01	6.37E+02	9.82E+01	5.81E+01	1.03E+02	9.72E+01	9.55E+01
Fe	1.97E+00	5.67E+00	8.78E+00	1.11E+01	4.24E+00	1.45E+01	9.61E+01	6.38E+01	6.38E+01	1.29E+03	1.99E+02	1.18E+02	2.09E+02	1.97E+02	1.93E+02
Co	1.42E+00	4.08E+00	6.32E+00	7.99E+00	3.05E+00	1.04E+01	6.92E+01	4.59E+01	4.59E+01	7.75E+02	1.20E+02	7.07E+01	1.25E+02	1.18E+02	1.16E+02
Ni	1.38E+00	3.98E+00	6.16E+00	7.79E+00	2.97E+00	1.01E+01	6.74E+01	4.47E+01	4.47E+01	9.05E+02	1.39E+02	8.25E+01	1.46E+02	1.38E+02	1.36E+02
Cu	1.59E+00	4.58E+00	7.10E+00	8.98E+00	3.42E+00	1.17E+01	7.77E+01	5.16E+01	5.16E+01	7.39E+02	1.14E+02	6.74E+01	1.20E+02	1.13E+02	1.11E+02
Zn	1.69E+00	4.88E+00	7.56E+00	9.56E+00	3.65E+00	1.25E+01	8.27E+01	5.49E+01	5.49E+01	8.33E+02	1.28E+02	7.60E+01	1.35E+02	1.27E+02	1.25E+02
Se	1.49E+00	4.30E+00	6.67E+00	8.43E+00	3.22E+00	1.10E+01	7.30E+01	4.84E+01	4.84E+01	9.79E+02	1.51E+02	8.93E+01	1.58E+02	1.49E+02	1.47E+02
Sr	5.56E-01	1.60E+00	2.48E+00	3.13E+00	1.20E+00	4.08E+00	2.71E+01	1.80E+01	1.80E+01	3.64E+02	5.61E+01	3.32E+01	5.89E+01	5.56E+01	5.46E+01
Mo	1.41E+00	4.06E+00	6.29E+00	7.95E+00	3.03E+00	1.04E+01	6.88E+01	4.57E+01	4.57E+01	9.24E+02	1.42E+02	8.43E+01	1.49E+02	1.41E+02	1.38E+02
Cd	1.42E+00	4.08E+00	6.32E+00	7.99E+00	3.05E+00	1.04E+01	6.92E+01	4.59E+01	4.59E+01	6.59E+02	1.02E+02	6.01E+01	1.07E+02	1.01E+02	9.88E+01
Pb	1.36E+00	3.93E+00	6.09E+00	7.70E+00	2.94E+00	1.00E+01	6.66E+01	4.42E+01	4.42E+01	6.17E+02	9.51E+01	5.63E+01	9.98E+01	9.42E+01	9.25E+01

7.2.4 NIST Standard Reference Material 6150

Diesel particulate matter Standard Reference Material (SRM) 1650 was generated from the heat exchangers of a dilution tube facility following 200 engine hours of particle accumulation from several direct injection four-cycle diesel engines operated under a variety of conditions. It is considered to be representative of heavy-duty diesel engine particulate emissions *[123]*. Although the metals content of SRM 1650 is not certified by NIST, Huggins et al. used Particle Induced X-ray Emission (PIXE) to quantify the concentrations of 15 elemental components, presented below in Table 7-3. The results obtained via the ICP-MS methodology used in the current study agree very well with the data obtained by Huggins et al. for 10 of the 14 elements that were common to each technique. The ICP-MS method detected three additional elements above MDL not detected by the PIXE method.

Table 7-3: ICP-MS analysis of NIST SRM 1650

	SRM 1650		
Element (m/z)	Robert et al. ICP-MS	Huggins et al. PIXE	% diff (abs Δ / avg)
	ug/g	**ppmm**	**%**
Sodium / 23	***0.1***	< dl	
Magnesium / 25	46.9	< dl	
Aluminum / 27	***61.7***	< dl	
Silicon / 28	***57.2***	160	95%
Phosphorus / 31	***662.3***	740	11%
Sulfur / 34	5.35%	1.45%	115%
Chlorine / 35		120	
Potassium / 39	***12.5***	< dl	
Calcium / 40	2162.0	2300	6%
Titanium / 47	***0.0***	< dl	
Vanadium / 51	3.4	< dl	
Chromium / 52	70.3	62	13%
Manganese / 55	14.0	15	7%
Iron / 57	632.0	690	9%
Nickel / 60	***66.8***	50	29%
Copper / 63	56.6	50	12%
Zinc / 66	***999.6***	870	14%
Arsenic / 75	***1.7***	3.00	55%
Bromium / 79	7992.5	3.50	200%
Strontium / 88	5.7	< dl	
Cadmium / 111	6.2	< dl	
Lead / 208	31.3	23	30%

BOLD ITALICS indicates ICP-MS data that is below MDL

7.2.5 Particulate Matter Analysis

One half of each PM sample filter was analyzed using Ion Chromatography as reported in Chapters 2 and 3 by Robert et al [40, 93]. The second halves were analyzed in this study. Each half filter was extracted in a matrix of 75% acetone (Optima Grade, Fischer Scientific) and 25% 1N NHO3 (Trace Metal Grade, Fischer Scientific and MilliQ) (m/v). The half filters were immersed in 30 mL of this solvent in 50 mL Corning vials and sonicated without heating for 30 minutes. The darkened extract was then transferred to secondary 50 mL Corning vials for direct injection into the ICP-MS.

Laboratory calibration standards were made from commercially available stock solutions a 23-element standard, a rare earth standard, and mixtures of 15 individual commercially available single-element standards (SPEX CertiPrep Group, Metuchen, NJ). These stock solutions were diluted using the 75/25 acetone/1N HNO3 solvent. Seven-point calibration curves were run for each set of standards with standard concentrations ranging from 10 – 1000 ppb (ng/mL).

PM extracts were analyzed using the methodology described in Chapter 6 by Robert et al *[122]* for the analysis of gasoline, diesel fuel, and motor oil samples from the same test vehicles, with the carrier gas flow rate and oxygen flow rate differences discussed previously. Raw data files were converted to count-per-second data using the FileView32 program (Agilent). Calibration curves were manually generated, reviewed for QA/QC (blank subtraction, slope, R^2) and applied to the raw count-per-second data as applicable to yield data in units of ppb. Extract concentration (ppb) units were converted to mass units per filter (ng/filter) based on the volume of extract in each vial and accounting for the fact that only one half of each original filter was extracted. Mass per filter units were converted to mass per kilometer (ng/km) emission factors based on the methodology presented by Robert et al [40], accounting for sampling times, instrument flow rates, emission dilution ratios, and distances traveled during each chassis dynamometer test.

7.2.6 Expected Interferences and Mode/Isotope Choices for Data Reporting

A discussion of expected interferences using the current type of ICP-MS technique was presented by Robert et al *[122]*. In that study, elemental concentration data obtained in differing instrument modes and for differing element isotopes was averaged within data sets because the variability between samples was greater than the variability between modes or isotopes. Similar effects are expected in the current study due to interaction between the acetone / nitric acid matrix with argon and oxygen. However, because additional quality assurance measures were available and utilized in the current study, the choice of instrument mode and isotope data reported is case-specific based on the following.

The complete raw data set was screened based on the agreement between duplicate measurements and the agreement between co-located measurements. In the former case one RAAS sample from each test was re-run and linear regressions were performed on each element across samples within the LDGV data set and within the HDDV data set. In the latter case linear regressions were performed on each element based on co-located measurements within each RAAS unit; additionally the sum of the MOUDI stages ($PM_{1.8}$) was compared to their co-located RAAS measurement ($PM_{1.8}$). This exercise yielded three QA/QC metrics for each element in each mode for each isotope. In this study, the emission factors reported are those whose (a) linear regression of duplicates had a slope between 0.7 and 1.3 and an R^2 higher than 0.9, (b) linear regression of co-located RAAS measurements had a slope between 0.7 and 1.3 and an R^2 of 0.9, (c) sum of MOUDI versus RAAS value was between 0.5 and 1.5, and (d) size distributions were continuous. If the data for more than one mode and/or isotope per

element passed each of these four QA/QC metrics that data was averaged so that for each element only one emission factor is presented in the current study. Based on these requirements, data is reported for nineteen elements in this study. Of the 285 possible elemental size distributions possible (19 elements x (9 LDGV data sets + 6 HDDV data sets)) only 59 of them, or 21%, met all four QA/QC requirements.

7.3 Results and Discussion

7.3.1 Elemental Composition of LDGV and HDDV Ultrafine and Fine PM Fractions

Table 7-4 presents the LDGV and HDDV ultrafine elemental composition emission factors for the 59 data sets passing all QA/QC requirements. Table 7-5 presents analogous emission factor data for the fine PM fraction. In both tables, data is only reported that passes all QA/QC metrics as discussed previously. Data below the official MDL but that passes multiple internal QA/QC requirements suggesting that it may be valid is (shaded / in italics). All units are emission factors in ng/km. A large number of elements are below the MDL because the dilution factors employed in the study had to be sufficiently large to generate realistic particle size distributions. The LDGV and HDDV data sets have 9 of 19 reported elements in common. Zn was the most ubiquitous element throughout the data set, present in all but one of the 15 data sets. Al, K, Ni, and Cu were also present in both sample sets to similar degrees, as measured by the number of samples detected divided by the total number of distributions possible (± 10% LDGV vs. HDDV). Mg, Ca, and Pb were found in both the LDGV and HDDV sets but not to similar degrees; Mg and Ca were found more frequently in the HDDV set than the LDGV data set whereas the reverse was true for Pb. S, Cr, Mn, Fe, and Co were found in the LDGV data set but not in the HDDV data set; conversely Na, Se, Sr, Mo, and Cd were found in the HDDV data set but not in the LDGV data set. Thus, aside from Na, the LDGV data set had unique elements of lower molecular weight than the HDDV data set, and visa-versa.

As reported in Tables 7-4 and 7-5, for common elements the concentrations in HDDV diesel fuel were generally observed to be higher than in LDGV gasoline samples. The variability within each data set is high with up to two orders of magnitude difference between elemental concentrations across vehicle samples. Likewise, with the exception of the two oldest HDDVs, the abundance of elements detected within each data set does not correlate well with vehicle type, age, or mileage. Within the LDGV data set among similar vehicle type, the UC cycle emits higher concentrations of elements that the FTP cycle, a result consistent with carbon measurements for this data set as reported by Robert et al [40]. Within the HDDV data set, the 56k 5-mode HHDDT test emits a greater mass of elemental matter than the idle/creep mode, consistent with the findings of Robert et al. on a mass basis [93].

The two largest elemental concentrations observed in this study are both HDDV $PM_{1.8}$ emission factors, specifically 29 ug/km of P for HDDV vehicle #1 (1998 Freightliner) and 28 ug/km P for HDDV vehicle #3 (1991 Volvo). Both of these elements are motor oil additives; their intermittent presence in the HDDV sample set underscores the inherent sources of variability in case-specific vehicle emissions and has implications for both ambient PM and exposure studies.

Table 7-4: LGDV and HDDV ultrafine PM elemental emission factors measured using ICP-MS.

	LIGHT-DUTY GASOLINE VEHICLES (ng/km elements, ug/km C)									HEAVY-DUTY DIESEL VEHICLES (ng/km elements, mg/km C)					
test ID	LDGV-2	LDGV-3	LDGV-4	LDGV-6	LDGV-7	LDGV-8	LDGV-9	LDGV-10	LDGV-11	HDDV-1	HDDV-2	HDDV-3	HDDV-4	HDDV-5	HDDV-6
vehicle class / ID	LEV	TWC PC	TWC PC	TWC LDT/SUV			OCAT	NCAT	SMOKER	#1 IDLE/CREEP	#1 HHDDT	#2 HHDDT	#2 HHDDT	#3 HHDDT	#4 HHDDT
driving cycle	FTP	FTP	UC	UC	CC	FTP	FTP	FTP	FTP	56k	56k	56k	66k	56k	56k
element															
EC	36.65	57.75	111.09	642.44	21.30	145.97	178.54	944.74	228.60	116.22	16.79	13.29	16.29	49.24	55.79
OM	10.39	45.49	273.78	4293.35	255.59	259.34	1659.41	835.93	6668.48	144.37	8.49	8.55	5.27	6.08	11.65
Na														188.03	
Mg					6.72						6410.93		6653.68		766.70
Al									13.90			16.57			
P					594.98		1812.71							6828.78	
S		8.57		356.42	196.05	204.09									
K				10.04		24.32								1966.58	
Ca				4.42							2199.22			192.71	1099.76
Ti															
V															
Cr			22.55												
Mn			1.55												
Fe								3.54							
Co			0.04				0.37								
Ni			14.23				113.85							374.16	35.18
Cu			1.35		0.89				2.78				4.01	1.08	35.35
Zn	0.08		8.40	1.53	0.54	0.69	2.35	2.56	15.08	174.87	13.27	7.86	48.29	127.05	1190.18
Ga															
Ge															
As															
Se											8.73				
Sr														1.22	4.13
Mo														2.90	
Ag															
Cd															0.72
Sn															
Sb															
Ba															
Pb			0.64				0.00	0.13	0.78						39.60

Table 7-5: LGDV and HDDV fine PM elemental emission factors measured using ICP-MS.

	LIGHT-DUTY GASOLINE VEHICLES (ug/km)									HEAVY-DUTY DIESEL VEHICLES (ug/km)					
test ID	LDGV-2	LDGV-3	LDGV-4	LDGV-6	LDGV-7	LDGV-8	LDGV-9	LDGV-10	LDGV-11	HDDV-1	HDDV-2	HDDV-3	HDDV-4	HDDV-5	HDDV-6
vehicle class / ID	LEV	TWC PC	TWC PC	TWC LDT/SUV			OCAT	NCAT	SMOKER	#1 IDLE/CREEP	#1 HHDDT	#2 HHDDT	#2 HHDDT	#3 HHDDT	#4 HHDDT
driving cycle	FTP	FTP	UC	UC	CC	FTP	FTP	FTP	FTP	56k	56k	56k	66k	56k	56k
element															
EC	153.13	336.94	636.77	1609.82	874.97	216.45	675.56	2646.95	6166.62	380.56	119.96	87.91	85.84	265.60	428.58
OM	155.26	416.66	624.49	4801.96	1196.90	600.88	11020.74	3849.82	148079.75	789.76	71.75	67.58	62.90	49.53	108.59
Na														624.17	
Mg					18.50						28555.32		16760.72		3344.95
Al									111.34			48.74			
P					2377.94		8077.26							28262.59	
S		51.40		1542.57	643.14	572.86									
K				39.20		136.44								7042.66	
Ca				93.85							4504.84			1072.77	5851.07
Ti															
V															
Cr			146.69												
Mn			25.44												
Fe								189.66							
Co			1.63				1.45								
Ni			234.83				405.56							1517.19	541.57
Cu			18.73		1.69				38.67				25.79	8.13	125.97
Zn	1.02		75.15	68.79	2.65	36.39	144.87	28.54	134.88	1245.99	215.98	127.81	274.10	601.05	6826.34
Ga															
Ge															
As															
Se											44.47				
Sr														6.01	17.82
Mo														12.15	
Ag															
Cd															5.19
Sn															
Sb															
Ba															
Pb			11.69				5.24	4.44	14.39						290.08

7.3.2 LDGV and HDDV Elemental Size Distributions

Figure 7-1 presents elemental size distributions for the LDGV data set; Figure 7-2 presents this data for the HDDV data set. In both figures, the minimum, average, and maximum emission factors are plotted for each MOUDI stage. The text within each panel indicates the number of samples within each data set for which data passed QA/QC metrics as discussed previously, the numeric value for the RAAS $PM_{1.8}$ emission factor, and the value of the summed MOUDI divided by the RAAS measurement. Therefore, each panel represents only a subset of the data possible and is not necessarily indicative of a class average.

Mass distributions for 14 elements found in LDGV PM are shown in Figure 7-1. These elements can be classified into three groups. The first group contains Mg, K, Cr, Mn, Co, and Ni whose mass distributions peak between 56 nm and 180 nm. The second group contains Ca, Fe, and Zn whose mass distributions peak above 560 nm. The third group is bimodal and is comprised of Al, P, S, Cu, and Pb – in each of these bimodal distributions the smaller mode (< 320 nm) is greater in magnitude than the larger mode (> 560 nm).

Mass distributions for 14 elements found in HDDV PM are shown in Figure 7-2. The same three groups delineated for the LDGV data set can be ascribed to the HDDV data set. Mass distributions for Mg, K, Ca, Cu, Zn, Se, Sr, Cd, and Pb are uni-modal and peak between 56 nm and 180 nm. In contrast to the LDGV data set, none of the HDDV mass distributions are uni-modal that peak in larger sizes. The mass distributions for Na, Al, P, Ni, and Mo are bimodal; however the magnitude of their second modes are not as large relative to the first mode as in the LGDV data set. The second modes of the HDDV mass distributions also peak at a smaller size (generally < 560 nm) than in the LDGV data set.

Figures 7-1 and 7-2 convey several aspects of the sample set as a whole. First, the fractional nature of the data set is apparent; for instance 14 of the 28 panels are based on n=1 measurements. Secondly, the large variability between the minimum and maximum measurements in several cases (i.e. LDGV Zn) is evident. Finally, some notable differences are evident between the distributions for some elements in the LDGV data set versus the HDDV data set. The peaks in the LDGV Ca and Zn distribution peaks between 560 nm and 780 nm whereas HDDV Ca and Zn peak much lower between 100 nm and 180 nm. Cu has a strong bi-modal distribution in the LDGV data set but a uni-modal distribution in the HDDV data; the converse is true for Pb.

As reported by Robert et al. [40, 93], the peak in the reconstructed mass distributions, and for elemental carbon and organic matter, was between 100 and 180 nm for almost every LDGV and HDDV test. Thus, observed elemental bi-modal distributions and uni-modal distributions at that peak at larger sizes are indicative of elements associated disproportionately with PM mass.

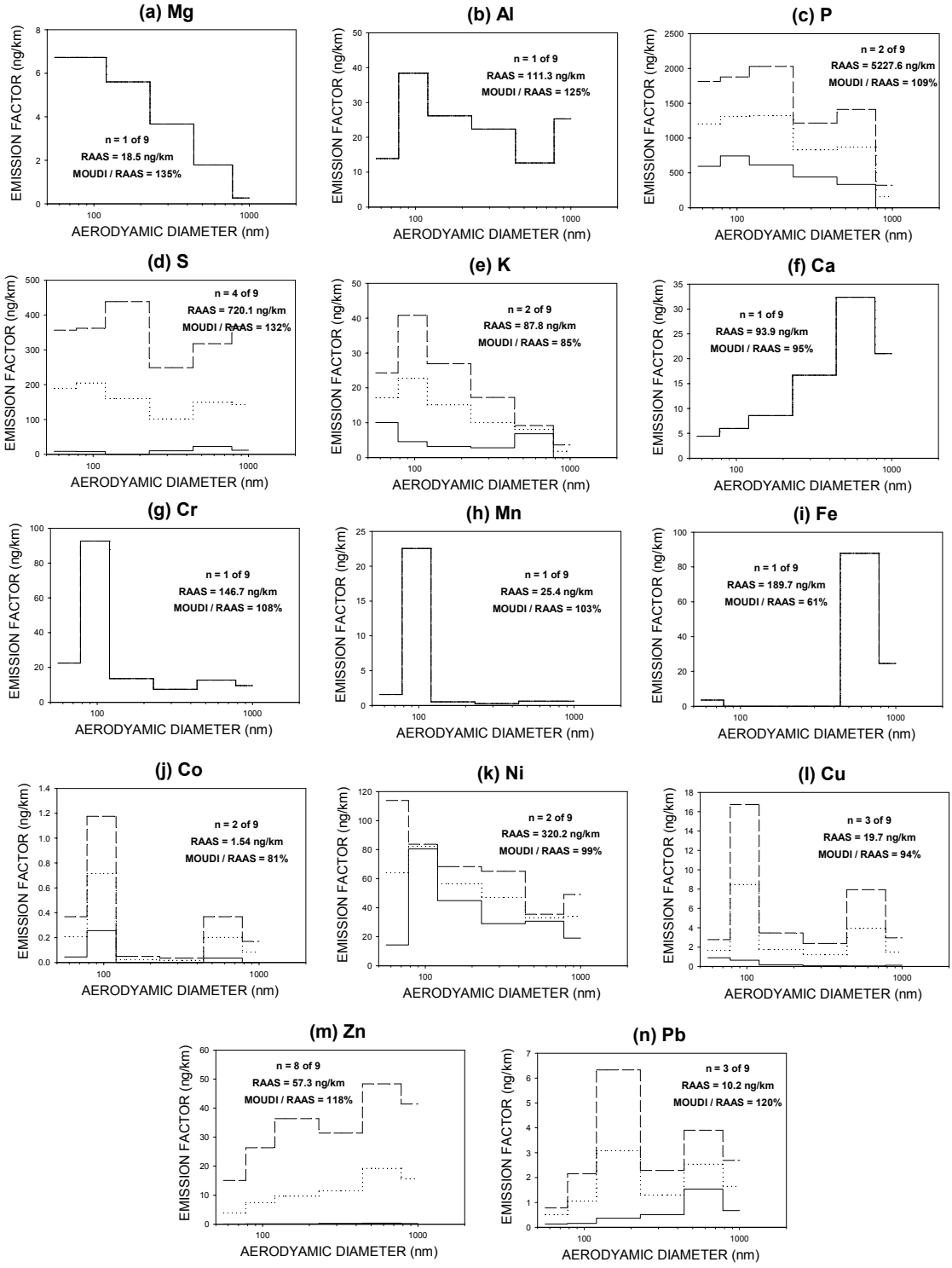

Figure 7-1: Size distributions of elements measured in LGDV PM emissions using ICP-MS.

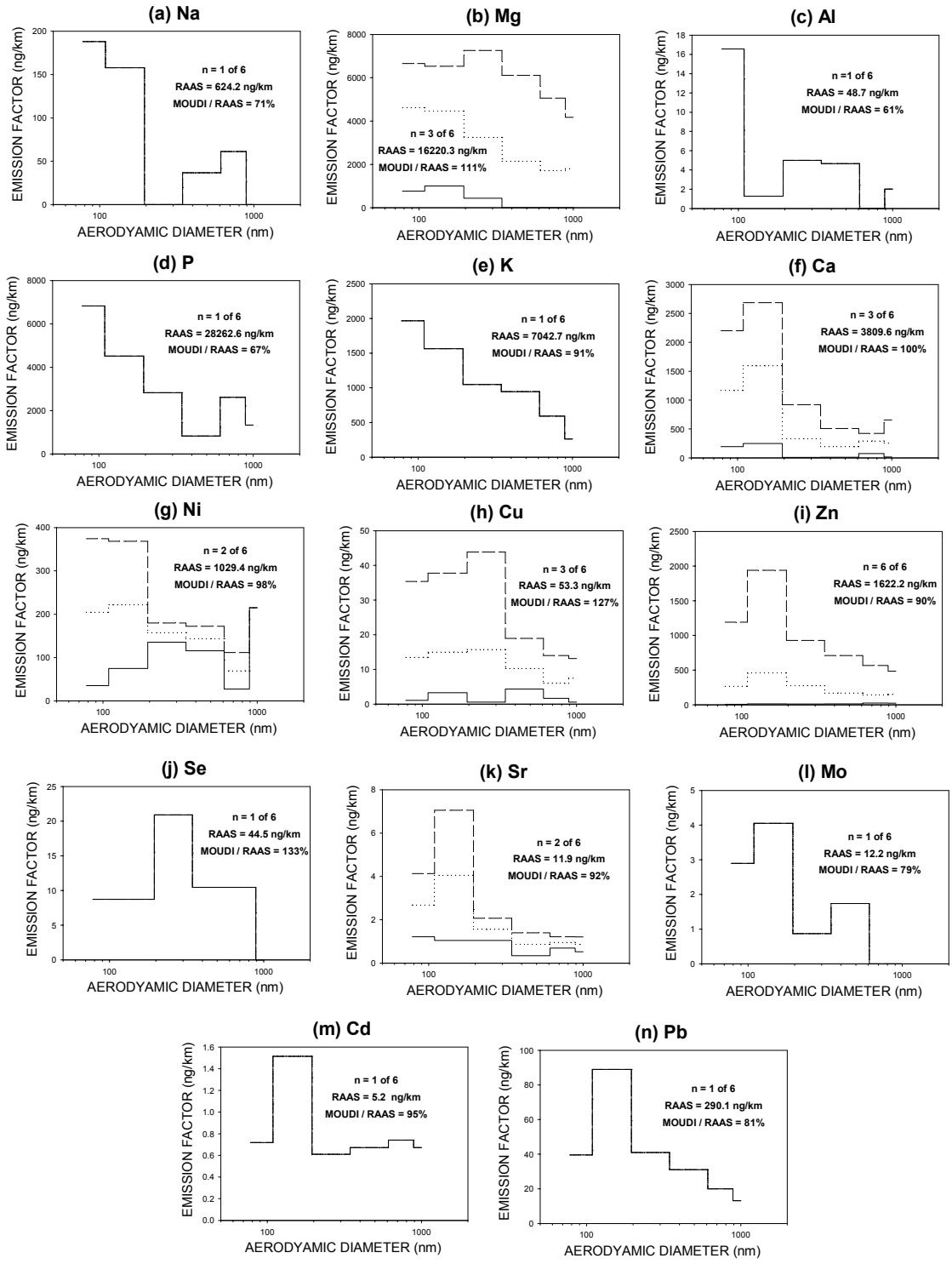

Figure 7-2: Size distributions of elements measured in HDDV PM emissions using ICP-MS.

7.3.3 PM Composition versus Gasoline, Diesel Fuel, and Motor Oil Composition

All of the elements in Tables 7-4 and 7-5 were detected in either the gasoline, diesel fuel, and/or motor oil samples from the same vehicles as reported by Robert et al *[122]*. Although the PM emissions data set is fractional – this may be due to the effects of varying dilution ratios, driving cycles, MDLS, or other factors – several relationships to fuel and oil compositions are evident. Table 7-6 summarizes the result of these comparisons qualitatively. An 'X' in the PM column indicates that there is an evident relationship between the relative concentrations of that element in the PM sample as well as in either the fuel or the oil sample. An entry of 'low', 'med', or 'high' in either the fuel or oil columns indicates the strength of the correlation with PM data for that combustion component. Rows without entries indicate that no qualitative relationship was observed and an entry of 'ND' indicates that the element of interest was not detected above MDL in ether the PM, fuel, or oil samples.

Table 7-6: Strength of qualitative relationships of PM composition to gasoline, diesel fuel, and/or motor oil compositions.

	LDGVs			HDDVs		
ELEMENT	PM	FUEL	OIL	PM	FUEL	OIL
Na	ND	ND	ND	X		low
Mg	X		high			
Al	X			X		low
P	X	med	med	X		low
S				ND	ND	ND
K	X	med		X		low
Ca	X	high		X	high	
Cr	X		high	ND	ND	ND
Mn	X		high	ND	ND	ND
Fe	X	high		ND	ND	ND
Ni				X		med
Cu				X	high	low
Zn	X	low		X	high	
Se	ND	ND	ND	X	high	high
Sr	ND	ND	ND	X	high	med
Mo	ND	ND	ND	X		low
Cd	ND	ND	ND	X	high	
Pb	X		high	X	high	

Five elements detected in LDGV exhaust PM correlate with the results obtained from the analysis of gasoline sampled and composited from seven vehicle groups – LEV PCS, LEV LDT/SUVs, TWC PCs, TWC LDT/SUVs, OCATs, NCATs, and SMOKERS – as reported by Robert et al. [122]. Ca was only observed in the PM phase for TWC LDT/SUVs and was most abundant for the same vehicles in the gasoline samples. The same was true for Fe with respect to NCATs. Relative high concentrations of P and K were also observed in the PM and gasoline samples for TWC LDT/SUVs. Although not as evident, Zn in PM correlated better with gasoline compositional trends than for oil; it is likely that there are important PM contributions from both fluid sources.

Five elements detected in LDGV exhaust PM correlate with the results obtained from the analysis of composited LDGV motor oils. Mg was only observed for TWC LDTs/SUVs in the PM phase and was most abundant for these vehicles in the oil samples. Cr and Mn were only observed in for TWC PCs in the PM phase and second in abundance in the oil samples only to the LEVs; LEV PM data for Cr and Mn was most likely not detected due to the very low PM mass collected during these tests. It is noteworthy that for these examples, PM data was detected from tests using the UC cycle, and not for tests of the same vehicles using the FTP cycle – this finding is consistent with the observation that reconstructed PM emission factors based on carbonaceous compositional data are lower for the FTP cycle than the UC cycle [40]. In decreasing order, Pb was detected in the PM phase for the SMOKERs, TWC PCs, and LEVs; in the oil samples the most abundant concentrations were for the SMOKERs, TWC PCs, OCATs, and LEVs. There is a weaker correlation for P, which was most abundant in the PM phase for the OCATs, and TWC LDT/SUVs but most abundant in the oil for TWC LDT/SUVs.

No distinct correlations were observed in the LDGV data set between PM elemental composition and gasoline / motor oil composition for Al, S, Ni, or Cu, suggesting that the source of these elements in the vehicle exhaust may be a function of the vehicles themselves, such as contact with engine parts, gasoline tank alloys, etc. One interesting observation is that S was observed only in TWC exhaust, although the concentrations in gasoline and motor oil were similar across all vehicle classes.

Similar comparisons can be made between the HDDV PM, diesel fuel, and motor oil data sets. The abundance and magnitude of elements detected in the HDDV PM data set was generally greatest for the oldest vehicle tested, a finding consistent with the results of the diesel fuel analyses. Ca, Cu, Zn, Sr, Cd, and Pb were all detected in the highest concentrations for HDDV vehicle #4 (1984 Kenworth) in both the PM samples and the diesel fuel samples. Conversely, none of the PM samples correlated well with the motor oil samples for these elements. Se was most abundant in the PM, diesel fuel, and motor oil sample for the same vehicle. However, other than Se, there are no strong correlations with the diesel PM and the motor oil for other elements. Ni and Sr were abundant in both the PM and motor oil samples for HDDV vehicle #3 (1991 Freightliner), and only weak associations between PM and motor oil composition were observed for Na, Al, P, K, Cu, and Mo.

Comparison of the elemental composition of PM emissions of LDGVs and HDDVs to their respective fuels and motor oils is not quantitative but does yield several important results. Although no generalities can be concluded, it is evident that elements present in the base fuels and oils can be detected in the PM emissions. Whereas the composition of LDGV PM emissions appear to be impacted by both gasoline and motor oil components, the composition of HDDV PM emissions appear to be impacted primarily from components – most likely additive packages – to diesel fuel. Although Zn is the most ubiquitous element in both LDHV and HDDV PM emissions, the relative contributions from fuel and oil remain unclear.

Many other factors influence the composition of exhaust PM, including the composition of intake air, combustion conditions, contact of fuels and oils with surfaces and components within the vehicle, vehicle maintenance, driving conditions and practices, emissions reductions technologies, and other factors. This study shows that despite these other factors the elemental components of fuels and oils are major contributors to exhaust PM composition.

7.3.4 Comparison of Results to Other Studies

An important consideration in the current study is how the resulting emission factor data compares with similar data reported from other studies. Data on the elemental composition of PM emissions from light-duty gasoline vehicles is limited and no opportunities for comparison to previous results were realized. However, there have been a number of previous studies that characterized the metals content of diesel particulate matter. Wang et al. [118] reported elemental concentrations of diesel PM from a non-catalyst turbo-charged diesel engine using filter digestion and subsequent ICP-AES analyses. Sharma et al. [32] reported elemental the concentration of metals in diesel PM exhaust from a mid-sized Mahindra DI-2500 diesel engine analyzed using an atomic adsorption spectro-photometer. Both of these studies utilized engine dynamometers and were performed outside of the United States, both aspects making comparison to the current study qualitative due to differences in diesel fuels and motor oil compositions, in addition to study sampling and analysis differences. Saitoh et al. [24] reported data on the composition of diesel PM2.5 from a diesel truck tested on a vehicle chassis dynamometer in Japan and analyzed using Particle Induced X-Ray Emission (PIXE) methodology; thus these results, although still expected to be dissimilar, are the most pertinent for comparison to those reported in this study.

Table 7-7 summarizes the results reported by previous studies and the current study for elements detected in diesel exhaust PM. Emission factors from the current study have been converted to mass concentrations within the vehicle exhaust (ug m^{-3}) for direct comparison to the results from the previous three studies. The averaged LDGV values from the current study are also reported for comparison. Only one element, Zn, was detected in the current study for the idle/creep-only test. As reported by Sharma et al., but in contrast to Saitoh et al, the Zn concentration in the idle/creep test is higher than that from the 5-mode (i.e. 56k and/or 66k inertial load) tests. The concentrations of Mg, Ca, Cu, Zn, and Pb are on the order of the results reported by Saitoh et al. for a vehicle chassis dynamometer study, and values for Na and Ni were within a factor of ten. Data for S was reported by Saitoh but not detected in the current study; this may be due to the low-sulfur fuels currently in use in California. Conversely, P and K were reported in the current study by not by Saitoh et al.; these are fuel and/or oil additives and may be present only on a case basis. The large variability in reported results between all four studies summarized in Table 7-7 mirror the large variability between results obtained from different individual vehicles in the current study.

Table 7-7: Comparisons of elemental emissions measurements to other studies.

	DIESEL ENGINE / VEHICLE EXHUAST							LDGV
	Wang et al.	Sharma et al.		Saitoh et al. $PM_{2.5}$		current study $PM_{1.8}$		
element	100%	idle	100%	idle	40%	idle/creep	5-mode	avg
Na	NR	NR	NR	44	290	ND	6	ND
Mg	138	125	87	ND	139	ND	174	***0.02***
Al	641	NR	NR	NR	NR	ND	***0.2***	0.04
P	NR	NR	NR	NR	NR	ND	270	3.14
S	NR	NR	NR	130	274	ND	ND	0.39
K	NR	NR	NR	NR	NR	ND	67	0.03
Ca	831	936	815	2	55	ND	38	0.05
Cr	87	59	32	NR	NR	ND	ND	0.07
Mn	21	NR	NR	0.4	4	ND	ND	0.01
Fe	543	258	172	0.6	45	ND	ND	0.08
Co	39	NR	NR	NR	NR	ND	ND	***0.00***
Ni	51	42	25	0.1	0.8	ND	10	0.16
Cu	55	NR	NR	0.3	3	ND	1	0.01
Zn	111	86	68	2	17	308	64	0.03
Se	NR	NR	NR	NR	NR	ND	***0.4***	ND
Sr	14	NR	NR	NR	NR	ND	***0.1***	ND
Mo	82	NR	NR	NR	NR	ND	***0.1***	ND
Cd	11	ND	ND	NR	NR	ND	***0.1***	ND
Pb	41	35	18	0.3	3	ND	3	0.00

Bold italics indicates data below MDL in the current study

7.4 Conclusions

The size-resolved elemental composition of particulate matter emissions from light-duty gasoline and heavy-duty diesel vehicle chassis dynamometer studies was measured using Inductively Coupled Plasma – Mass Spectrometry methods. Zn was the most abundant element detected throughout the data set, with $PM_{1.8}$ emission factors ranging from 36 – 6826 ng/km. Al, K, Ni, and Cu were also present in both LDGV and HDDV PM; however the LDGV data set contained unique elements of lower molecular weight than the HDDV data set. Elemental size distributions were either uni-modal peaking at small sizes (<320 nm), uni-modal peaking at larger sizes (>560 nm), or bi-modal. Ca and Fe were well correlated between the LDGV PM samples and previously reported LDGV gasoline concentrations, as were Mg, Cr, Mn, and Pb between PM samples and previously reported LDGV motor oil concentrations. For HDDVs, Ca, Cu, Zn, Se, Sr, Cd, and Pb were all well correlated between PM samples and previously reported HDDV diesel fuel concentrations, with no strong correlations between PM samples and previously reported HDDV motor oil concentrations.

8 SIZE AND COMPOSITION DISTRIBUTIONS OF PARTICULATE MATTER EMISSIONS FROM A BUSY CALIFORNIA FREEWAY

8.1 INTRODUCTION

The contribution of freeway emissions to ambient particulate matter (PM) concentrations is of interest for several reasons. Large populations live, work, or attend school within close proximity to major freeways – it has been reported that up to 10% of California schools are located within 150m of medium-to-high trafficked roads *[124]*. This close proximity to heavily-trafficked roads is an obvious source of PM exposure, with likely substantial motor vehicle contributions, having implications for negative health impacts such as respiratory symptoms *[110]*. Previous research has observed the proximity of residence to a major freeway increases the prevalence and severity of asthma and respiratory stress in children *[125]* and that exposure to traffic related PM disproportionately negatively affects the poor and ethnic minority groups *[124]*.

Previous studies reported size-resolved carbonaceous, ionic, and elemental composition measurements of Light-Duty Gasoline Vehicle (LDGV) and Heavy Duty Diesel Vehicle (HDDV) PM emissions from chassis dynamometer experiments *[126, 127]*. Related research investigated the elemental composition of gasoline, diesel fuel, and motor oil from the same LDGVs and HDDVs [122, 128]. Those studies observed several elemental components of the motor vehicle fuels and oil in the PM emissions.

This study reports size-resolved carbonaceous, ionic, and elemental composition of ambient background, freeway, and downwind locations near a California freeway, with emphasis on linkages to previous findings. Time-weighted and averaged freeway and downwind size and composition distributions are compared to a background location. Background-subtracted mass contribution of the freeway to ambient PM loads is compared to the previous LDGV and HDDV measurements. Observed trends between motor vehicle PM freeway contributions and chassis dynamometer data are unique and allow a connection to be made between the freeway PM composition and the composition of motor vehicle fuels and oils.

8.2 METHODS

8.2.1 I-5 Freeway Study

A week-long ambient PM sample collection was conducted in the vicinity of Interstate 5 (I-5) freeway in San Diego, CA during July 2004. Measurements were made at three different physical locations (see Figure 8-1) as well as over three distinct time periods. Sampling was conducted from the afternoon of Wednesday, July 21, 2004

through the evening of Tuesday, July 27, 2004, spanning a period of approximately 151 hours.

Ambient background aerosol was collected continuously over the entire seven day experiment. Freeway and downwind locations were sampled in three discreet periods. The first period, WEEKDAY-1, spanned a 44 hour period from Wednesday afternoon to Friday morning, capturing several traffic rush hour periods and representative of typical weekday traffic. The second period, WEEKEND, spanned a 56 hour period from Friday afternoon to Sunday night, capturing a noticeably different mixture of vehicle types. The third and final period, WEEKDAY-2, spanned a 46 hour period from Monday morning to Tuesday evening, again capturing several weekday traffic rush hour periods with a larger percentage of diesel vehicles than during the WEEKEND sample.

The ambient background location sampling station was located on the roof of Urey Hall on the campus of the University of California, San Diego. This location was approximately 12 meters above ground level, at an elevation of 140 meters above sea level. It was approximately 1000 m east of the Pacific Ocean with minimal development and few roads in-between. Sampling at this site consisted of several PM measurement instruments. An Andersen Reference Ambient Air Sampler (RAAS) (Andersen Instruments, Smyrna, GA) was configured to collect $PM_{1.8}$ using an AIHL cyclone with an instrument flow rate of 60 Lpm (10 Lpm per sampling leg). It was loaded with an array of 47mm quartz filters (QAO47, Pall Corp., baked at 550°C for 48-hrs), Teflon filters (Teflo R2PJ047, Pall Corp., untreated), nylon filters (Pall Nylasorb 1.0 um), and glass fiber filters (Pall Type A/E). A PM_{10} inlet was affixed to each RAAS and was loaded with one 47mm quartz filter, one 47mm nylon filter, and one 47mm glass fiber filter (flow rate ~5 Lpm each). One Micro Orifice Uniform Deposit Impactor (MOUDI) was loaded with 47 mm Al foil substrates (MSP Corp., baked at 550°C for 48-hours) and a quartz 37mm afterfilter (Pallflex 2500QAT-UP, baked at 550°C for 48-hours); a second MOUDI was loaded with 47mm Teflon filters and a 37mm Teflon afterfilter (untreated). Both MOUDIs operated at flow rates of 30 Lpm. A scanning mobility particle sizer (SMPS) (SMPS Model 3080, DMA Model 3081, CPC Model 3025A, TSI Incorporated, Shoreview MN) also ran continuously at the background location, with a scanning range of 17 – 764 nm.

The freeway location sampling site was located approximately 18 m east of I-5 just south of exit number 29 east of the UCSD campus, 1340 m east of the background site. The freeway station was configured with one RAAS, a PM_{10} inlet, three foil MOUDIs, one Teflon MOUDI, and a foil-loaded nano-MOUDI (MSP Corporation, Shoreview, MN. The freeway site was located next to a UCSD sampling trailer that housed an SMPS, an Aerodynamic Particle Sizer (APS), and a variety of other instrumentation including an aetholometer and an Aerosol Time of Flight Mass Spectrometer (ATOFMS). A meteorological station was also positioned in the immediate vicinity of the freeway site and UCSD sampling trailer.

The downwind location sampling site was located approximately 24 m northeast of the freeway site and 37 m east of I-5. The downwind site was configured with one

RAAS, a PM_{10} inlet, one foil MOUDI, one Teflon MOUDI, an SMPS (11 – 496 nm), and an APS (< 20 μm).

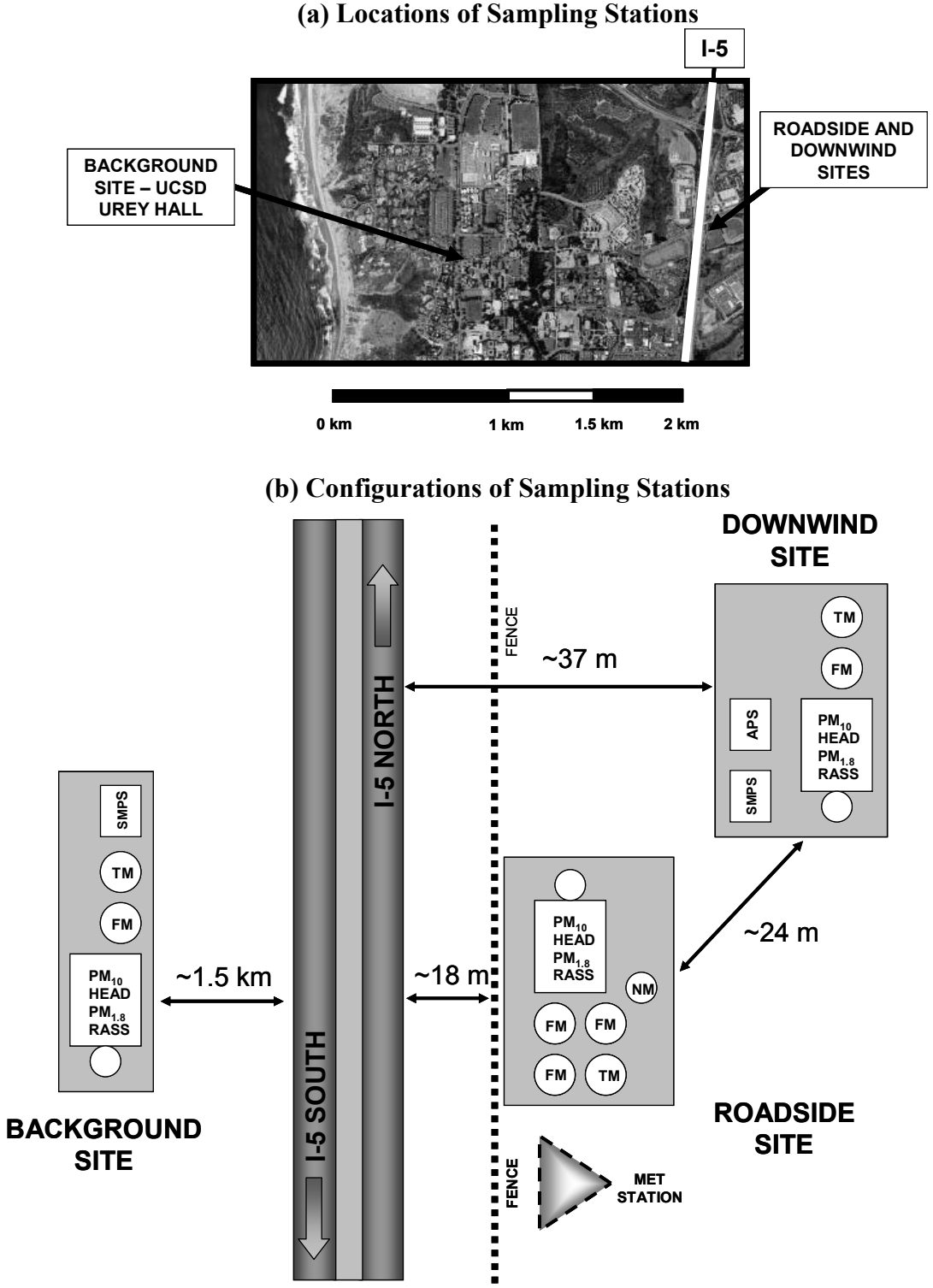

Figure 8-1: Location and configuration of sampling sites upwind and downwind of the freeway. Note that panel b is not to scale.

8.2.2 Chassis Dynamometer Testing

Results from this freeway study are compared to measurements of particulate matter emissions testing results obtained in two previous chassis dynamometer experiments. PM emissions of 30 LDGVs of various technology classes were collected using three driving cycles at the California Air Resources Board's (CARB's) Hagen-Smit laboratory in El Monte, CA as reported by Robert et al [40]. PM emissions from four HDDVs were collected using partial or full driving cycles and under varying simulated inertial loads at the West Virginia University portable dynamometer facility in Riverside, CA as reported by Robert et al [93].

8.2.3 Sample Analyses

Collected samples were sealed in Petri dishes with Teflon tape and stored in laboratory freezers (-16 °C) until analysis. Laboratory analyses included gravimetric (Teflon and foil substrates), elemental carbon (EC) and organic carbon (OC) content (quartz and foil substrates), ionic species content (Teflon substrates), and elemental composition (Teflon substrates). Gravimetric analyses were performed before and after sample collection using a Cahn 28 microbalance in a temperature (20-25 °C) and relative humidity (30-40 %) controlled environment. EC and OC content were obtained using thermal optical transmittance (TOT) method (Carbon Aerosol Analysis Lab Instrument, Sunset Laboratories, Tigard, OR) employing the NIOSH 5040 protocol *[41]* as described by Birch and Cary *[42]*. Anion content (chloride, nitrate, phosphate, sulfate) and cation content (sodium, ammonium, potassium, magnesium, calcium) were determined using ion chromatography (DX-600 workstation, Dionex Corporation, Sunnyvale, CA). Elemental composition was determined using Inductively Coupled Plasma – Mass Spectrometry (ICP-MS) methodology (Agilent 7500ce ICP-MS, Agilent Technologies, Palo Alto, CA) as described by Robert et al. *[128]*.

8.3 Data Reduction and Quality Assurance

Mass size distributions and corresponding RAAS $PM_{1.8}$ data for the LDGV and HDDV sample sets were generated via mass reconstruction using EC, organic matter (OC x 1.4), and ionic species data as described by Robert et al. [40, 93], a process that utilizes sample test parameters such as instrument flow rates, sampling times, vehicle distances traveled, and dilution ratios. Data in these studies were reported as emission factors on a mass per kilometer basis ($\mu g\ km^{-1}$ in the LDGV study and $mg\ km^{-1}$ in the HDDV study). Motor vehicle PM elemental data was not a significant contributor to the total reconstructed mass data in either study, but was also converted to emission factor (ng/km) data as reported by Robert et al. *[128]*.

Data in the current study were converted to ambient mass concentrations in units of $ng\ m^{-3}$ based on instrument flow rates and sampling times. A time-weighted mass average for the freeway and downwind sampling locations was determined based on the

number of hours elapsed during the WEEKDAY-1, WEEKEND, and WEEKDAY-2 sampling periods as compared to the total number of hours sampled across all three periods. Across all studies ultrafine PM is defined as PM between 56 nm and 100 nm aerodynamic diameter and fine PM is defined as PM less than 1800 nm aerodynamic diameter.

To obtain the contribution of the freeway to the ambient background signal, as well as any diluted freeway signature at the downwind location, the background concentration of each species was subtracted from the freeway and downwind data as scaled to the concentration of vanadium at each location. The decision to background subtract based on the relative amounts of vanadium between locations was made for several reasons. First, based on an assessment of the both the spatial and temporal variability in species concentrations, it became obvious that turbulent mixing near the freeway had an impact on downwind concentrations. Second, vanadium was present in the background signal at a concentration of ~6 ng m^{-3}, and at the freeway location in the same weighted average concentration. Vanadium thus serves as a good marker for the background signal; the effect of this approach on the scaling of background concentrations for subtraction from the freeway data is insignificant but becomes a factor in the downwind data set due to turbulent down-mixing as will be discussed.

Several QA/QC metrics were utilized to ensure the validity of speciated data reported in this study. Data was subjected to the same QA/QC acceptance testing as described by Robert et al. *[128]*, which considered agreement between duplicate measurements, agreement between co-located measurements, agreement between the MOUDI sum and the RAAS, and continuous size distributions in order to select and / or average ICP-MS mode and element isotope data combinations for reporting. An additional QA/QC metric available in this study is the comparison of the sum of the MOUDI to the RAAS after background subtraction from the freeway and downwind time-weighted data sets. A favorable agreement in this case indicates that the size-resolved freeway PM contribution adds up to the fine freeway PM contribution, providing additional confidence in these data. QA/QC data is included in figure panels throughout this study for reference.

8.4 RESULTS AND DISCUSSION

8.4.1 Meteorological Data

Figure 8-2 provides a synopsis of the meteorological conditions prevalent during the testing period. The data shown are from the met station depicted in Figure 8-2, located adjacent to the freeway sampling location. Wind speed and direction measurements were taken at a height of 10m. The line plots in Figure 8-2 provide continuous wind speed, wind direction, and ambient temperature and relative humidity data while the polar plots in Figure 8-2 provide wind speed and direction data for discreet six hour time periods corresponding to the x-axis labels on the line plots.

With few exceptions the prevailing winds approached from the west to southwest. Wind direction was very constant with only a slight diurnal variation of ~20°. Wind speed was generally between 0.5 and 1.5 m s^{-1} and exhibited a stronger diurnal pattern of higher wind speeds during the day. Temperatures were not bounded by extremes, ranging only from 19 °C to 23 °C over a seven day period. The diurnal pattern of warmer temperatures during the day was accompanied by an inverse pattern of lower relative humidities during the day. Relative humidity ranged from 76% - 98%; however only four six-hour periods (out of 27) exceeded 90%.

The combination of constant wind speed and direction, accompanied by relatively stable (i.e. not extreme) variations in ambient temperature and relative humidity created an idyllic environment for a study in which the contribution of a line source to ambient PM concentrations is of interest. Based on the stable meteorology it can be concluded that the data obtained originated west of the sampling stations – from the oceans or directly inland for the background sample and from the I-5 Interstate in the case of the freeway and downwind samples.

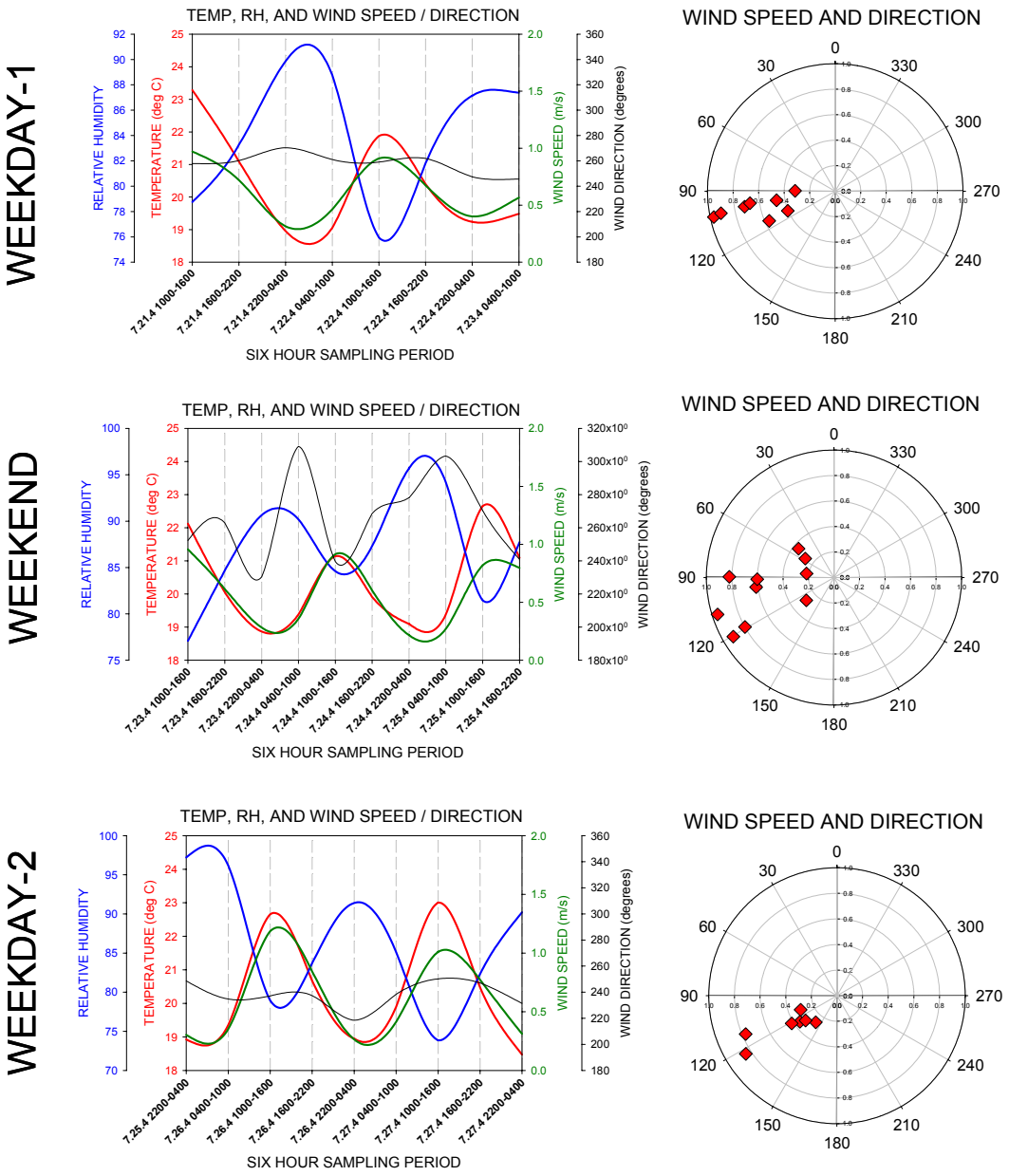

Figure 8-2: Meteorological data summary during freeway sampling.

8.4.2 Size and Composition Distributions

Figure 8-3 presents reconstructed mass distributions for the background and time-weighted averaged freeway and downwind sampling locations in units of ug m^{-3}. The reconstructed distributions are based on EC, OM, ionic species data (SO_4^{-2}, Na^{+}, NH_4^{+}, and Ca^{+2}), and elemental data; elemental data is summed and individual species mass distributions may be found in Figure 8-3.

The background, freeway, and downwind fine PM mass size distributions were uni-modal and peaked between 560 nm and 1000 nm. The background fine PM concentration, based on reconstructed composition information, was 14 ug m^{-3}. Almost 70% of this mass was sulfate (9.7 ug m^{-3}), followed by ammonium (2.0 ug m^{-3}), and elemental mass (1.3 ug m^{-3}). Organic matter (0.6 ug m^{-3}), sodium (0.2 ug m^{-3}), EC (1.2 ug m^{-3}), and calcium (0.0 ug m^{-3}) comrpise less than 10% of the background $PM_{1.8}$ mass. The concentration of ultrafine PM in the background sample was 0.8 ug m^{-3}. The composition of ultrafine PM in the background sample was markedly different than that in the fine PM fraction and was domintated by OM (53%), EC (29%), and ammonium (14%) with only trace amounts of other species detected.

Background EC had a mass distribution peak between 100 and 180 nm, an observation consistent with motor vehicle emission distributions from the LGDV and HDDV chassis dynamometer studies. There were roads between the background site and the ocean, as well as traffic in the vicnity of the UCSD campus. The EC concentration was much less than that observed at the freeway and downwind locations. The OM distribution was bimodal with a mode of larger magnitude between 320 and 560 nm and a mode of smaller magnitude above 1000 nm. Both Na^{+} and Mg^{+2} had mass distributions starting at 320nm and increasing in magnitude to the MOUDI $PM_{1.8}$ cutoff diameter; fine Na^{+} is most likely the tail of a corse mode signature from sea salt. SO_4^{2-}, NH_4^{+}, and Ca^{+2} were all uni-modal and peaked between 560 and 1000 nm.

As shown in Figure 8-4, elemental data in the background sample was dominated by Na, which has a mass distribution starting at 320nm and increasing in magnitude to the MOUDI $PM_{1.8}$ cutoff diameter; this matches the observation of Na^{+} from the ionic species data. This is most likely the tail of a corse mode Na signature from sea salt. The next most abundant elements in background fine PM were Ni, Fe, and Mg; other elements detected included Cu, Sr, Pb, V, Ga, As, Ag, Sn, and Sb. Na was the only element observed with a maximum in its size distribution above 1000 nm. As and Sn were both bi-modal with a mode of smaller magnitude between 100 and 180 nm and a mode of larger magnitude between 320 and 560 nm. Mg, Fe, Ni, Cu, and V were uni-modal with a peak between 320 and 560 nm; V is a marker for off-shore shipping and was used as a tracer for background subtraction at the freeway and downwind sites as previously discussed. Sr, Pb, Ga, Ag, and Sb were also uni-modal but their mass distributions peacked between 560 and 1000 nm.

The freeway fine $PM_{1.8}$ concentration was 19.4 µg m^{-3}, representing a 6.4 µg m^{-3} increase above the background signal. Approximatley 50% of this mass was sulfate (9.9 µg m^{-3}), which was within 5% of the concentration in the background signal. Other primary species in the roadside fine PM were ammonium (19%, 3.8 µg m^{-3}) and elemental components (16%, 3.4 µg m^{-3}), and lower but still significant amounts of elemental carbon (8% 1.4 µg m^{-3}) and organic matter (6% ,1.1 µg m^{-3}). In contrast to the background signal, the ionic form of sodium was not measured reliably in the freeway sample in either the fine or ultrafine PM fraction. The concentration of ultrafine PM in the freeway sample was 5.8 µg m^{-3}, and increase of 5.0 µg m^{-3} above the background sample. The composition of ultrafine PM in the freeway sample was dominated by

elemental species (58%) and elemental carbon (25%), with lesser amounts of OM (8%), and ammonium (6%) and sulfate (4%).

These freeway data clearly show higher concentrations of several PM components in the freeway environment as compared to the background site; freeway signatures (background-subtracted time-weighted freeway data) are presented later in this report. These analyses include size and composition information for carbonaceous, ionic, and individual elemental species. Of note, the time-weighted average of fine PM vanadium in the freeway sample was 6.0 ng m^{-3}, compared to 5.7 ng m^{-3}. As mentioned previously vanadium was used as a tracer to scale the background signal for subtraction from the freeway data; the scaling facor was near unity for the freeway site.

The downwind fine $PM_{1.8}$ concentration was 16.1 µg m^{-3}, representing a 3.3 µg m^{-3} decrease in concentration from the freeway site but still a 2.1 ug $m^{-}3$ increase above the background signal. Although the fine PM mass concentration is lower than the freeway sample (due to dilution with background air) the relative abundances of species are similar with 56% sulfate, 19% ammonium, 9% elemental species, 6% organic matter and calcium, and 5% elemental carbon. The composition of the ultrafine PM in the downwind sample appears to be a hybrid of the background and freeway ultrafine PM samples. EC accounts for 32% of the downwind ultrafine PM,with 31% from OM, 20% calcium, 13% ammonium, and 4% sulfate.

There was approximately 9 ug m^{-3} of coarse PM, defined as $PM_{10-1.8}$, observed in the background signal. 3.8 ug m^{-3} (42%) was Na^{2+}, a sea salt speices transported inland from the Pacific Ocean. Elemental species accounted for 27% of the background coarse PM signal; 11% from those elements presented in Figure 8-4 (dominated by 1.0 ug m^{-3} of Mg with lesser amounts of Ga, As, and Sr) and an additional 16% from other elements presented in Figure 8-4 (dominated by 1.2 ug m^{-3} of K with lesser amounts of Co, Ti, Na, Zn, S, and Mn). The background signal also contained a large contribution of coarse mode organic matter at a concentration of 1.6 ug m^{-3} (17%) as well as appreciable amounts of nitrate at 0.8 ug m^{-3} (9%) and calcium at 0.4 ug m^{-3} (4%). There was no coarse mode EC or sulfate observed in the background coarse PM signal.

The time-weighted average freeway coarse PM concentration was 4.0 ug m^{-3} higher than that of the background signal, with increases in the concentraitons of sulfate (3.5 ug m^{-3}), OM (1.0 ug m^{-3}) and NH^{4+} (1.0 ug m^{-3}) but also significant (~0.5 ug m^{-3}) decreases in Al, Ca, and Na^{+}. The time-weighted average downwind coarse PM concentration was 5.0 ug m^{-3} higher than that of the background signal and of similar composition to the freeway data, indicating that the coarse PM fraction did not settle appreciably in the additional 19m traveled downwind from the site, although the slight incrase could signify gravitational settling of coarse PM from agove the sampling instrument inlet height(s).

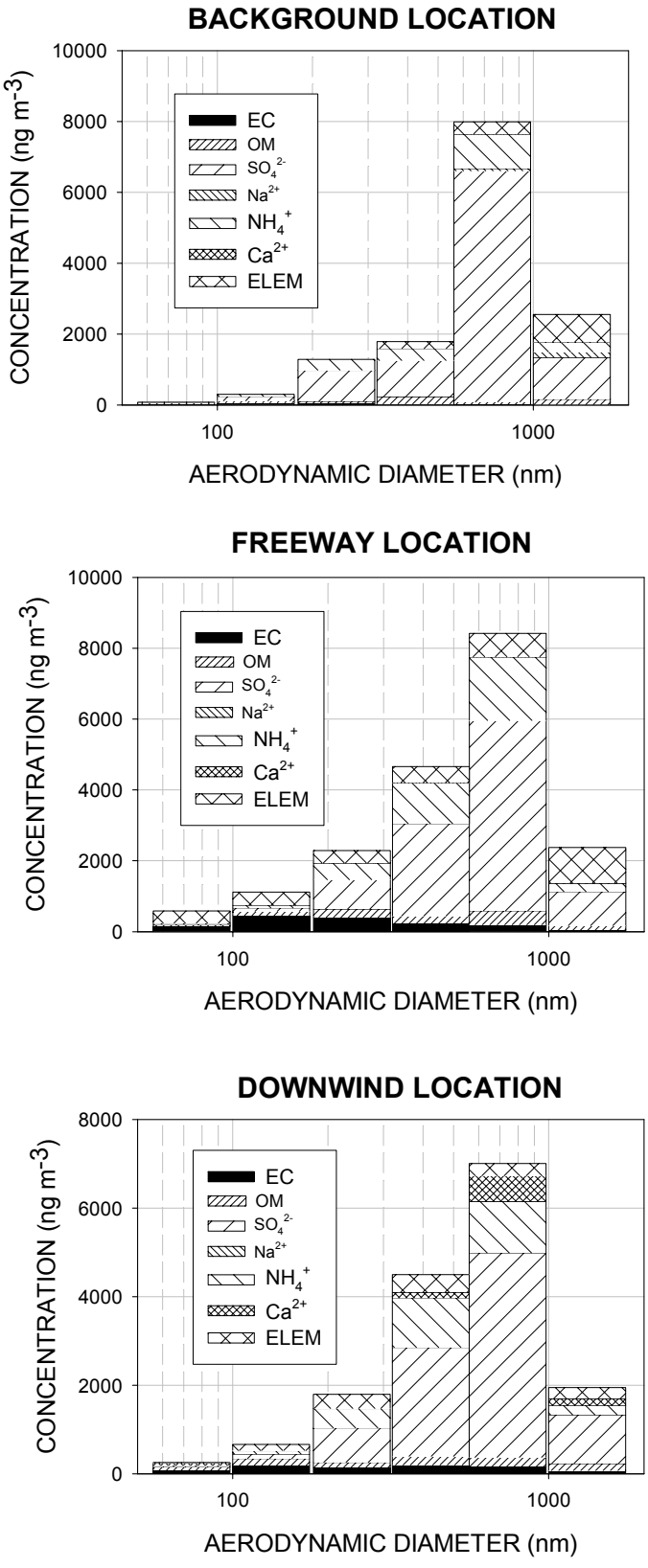

Figure 8-3: Size and composition distributions of particulate matter species measured upwind and downwind of the I-5 freeway.

These downwind data reveal a dilution of the freeway fine and ultrafine concentrations between the two sites. It is very likely that in addition to dilution there are other physical and chemical processes such as nucleation, condensation, coagulation, and secondary organic aerosol formation that impact both the size and composition distributions of both fine and ultrafine PM. These processes and effects are also expected to be a function of the distance from the freeway, an important consideration for exposure analyses. For example, Janssen et al. showed that the concentrations of air pollutants in and outside schools near motorways are significantly associated with distance, traffic density and composition, and percentage of time downwind *[112]*. However, since the focus of this report is the contribution of the freeway to ambient PM loads, and comparison of the freeway signature to previous chassis dynamometer source profiles, there is no further analyses of the background-subtracted downwind data.

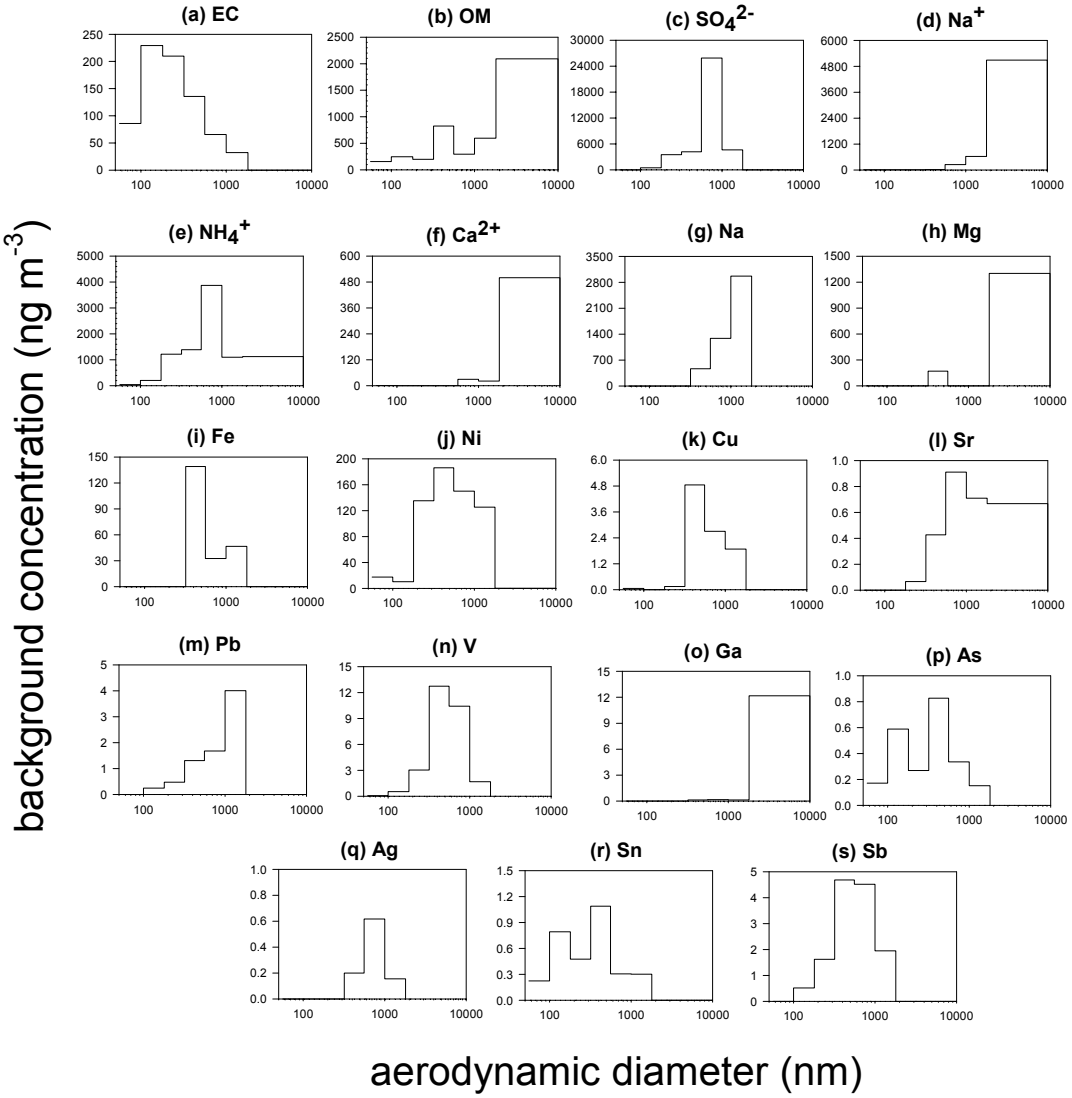

Figure 8-4: Detailed size and composition distributions of particulate species measured at the upwind sampling location.

Harrison et al. *[120]* reported the metals content of PM in a roadside environment in the United Kingdom. $PM_{2.0}$ mass was 12.8 μg m-3; the major ionic species were chloride, sulfate, nitrate, and ammonium. PM_{10} elemental species included, in descending order by concentration, Fe, Mg, Ca, Pb, Zn, and Ba all above 20 ng m^{-3} and Cu, Mn, Ni, Sr, and Se all between 1.0 ng m^{-3} and 12.0 ng m^{-3}. Each of these elements was detected in the freeway sample in the current study with the exception of Ba. Lough et al. *[121]* also reported the metals concentrations of PM_{10} from a roadside tunnel sample in Milwaukee, WI. The most abundant elements detected using ICP-MS methodology, in order of decreasing abundance, included OC and EC, Fe, Mg, Na, Ni, Cu, Zn, Cr, Mn, and Sn; all but the last three of these elements are present in the freeway $PM_{1.8}$ data in this study. The only element reported from XRF analysis present in the current study was Ca. Lin et al. *[109]* reported characteristics of metals in ultrafine (D_p < 100 nm), fine (D_p < 2500 nm), and coarse mode PM (< 10 μm). Particles were collected near a roadside in Taiwan, acid-digested using a microwave process, and quantified using ICP-MS methodologies. Na was the most abundant element measured, similar to the results of the current study, with a coarse PM mode tail into the fine PM mode. Ca, Fe, Zn, Pb, Sr, Ni, Cu, Cd, V, and Sb were also measured in the ultrafine, fine, and coarse modes. Several elements were detected that were not present in the current study such as Al, K, Ba, and Ag.

8.4.3 Freeway versus Dynamometer Signatures

Figure 8-5 provides a comparison between the background-subtracted and time-weighted averaged freeway data and the averaged LDGV and HDDV chassis dynamometer signatures for EC, OM, ionic species, and elemental components of fine PM. Units are expressed as concentrations in ng m^{-3} for the freeway contributions (solid line), emission factors in μg km^{-3} for LDGVs (dotted line), and emission factors in mg km^{-1} for HDDVs (dashed line). Panels are shown for each species for which there was a roadside contribution and for which there were one or both vehicle type signatures, regardless of a positive association between the measurements.

Several species were present in the roadside contribution distributions that, when superimposed on the vehicle chassis dynamometer signatures, reveal an apparent overlap. For instance, the freeway contribution of elemental carbon (panel a) is log-normal and peaks between 100 and 180 nm, as do both the LDGV and HDDV chassis dynamometer emissions. This result implicates both LDGVs and HDDVs as sources of the freeway EC addition to the background aerosol. The freeway contribution of OM (panel b) is bi-modal, with a mode of smaller magnitude peaking between 180 and 320 nm and a mode of larger magnitude peaking between 560 and 1000 nm. Although the average HDDV chassis dynamometer OM distribution peaks between 100 and 180 nm, the averaged LDGV OM distribution (dominated mathematically by SMOKERS) peaks in alignment with the freeway contribution.

Several other chassis dynamometer signatures appear related with the freeway contribution signatures. The freeway contribution distribution of S parallels that of LDGVs. The freeway contribution of elemental (not ionic) calcium and zinc are bimodal; the first mode between 100 and 180 nm aligns with the HDDV data and the second mode between 560 and 1000 nm aligns with the LDGV data. Both Mn and Fe freeway signatures are uni-modal and are aligned with uni-modal LDGV distributions. The results for Ca, and Zn are particularly interesting as these two elements were detected in abundance in gasoline, diesel fuel, and/or motor oil by Robert et al. [122] and also in LDGV and/or HDDV exhaust PM by Robert et al. *[128]*.

The freeway and motor vehicle distributions in the remaining panels in Figure 8-5 do not have the same degree of similarity, but there are certainly other processes that can explain the freeway contribution information. For example, both Fe and Cu are uni-modal and peak at larger sizes; these metals are known components of brake dust which in turn can be re-suspended by a heavily trafficked freeway. Davis et al. *[129]* detected Cu, Cd, Zn, and Pb in extracts from automobile brake runoff and diluted used oil samples, a result supporting the identification of these two sources as possible contributors to freeway PM composition.

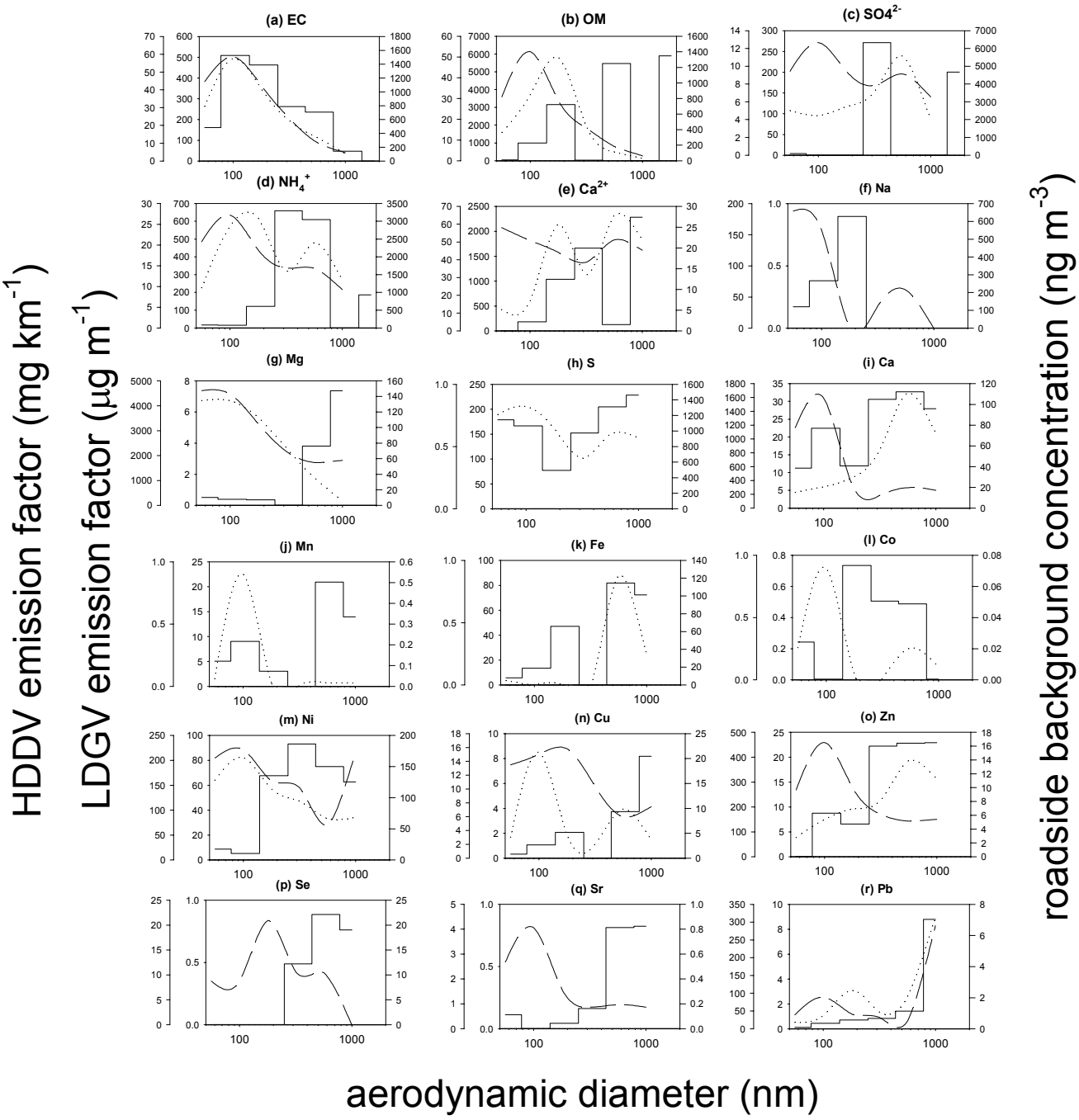

Figure 8-5: Detailed size and composition distribution of particulate matter from the I-5 freeway vs. chassis dynamometer signatures.

8.4.4 Temporal Analyses

Figure 8-6 presents the background-subtracted freeway signatures for those species that exhibit weekday-weekend dependence. The gray bar in the middle of each bar set represents the concentration of that species (ng m^{-3}) during the WEEKEND sample, bracketed by black bars to the left (WEEKDAY-1 sample) and to the right (WEEKDAY-2 sample). As shown in panel (a), EC concentrations attributed to the freeway are notable higher during the weekday samples as compared to the weekend sample below 180 nm. Conversely, panel (b) shows that the concentrations of OM from the freeway were notably higher during the weekend period than the weekday periods above, illustrating a clear weekend effect with EC and OM.

The results of the carbonaceous data is in agreement with the observed traffic patterns during the three discrete sampling periods, During the weekday periods, a higher number and percentage of HDDVs were observed, whereas during the weekend a higher number (weekend holiday traffic) and percentage of LGDVs were observed on the freeway. This finding is supported by the emission factor and size distribution data for the LDGV and HDDV chassis dynamometer experiments, in that HDDV emission factors of EC are much higher than that of LDGVs, and visa-versa for LDGV OC from SMOKERs versus HDDVs. In addition to EC and OM, Ca, Zn, Fe, Cu, Zn, Se, Pb, Ga, As, and Sb all show a predominance during the weekend of larger particles; only As shows a weekday predominance or one for smaller particles. This data is more difficult to interpret and is shown for informational purposes; each of these except As was detected in gasoline, diesel fuel, and motor oil and several also in LGDV / HDDV PM. Their weekday-weekend effect may indicate that they may largely be attributed to LDGVs, or there may have been some other factor (i.e. increased average speed of driving) that re-suspended a greater mass of particles with these elements from the freeway surface.

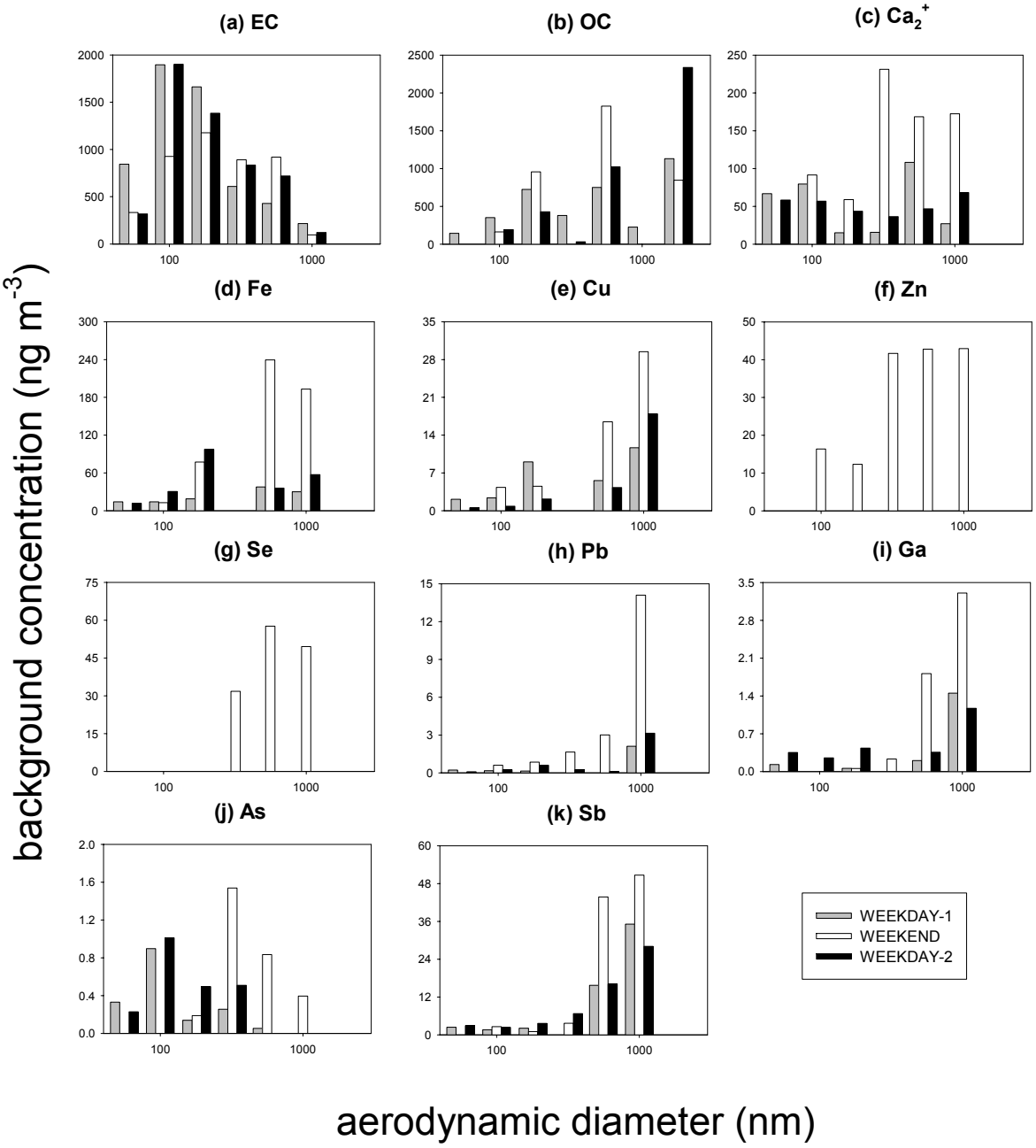

Figure 8-6: Temporal variation of detailed size and composition distributions in the roadside environment. The gray bar in the middle of each cluster represents the concentration of that species (ng m-3) during the WEEKEND sample, bracketed by black bars to the left (WEEKEND-1 sample) and to the right (WEEKDAY-2 sample).

8.5 Conclusions

Size-resolved particulate matter (PM) samples were collected near a busy freeway in San Diego, CA over a 7 day period in the summer of 2004. Samples were collected at a site ~1000m upwind of the freeway, a site 18m downwind of the freeway, and a site 37 m

downwind of the freeway during two discrete weekday and one weekend period. Samples were analyzed for organic carbon, elemental carbon, water-soluble ions, and elements. Comparisons were made to previously reported light-duty gasoline vehicle (LDGV) and heavy-duty diesel vehicle (HDDV) PM emissions measured using chassis dynamometers. All upwind and downwind fine PM mass distributions peaked between 560 nm and 1000 nm and were dominated by sulfate, with significant quantities of ammonium and various trace elements. The difference between upwind and downwind concentrations was small, but an effective emissions signature was still detected within the uncertainty limits of the measurements. The fine PM mass concentrations measured 18 m and 37 m downwind of the freeway were 5.4 μg m^{-3} and 3.1 μg m^{-3} greater, respectively, than the fine PM concentrations measured at the upwind location. These signals reflect both a freeway contribution to ambient PM as well as the effects of downwind dilution.

The freeway emissions signature for elemental carbon had a size distribution that peaked between 0.1 – 0.18 μm, analogous to both the LGDV and HDDV chassis dynamometer signatures. The organic carbon size distribution signature from the freeway was similar to the LDGV chassis dynamometer emissions with maxima between 0.18 – 0.32 μm. Freeway emissions of particulate Ca and Zn had size distributions that were bimodal and had similar shape to HDV dyanometer emissions between 0.1-0.18 μm and LDGV dynamometer emissions between 0.56-1.0 μm. Both Ca and Zn have been measured previously in gasoline, diesel fuel, and motor oil from LDGVs and HDDVs; these results illustrate plausible linkages between motor vehicle combustion components and fine PM contributions from a busy freeway. Concentrations of Cu, Fe, and Sr all had size distributions that peaked at sizes larger than 1 μm particle diameter, consistent with their presence in brake and / or road dust.

Elemental carbon and organic carbon emissions both exhibited weekday-weekend effect. Greater concentrations of elemental carbon were observed during the weekday sampling periods below 0.18 μm, with greater concentrations of organic carbon observed during the weekend period above 0.18 μm. These findings were consistent with the observed local traffic patterns with a higher number and percentage of HDDVs present during the weekday versus the weekend sampling periods.

9 SEPARATING LUBRICATING OIL VS. FUEL CONTRIBUTIONS TO PARTICULATE MATTER EMISSIONS FROM LIGHT DUTY GASOLINE AND HEAVY DUTY DIESEL VEHICLES

9.1 Introduction

Motor vehicles have been identified as one of the major sources of airborne particulate matter (PM) with aerodynamic diameter smaller than 2.5 μm (PM2.5) *[79-81]*. Recent studies show that motor vehicles also emit significant quantities of ultrafine particles with aerodynamic diameter smaller than 0.1 μm (PM0.1) [40, 58, 127]. Both PM2.5 and PM0.1 have been implicated as potential sources of negative health effects *[1-9]*. Recent attention has focused on the relative toxicity of particles emitted from different sources to provide enhanced information for the design of efficient emissions control programs. The accurate quantification of motor vehicle contributions to ambient PM2.5 and PM0.1 concentrations is necessary to identify potential threats to public health.

The majority of the PM emitted from motor vehicles is composed of carbonaceous material with a mass distribution that peaks between 0.1-0.3 μm with a tail that extends into the PM0.1 size range [40, 58, 93]. The only possible feedstocks for these carbonaceous PM emissions are (a) the fuel that powers the motor vehicles and (b) the lubricating oil used in the engines. The chemical signature of lubricating oil has been identified in the PM exhaust from both gasoline- and diesel-powered vehicles *[14, 75]* and heavy PAHs thought to be derived from gasoline have also been identified in light duty vehicle exhaust *[105, 130]*. It therefore seems likely that both fuel and lubricating oil contribute to the motor vehicle tailpipe emissions.

The health effects of particles derived from lubricating oil, gasoline, and diesel fuel may be quite different. Lubricating oil is composed of a heavier fraction of crude oil base stock with small quantities of additives to improve wear performance. Gasoline and diesel fuel are lighter fractional distillates of crude oil with various additives to enhance combustion characteristics. The chemical composition of the PM derived from motor oil, gasoline, and diesel fuel is different and their health effects may also be different. A need exists to separately quantify the ambient concentrations of PM derived from lubricating oil, gasoline, and diesel fuel to determine if particles derived from any one of these sources is particularly toxic.

The purpose of the current study is to separately quantify fuel and oil contributions to PM emissions from 5 classes of light duty gasoline vehicles (LDGVs) and 4 heavy duty diesel vehicles (HDDVs) operated under realistic driving cycles. Organic compounds are identified that can act as unique tracers for lubricating oil, gasoline, and (approximately) diesel fuel. Multiple regression analysis is used to derive source profiles that list the amount of PM emitted per unit of each tracer compound. The contribution that fuel and oil make to the size distribution of PM emitted from LDGVs and HDDVs is also presented.

9.2 Methods

9.2.1 Sample Collection

Size-resolved concentrations of elemental carbon (EC), organic carbon (OC) and individual organic compounds were measured in particulate matter emitted from heavy duty diesel vehicles and light duty gasoline vehicles operated under transient driving cycles on chassis dynamometers as discussed in Chapters 2-5 *[93, 130-132]*. A dilution sampling system was employed to mix hot tailpipe exhaust with clean air to mimic the atmospheric dilution process without contaminating the emissions signature with material from other sources. Dilution ratios employed in each test were specifically chosen to be as large as possible to create realistic particle size distributions while still concentrating the sample sufficiently to collect enough mass for subsequent chemical analysis. Dilution factors ranged from 129-584 during diesel testing and 38-393 during gasoline testing. Particulate matter samples were collected with Reference Ambient Air Samplers (RAAS) (Andersen, Smyrna, GA) and Micro Orifice Uniformm Deposit Impactors (MOUDIs) (MSP Corporation, Shoreview, MN). Further details of sample collection are provided in Chapters 2-5 *[93, 130-132]*.

9.2.2 Sample Extraction and Analysis for Organic Compounds

The concentration of elemental carbon (EC) and organic carbon (OC) in all RAAS and MOUDI samples was measured using the NIOSH thermal optical analysis method with a Sunset Labs carbon analyzer (Sunset Labs, Tigard, OR). The remaining portion of each sample was then extracted from the collection media with ~15 mL of dichloromethane and then evaporated under nitrogen to a final volume of 50 μL. A known amount of an isotopically labeled sterane (ααα-20R-cholestane-d_4) and two isotopically labeled PAHs (chrysene-d_{12} and dibenz[ah]anthracene-d_{14}) was spiked onto each sample before extraction to serve as recovery and quantification internal standards. All sample quantification was carried out relative to these interal standards to increase the precision and accuracy of the results. Sample analysis was performed with gas chromatography (GC) and ion trap mass spectrometry (ITMS). Further details of the procedures used for chemical analysis of organic compounds are provided by Riddle et al. [103, 130].

9.3 Results and Discussion

9.3.1 Regression Analysis

Figures 9-1 and 9-2 in the current chapter illustrate normalized particle size distributions of total carbon and trace organic species measured during thelight duty gasoline vehicle (LDGV) and heavy duty diesel vehicle (HDDV) tests. Total carbon concentrations in each particle size fraction are illustrated with the open bars in each chart. Elemental carbon and organic carbon size distributions were highly correlated in all tests such that the normalized total carbon size distribution also represents the EC and OC size distributions. The individual trace organic compounds shown in Figures 9-1 and

9-2 are representative of numerous additional organic compounds. Statistical analysis of all the GC-ITMS measurements revealed that organic compounds could be generally classified into two groups based on their size distributions. Two hopanes (17α(H)-21β(H)-29-norhopane and 17α(H)-21β(H)-hopane) and two steranes (αββ-20R-stigmastane and αββ-20S-stigmastane) had nearly identical size distributions in all samples. The likely source for these compounds was lubricating oil [13, 14, 75]. Size distributions of heavy PAHs benzo[ghi]perylene and coronene were highly correlated in light duty gasoline vehicle tests and were likely derived from unburnt gasoline and incomplete combustion [105]. Tests on gasoline and diesel vehicles discussed in Chapters 4 and 5, respectively, have shown that heavy PAHs are emitted primarily from gasoline vehicles while light, 3- and 4-ring PAHs are found at very high levels in diesel engine exhaust [103, 130]. Size distributions of light PAHs fluoranthene and pyrene were highly correlated during heavy duty diesel vehicle tests and were likely derived from incomplete combustion of diesel fuel.

Figures 9-1 and 9-2 of the current study show that the size distribution of 17α(H)-21β(H)-29-norhopane is not always correlated with the measured size distribution of total carbon emissions. Likewise, the size distributions of PAHs differ from the size distribution of total particulate carbon emissions in several important cases. Oil and fuel contributions to total carbon emissions appear to be separate and distinct. Variations in emissions control technology, engine load, and driving cycle affect the size distribution of EC and OC emissions [126, 127]. The results of the current study suggest that these factors also affect oil- and fuel-derived contributions to carbon emissions. This finding motivates the separate treatment of fuel and lubricating oil contributions to carbonaceous particulate matter emissions from motor vehicles.

One technique to separately identify the influence of multiple independent variables (fuel and lubricating oil) on a dependant variable (carbon emissions) is multivariate regression using the different particle size fractions as separate observations within each test. A simple regression model with the form y = a*x1 + b*x2 can be fit to each sample with parameters “a” and “b” found to minimize the residual concentration. In this approach “x1” and “x2” represent organic tracer compounds present in lubricating oil and fuel, respectively, while “a” and “b” represent the amount of carbon per unit of tracer compound. Hopanes and steranes will be used as lubricating oil tracers while PAHs will be used as fuel tracers. Some PAHs may partition into the lubricating oil over time but the dominant source of PAHs in the emissions is expected to be from the fuel.

The inclusion of multiple hopanes and steranes in the regression analysis did not add information to the analysis because all species within this compound class had size distributions that were highly correlated. Furthermore, including multiple hopanes and steranes dilutes the true power of the regression analysis since each sample set is limited to 6 observations (different MOUDI size fractions). In the present study, the average concentration of all hopanes and steranes were expressed as an equivalent mass concentration of 17α(H)-21β(H)-29-norhopane for the concentration of “oil tracer”. Likewise, statistical analysis showed that PAH size distributions emitted from light duty gasoline and heavy duty diesel vehicles had very similar shapes. The concentrations of

two heavy PAHs (coronene and benzo[ghi]perylene) were expressed as the equivalent mass concentrations of benzo[ghi]perylene for the gasoline "fuel tracer" and the concentrations of the two light PAHs (fluoranthene and pyrene) were expressed as the equivalent mass concentration of fluoranthene for the diesel "fuel tracer". Equivalent concentrations of each compound were calculated by multiplying the actual compound mass with the ratio of the (surrogate compound mass / actual compound mass) determined from regression across all 6 size fractions. This approach gives equal weighting to the information in all trace compounds even though the absolute value of some compound concentrations may be larger than others.

Multiple regression analysis was performed twice for each sample set in the current study to separately identify oil and fuel contributions to EC and OC. The amount of carbon (either EC or OC) in each of the 6 PM samples collected by the MOUDI was fit using the equation

Carbon = (μg C / ng oil tracer) * oil tracer + (μg C / ng fuel tracer) * fuel tracer (1)

Table 9-1 illustrates the results of this analysis for lubricating oil and fuel contributions to EC and OC emitted from light-duty gasoline vehicles (LDGVs) and heavy-duty diesel vehicles (HDDVs). The uncertainty ranges shown in Table 9-1 are 95% confidence intervals. Some of the coefficients shown in Table 9-1 have uncertainty ranges that are comparable to the predicted value. This is caused by similarity in the size distributions for oil and fuel tracers during some of the chassis dynamometer tests. In other tests there were large differences between oil and fuel tracer size distributions, clearly emphasizing the fact that oil and fuel contributions to EC and OC emissions are separate (see Figures 9-1 and 9-2 along with associated discussion). The agreement between the linear fit described by equation (1) to the concentration of EC and OC in each sample is summarized using the correlation coefficient (R^2). The two parameter regression model with separate oil and fuel contributions had $R^2 \geq 0.93$ for all tests. Attempts to fit the measured EC size distributions from HDDVs using only oil tracers produced correlation coefficients (R^2) ranging from 0.67 – 0.98. Attempts to fit the measured OC size distributions from HDDVs using only fuel tracers produced correlation coefficients (R^2) ranging from 0.73 – 0.99. Single variable fits for gasoline vehicles were even less accurate, emphasizing the fact that both fuel and oil made contributions to EC and OC emissions from all vehicles.

Figures 9-3 to 9-6 illustrate reconstructed carbon concentrations measured in each particle size fraction using Equation 1 vs. measured concentrations. Carbon concentrations in different size fractions span a continuous range of values during each chassis dynamometer test. Predicted carbon concentrations show good agreement with measurements across the entire range of concentrations. Regression statistics are usually not dominated by a single large observation. The ultrafine size fraction (PM0.1) is denoted by an open circle in Figures 9-3 to 9-6 and usually falls in the middle of the measured range of values. Based on these results, equation 1 and the values listed in Table 9-1 appears to explain the size distribution of EC and OC emitted from LDGVs and HDDVs operated under realistic driving cycles. The contributions that lubricating oil

and fuel make to ultrafine particle concentrations should be accurately represented by this analysis

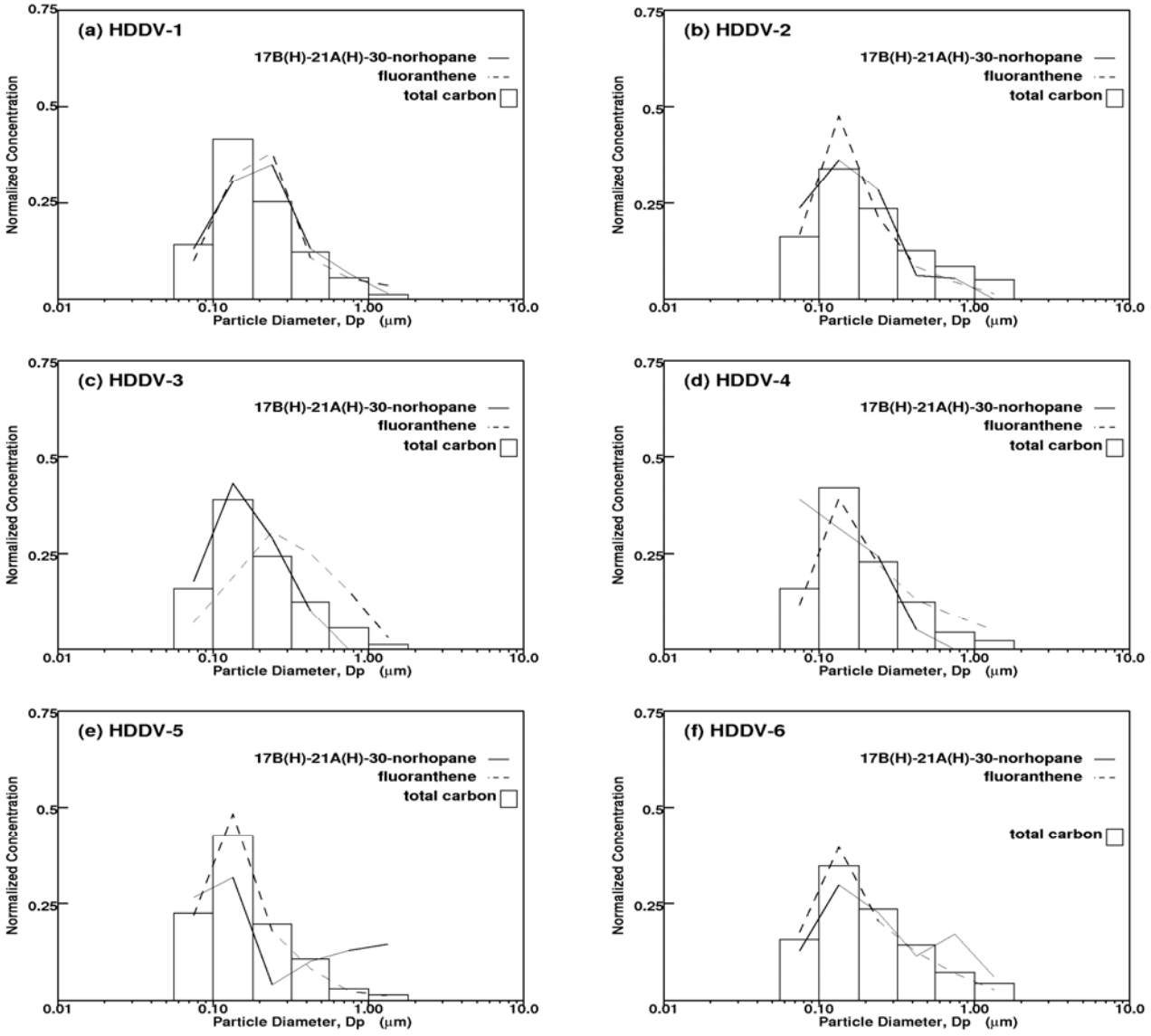

Figure 9-1: Normalized size distribution of total carbon, 17α(H)-21β(H)-29-norhopane, and fluoranthene emitted from diesel vehicles operated on a chassis dynamometer under transient driving cycles. Normalized concentrations in each size fraction are calculated by dividing the mass by the total measured PM1.8 mass.

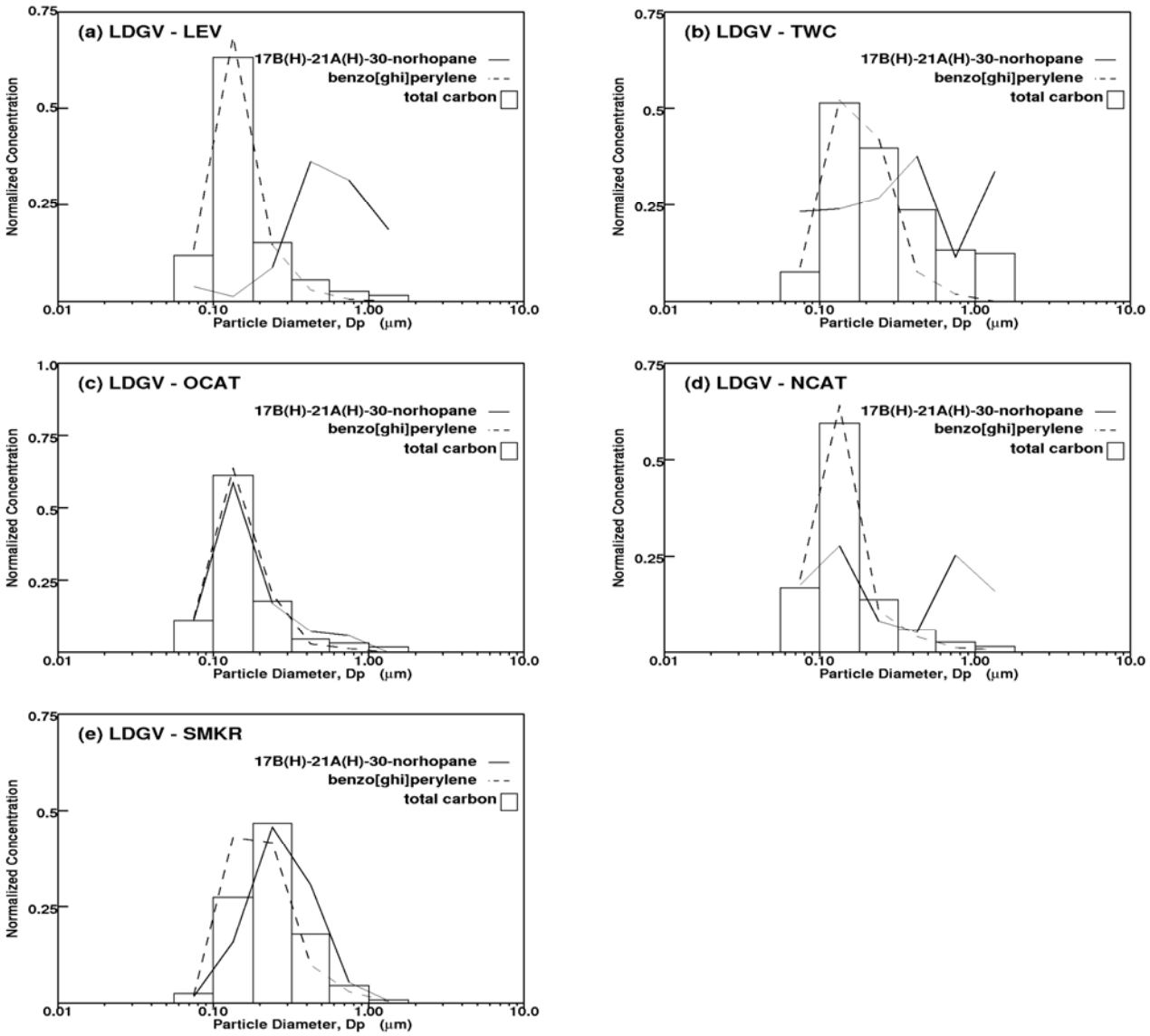

Figure 9-2: Normalized size distribution of total carbon, 17α(H)-21β(H)-29-norhopane, and benzo[ghi]perylene emitted from gasoline vehicles operated on a chassis dynamometer under transient driving cycles. Normalized concentrations in each size fraction are calculated by dividing the mass by the total measured PM1.8 mass.

Table 9-1: Results of the multivariate correlation analyses of fuel and oil tracers with both elemental and organic carbon for heavy duty diesel vehicles and light duty gasoline vehicles operated on chassis dynamometers. Oil tracers concentrations are 17α(H)-21β(H)-29-norhopane, 17α(H)-21β(H)-hopane, αββ-20R-stigmastane and αββ-20S-stigmastane normalized to the concentration 17α(H)-21β(H)-29-norhopane . Fuel tracer concentrations for gasoline vehicles are benzo[ghi]perylene and coronene normalized to the concentration of benzo[ghi]perylene. Fuel tracers for diesel vehicles are fluoranthene and pyrene normalized to the concentration of fluoranthene. Uncertainty estimates are 95% confidence intervals.

	Elemental Carbon (µg EC / ng tracer)			**Organic Carbon (µg OC / ng tracer)**		
	Oil tracer	**Diesel fuel tracer**	**R^2**	**Oil tracer**	**Diesel fuel tracer**	**R^2**
Diesel Vehicles						
HDD-1	2.6 ± 0.64	7.1 ± 9.8	0.97	5.6 ± 2.8	11.2 ± 42.1	0.94
HDD-2	5.6 ± 8.7	4.95 ± 4.92	0.93	4.6 ± 3.2	2.2 ± 1.8	0.97
HDD-3	8.7 ± 0.37	5.4 ± 0.62	1.00	7.9 ± 0.48	2.7 ± 0.81	0.99
HDD-4	0.24 ± 0.51	24.0 ± 1..5	0.99	0.0 ± 0.45	15 ± 1.4	0.99
HDD-5	2.2 ± 4.7	12.3 ± 1.6	0.96	0.71 ± 0.94	1.95 ± 0.31	0.98
HDD-6	9.8 ± 4.6	8.5 ± 1.6	0.97	0.045 ± 0.69	2.6 ± 0.23	0.99
Gasoline Vehicles	**Oil tracer**	**Gasoline fuel tracer**		**Oil tracer**	**Gasoline fuel tracer**	
LEV	0.82 ± 0.28	6.3 ± 0.11	1.00	1.0 ± 0.28	1.4 ± 0.11	0.99
TWC	1.1 ± 0.79	1.7 ± 0.13	0.99	1.50 ± 0.70	0.97 ± 0.12	0.99
OCAT	1.45 ± 0.39	0.036 ± 0.20	0.99	2.9 ± 1.3	4.0 ± 0.66	1.00
NCAT	1.1 ± 1.2	0.34 ± 0.026	0.99	3.5 ± 1.6	0.25 ± 0.034	0.98
SMKR	0.20 ± 0.055	0.047 ± 0.014	0.97	3.7 ± 0.46	0.91 ± 0.12	0.99

Table 9-1 shows that the amount of EC associated with each unit of oil tracer in the present study ranged from 0.24 – 9.8 (µg EC / ng tracer) for diesel vehicles depending on the vehicle age, driving cycle, and simulated load. The test with the highest simulated load (HDD-4) had the lowest amount of EC associated with each unit of oil tracer (0.24 µg EC / ng tracer). The same vehicle tested with the identical driving cycle but with 15% lower inertial load exhibited one of the highest EC concentrations per unit of oil tracer (8.7 µg C / ng tracer). Vehicle load is correlated with exhaust temperature [95] which appears to modify either the amount of tracer compound or the fraction of motor oil that is measured as EC in the vehicle exhaust. Previous analysis has revealed that higher loads shift the size distribution of motor oil tracer compounds to smaller sizes with less size shift observed for EC [103].

The amount of EC associated with each unit of oil tracer emitted from gasoline vehicles was more constant than that observed for diesel vehicles. Gasoline vehicles emitting visible smoke (SMKR) had the lowest ratios of EC per unit of oil tracer at approximately 0.2 (µg C / ng tracer). It seems likely that these vehicles emitted motor oil with minimal chemical modification. All other gasoline vehicle categories emitted approximately 1 (µg EC / ng oil tracer) under the FTP driving cycle indicating that at least some of the motor oil was chemically altered by the combustion process.

The amount of EC associated with fuel tracers varied from 5 – 24 (µg EC / ng tracer) for diesel vehicles depending on engine load condition. Test HDD-4 that operated under the highest inertial load conditions (66,000 lbs inertial weight) had the highest EC

emissions with 24 (μg EC / ng fuel tracer). Test HDD-5 was a vehicle operated at the standard inertial load (56,000 lbs) under the standard 5-mode transient driving cycle but this vehicle only had 280 hp compared to 460 hp (HDD-1, HDD-2)and 510 hp (HDD-3, HDD-4) in other tests. The increased production of soot from diesel engines under high load conditions is well documented and the ability of the regression analysis to identify this feature in the measurements increases confidence in the regression approach.

The amount of EC associated with fuel tracers emitted from gasoline vehicles spanned the range from ~0 – 6.3 (μg EC / ng tracer). The LEV's emitted the greatest amount of EC per unit of fuel tracer while the smoking vehicles (SMKR) emitted the smallest amount of EC per unit of fuel tracer. Time-resolved analysis showed that LEVs operated under the FTP driving cycle emitted most of their PM during the cold-start phase of the test when the combustion conditions were fuel-rich and the exhaust system was relatively cold [126]. The enhanced emission of soot from gasoline-powered vehicles under cold fuel-rich conditions has been identified in previous studies [97], once again building confidence in the regression analysis method. Smoking vehicles emitted unburned motor oil with little chemical modification. The low amount of EC per unit of fuel tracer from the SMKRs suggests that little pyrolized fuel was emitted from these vehicles.

The amount of organic carbon (OC) associated with each unit of oil tracer ranged from ~0 – 7.9 (μg OC / ng tracer) for diesel vehicles and 1.1 – 3.7 (μg OC / ng tracer) for gasoline vehicles. In most cases, the amount of OC associated with each unit of fuel tracer was comparable in magnitude, with values ranging from ~2.2 – 15 (μg OC / ng tracer) for diesel vehicles and 0.25 – 4.0 (μg OC / ng tracer) for gasoline vehicles.

Figure 9-7a illustrates the total particulate carbon (=EC + OC) per unit of 17α(H)-21β(H)-29-norhopane emitted from HDDVs and LDGVs. Lubricating oil that passes through the engine should retain a characteristic ratio of (total carbon / 17α(H)-21β(H)-29-norhopane) that reflects the relative concentration of the hopane in the oil. The degree to which the lubricating oil chars in the combustion chamber (converting OC to EC) should not affect the total carbon concentration. All of the LDGVs illustrated in Figure 9-7a exhibit a relatively constant ratio of total carbon per unit of 17α(H)-21β(H)-29-norhopane with values ranging from 2.5-4.5 (μg C / ng 17α(H)-21β(H)-29-norhopane). The uncertainty range around the HDDV predictions is greater than for LDGVs because hopane size distributions are similar to light PAH size distributions in the HDDV exhaust. Generally speaking, the HDDVs tested in the current study appear to emit ~3-10 (μg C / ng 17α(H)-21β(H)-29-norhopane). The enhancement of carbon emissions per unit of norhopane in HDDVs vs. LDGVs may be due to the use of heavier grade oils in the diesel engines. The only feature of Figure 9-7a that does not fit the expected pattern is the large different between test HDD-3 and HDD-4 that used the same vehicle under different load conditions. The reason for this discrepancy is unknown.

Figure 9-7b illustrates the total particulate carbon emitted per unit of fluoranthene (HDDVs) and per unit of benzo[ghi]perylene (LDGVs) during chassis dynamometer tests. The amount of particulate matter produced from each unit of fuel input is expected

to depend on engine technology, emissions control technology, and driving cycle. Most HDDVs emitted ~8-19 (µg C / ng fluoranthene) under normal load conditions, with ~40 (µg C / ng fluoranthene) observed during test HDD-4 that used higher load conditions. The same test predicted relatively low concentrations of carbon per unit of norhopane. Once again, the explanation for this single outlier is not obvious. Gasoline vehicles emitted ~1-10 (µg C / ng benzo[ghi]perylene), with the highest relative concentrations observed in relatively "clean" vehicles that released the majority of their particulate matter emissions during the cold-start phase of the FTP driving cycle.

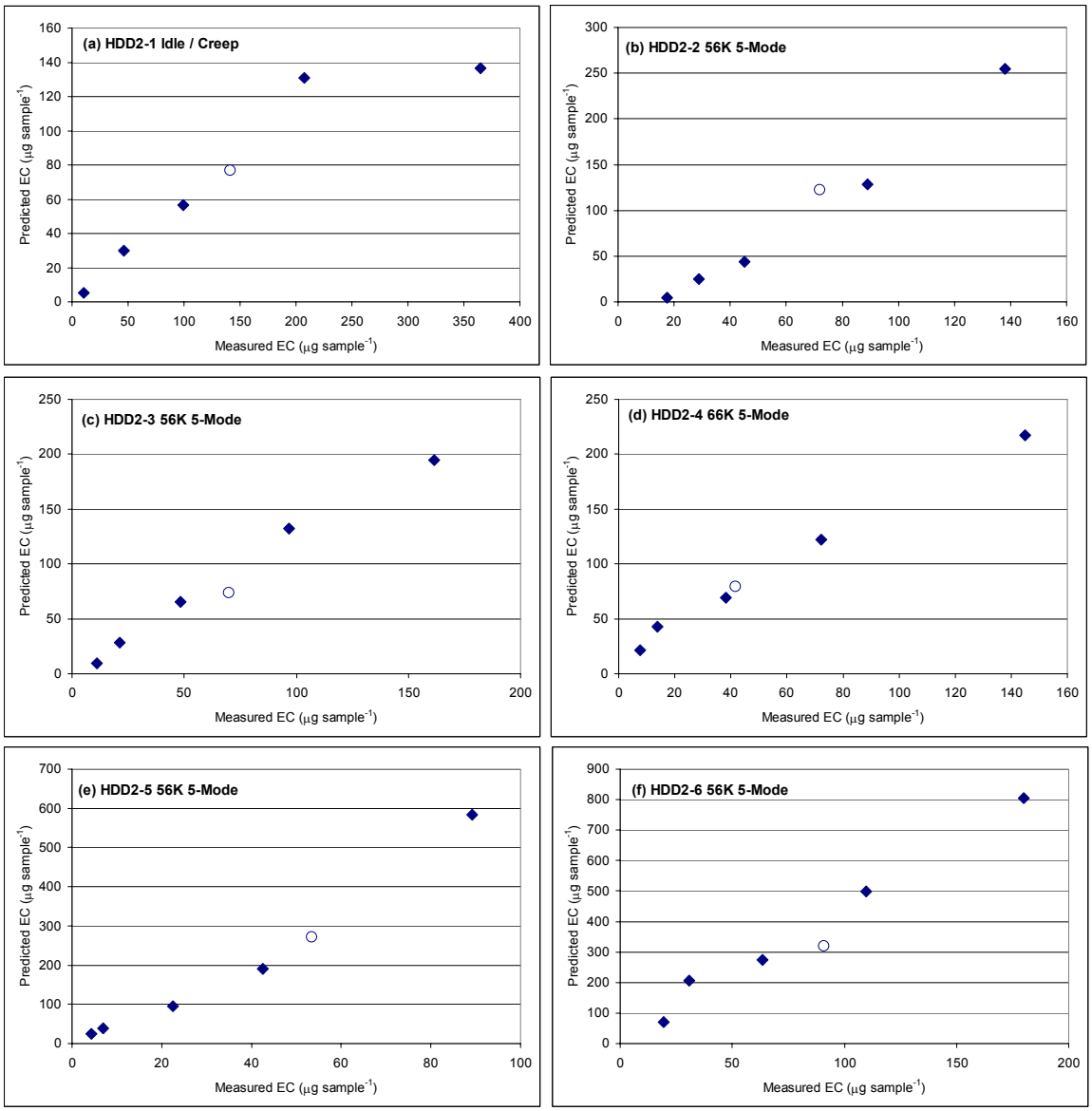

Figure 9-3: Comparison between measured concentrations of EC collected on each MOUDI stage during HDDV tests vs. predicted concentrations using equation (1). Correlation coefficients (R^2) are displayed in Table 1. The open circle represents the ultrafine (PM0.1) stage.

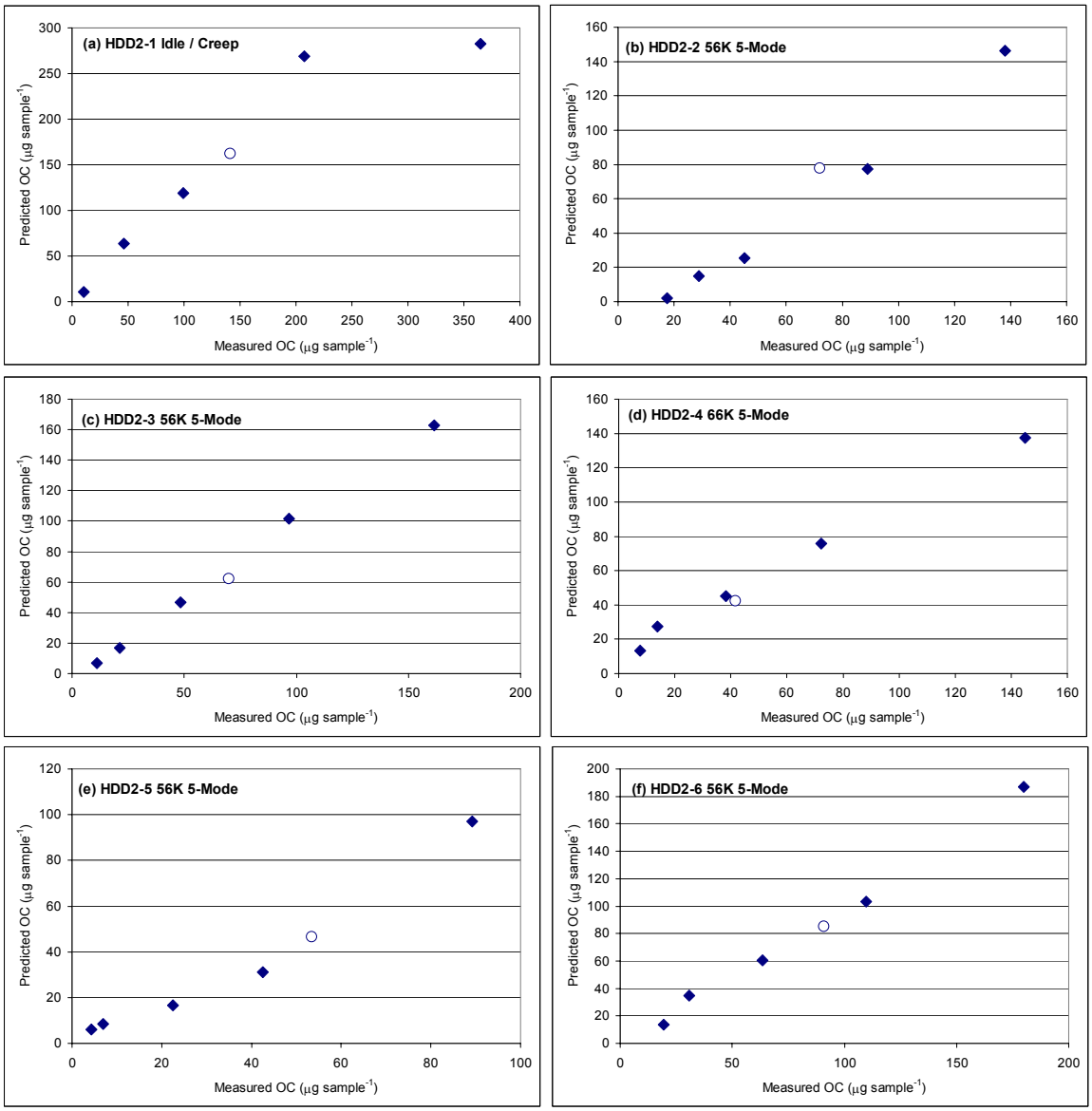

Figure 9-4: Comparison between measured concentrations of OC collected on each MOUDI stage during HDDV tests vs. predicted concentrations using equation (1). Correlation coefficients (R^2) are displayed in Table 9-1. The open circle represents the ultrafine (PM0.1) stage.

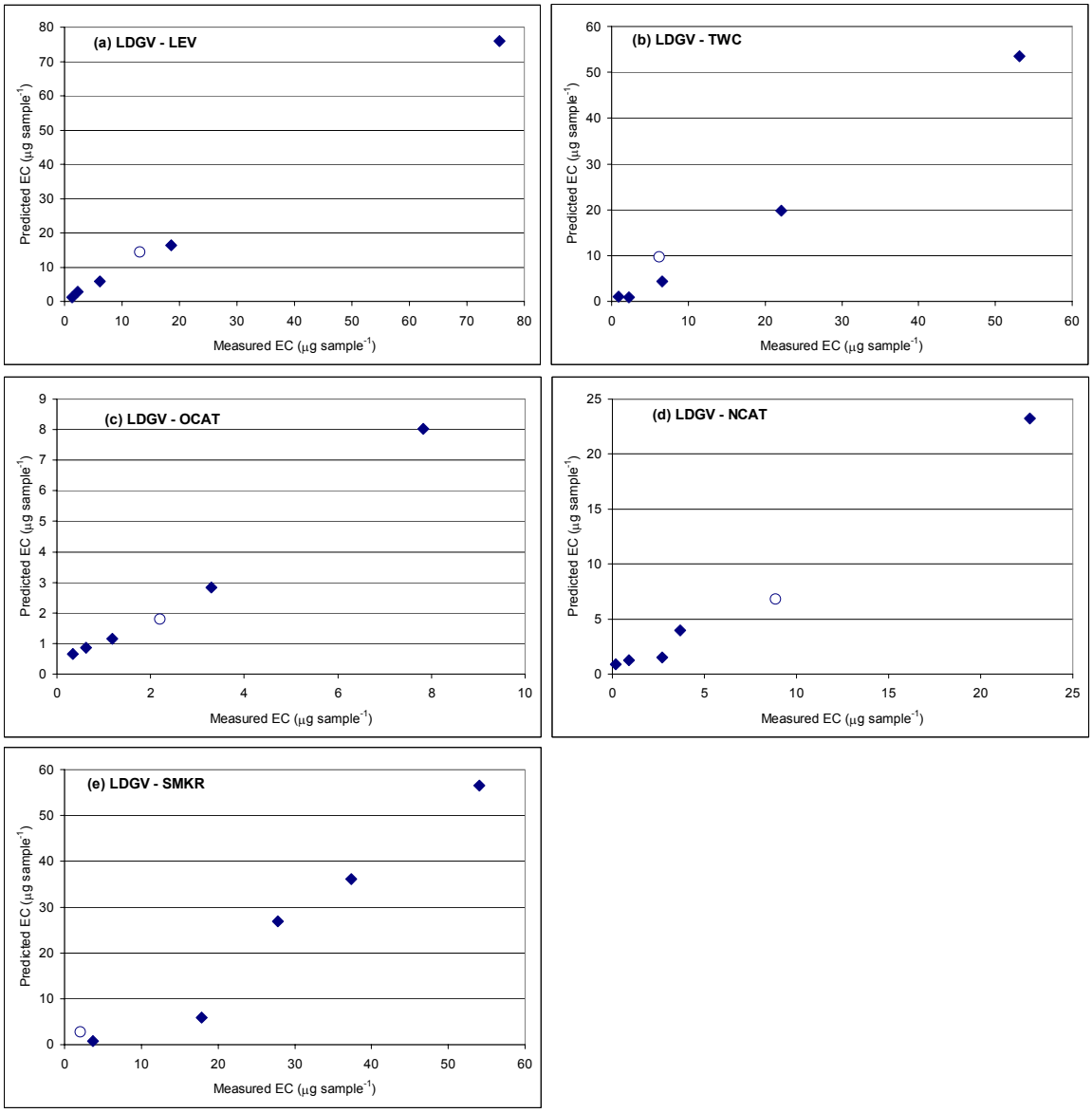

Figure 9-5: Comparison between measured concentrations of EC collected on each MOUDI stage during LDGV tests vs. predicted concentrations using equation (1). Correlation coefficients (R^2) are displayed in Table 9-1. The open circle represents the ultrafine (PM0.1) stage.

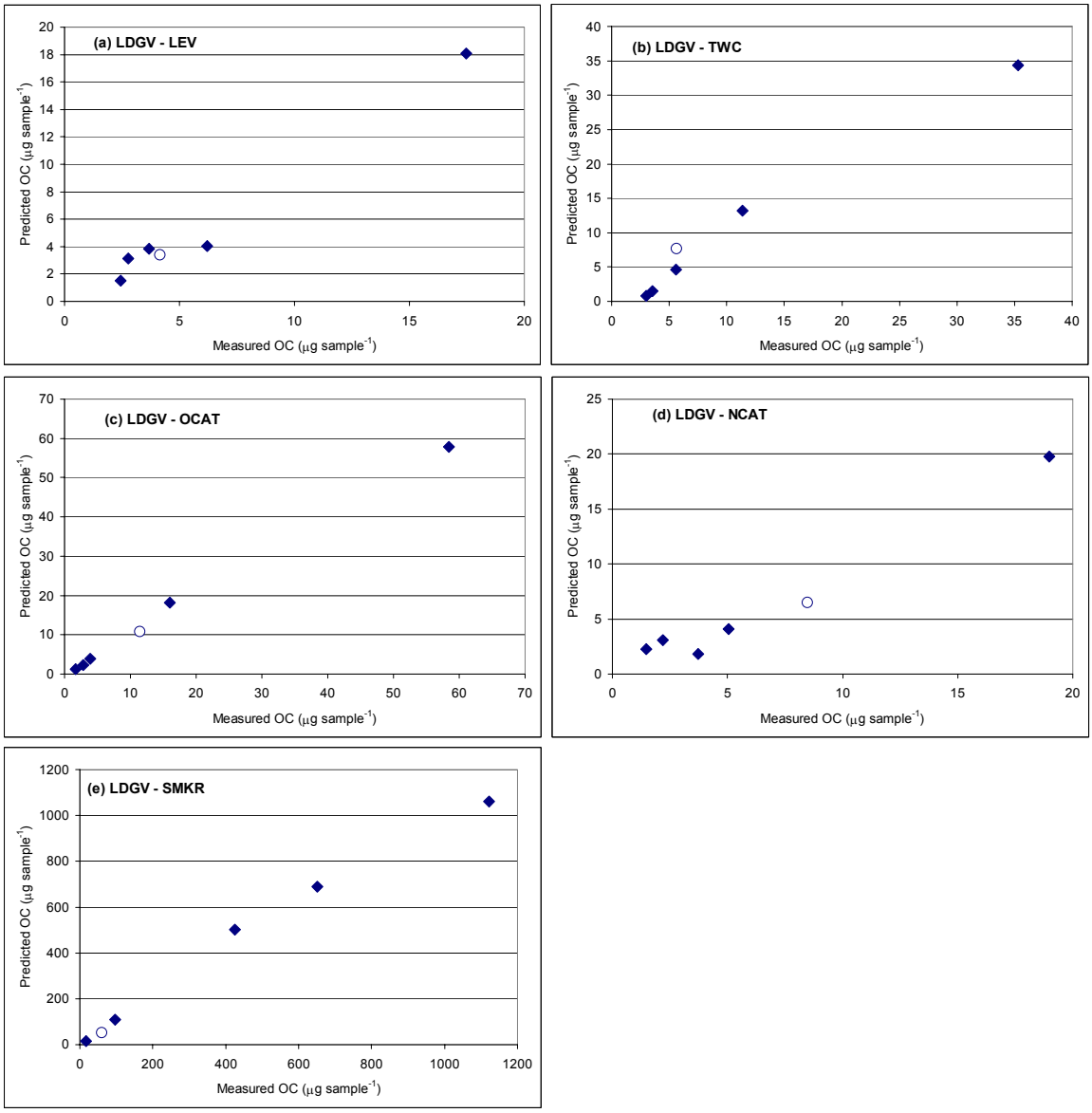

Figure 9-6: Comparison between measured concentrations of OC collected on each MOUDI stage during LDGV tests vs. predicted concentrations using equation (1). Correlation coefficients (R^2) are displayed in Table 9-1. The open circle represents the ultrafine (PM0.1) stage.

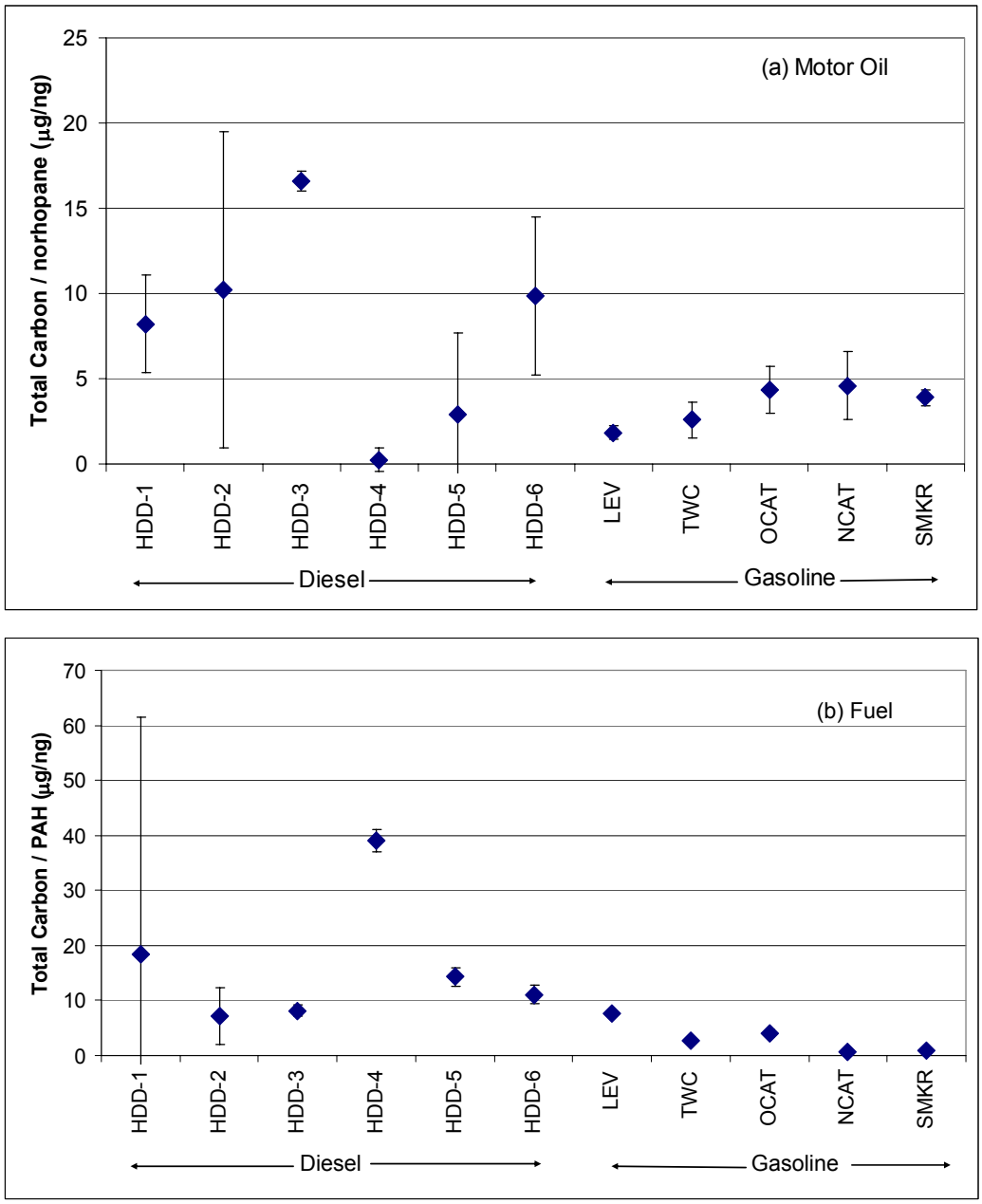

Figure 9-7: Quantity of total particulate carbon (=EC+OC) associated with each unit of norhopane derived from motor oil (panel a) and PAH derived from fuel (panel b) during HDDV and LDGV testing. Note that the PAH used for diesel fuel was fluoranthene and the PAH used for gasoline was benzo(ghi)perylene. The uncertainty range corresponds to 95% confidence intervals for the regression analysis summarized in Table 9-1.

9.3.2 Size-Resolved Source Profiles

Figure 9-8 shows source contributions to each μg of particulate carbon emitted from Heavy Duty Diesel Vehicles (HDDVs) predicted using the regression factors shown in Table 9-1 and the size-resolved emissions rates of each trace organic compound as discussed in previous studies [103]. EC and OC associated with oil and fuel tracers are shown separately in each panel. Residual concentrations (positive and negative) are shown as "unknown" in each figure. All reconstructed diesel source profiles had a peak in the size bin between 0.1 – 0.18 μm aerodynamic diameter but source contribution trends depend strongly on vehicle age and load. Test with the highest loads relative to engine horsepower (HDDV-4 and HDDV-5) had the greatest amount of EC associated with diesel fuel and the least amount of EC associated with lubricating oil. This matches the expected behavior of compression igninition engines operating in fuel-rich conditions. The test with the lowest load (HDDV-1) had the most OC associated with lubricating oil. Fuel contributions to OC size distributions were relatively consistent across all tests except HDDV-3. All of the reconstructed carbon size distributions shown in Figure 9-3 closely match the measured carbon size distributions reported in Chapter 2 [93] as would be expected since the correlation coefficients (R^2) shown in Table 9-1 are very close to unity.

Figure 9-4 shows source contributions to each μg of particulate carbon emitted from Light Duty Gasoline Vehicles (LDGVs) predicted using the regression factors shown in Table 9-1 and the measured emissions rates of tracer compounds [130]. All reconstructed LDGV source profiles peak between 0.1 – 0.18 μm particle diameter except SMKRs which peak between 0.18 – 0.32 μm particle diameter. These size distributions closely match measured size distribution of EC and OC reported in Chapter 3 [132]. Fuel contributions to EC dominate the carbonaceous emissions from LEVs, TWCs, and NCATs. Each of these samples was dominated by emissions released without a functioning catalyst. In the case of LEVs and TWCs, a significant fraction of the emissions were released when the engine was operating under "cold-start" conditions in a fuel-rich mode and before the catalyst reached operating temperature. Enhanced EC production from spark ignition engines is expected under these conditions. Fuel contributions to OC are also significant in all LDGV samples but little trend is observed between the different vehicle categories. Oil contributions to OC are most significant from the smoking vehicles (SMKRs) as would be expected since the majority of the smoke emissions are likely motor oil. Oil OC emissions are also significant from vehicles equipped with oxidation catalysts (OCATs), although the absolute emissions rates from these vehicles (μg / km) are much lower than emissions from SMKRs [132].

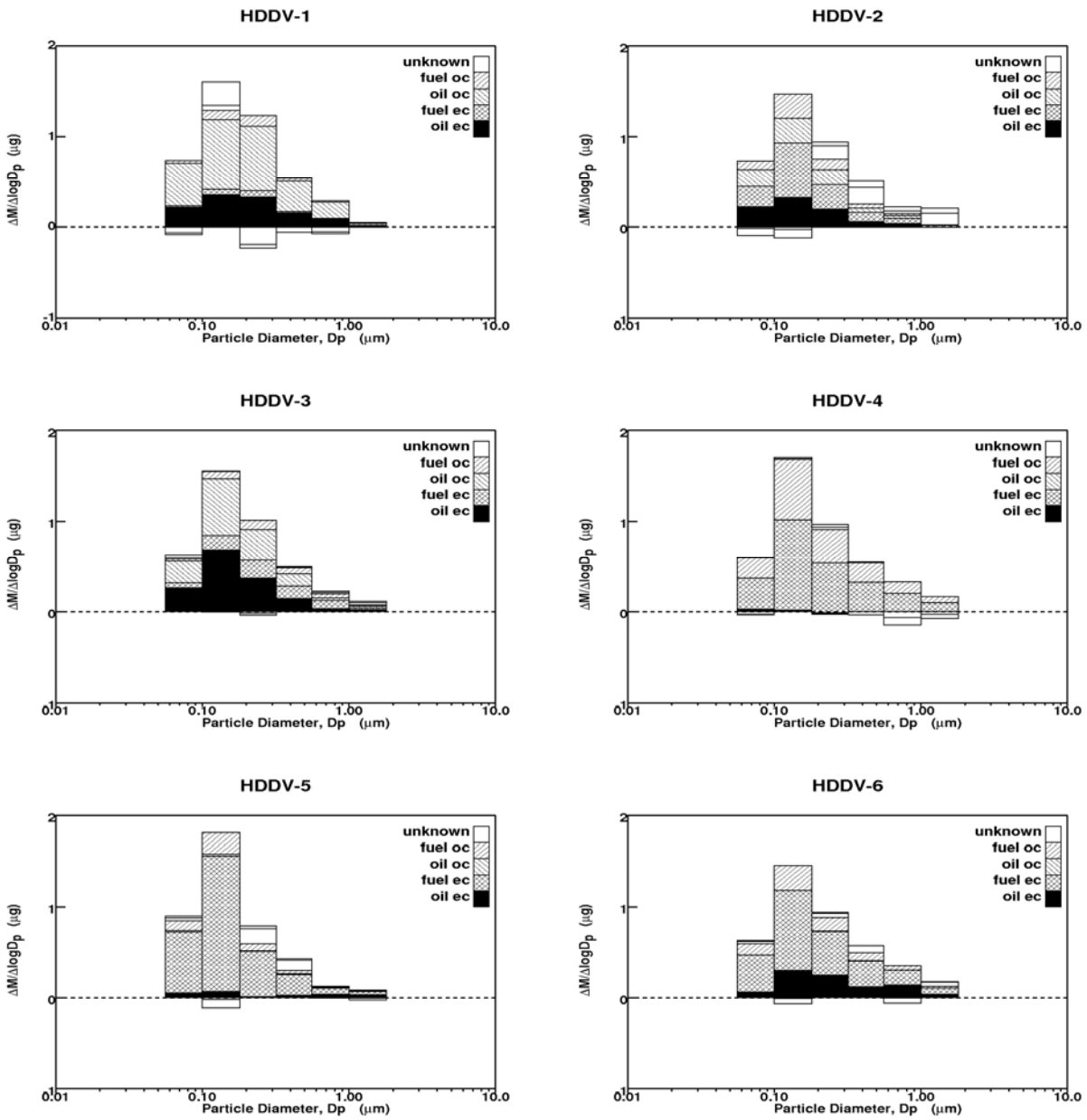

Figure 9-8: Constructed source profiles for 1 µg of particulate matter emitted from Heavy Duty Diesel Vehicles (HDDVs) operated under HHDDT driving cycles. Each panel represents emissions from a different HDDV. Test HDDV-1 used only the idle+creep portion of the HHDDT driving cycle while all other tests used the full 5-modes of the HHDDT including transients and high speed cruises. All tests used a simulated inertial weight of 56,000 lbs except for HDDV-4 which used a simulated weight of 66,000 lbs.

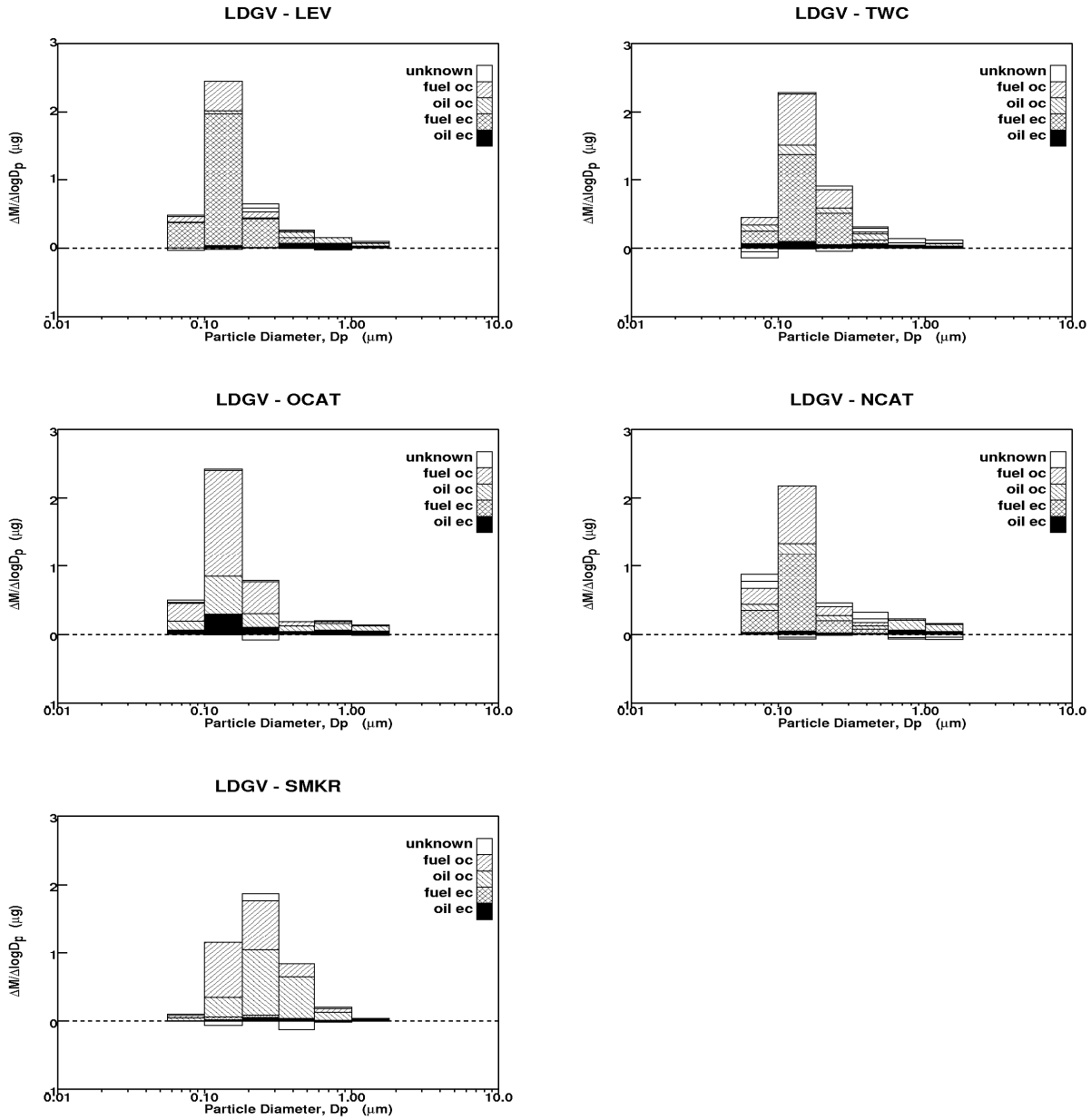

Figure 9-9: Constructed source profiles for 1 µg of particulate matter emitted from Light Duty Gasoline Vehicles (LDGVs) operated under the Federal Test Procedure driving cycle. Each panel represents an average of multiple vehicles within different emissions control technology classes: Low Emission Vehicles (LEVs), Three Way Catalyst vehicles (TWC), Oxidation Catalyst vehicles (OCAT), Non-catalyst vehicles (NCAT), and smoking vehicles (SMKR).

9.4 Conclusions

Size-resolved samples of particulate matter emitted from heavy duty diesel vehicles (HDDVs) and light duty gasoline vehicles (LDGVs) were analyzed for elemental carbon (EC), organic carbon (OC), and individual organic compounds. The size distribution of EC and OC was well correlated in all tests. Hopane and sterane size distributions did not match the total carbon size distribution, suggesting that emission of lubricating oil are not the dominant source of particulate carbon in the exhaust. Regression analysis using 17α(H)-21β(H)-29-norhopane as a tracer for motor oil and flouranthene as a tracer for diesel fuel was able to explain the size distribution of particulate EC and OC emissions from HDDVs. A similar regression analysis performed using 17α(H)-21β(H)-29-norhopane as a tracer for lubricating oil and benzo[ghi]perylene as a tracer for gasoline was able to explain the size distribution of particulate EC and OC emitted from LDGVs. Fuel contributions to particulate matter exhaust from both HDDVs and LDGVs were very significant. EC emissions from all diesel vehicles operated under relatively high load conditions were dominated by fuel contributions. OC emissions from diesel vehicles were more evenly apportioned between fuel and oil contributions. EC emissions from LDGVs operated under fuel-rich conditions were also dominated fuel contributions. Fuel contributions also accounted for the majority of the OC emissions from LDGVs except for vehicles emitted visible smoke for which oil contributions to OC were slightly greater than fuel contributions.

The results of the current study clearly illustrate that fuel and lubricating oil make separate and distinct contributions to particulate matter emissions from motor vehicles. These particles should be tracked separately during ambient source apportionment studies since the atmospheric evolution and ultimate health effects of these particles may be different. The regression between tracer concentrations and EC/OC illustrated in this study provides source profile information that can be used in future ambient source apportionment studies.

10 SOURCE APPORTIONMENT OF ULTAFINE (PM0.1) AIRBORNE PARTICLES IN A ROADSIDE ENVIRONMENT

10.1 Introduction

Source apportionment studies for airborne particles have historically focused on PM10 (aerodynamic particle diameter Dp < 10 μm) (see for example [133-136]) or PM2.5 (aerodynamic particle diameter Dp < 2.5 μm) (see for example [81, 134, 137-139]). Recent evidence suggests that the ultrafine particle size fraction (Dp < 0.1 μm) may also be associated with adverse health effects [5, 10, 83-85]., but only preliminary estimates have been made about source contributions to PM0.1 concentrations based on emissions inventory estimates [61]. The size distribution of particles emitted from primary combustion sources extends into the ultrafine size range [58, 140] suggesting that fuel combustion may be one of the largest sources of ultrafine particle to the atmosphere. Transportation typically accounts for a large fraction of the fuel combustion in many urban areas, and it would be useful to study source contributions to ultrafine particles in a roadside environment as a first step towards a more comprehensive understanding of ultrafine source apportionment.

Source apportionment studies typically use chemical "fingerprints" or "source profiles" to quantify contributions to ambient PM concentrations. PM10 source profiles have been primarily constructed with elemental information because a large fraction of PM10 mass is made up by metals found in the earth's crust such as Si, Fe, and Ca and because elemental measurement techniques such as X-Ray Fluorescence (XRF) have been available to researchers for decades. The majority of primary PM2.5 particulate matter is typically composed of carbonaceous material. The concentration of metals in the PM2.5 size fraction is lower than in the PM10 size fraction producing greater relative uncertainty in PM2.5 source apportionment calculations that only use elemental source profiles. Additional PM2.5 source profiles have recently been developed that use organic molecular markers with greater source specificity [13, 14, 75, 141-151] leading to improved estimates for PM2.5 source contributions [79]. The PM0.1 size fraction is also dominated by carbonaceous material [61] suggesting that molecular markers will be the most useful method to construct source profiles for particles in the ultrafine size range.

The purpose of this chapter is to report the results of a source apportionment study for ultrafine particles adjacent to a busy freeway in San Diego, California using molecular markers as tracers. Size distributions of particle-phase hopanes, steranes, and PAHs measured next to Interstate 5 (I5) are reported for 6 size fractions 0.056 – 0.1, 0.1 – 0.18, 0.18 – 0.32, 0.32 – 0.56, 0.56 – 1.0, and 1.0 – 1.8 μm particle aerodynamic diameter. Comparisons are made to the size distribution of trace organic emissions from gasoline and diesel-powered vehicles measured during previous chassis dynamometer studies as reported in Chapters 4 and 5 [93, 103, 130, 132]. The source-resolved profiles developed in Chapter 9 are then used to calculate source contributions to PM0.1 carbon concentration in the roadside environment.

10.2 Methods

10.2.1 Sample Collection

Size-resolved samples of airborne particulate matter were collected at one site upwind (west) and two sites downwind (east) of the Interstate 5 (I5) freeway in San Diego, California. The upwind sample was collected on the roof of Urey Hall on the campus of the University of California, San Diego approximately 1500 m upwind of the southbound lane of I5. The first downwind sample was collected along the perimeter fence of I5 approximately 18 m east of the northbound lane, while the second downwind sample was collected approximately 37m east of the northbound lane. Samples were collected using Micro Orifice Uniform Deposit Impactors (MOUDIs) (MSP Corporation, Shoreview, MN) on aluminum foil substrates that were baked at 500^{o}C for 48 hrs prior to use to remove background carbon. Additional samples were collected on pre-baked quartz filters (Gellman QAO47) using Reference Ambient Air Samplers (RAAS) (Andersen Instruments). Both MOUDI and RAAS samplers employed an AIHL-design cyclone [35] to remove particles larger than 1.8 μm in aerodynamic diameter from the sample stream. All samples were collected between July 21-27, 2004. Further details of the sample collection methodology, meteorological conditions during sampling, and inorganic composition of the collected airborne particles are provided by Robert et al. [152].

10.2.2 Sample Extraction and Analysis for Organic Compounds

Sample extraction and analysis methodology is identical to that described in Chapters 4 and 5. Co-located MOUDI and RAAS samples were combined by size and extracted together in order to obtain sufficient mass for organic analysis. Sampling substrates were spiked with an isotopically labeled sterane (ααα-20R-cholestane-d_4) and two isotopically labeled PAHs (chrysene-d_{12} and dibenz[ah]anthracene-d_{14}) then allowed to dry. All samples were extracted by sonication in ~15 mL of dichloromethane. Extracts were then evaporated under nitrogen to a final volume of 50 μL.

Separation of the analytes was performed on an Agilent J&W DB-XLBMSD capillary GC column (30m x 0.25mm i.d. x 0.25 μm film thickness). Mass spectra were measured for each sample using a Varian 3400 gas chromatograph (GC) coupled with a Varian 2000 ion-trap mass spectrometer (ITMS) operated in electron impact (EI) ionization mass spectrometry/selected ion monitoring (SIM) mode. PAHs were measured by monitoring for the parent ion masses. Hopanes and steranes were monitored by scanning for their predominant fragment ions, m/z =191 and m/z=217/218 respectively. Other operating parameters of the GC-ITMS are those recommended by the manufacturer. Chemical species were identified by comparison to authentic standards or by comparison of relative retention times and mass spectra to those in the literature [104]. Further details of the procedures used for chemical analysis of organic compounds are provided by Riddle et al. [103, 130].

10.3 Results and Discussion

10.3.1 Measured Tracer Size Distributions Adjacent to the Roadway

The average normalized size distributions of lubricating oil tracers (hopanes and steranes), light PAHs, and heavy PAHs measured at 18 m and 37 m downwind of roadway are shown in Figure 10-1. Normalized size distributions were constructed by dividing the mass in each size fraction by the total PM1.8 mass summed across all size fractions. Size distributions for the samples collected 18 m downwind of the freeway are shown in the left column of Figure 10-1 while size distributions measured 37 m downwind of the freeway are shown on the right. Uncertainty bars shown in Figure 10-1 are one standard deviation of the individual compound values used to calculate the average within each size fraction.

Figure 10-1 panels a and b show that the normalized particulate hopane and sterane size distributions observed during the current study have a peak in the 0.10 – 0.18 μm size fraction at both 18 m and 37 m downwind of the freeway. The size distributions for the location 37 m downwind of the freeway show more variability than the distributions measured 18 m downwind due to the lower sample mass available for analysis. Size distributions for both the light and heavy PAHs (Figure 10-1 panels c-f) also peak in the 0.10 – 0.18 micron size fraction at both downwind locations. The relative amount of mass in the ultrafine size fraction is slightly higher 18 m downwind vs. 37 m downwind for all three classes of chemicals presented.

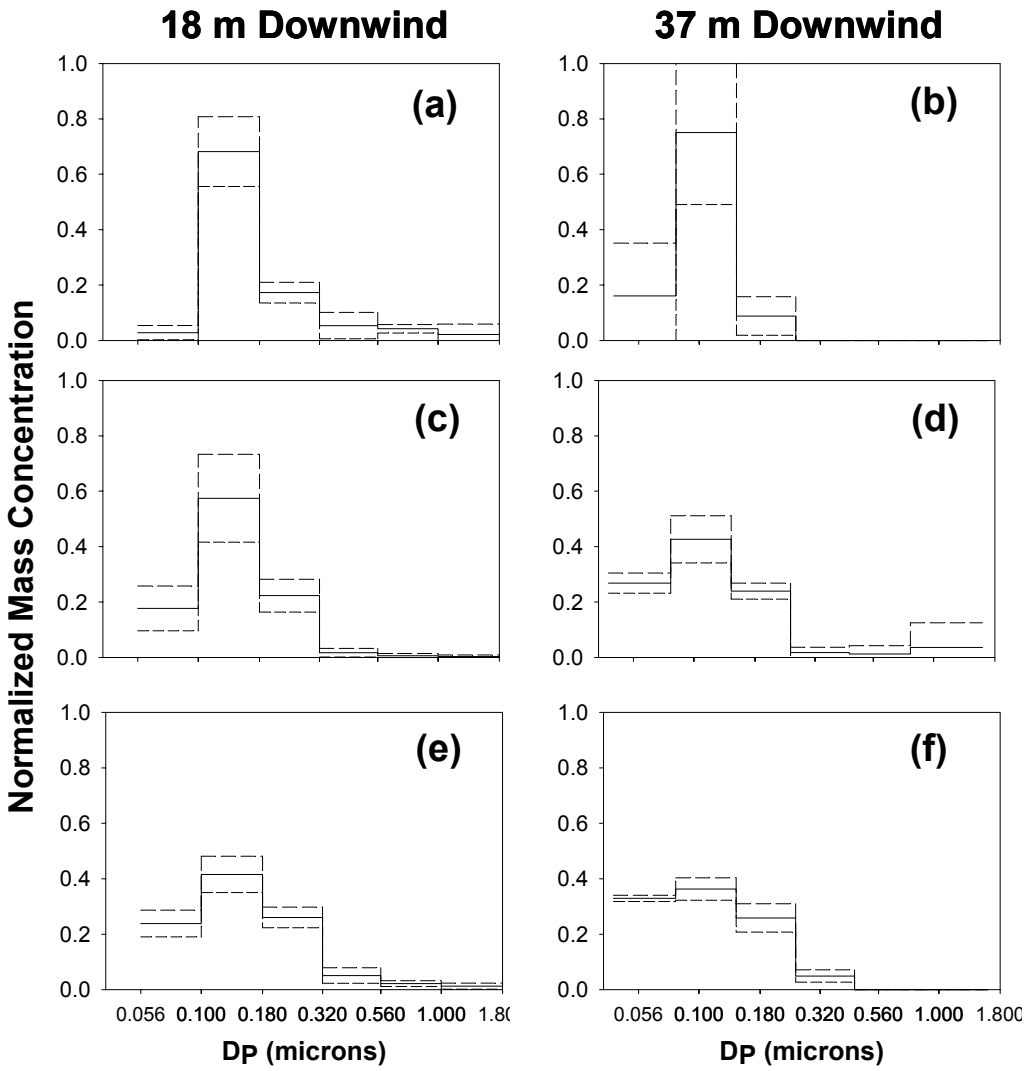

Figure 10-1: Average lubricating oil (hopane and sterane) tracer (panels a and b) normalized size distributions, average light PAH (panels c and d) normalized size distributions, and average heavy PAH (panels e and f) normalized size distributions 18 m and 37 m downwind of the freeway. Samples were normalized to collected PM1.8 analyte mass.

The organic compound size distributions measured in the roadside environment (shown in Figure 10-1) have a strong resemblance to the organic compound size distributions measured during chassis dynamometer studies [103, 130]. All hopane, sterane, and PAH size distributions associated with emissions from heavy duty diesel vehicles operated on a chassis dynamometer had an approximately log-normal shape with a peak between 0.10 – 0.18 μm aerodynamic diameter [103]. Likewise, PAH emissions from light duty gasoline vehicles operated on a chassis dynamometer had log-normal size distributions that peaked between 0.10 – 0.18 μm for all vehicle categories except those emitting visible smoke (PAH size distribution peak shifted to 0.18 – 0.32 μm) [130]. The geometric mean of PAH size distributions measured in the roadside environment during the current study are somewhat greater than those measured in either the heavy duty diesel vehicle or the light duty gasoline vehicle chassis dynamometer tests. This suggests

that the size distribution of EC and OC derived from diesel fuel and gasoline will also be broader in the roadside environment than in the chassis dynamometer tests.

Coronene and benzo[ghi]perylene were highly correlated in the roadside environment with a regression slope of 0.47. This ratio was slightly smaller than the coronene / benzo[ghi]perylene ratios of 0.57, 0.94, 0.99, 1.1, and 0.61 measured from LEVs, TWCs, OCATs, NCATs, and SMKRs during chassis dynamometer testing [130]. Likewise, pyrene and fluoranthene were highly correlated in the roadside environment with a regression slope of 1.3. This suggests that pyrene and fluoranthene concentrations in the roadside environment are generated by a common source that is likely to be heavy duty diesel vehicles. Pyrene / fluoranthene ratios measured during chassis dynamometer testing of heavy duty diesel vehicles ranged from 1.6 – 2.4 [103].

Hopane and sterane size distributions emitted from light duty gasoline vehicles during chassis dynamometer tests varied depending on the emissions control technology used on the vehicle and the operating condition (cold vs. warm start). Vehicles without an operating catalyst and vehicles dominated by cold-start emissions before the catalyst reached operating temperature emitted bimodal hopane and sterane size distributions with the larger mode measured at particle diameter greater than 0.32 μm. The absence of hopane and sterane size distributions with bimodal shape in the current study suggests that emissions from this type of vehicle were not dominant in the roadside environment.

10.3.3 Size-Resolved Source Apportionment of Carbonaceous Particulate Matter in the Roadside Environment

PM2.5 emission estimates from different categories of motor vehicles driving on the I5 freeway in San Diego were obtained using the California Air Resources Board (CARB) Emission Factors (EMFAC) model for San Diego County. EMFAC results for July 2004 predict that 55% of the on-road PM2.5 emissions originate from diesel-powered vehicles, 44% originates from catalyst-equipped gasoline-powered vehicles (TWC), and 1% originates from non-catalyst-equipped gasoline-powered vehicles (NCAT). These factors were combined with the information shown in Table 9-1 to construct weighted-average profiles for lubricating oil and gasoline contributions to EC and OC in the roadside environment. Tracer mass was associated with the same amount of organic carbon regardless of size fraction, thus these equations can be utilized to determine the EC and OC in all fine size fractions. All catalyst-equipped gasoline vehicle emissions were represented using the TWC values, and all heavy duty diesel vehicles were represented using HDDV-5 values. These tests were chosen because the source profiles fell in the middle of the range of observed values (see Figure 9-7). The resulting equations for EC and OC were

$$\begin{aligned} EC \quad &= 1.6\ (\mu g\ EC / ng\ oil\ tracer) * oil\ tracer \\ &+ 6.2\ (\mu g\ EC / ng\ gasoline\ tracer) * gasoline\ fuel\ tracer \\ &+ 12.3\ (\mu g\ EC / ng\ diesel\ tracer) * diesel\ tracer \end{aligned} \qquad (1)$$

$$\begin{aligned} OC &= 0.87\ (\mu g\ OC / ng\ oil\ tracer) * oil\ tracer \\ &+ 1.4\ (\mu g\ OC / ng\ gasoline\ tracer) * gasoline\ fuel\ tracer \\ &+ 1.95\ (\mu g\ OC / ng\ diesel\ tracer) * diesel\ tracer \end{aligned} \quad (2)$$

Equations (1) and (2) were used to predict size distributions of EC and OC concentrations in the roadway environment using the measured organic tracer concentrations illustrated in Figure 10-1. The predicted EC and OC concentrations were then compared to concentrations measured at the roadway [152]. The roadway carbon signature was first background subtracted using upwind carbon size distribution measurements so that the traffic contribution was more clearly visible. Background concentrations measured approximately 12 m above the surface are larger than concentrations measured 1m above the surface due to depositional losses and the development of a logarithmic concentration gradient adjacent to the ground [153]. Background subtraction was further complicated by the fact that turbulent eddies generated by the topography of the roadway and the vehicles traveling on the roadway caused differing amounts of vertical mixing at the location 18 m downwind of the roadway vs. 37 m downwind of the roadway. Vanadium was used as a marker to determine appropriate amounts of background subtraction at each location. Vanadium is commonly detected in the emissions from ships burning residual fuel oil that likely account for the majority of the "background" aerosol in the vicinity of San Diego coastline. Vanadium concentration were measured to be 5.7 ng m^{-3} at Urey Hall (the background location), 6.0 ng m^{-3} 18 m downwind of the roadway, 2.2 ng m^{-3} 37 m downwind of the roadway. The sharp variation in background concentrations at 18 m vs. 37 m downwind of the roadway illustrates the great effect of down-mixing caused by mechanical turbulence adjacent to the freeway. These trends emphasizes that care must be exercised when interpreting measurements in the roadway environment so that changes in particle size and composition are attributed to the correct source and not to changes in vertical mixing.

Figure 10-2 illustrates predicted source contributions to the size distribution of EC and OC 18 m and 37 m downwind of the roadway. Residual concentrations (positive or negative) are shown as "unknown" in each size fraction. Both measured and predicted EC concentrations emitted from the roadway are larger than OC concentrations. EC concentrations decreased by 25-33% between 18 m – 37 m downwind of the roadway due to dilution with background air. The peak in both the measured and predicted EC size distribution occurred between 0.1 – 0.18 μm particle aerodynamic diameter. Lubricating oil, diesel fuel, and gasoline all contributed to EC concentrations across the full size range, with the highest concentrations in size fractions below 0.18 μm particle diameter. Lubricating oil, diesel fuel, and gasoline account for the majority of the ultrafine EC in the roadside environment.

The peak in the OC size distribution at both 18m and 37m downwind of the freeway occurred between 0.56 – 1.0 μm particle diameter. OC concentrations decrease by 24-33% between 18 m – 37 m downwind of the roadway (similar to EC trends). Predicted source contributions to OC concentrations in the PM0.18 size fraction are 27-71% greater than measured concentrations at the sampling location 18 m downwind of

the roadway. Predicted source contributions to PM0.18 OC concentrations 37 m downwind of the freeway are very close to measured concentrations, suggesting that the additional dilution that occurs between 18m – 37m causes some of the most volatile organic compounds to evaporate from the particles yielding a more representative near-field source characterization that matches the conditions in the chassis dynamometer tests.

A fraction of the EC was not explained by the regression model using lubricating oil and fuel tracers. This "unknown" EC may have been produced by other sources in size fractions larger than 0.18 μm. Possible sources of this additional EC include road, brake, and/or tire dust, all of which contain a significant amount of elemental carbon [150, 154]. It is unlikely that these mechanical generation sources produced EC in the ultrafine size fraction. Likewise, a significant amount of "unknown" OC was observed both at 18 m and 37 m downwind of the roadway. The size distribution of this excess OC peaks between 0.56 – 1.0 μm particle aerodynamic diameter. This material may reflect contributions from road dust or secondary organic aerosol formation.

An alternative explanation for the underprediction of ultrafine EC and OC in the roadside environment is that the fluoranthene tracer used to estimate diesel fuel contributions partially volatilized during sample collection, yielding underpredictios for the diesel fuel contribution to ambient particulate matter. Traditional CMB applications use EC as a tracer for diesel engine source contributions after the concentration of EC from all other minor sources has been subtracted. The same approach can be adopted in the current study by calculating the amount of EC associated with gasoline and lubricating oil and then assigning the remaining EC to diesel engines. The ratio of OC/EC from diesel engines in the fine particle size fraction has been measured to be 1/2.56 = 0.39 in previous studies (see Chapter 13). This value is consistent with the range of EC/OC values measured during HDDV testing in the current study (see Chapters 2, 3) and will be used in the current analysis.

Figure 10-3 illustrates the predicted source contributions to EC and OC concentrations in the roadside environment if all residual EC not attributed to lubricating oil and gasoline is assigned to diesel engines. EC concentrations across the entire size range are dominated by contributions from diesel engines when this assumption is made. PM0.18 OC concentrations are overpredicted by 50-100% using this approach because of the additional diesel OC that is carried along with the EC. It is interesting to note that some residual OC underpredictions remain for size fractions larger than 0.18 μm, yielding a total fine (PM1.8) OC prediction that is approximately balanced. The size-resolved measurements clearly indicate that this "balance" is achieved with overpredictions at smaller particle sizes and underpredictions for larger particles which is not physically possible. These results suggest that either the residual ultrafine EC shown in Figure 10-2 is from sources other than diesel engines or that the ratio of OC/EC in the ultrafine particulate exhaust from diesel engines is less than 0.39. In either case, the traditional CMB approach of treating EC as a tracer species does not appear to yield good results for the ultrafine size fraction in the current study.

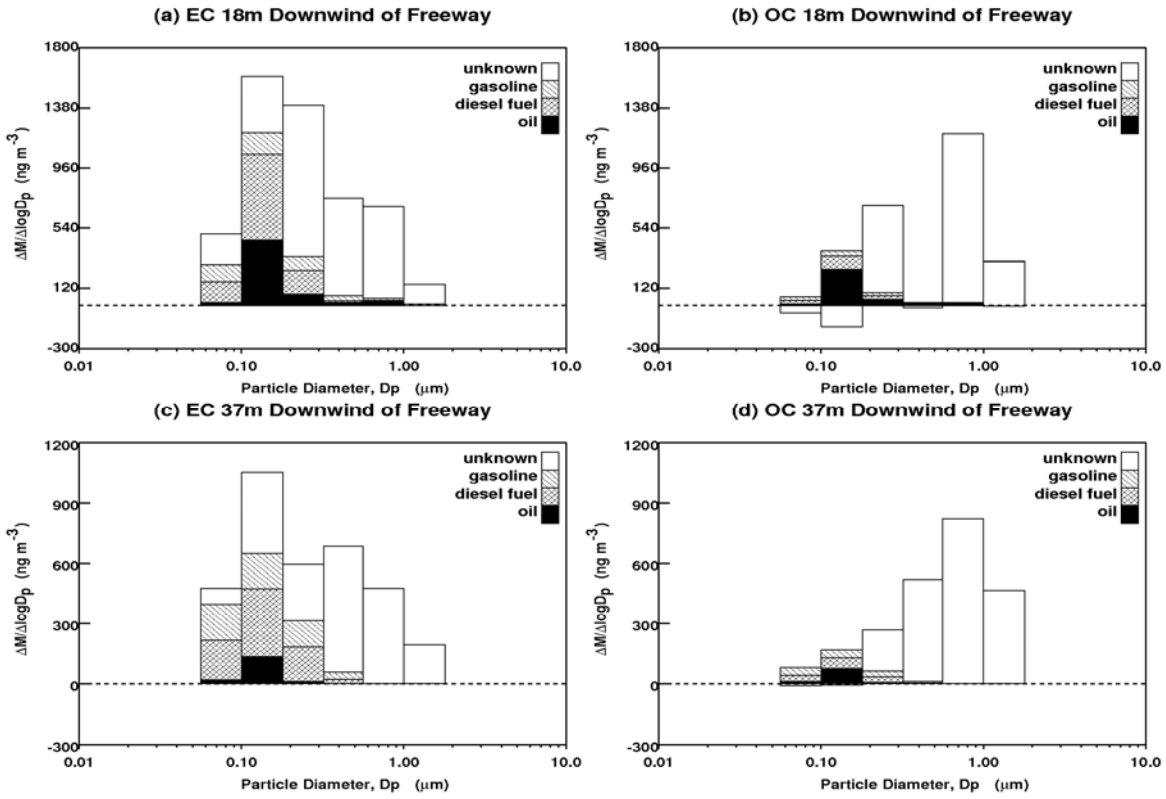

Figure 10-2: Estimated source contributions to Elemental Carbon (EC) and Organic Carbon (OC) measured at 18m and 37m downwind of a busy freeway in San Diego, California. Residual concentrations are shown as "unknown". Diesel fuel concentrations use fluoranthene as a tracer.

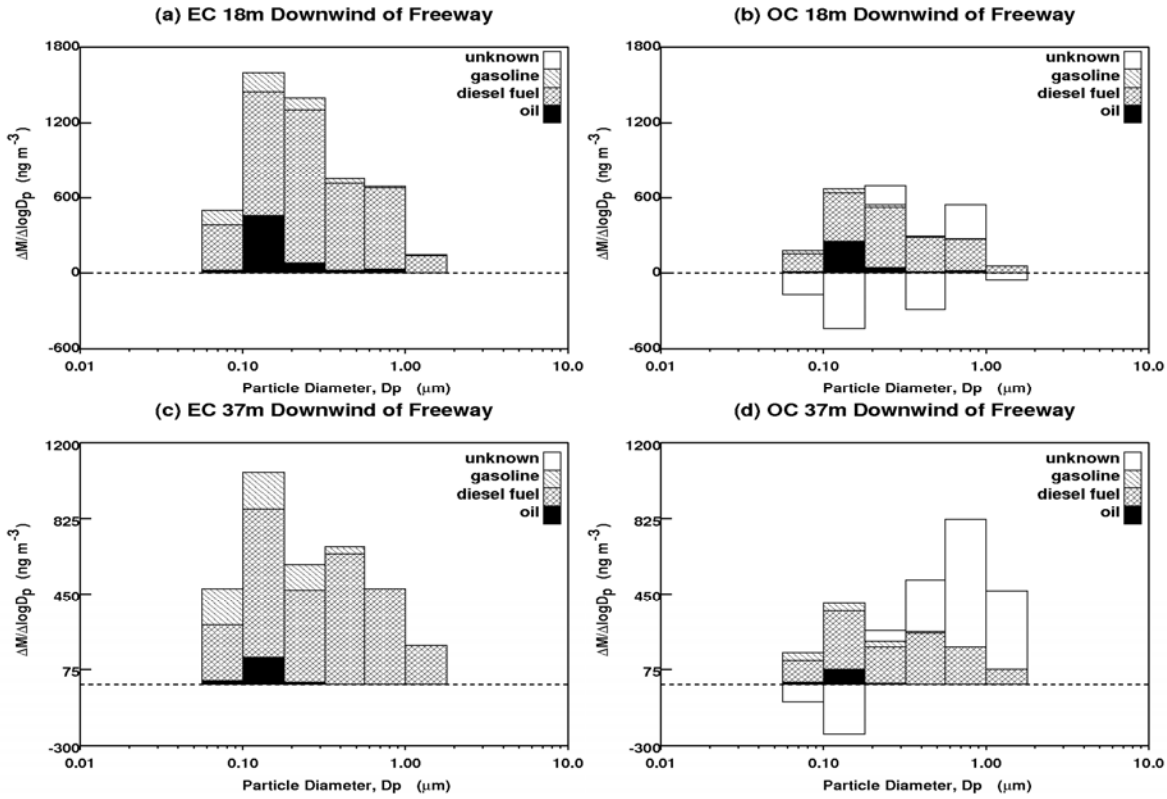

Figure 10-3: Estimated source contributions to Elemental Carbon (EC) and Organic Carbon (OC) measured at 18m and 37m downwind of a busy freeway in San Diego, California. Residual concentrations are shown as "unknown". Residual EC concentrations are assigned to diesel fuel with an OC/EC ratio of 0.39.

10.3.4 Source Contributions to Ultrafine PM in the Roadside Environment

Figure 10-4 illustrates predicted source contributions to ultrafine (Dp < 100 nm) EC and OC concentrations 18 m and 37 m downwind of the roadway calculated based on the results illustrated in Figure 10-2. Motor oil (from either gasoline or diesel engines) accounts for 4% of PM0.1 EC and 12-19% of PM0.1 OC. Predicted gasoline-fuel and diesel-fuel contributions to PM0.1 EC and PM0.1 OC are nearly identical. Diesel-fuel contributions to PM0.1 EC (29-41%) are slightly greater than gasoline-fuel contributions (23-36%). The opposite trend is observed for PM0.1 OC concentrations with slightly greater predicted contributions from gasoline-fuel (43-49%) than diesel-fuel (36-39%). Approximately 17-44% of the PM0.1 EC mass was unaccounted for.

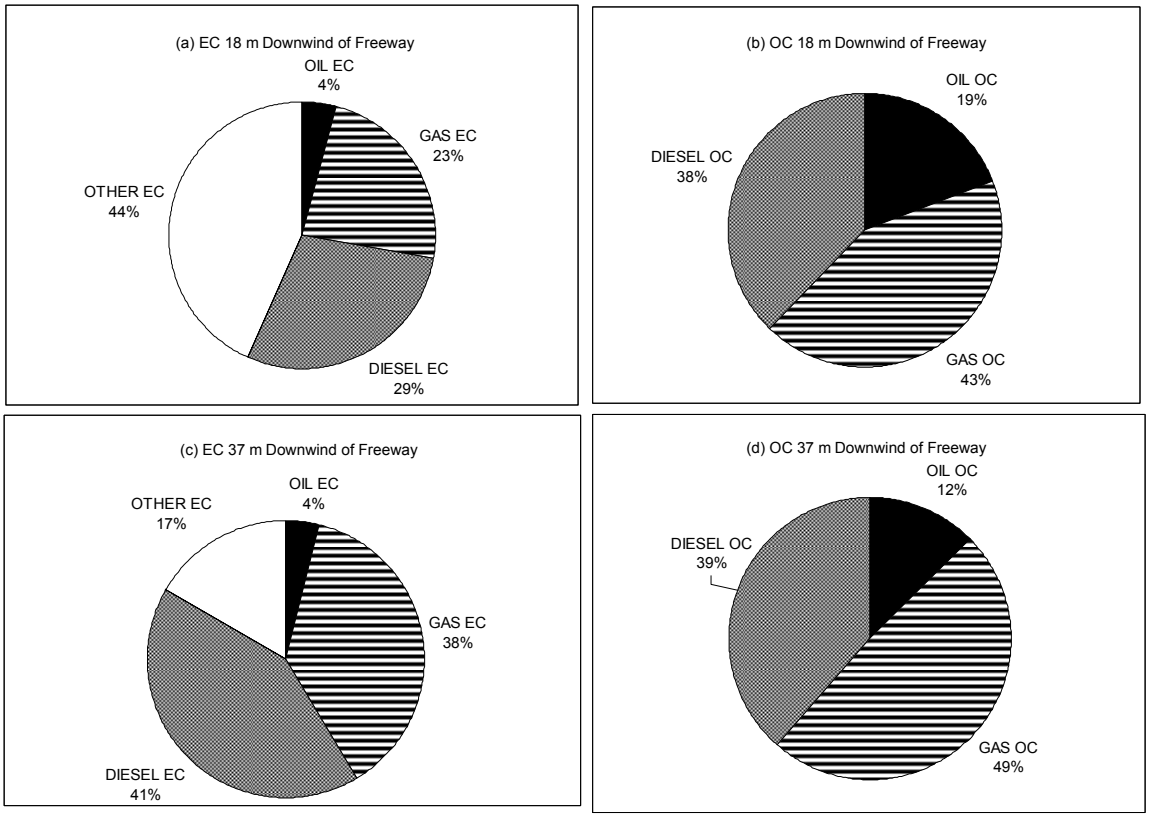

Figure 10-4: Calculated source contributions to elemental carbon (EC) and organic compounds (OC) in the PM0.1 size fraction 18 m downwind of the freeway (panels a, b) and 37 m downwind of the freeway (panels c, d). Oil EC and OC includes contributions from all vehicle types. Gas EC and OC refer to contributions derived from gasoline only. Diesel EC and OC refer to contributions derived from diesel fuel only. Flouranthene is used as a tracer for diesel fuel contributions.

10.4 Conclusions

Size distributions of particulate hopanes, steranes, and polycyclic aromatic hydrocarbons (PAHs) were measured at one site upwind (west) and two sites downwind (east) of the Interstate 5 (I5) freeway in San Diego, California. Particulate matter was collected with cascade impactors and filter samplers. Samples were extracted using organic solvents and analyzed using GC-MS. Size distributions of hopanes and steranes peaked in the 0.10 – 0.18 μm size range which corresponds with previous vehicular studies of lubricating oil size distributions. Light, particle-phase 4-ring PAHs have the same size distributions at the roadside and in heavy-duty diesel vehicle exhaust measurements while the heavy PAH size distribution matches that seen for gasoline powered vehicles.

Regression analysis was performed on motor vehicle hopane, sterane, and PAH emissions to apportion elemental carbon and organic carbon emissions to fuel and motor oil. EMFAC results for July 2004 were used to weight motor oil and gasoline vehicle emissions profiles to create an appropriate on-road average profile. The resulting equations were used to predict size distributions of EC and OC concentrations in the

roadway environment using the measured organic tracer concentrations. The peak in both the measured and predicted EC size distribution occurred between 0.1 – 0.18 μm particle aerodynamic diameter. Lubricating oil, diesel fuel, and gasoline all contributed to EC concentrations across the full size range. Ultrafine OC concentrations measured 18 m downwind of the roadway were lower than the predicted values by 27-71%. Ultrafine OC concentrations measured 37 m downwind of the roadway were in good agreement with predicted values from gasoline fuel, diesel fuel, and motor oil.

Motor oil accounted for approximately 4% of the ultrafine EC and12-19% of the ultrafine OC in the roadside environment. Gasoline fuel accounted for 43-49% of the ultrafine OC in the roadside environment while diesel fuel accounted for 38-39% of the ultrafine OC. Gasoline fuel contributed 23-38% of the ultrafine EC tin the roadside environment while diesel fuel contributed 29-41% of the ultrafine EC. Ultrafine EC from some other source accounted for 17-44% of the PM0.1 EC mass. These results highlight the significant contribution that fuel (both gasoline and diesel) make to ultrafine particle concentrations in the roadside environment.

11 SIZE DISTRIBUTION OF TRACE ORGANIC SPECIES EMITTED FROM BIOMASS COMBUSTION AND MEAT CHARBROILING

11.1 Introduction

According to the United States Environmental Protection Agency, biomass combustion accounts for approximately one third of the fine particulate matter (Dp < 2.5 μm; PM2.5) emissions to the atmosphere in the United States each year (http://www.epa.gov/ttn/chief/trends/index.html). The health effects of these emissions are uncertain, but epidemiological studies clearly show a relationship between increased PM2.5 concentrations in the atmosphere and increased mortality [155]. Recent studies have suggested that the ultrafine size fraction (Dp<0.1 μm) may pose an enhanced risk to human health [5, 83-85] possibly because ultrafine particles are small enough to pass through cell membranes allowing them to deliver potentially toxic compounds to cells [10].

Atmospheric particles in different size fractions typically have different source-origins and chemical compositions. The coarse particle size fraction (Dp < 10 μm) is typically dominated by windblown crustal material that can be characterized through elemental composition measurements (see for example [156]). The primary component of the fine particle size fraction (Dp < 2.5 μm) typically is dominated by combustion sources that can be characterized by organic compounds (see for example [14, 147, 157-159]). Preliminary measurements show that the ultrafine size fraction is also dominated by organic compounds [61, 65, 160], but the concentrations of organic compounds contained in ultrafine particles have only been reported for gasoline- and diesel-powered motor vehicles [90, 103, 159, 161], not for other types of combustion sources with the exception of polycyclic aromatic hydrocarbons (PAH) from residential wood combustion [162]. Additional source profiles must be developed for the ultrafine size fraction to carry out accurate PM0.1 source apportionment calculations.

The purpose of this study is to report the concentration of organic molecules detected in the emissions from pine, California oak, east coast oak, eucalyptus, rice straw, cigarette smoke, and meat cooking in six size fractions between 0.056 – 1.8 μm particle diameter. Concentrations of polycyclic aromatic hydrocarbons (PAHs) and other organic compounds useful for source apportionment studies are described for each size fraction. The degree to which each compound has an emissions size distribution that is correlated with organic carbon (OC) and elemental carbon (EC) size distributions is analyzed and suitable tracers for ultrafine source apportionment studies are suggested.

11.2 Methods

Source Sample Collection: Softwood (pine and eucalyptus), hardwood (east coast and California oaks), meat cooking, and cigarette smoke samples were collected at the California Institute of Technology between 1995 - 1997 [140, 141, 163, 164]. Rice straw (Oryza sativa, M202 variety) combustion samples were collected at the National Risk

Management Laboratory of the U.S. Environmental Protection Agency in 2002 [165]. The source sampling methodology for each test was similar and only a brief overview is provided in the current study (the reader is directed to the references listed above for additional details). Prior to the combustion phase of each test, the biomass was pre-weighed and arranged in a typical configuration for use. For hardwoods and softwoods, fuels were burned in a residential fireplace [141]. Rice straw was arranged in an open agricultural burn pattern and combusted within a ~28m^3 custom enclosure [165]. Cigarettes were smoked by an individual in en enclosed area; thus emissions are a combination of both mainstream and sidestream smoke [164]. Meat cooking was carried out in a commercial cafeteria [163]. All combustion emissions were mixed with clean background air using the dilution sampler described by Hildemann et al. [36]; rice straw emissions were diluted using a slightly modified version of this dilution sampler [165].

PM emissions were collected after dilution using denuder-filter-PUF sampling trains and Micro-Orifice Uniform Deposit Impactors (MOUDIs). Bulk PM2.5 samples for organic analysis were collected on quartz filters; the results of these analyses are reported elsewhere [141, 163, 165]. Size-resolved PM samples in 6 size fractions from 0.056 - 1.8μm were collected on pre-weighed aluminum substrates. A detailed description of the organic and inorganic size distribution results is provided by Kleeman et al. [140]. All sample collection media was pre-baked at 500^{o}C for more than 24 hrs to reduce background carbon concentrations.

Organic Compound Quantification: Samples analyzed in the current study were stored on the original collection media in petri dishes that were lined with baked aluminum foil and sealed with Teflon tape at -18^{o}C until shortly before analysis. Each sample was spiked with two deuterated internal standard solutions and were then allowed to dry. The samples were sonicated twice for 15 min in 10 mL of dichloromethane (DCM) at 0^{o}C. The two extracts were then combined, concentrated, filtered, and further concentrated to a volume of ~100 μL.

Wood, rice straw, and cigarette smoke extracts were analyzed by gas chromatography / mass spectrometry (GC-MS) (Agilent 6890 GC coupled with a Agilent 5973 MSD, Agilent Technologies, CA). The GC-MS is equipped with an Agilent HP-5MS capillary column that was 30 m long with an ID of 0.25 mm and a 0.25 μm coating. The GC inlet was operated in splitless mode with a 1 to 3 μL injection volume. The oven started at 30 °C and ramped at 6 °C min-1 up to 325 °C. Meat smoke samples were analyzed using a Varian 3400 GC coupled with a Varian 2000 ion-trap mass spectrometer (ITMS) operated in electron impact (EI) ionization mass spectrometry/selected ion monitoring (SIM) mode (GC-ITMS). All GC-MS and GC-ITMS operating parameters are those recommended by the manufacturer. Chemical species were identified by comparison to authentic standards or by comparison of relative retention times and mass spectra to those in the literature.

Compound quantification was accomplished using the internal standard method in which the response ratio of each target analyte relative to a known concentration of dueterated internal standard was determined [165]. Calibration curves were generated based on the

mass and peak ratios of authentic standards to compounds of interest based on their predominance in airborne combustion-derived fine PM (i.e. PAHs) or for their applicability as biomass combustion source tracers (i.e. cellulose pyrolysis products). These same peak ratios were determined in sample extracts and converted to mass ratios. Using the mass of internal standards spiked on the substrate, these mass ratios are converted to mass of analyte on the substrate.

Compounds reported in this study were classified into two groups: (1) polycyclic aromatic hydrocarbons (PAHs) that may have direct health impacts, and (2) other organic compounds that are useful for source apportionment. The PAH group includes 16 species ranging in molecular weight (M.W.) from 202 - 276 g $mole^{-1}$ ($C_{16}H_{10}$ – $C_{22}H_{12}$). The second group includes 25 species ranging in M.W. from 124.1 – 412.7 g $mole^{-1}$ ($C_7H_2O_2$ – $C_{29}H_{48}O$). A specific list of these compounds is provided in Tables 9-1.

Levoglucosan is typically extracted with polar solvents such as methanol (MEOH) or isoproponal (IPA) followed by reaction with a derivatization reagent such as bis(trimethylsilyl)trifluoroacetamide (BSTFA) that promotes elution through the GC column [166]. In the current study, levoglucosan was analyzed in the DCM extract without derivatization. The levoglucosan internal standard, ^{13}C-labelled levoglucosan, went through the same procedure and therefore accounts for extraction efficiency and quantification effects. Tests conducted on co-located samples extracted with DCM vs. DCM+MEOH yielded consistent results using this approach. The only potential disadvantage of this technique is increased minimum detection limits for levoglucosan due to poor chromatographic resolution of the underivatized compound through the GC column.

11.3 Results

11.3.1 Quality Assurance

Figures 11-1 and 11-2 show fine particle emission factors for 14 PAHs and 25 other organic compounds emitted from the combustion of wood, rice straw, and cigarettes that were measured using co-located MOUDI and denuder-filter-PUF samplers. Fine particle MOUDI results were constructed by summing each stage of the impactor to yield an integrated fine particle concentration. Fine particle filter results were measured with a denuder-filter-PUF sampling train and have been reported previously by Schauer et al. [141, 164] and Hays et al. [165]. PAH concentrations measured by both MOUDI and denuder-filter-PUF samplers varied between 0.01 – 10 (ng PAH / μg total carbon (TC)). Concentrations of other organics span an even larger range from 0.0001 – 1000 (ng compound / μg TC). The relative trends for all compounds concentrations measured with MOUDIs and denuder-filter-PUF samplers follow the same general pattern. Concentrations of heavy PAHs measured using the MOUDIs and denuder-filter-PUF techniques were generally in good agreement. The concentrations of lighter compounds such as fluoranthene, pyrene, and retene appeared to be higher when measured with the

denuder-filter-PUF samplers than with MOUDIs. This trend could be caused by volatilization losses associated with the higher flow rates and decreased pressure in the MOUDI. Levoglucosan was the most abundant organic species measured using both techniques, with concentrations ranging from 10-200 (ng levoglucosan / μg TC) depending on the source. Levoglucosan emissions from wood and rice straw combustion measured in the fine particle size fraction by the MOUDIs were generally 2-3 times lower than those measured by the denuder-filter-PUF systems. Several data files were discovered to be corrupted during the final quantification of levoglucosan, resulting in missing levoglucosan values for approximately half of the MOUDI stages from each test. Levoglucosan was also quantified in its native (underivatized) form in the current study which led to higher minimum detection limits (MDLs) and missing values for some stages with relatively low concentrations. Vanillin and coniferaldehyde concentrations measured with MOUDIs were also lower than denuder-filter-PUF measurements.

The upper half of Table 11- 1 shows the particulate concentration of 16 PAHs normalized by the concentration of total carbon emitted from the combustion of pine, California (CA) oak, east coast (EC) oak, eucalyptus, rice straw, cigarettes, and meat cooking in the fine particle size fraction (Dp < 1.8 μm). These units are convenient because they can be used directly in source apportionment studies. Surprisingly, coronene and MW 302 isomers were detected in the PM1.8 fraction of pine wood combustion at concentrations of 0.1-0.7 (ng / μg TC). No other biomass source emitted these compounds, and it is unknown if they were produced by the combustion process or if they reflect some source of contamination. Heavy PAH compounds such as coronene and MW 302 isomers have been measured in the exhaust of gasoline-powered motor vehicles at much higher concentrations (~3 orders of magnitude) than those detected in pine wood smoke [161]. Coronene and MW 302 isomers should therefore only pose a significant confounding factor for source apportionment studies when wood smoke concentrations are approximately 1000 times larger than gasoline-powered motor vehicle concentrations.

Light PAHs fluoranthene and pyrene were measured in pine wood smoke emissions with a concentration of approximately 0.1 (ng / μg TC). These compounds were also measured in the exhaust from heavy duty diesel engines but at much higher concentrations of approximately 50-650 (ng / μg TC) [103]. Therefore, light PAHs from pine wood combustion will only confound diesel engine source attribution calculations that use fluoranthene and pyrene when wood smoke concentrations are 500 – 6500 times larger than diesel engine concentrations.

Table 11-1: PM1.8 emissions of trace organic compounds from biomass combustion sources. OC = organic carbon, EC = elemental carbon, TC = total carbon (=OC+EC).

Compound Name		Pine		CA Oak		EC Oak		Eucalyptus		Rice Straw		Cigarettes
OC (g / kg biomass)		6.55		3.03		2.83		4.59		3.91		3.16[a]
EC (g / kg biomass)		0.21		0.03		0.07		0.12		0.63		0.85[a]
PAHs (ng / µg TC)												
Fluoranthene	4a	0.119 ± 0.007	2	0.191 ± 0.012	2	0.215 ± 0.013	2	0.105 ± 0.007	2	0.027 ± 0.002	3	0.048 ± 0.005
Acephenanthrylene	4a	0.059 ± 0.004	2	0.089 ± 0.006	2	0.107 ± 0.007	2	0.054 ± 0.004	2	0.004 ± 0	3	0.019 ± 0.003
Pyrene	4a	0.105 ± 0.006	2	0.177 ± 0.011	2	0.21 ± 0.012	2	0.103 ± 0.007	4a	0.026 ± 0.002	4a	0.043 ± 0.004
Benzo(ghi)fluoranthene	4a	0.311 ± 0.017	1	0.6 ± 0.038	2	0.873 ± 0.047	2	0.396 ± 0.028		0.068 ± 0.008	4a	0.139 ± 0.026
Benz(a)anthracene	4a	0.081 ± 0.005	1	0.153 ± 0.009	1	0.198 ± 0.011	2	0.093 ± 0.006	4a	0.032 ± 0.002	4b	0.031 ± 0.004
Chrysene/Triphenylene	4a	0.072 ± 0.004	2	0.167 ± 0.01	1	0.21 ± 0.012	2	0.101 ± 0.007	4a	0.027 ± 0.001		0.056 ± 0.003
Benzo(b)fluoranthene / benzo(k)fluoranthene	4a	0.134 ± 0.008	1	0.25 ± 0.016	2	0.456 ± 0.025	2	0.19 ± 0.015	4a	0.046 ± 0.004	4b	0.033 ± 0.01
Benzo(j)fluoranthene	4a	0.04 ± 0.003	1	0.065 ± 0.008	1	0.125 ± 0.009	2	0.052 ± 0.005	4a	0.019 ± 0.003	4b	0.01 ± 0.009
Benzo(e)pyrene	4a	0.051 ± 0.003	1	0.093 ± 0.006	2	0.162 ± 0.009	2	0.069 ± 0.005	4a	0.02 ± 0.002	4b	0.023 ± 0.006
Benzo(a)pyrene	4a	0.085 ± 0.005	1	0.14 ± 0.009	1	0.295 ± 0.016	2	0.121 ± 0.01	4a	0.03 ± 0.002	4b	0.026 ± 0.006
Perylene	4a	0.015 ± 0.001	2	0.024 ± 0.004	1	0.048 ± 0.004	2	0.021 ± 0.002	4a	0.01 ± 0.001	4a	0.024 ± 0.006
Indeno(cd)pyrene	1	0.071 ± 0.003	2	0.068 ± 0.005	2	0.167 ± 0.007	2	0.062 ± 0.004		0.019 ± 0.002	4a	0.017 ± 0.006
Benzo(ghi)perylene	1	0.052 ± 0.003	1	0.057 ± 0.008	2	0.139 ± 0.008	2	0.05 ± 0.005		0.015 ± 0.003		0.023 ± 0.012
Indeno(cd)fluoranthene	1	0.022 ± 0.002	1	0.019 ± 0.009	1	0.051 ± 0.006	2	0.018 ± 0.004		0.01 ± 0.003		0 ± 0.015
Coronene	4a	0.092 ± 0		0 ± 0		0 ± 0		0 ± 0		0 ± 0		0 ± 0
MW302 isomers		0.745 ± 0		0 ± 0		0 ± 0		0 ± 0		0 ± 0		0 ± 0
Other (ng / µg TC)												
Levoglucosan[b]	1	44.38 ± 1.105		76.90 ± 5.512	2	132.5 ± 3.666		156.1 ± 4.538		69.07 ± 2.034	2	35.307 ± 1.015
Retene	4a	0.2 ± 0.012	2	0.109 ± 0.011	1	0.049 ± 0.007	1	0.017 ± 0.004		0.007 ± 0.003		0 ± 0.008
1,8-Naphthalic anhydride	4a	0.039 ± 0.006	2	0.126 ± 0.017	1	0.14 ± 0.014	2	0.074 ± 0.008		0.017 ± 0.008		0.001 ± 0.024
1H-Phenalen-1-one	4a	0.164 ± 0.011	2	0.235 ± 0.02	1	0.285 ± 0.021	2	0.192 ± 0.012	2	0.02 ± 0.005	1	0.064 ± 0.017
1-Phenyl-Naphthalene	1	0.011 ± 0.007	2	0.002 ± 0.02	2	0.005 ± 0.017		0 ± 0.01		0 ± 0.009		0.006 ± 0.028
3,5-Dimethoxyphenol		0 ± 0.047		0 ± 0.144		0 ± 0.119		0 ± 0.07		0 ± 0.065		0.002 ± 0.2
4-Methylphenylacetone	1	0.175 ± 0.031	2	0.03 ± 0.038		0.028 ± 0.031	2	0.021 ± 0.019	2	0.076 ± 0.041		0.548 ± 0.088
Acenaphthenone	4a	0.02 ± 0.004	2	0.043 ± 0.013		0.03 ± 0.01	2	0.038 ± 0.006	4a	0.002 ± 0.005		0 ± 0.016
Acetosyringone	1	0.177 ± 0.092		13.9 ± 0.514	1	10.06 ± 0.423	2	12.17 ± 0.25	2	1.287 ± 0.142	3	0.193 ± 0.251
Acetovanillone	1	1.265 ± 0.08	2	0.755 ± 0.168	1	0.692 ± 0.149	2	0.561 ± 0.088	2	0.055 ± 0.03	3	0.058 ± 0.092
Anthracen-9,10-dione	4a	0.017 ± 0.004	2	0.034 ± 0.012	1	0.025 ± 0.01	2	0.018 ± 0.006	2	0.004 ± 0.005	3	0.01 ± 0.016

Benz(de)anthracen-7-one	4a	0.161 ± 0.018	1	0.305 ± 0.067	2	0.361 ± 0.053	2	0.208 ± 0.031		0.145 ± 0.026	4a	0.239 ± 0.101
Coniferyl aldehyde	1	31.94 ± 0.945	2	16.38 ± 0.483	1	16.51 ± 0.472	2	7.271 ± 0.279	2	0.344 ± 0.035	1	0.208 ± 0.034
Dimethoxycoumarin		0 ± 0.007		0 ± 0.022		0 ± 0.018		0 ± 0.011		0 ± 0.01		0 ± 0.03
Eugenol	1	0.014 ± 0.051	2	0.002 ± 0.156	2	0.008 ± 0.128	2	0.001 ± 0.076	2	0.001 ± 0.07		0 ± 0.217
Flourenone	4a	0.049 ± 0.005	2	0.06 ± 0.014	1	0.034 ± 0.01	2	0.022 ± 0.006	2	0.012 ± 0.005	3	0.035 ± 0.016
Guaiacol	1	0.063 ± 0.039	2	0.039 ± 0.118	2	0.066 ± 0.097	2	0.043 ± 0.058	2	0.005 ± 0.053	3	0.012 ± 0.164
Iso-eugenol	1	3.259 ± 0.112		0.703 ± 0.108	1	1.393 ± 0.107	2	0.278 ± 0.063	2	0.222 ± 0.048	3	0.206 ± 0.138
Methylchrysene	4a	0.01 ± 0.001	2	0.025 ± 0.003	1	0.047 ± 0.003	2	0.02 ± 0.002	4a	0.009 ± 0.001		0.02 ± 0.004
Methylfluoranthene	4a	0.307 ± 0.017		0.385 ± 0.023	1	0.491 ± 0.029	2	0.26 ± 0.017	2	0.184 ± 0.009	3	0.27 ± 0.015
Methylguaiacol	1	0.028 ± 0.059	1	0.009 ± 0.179	1	0.02 ± 0.148	2	0.011 ± 0.087	4a	0.003 ± 0.08		0 ± 0.249
Ethylguaiacol	1	0.013 ± 0.061	2	0.002 ± 0.185	1	0.004 ± 0.153	2	0.002 ± 0.09	2	0.003 ± 0.083		0 ± 0.257
Propylguaiacol	1	0.006 ± 0.053	2	0.001 ± 0.162		0.001 ± 0.133	2	0 ± 0.079		0 ± 0.073		0 ± 0.225
Sinapic aldehyde	1	0.846 ± 0.081	2	30.511 ± 0.9	1	37.7 ± 1.037	2	28.69 ± 0.613		0.275 ± 0.082	4a	0.534 ± 0.244
Syringealdehyde		0 ± 0.063		21.83 ± 0.697	1	20.29 ± 0.665	2	18.12 ± 0.394	2	0.495 ± 0.131	3	0.119 ± 0.265
Vanillin	1	1.887 ± 0.103	2	1.326 ± 0.182	1	0.912 ± 0.16	2	0.523 ± 0.095	2	0.187 ± 0.062	3	0.083 ± 0.092
Caffeine		0 ± 0		0 ± 0		0 ± 0		0 ± 0		0 ± 0	3	0.205 ± 0.025
Compound Name		**Meat Cooking**										
OC (g / kg meat)		10.7										
EC (g / kg meat)		0.097										
PAHs (ng / µg TC)												
Fluoranthene		0.014 ± 0.001										
Pyrene		0.008 ± 0.001										
Benzo(ghi)fluoranthene		0.002 ± 0.000										
Benzo(b)fluoranthene / Benzo(k)fluoranthene		0.005 ± 0.003										
Benzo(e)pyrene	1	0.002 ± 0.001										
Benzo(ghi)perylene	1	0.016 ± 0.001										
Phenanthrene		0.051 ± 0.002										
Other (ng / µg TC)												
Cholesterol	1	1.47 ± 0.010										

[a] OC and EC emissions from cigarettes have units of (mg / cigarette).
[b] PM1.8 concentrations are incomplete because data was lost for some stages during final quantification.

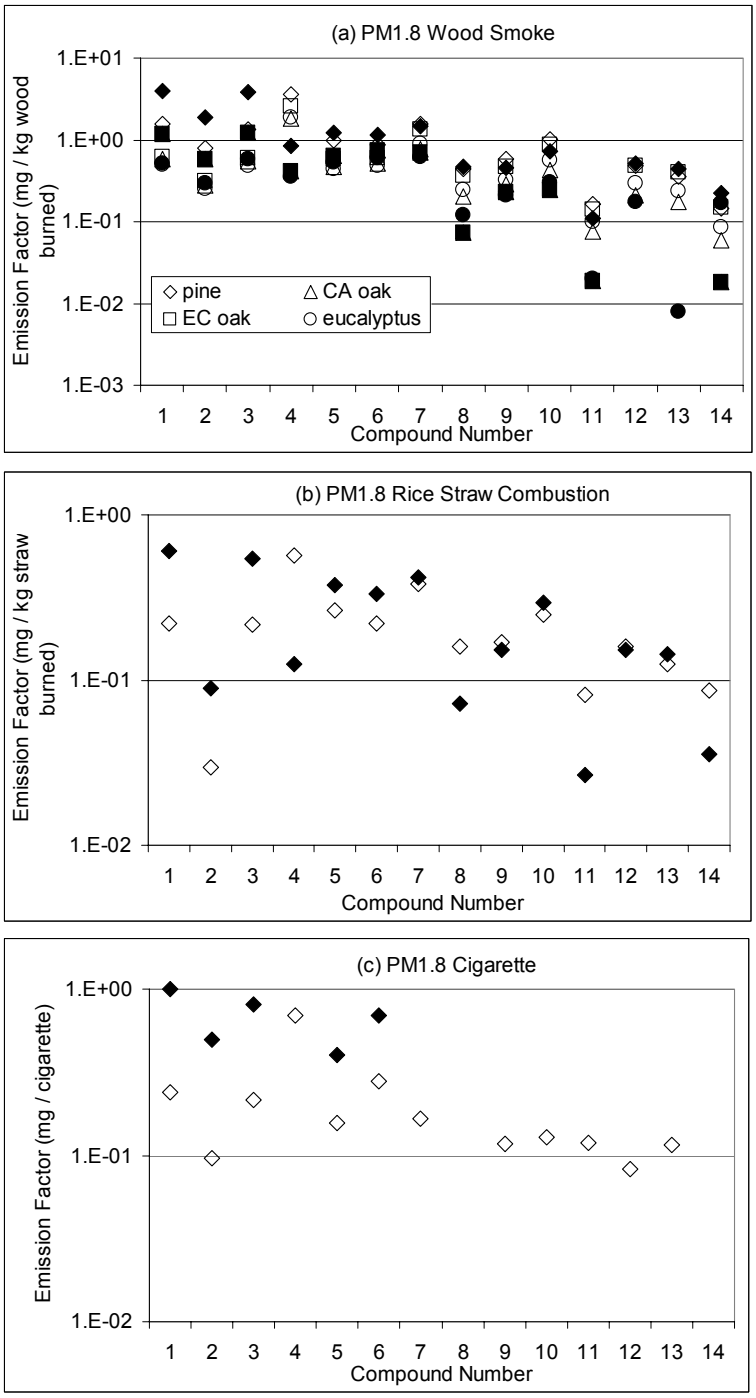

Figure 11-1: Comparison between organic compound emission factors for wood smoke measured with MOUDIs (open symbols) and filter samplers (closed symbols) from the fireplace combustion of wood [132]. Species correspond to (1) fluoranthene, (2) acephenanthrylene, (3) pyrene, (4) benzo(ghi)fluoranthene, (5) benz(a)anthracene, (6) chrysene/triphenylene (7) benzo(b)fluoranthene / benzo(k)fluoranthene, (8) benzo(j)fluoranthene, (9)benzo(e)pyrene, (10) benzo(a)pyrene, (11) perylene, (12) indeno(cd)pyrene, (13) benzo(ghi)perylene, and (14) indeno(cd)fluoranthene. Values below minimum detection limits are not shown.

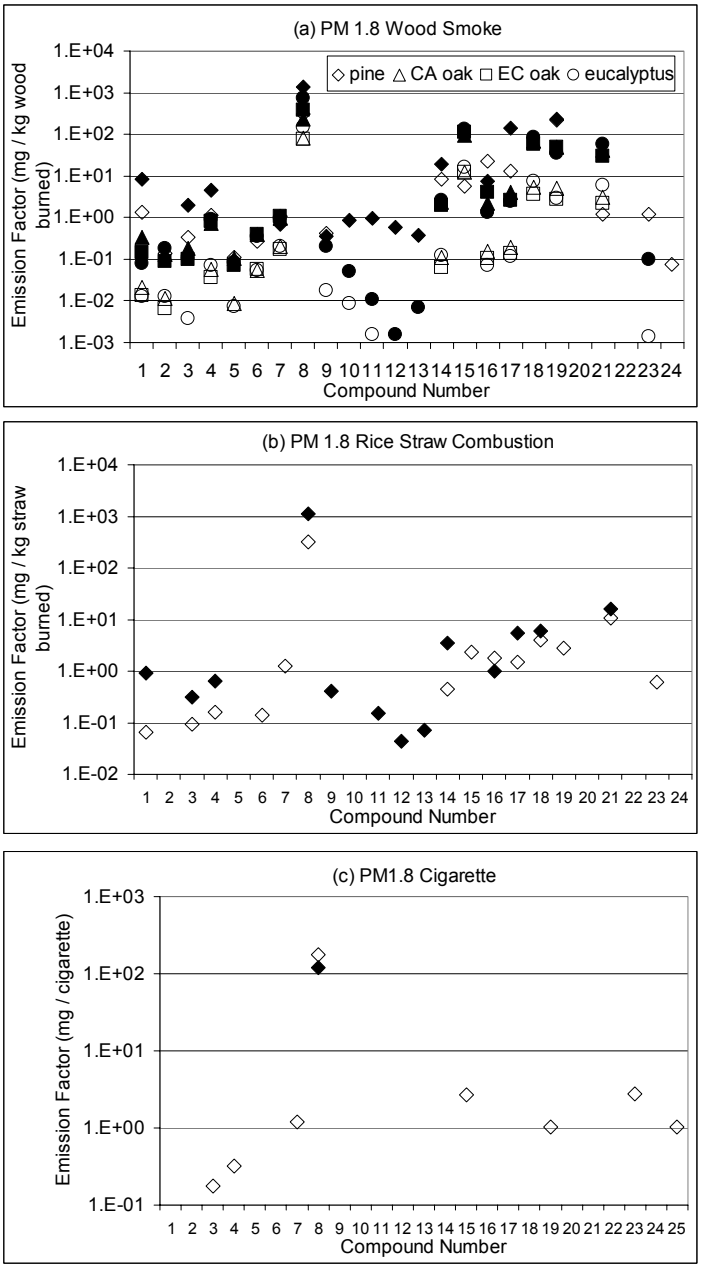

Figure 11-2: Comparison between organic compound emission factors for wood smoke measured with MOUDIs (open symbols) and filter samplers (closed symbols) from the fireplace combustion of wood [132]. Species correspond to (1) retene, (2) acenaphthenone, (3) flourenone, (4) 1H-phenalen-1-one, (5) anthracen-9,10-dione, (6) 1,8-naphthalic anhydride, (7) benz(de)anthracen-7-one, (8) levoglucosan, (9) guaiacol, (10) methylguaiacol, (11) ethylguaiacol, (12) propylguaiacol, (13) eugenol, (14) acetovanillone, (15) sinapic aldehyde, (16) iso-eugenol, (17) vanillin, (18) syringealdehyde, (19) coniferyl aldehyde, (20) 3,5-dimethoxyphenol, (21) acetosyringone, (22) dimethoxycoumarin, (23) 4-methylphenylacetone, (24) 1-phenyl-naphthalene, and (25) caffeine. Values below minimum detection limits are not shown.

11.3.2 Ultrafine Particle Emissions Profiles

The upper half of Table 11-2 shows the ultrafine (Dp < 0.1 μm) particulate concentration of 16 PAHs normalized by the concentration of total carbon (TC) emitted from the combustion of pine, California (CA) oak, east coast (EC) oak, eucalyptus, rice straw, cigarettes, and meat cooking. These units are convenient because they can be used directly in source apportionment studies. Figure 11-3 illustrates these same measurements with units of (mg / kg biomass burned) or (mg / cigarette). The most abundant PAH measured in ultrafine wood smoke emissions was benzo(ghi)fluoranthene with concentrations ranging from 0.4-0.7 (ng / μg TC) or 0.19 – 0.36 (mg / kg wood burned). Light PAHs fluoranthene and pyrene were measured in the ultrafine size fraction of wood smoke emissions with a concentration of approximately 0.1 (ng / μg TC). Fluoranthene and pyrene are present in the exhaust from heavy duty diesel engines at much higher concentrations of approximately 50-650 (ng / μg TC) [103]. Wood combustion will only be a significant source of light PAH emissions relative to diesel engine emissions when wood smoke particulate total carbon concentrations are 500 – 6500 times larger than diesel engine total particulate carbon concentrations.

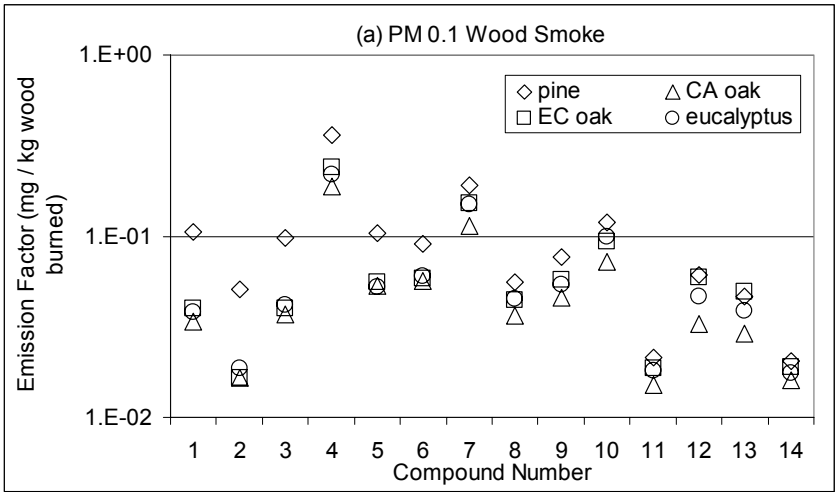

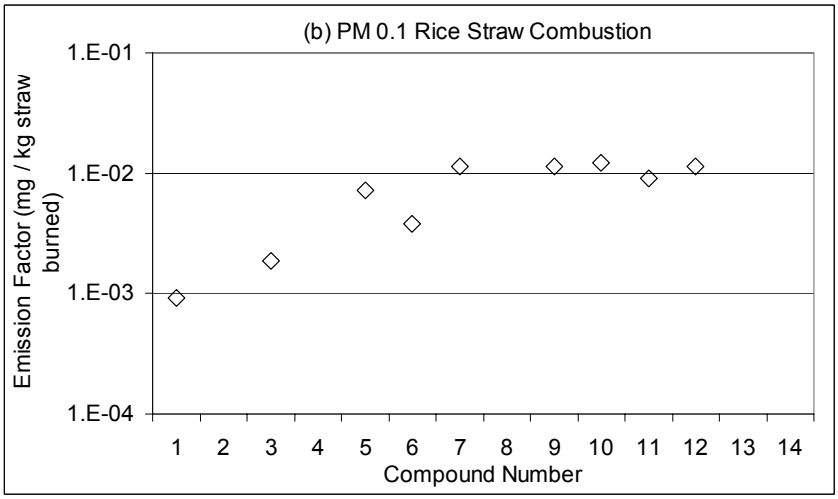

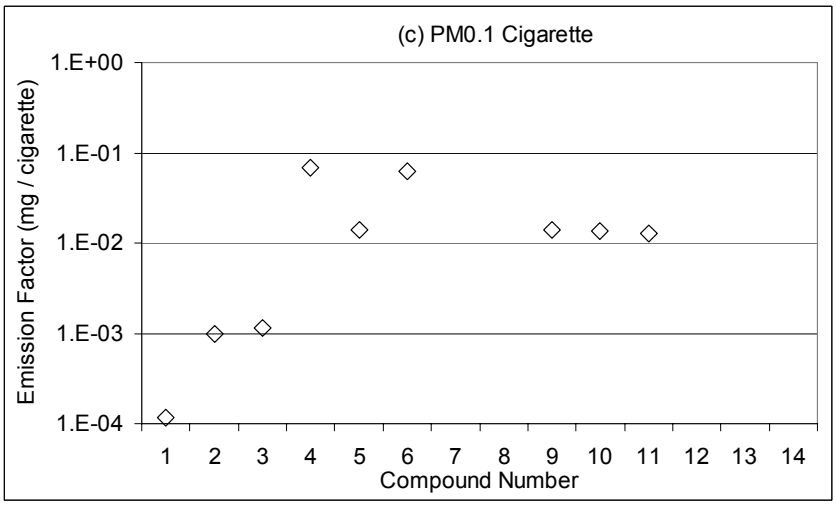

Figure 11-3: PM0.1 emission factors for (1) fluoranthene, (2) acephenanthrylene, (3) pyrene, (4) benzo(ghi)fluoranthene, (5) benz(a)anthracene, (6) chrysene/triphenylene (7) benzo(b)fluoranthene / benzo(k)fluoranthene, (8) benzo(j)fluoranthene, (9)benzo(e)pyrene, (10) benzo(a)pyrene, (11) perylene, (12) indeno(cd)pyrene, (13) benzo(ghi)perylene, and (14) indeno(cd)fluoranthene. Values below minimum detection limits are not shown.

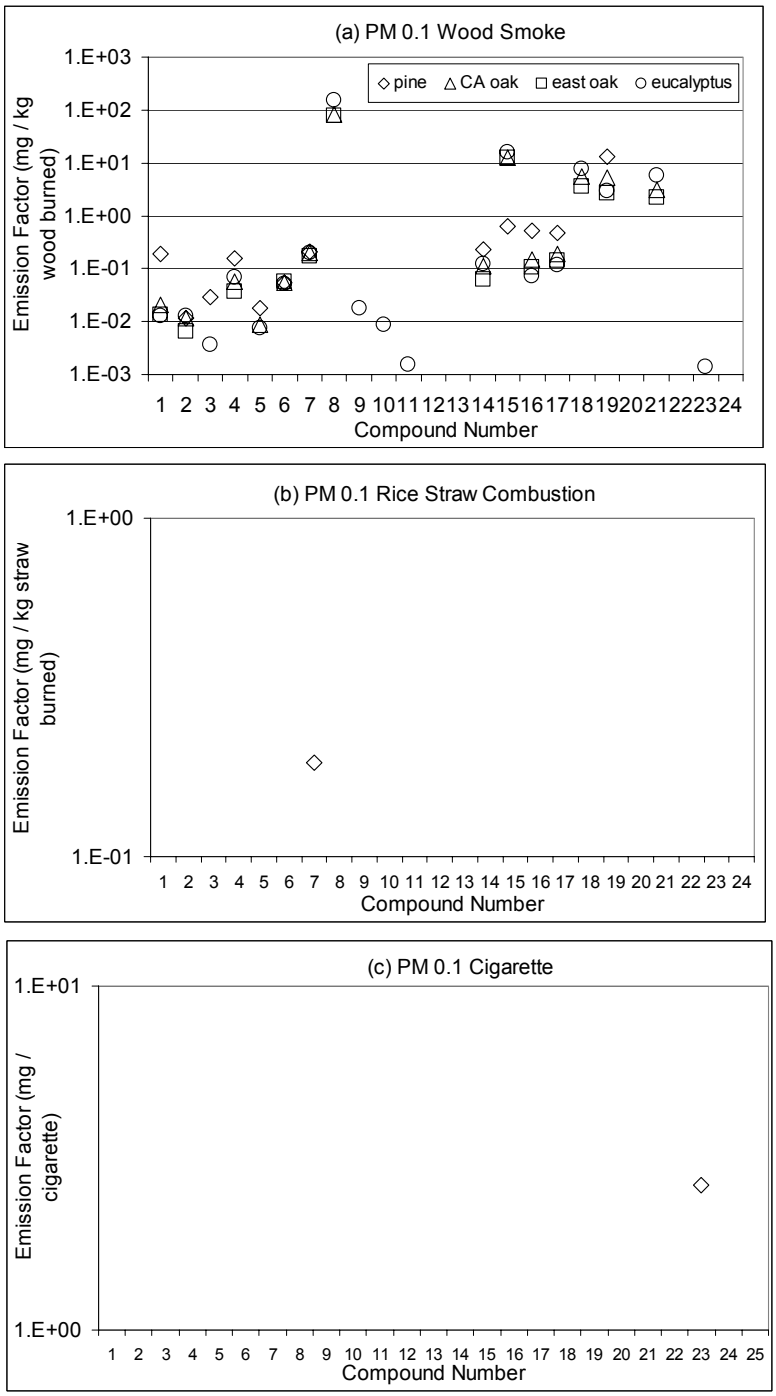

Figure 11-4: PM0.1 emission factors for (1) retene, (2) acenaphthenone, (3) flourenone, (4) 1H-phenalen-1-one, (5) anthracen-9,10-dione, (6) 1,8-naphthalic anhydride, (7) benz(de)anthracen-7-one, (8) levoglucosan, (9) guaiacol, (10) methylguaiacol, (11) ethylguaiacol, (12) propylguaiacol, (13) eugenol, (14) acetovanillone, (15) sinapic aldehyde, (16) iso-eugenol, (17) vanillin, (18) syringealdehyde, (19) coniferyl aldehyde, (20) 3,5-dimethoxyphenol, (21) acetosyringone, (22) dimethoxycoumarin, (23) 4-methylphenylacetone, (24) 1-phenyl-naphthalene, and (25) caffeine. Values below minimum detection limits are not shown.

Nine PAHs were detected in the ultrafine size fraction from rice straw combustion with the most abundant compound (benzo(a)pyrene) measured at ~0.07 (ng PAH / μg TC) or 0.01 (mg PAH / kg rice straw burned). All of the organic concentrations present in rice straw emissions are smaller than those in wood smoke emissions by a factor of approximately 2 - 10. The reduced concentration of PAHs in the ultrafine size fraction of rice straw smoke relative to wood smoke reflects the differences in biomass fuel composition and the different combustion conditions. Rice straw samples were combusted in an open burn chamber [165] while wood samples were burned in a residential fireplace [141]. The most abundant PAH measured in the ultrafine size fraction of cigarette smoke was benzo(ghi)fluoranthene with a concentration of 0.99 (ng PAH / μg TC) followed closely by chrysene/triphenylene (0.88 ng PAH / μg TC).

A much smaller number of compounds were quantified for meat cooking emissions because the primary emphasis was on trace organics that have been used in previous source apportionment studies rather than a general characterization of organics from this source. The most abundant PAH measured in the ultrafine size fraction of meat cooking emissions was phenanthrene (0.3 ng / μg TC). Fluoranthene and pyrene were also detected from meat cooking operations but at concentrations so small (<0.1 ng PAH / μg TC) that other sources such as diesel engines will dominate ambient concentrations under typical ambient conditions.

The ultrafine concentration of 27 additional organic compounds emitted from biomass combustion are listed in the lower half of Table 11-2 with units of (ng compound / μg TC) and illustrated graphically in Figure 11-4 with units of (mg compound / kg biomass burned). The most abundant compounds measured in wood smoke emissions were levoglucosan (~250 ng / μg TC), coniferaldehyde (~5-20 ng / μg TC), sinapic aldehyde (~1-40 ng / μg TC), and syringealdehyde (~0.3-15 ng / μg TC). Ultrafine levoglucosan concentrations are not available for pine smoke because the GC-MS datafile became corrupted during final quantification. Ultrafine coniferaldehyde concentrations were highest in the pine smoke emissions while the other aldehyde species were higher in oak and eucalyptus wood smoke. Levoglucosan concentrations in the ultrafine size fraction of rice straw and cigarette smoke were below the limit of quantification. The only additional organic compounds measured above detection limit in the ultrafine particle size fraction emitted from these sources were benz(de)anthracen-7-one in rice straw smoke (1.1 ng / μg TC) and 4-methylphenylacetone in cigarette smoke (38 ng / μg TC). Cholesterol was measured in the ultrafine size fraction of meat cooking emissions at a concentration of 3.7 (ng / μg TC).

11.3.3 Organic Compound Size Distributions

Figure 11-5 illustrates the normalized size distribution of total particulate carbon associated with pine, California oak, east coast oak, eucalyptus, rice straw, cigarette, and meat cooking smoke [140, 165]. Normalized size distributions were calculated by dividing the concentration in each size fraction by the total PM1.8 concentration associated with that source. Wood combustion sources have total particulate carbon size

distributions that peak between 0.1-0.18 μm particle aerodynamic diameter, while meat cooking carbon particles peak between 0.18 – 0.32 μm diameter. Cigarette and rice straw particulate carbon emissions peak between 0.32 – 0.56 μm particle diameter and 0.56 – 1.0 μm particle diameter, respectively.

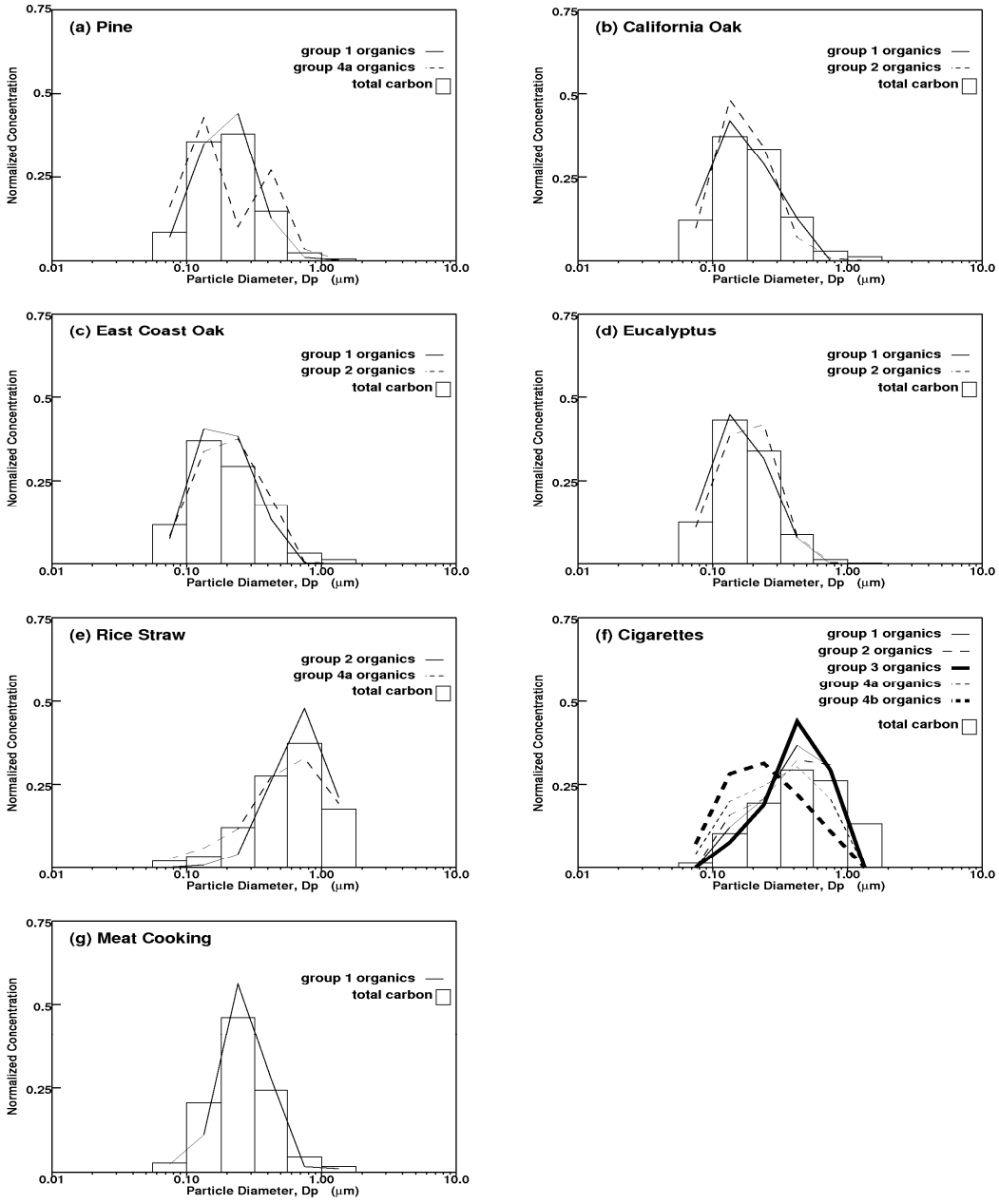

Figure 11-5: Normalized size distribution of total carbon emissions and trace organic species emitted from biomass combustion created by dividing the mass in each size fraction by the total PM1.8 mass. Group 1 organic size distributions correlate with both OC and EC (R2>0.9), group 2 organics correlate with OC (R2>0.9), group 3 organics correlate with EC (R2>0.9), and group 4 organics correlate with other organics but with OC or EC. Table 11-1 lists the compounds associated with each group.

Figure 11-5 also illustrates the normalized size distributions of trace organic compounds that may be useful for source apportionment calculations. Compounds were organized into different groups based on their size distributions. Group 1 organic compounds had size distributions that were highly correlated (R^2>0.9) with both EC and OC size distributions. Group 2 organic compounds had size distributions that were highly correlated (R^2>0.9) with OC only. Group 3 organic compounds had size distributions that were highly correlated (R^2>0.9) with EC only. Those organic compounds with size distributions that were highly correlated (R^2>0.9) with other organics but not well correlated with either OC or EC were assigned to group 4. More than 1 set of group 4 compounds may exist for each test. Averaged size distributions were calculated when a group contained more than one compound as a member. Table 11-1 lists the members of each organic size distribution group.

Figure 11-5a and Table 11-1 shows that only three PAH compounds emitted from pine wood combustion have size distributions that are well-correlated with both OC and EC size distributions (indeno(cd)pyrene, benzo(ghi)perylene, and indeno(cd)fluoranthene). The majority of the remaining PAH compounds emitted from pine wood combustion had a bimodal size distribution with a minimum between 0.18 – 0.32 μm particle diameter. No other biomass combustion source exhibited this size distribution profile suggesting that the result may stem from a measurement error. Levoglucosan, coniferylaldehyde, and iso-eugenol emitted from pine wood combustion each had size distributions that were correlated with both OC and EC.

Figures 11-5b-d and Table 11-1 show that the majority of the organic compounds emitted from California oak, east coast oak, and eucalyptus had size distributions that were highly correlated (R^2>0.9) with either OC and EC (group 1) or OC (group 2). OC and EC size distributions from these sources were similar [140], with OC peaking at slightly larger sizes. Group 2 organics therefore also peak at slightly larger sizes as shown in Figure 11-5b-d.

Figure 11-5e and Table 11-1 show two PAHs and fourteen other organic compounds had size distributions that correlated with OC (R^2>0.9) and eleven other compounds formed an independent correlated group that was shifted to slightly smaller particle sizes. The size distribution of levoglucosan emitted from rice straw combustion was not well correlated with OC, EC, or any other organic compound.

Figure 11-5f and Table 11-1 show that 1H-phenalen-1-one and coniferaldehyde present in cigarette smoke had size distributions that were well correlated with both OC and EC emissions (group 1). The levoglucosan size distribution in cigarette smoke was well correlated with OC only (group 2). Twelve compounds including caffeine, syringealdehyde, acetosyringone, and vanillin had size distributions that were correlated with EC (R^2>0.9) (group 3). Two additional groups of othe11- self-correlated organics were also detected in cigarette smoke (group 4a and 4b). Figure 11-3f illustrates that the size distribution of organics that is correlated with EC (group 3) had the sharpest peak centered between 0.32 – 0.56 μm particle diameter while the other self-correlated groups

have are generally shifted to slightly smaller particle sizes. Group 4b compounds that had the smallest mean diameter were composed of intermediate weight PAHs.

Figure 11-5g and Table 11-1 show that the size distribution of cholesterol was readily apparent in the meat cooking emissions with PM1.8 and PM0.1 concentrations well above detection limits. The cholesterol size distribution was highly correlated (R^2>0.9) with both OC and EC size distributions.

11.3.4 Proposed Tracers for Size-Resolved Source Apportionment Calculations

The resolution of source apportionment studies for airborne particulate matter is greatly increased by the use of unique tracers that are only released by a well defined class of sources. Organic compounds used in apportionment studies must also be stable in the atmosphere over periods of a few days to weeks if they are to be used as source tracers. Cholesterol has been used as a tracer for meat cooking activities in previous studies [79, 98, 167]. The cholesterol size distribution measurements in the current study are well correlated with EC and OC size distributions, suggesting that cholesterol can serve as an appropriate tracer for meat cooking contributions to ultrafine particle concentrations.

Levoglucosan was the most abundant organic compound measured in the PM1.8 size fraction of wood, rice straw, and cigarette smoke. This compound has been used as a tracer for biomass combustion in numerous previous studies [79, 98, 167]. Levoglucosan size distributions measured in the current study were not highly correlated with EC and OC size distributions from all biomass combustions sources because a significant number of levoglucosan measurements are missing due to corrupted data files discovered during the final phase of quantification. Additional data analysis was performed to determine if levoglucosan concentrations that are available suggest any enhancement or reduction in levoglucosan concentrations as a function of size.

Figure 11-6 compares levoglucosan vs. OC emissions rates in available MOUDI size fractions collected from pine, California oak, east coast oak, eucalyptus, rice straw, and cigarette smoke. The PM0.1 size fraction is denoted as an open circle (when available) to differentiate it from other size fractions. A regression line with an intercept of zero was added to each panel to illustrate the degree of correlation among the size fractions. Correlation coefficients between levoglucosan and OC range from R^2 = 0.05 – 0.99, but the missing data points make it difficult to evaluate the correlation using this statistic alone. What can be observed in Figure 11-6 is that all data points fall within a factor of 30% from the best-fit correlation line including PM0.1 measurements when they are available. These results suggest that the relative concentration of levoglucosan / OC is not a strong function of particle size in pine, rice straw, and cigarette smoke. The slope of the regression line shows that the ratio of levoglucosan to OC in the particulate emissions from wood combustion is 0.08 – 0.19 (μg levoglucosan / μg OC) which is in reasonable agreement with filter-based measurements [141]. Levoglucosan should therefore prove to be a reliable tracer in ultrafine source apportionment calculations when measurements are made above the minimum detection limits.

11.4 Conclusions

Size-resolved particulate matter emissions from pine, California oak, east coast oak, eucalyptus, rice straw, cigarette smoke, and meat cooking were analyzed for trace organic species using solvent-extraction followed by GC-MS analysis. Six particle size fractions were studied between 0.056, 0.1, 0.18, 0.32, 0.56, 1.0, and 1.8 μm particle diameter. The smallest particle size fraction analyzed was in the ultrafine (Dp < 0.1 μm) range that has been implicated as a potential health concern. Fourteen PAHs were detected in the ultrafine size fraction of wood smoke with the most abundant species (benzo[ghi]fluoranthene) emitted at a rate of 0.2 – 0.4 (mg / kg wood burned). Nine PAHs were detected in the ultrafine size fraction of rice straw smoke with the most abundant compound (benzo(a)pyrene) emitted at 0.01 (mg / kg rice straw burned). The most abundant PAH measured in the ultrafine size fraction of cigarette smoke was benzo(ghi)fluoranthene (0.07 mg / cigarette) followed closely by chrysene/triphenylene (0.06 mg / cigarette).

Besides PAHs, the most abundant compounds identified in the wood included levoglucosan (<MDL-150 mg / kg burned), acetovanillone (0.06-0.23 mg / kg burned), conferylaldehyde (2.7-13.21 mg / kg burned), iso-eugenol (0.07-0.53 mg / kg burned), and vanillin (0.12-0.46 mg / kg burned). The size distribution of each of these compounds was highly correlated (R^2>0.9) with the size distribution of particle-phase organic carbon (OC) and / or elemental carbon (EC). The only organic compounds besides PAHs detected in the ultrafine size fraction of rice straw and cigarette smoke were benz(de)anthracen-7-one (0.19 mg / kg rice straw burned) and 4-methylphenylacetone (2.64 mg / cigarette), respectively. Caffeine was measured in cigarette smoke size fractions greater than 0.1 μm with a total PM1.8 emissions rate of 1 (mg / cigarette). The most abundant organic species measured in meat cooking smoke was cholesterol with a size distribution that was highly correlated with both OC and EC. The concentration of each compound normalized by the concentration of total OC was relatively uniform for all particle sizes. Cholesterol and levoglucosan should prove to be useful tracers for meat cooking and wood smoke emissions in the ultrafine size range.

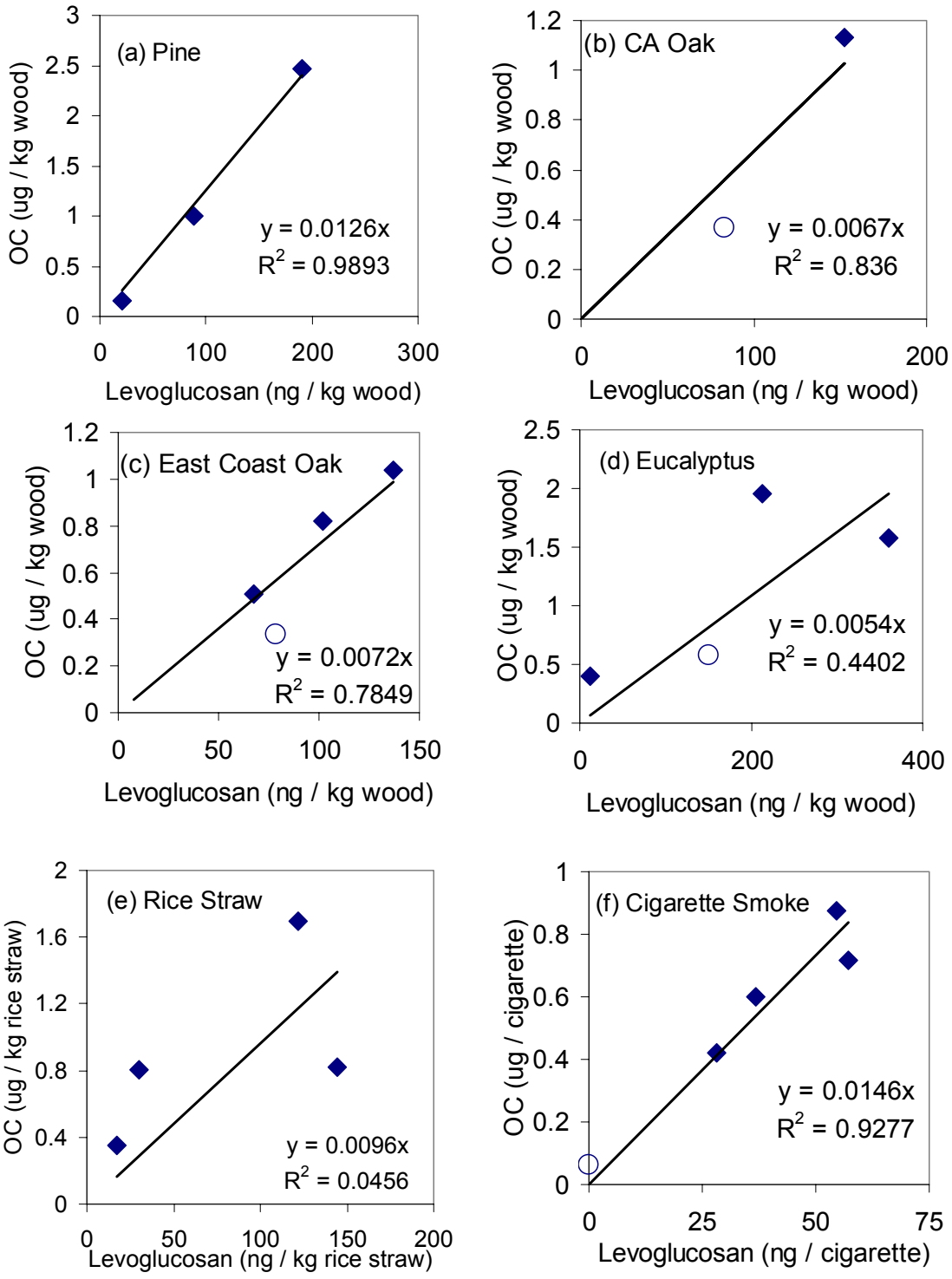

Figure 11-6: Correlation between levoglucosan and organic carbon measurements in different MOUDI size fractions. The PM0.1 size fraction is denoted by an open circle rather than a closed diamond. Only measurements above Minimum Detection Limits (MDL) are shown.

Table 11-2: PM0.1 emissions of trace organic compounds from biomass combustion sources. OC = organic carbon, EC = elemental carbon, TC = total carbon (=OC+EC).

Compound Name		**Pine**		**CA Oak**		**EC Oak**		**Eucalyptus**		**Rice Straw**		**Cigarettes**
OC (g / kg biomass)		0.57		0.37		0.33		0.58		0.09		0.06[a]
EC (g / kg biomass)		0.01		0.007		0.006		0.01		0.0		0.007[a]
PAHs (ng / µg TC)												
Fluoranthene	4a	0.183 ± 0.02	2	0.091 ± 0.099	2	0.117 ± 0.018	2	0.065 ± 0.01	2	0.005 ± 0.001	3	0.002 ± 0.001
Acephenanthrylene	4a	0.089 ± 0.012	2	0.045 ± 0.053	2	0.049 ± 0.015	2	0.032 ± 0.008	2	0 ± 0	3	0.014 ± 0.002
Pyrene	4a	0.169 ± 0.018	2	0.099 ± 0.088	2	0.117 ± 0.015	2	0.071 ± 0.008	4a	0.011 ± 0.001	4a	0.016 ± 0.002
Benzo(ghi)fluoranthene	4a	0.627 ± 0.065	1	0.506 ± 0.312	2	0.706 ± 0.078	2	0.373 ± 0.043		0 ± 0.227	4a	0.982 ± 0.357
Benz(a)anthracene	4a	0.179 ± 0.019	1	0.142 ± 0.075	1	0.165 ± 0.019	2	0.089 ± 0.011	4a	0.041 ± 0.009	4b	0.201 ± 0.104
Chrysene/Triphenylene	4a	0.158 ± 0.016	2	0.152 ± 0.081	1	0.173 ± 0.018	2	0.102 ± 0.01	4a	0.022 ± 0.003		0.884 ± 0.102
Benzo(b)fluoranthene / benzo(k)fluoranthene	4a	0.328 ± 0.035	1	0.304 ± 0.13	2	0.447 ± 0.051	2	0.254 ± 0.028	4a	0.066 ± 0.061	4b	0.02 ± 0.213
Benzo(j)fluoranthene	4a	0.097 ± 0.016	1	0.097 ± 0.067	1	0.131 ± 0.027	2	0.076 ± 0.015	4a	0.007 ± 0.061	4b	0.031 ± 0.213
Benzo(e)pyrene	4a	0.132 ± 0.014	1	0.123 ± 0.053	2	0.168 ± 0.019	2	0.092 ± 0.011	4a	0.067 ± 0.028	4b	0.196 ± 0.098
Benzo(a)pyrene	4a	0.206 ± 0.021	1	0.194 ± 0.073	1	0.276 ± 0.029	2	0.17 ± 0.016	4a	0.07 ± 0.028	4b	0.192 ± 0.098
Perylene	4a	0.037 ± 0.006	2	0.04 ± 0.033	1	0.055 ± 0.011	2	0.031 ± 0.006	4a	0.052 ± 0.028	4a	0.181 ± 0.098
Indeno(cd)pyrene	1	0.105 ± 0.009	2	0.088 ± 0.04	2	0.174 ± 0.016	2	0.079 ± 0.009		0.066 ± 0.028	4a	0 ± 0.173
Benzo(ghi)perylene	1	0.081 ± 0.011	1	0.078 ± 0.066	2	0.145 ± 0.02	2	0.066 ± 0.011		0 ± 0.098		0 ± 0.345
Indeno(cd)fluoranthene	1	0.035 ± 0.009	1	0.043 ± 0.07	1	0.056 ± 0.017	2	0.03 ± 0.009		0 ± 0.098		0 ± 0.345
Other (ng / µg TC)												
Levoglucosan	1	Footnote [b]		222.7 ± 45.3	2	230.43 ± 11.1		255.04 ± 6.15		0 ± 9.463	2	0 ± 21.548
Retene	4a	0.325 ± 0.037	2	0.057 ± 0.088	1	0.04 ± 0.018	1	0.022 ± 0.01		0.004 ± 0.052		0 ± 0.182
1,8-Naphthalic anhydride	4a	0.095 ± 0.029	2	0.147 ± 0.138	1	0.17 ± 0.055	2	0.089 ± 0.031		0 ± 0.159		0.043 ± 0.557
1H-Phenalen-1-one	4a	0.276 ± 0.039	2	0.152 ± 0.161	1	0.108 ± 0.037	2	0.118 ± 0.021	2	0 ± 0.107	1	0 ± 0.375
1-Phenyl-Naphthalene	1	0.005 ± 0.033	2	0.002 ± 0.167	2	0.001 ± 0.063		0 ± 0.035		0 ± 0.19		0 ± 0.669
3,5-Dimethoxyphenol		0 ± 0.236		0 ± 1.185		0 ± 0.448		0 ± 0.248		0 ± 1.348		0.157 ± 4.739
4-Methylphenylacetone	1	0.017 ± 0.063	2	0.021 ± 0.314		0 ± 0.119	2	0.002 ± 0.066	2	0 ± 0.357		37.605 ± 5.197
Acenaphthenone	4a	0.021 ± 0.019	2	0.031 ± 0.104		0.019 ± 0.035	2	0.022 ± 0.02	4a	0 ± 0.107		0 ± 0.375
Acetosyringone	1	0.052 ± 0.297		8.442 ± 4.23	1	6.549 ± 1.279	2	10.05 ± 0.709	2	0.201 ± 1.691	3	0 ± 5.945
Acetovanillone	1	0.403 ± 0.111	2	0.299 ± 1.385	1	0.185 ± 0.207	2	0.212 ± 0.114	2	0 ± 0.621	3	0 ± 2.184
Anthracen-9,10-dione	4a	0.031 ± 0.019	2	0.023 ± 0.095	1	0.006 ± 0.035	2	0.013 ± 0.02	2	0 ± 0.107	3	0 ± 0.375
Benz(de)anthracen-7-one	4a	0.365 ± 0.086	1	0.535 ± 0.55	2	0.513 ± 0.156	2	0.346 ± 0.087		1.098 ± 0.457	4a	0 ± 2.863

Coniferyl aldehyde	1	22.87 ± 1.148	2	13.92 ± 3.972	1	7.927 ± 0.559	2	5.003 ± 0.31	2	0 ± 0.226	1	0 ± 0.794
Dimethoxycoumarin		0 ± 0.036		0 ± 0.179		0 ± 0.068		0 ± 0.038		0 ± 0.204		0 ± 0.717
Eugenol	1	0.005 ± 0.256	2	0.004 ± 1.283	2	0 ± 0.485	2	0 ± 0.269	2	0 ± 1.459		0 ± 5.13
Flourenone	4a	0.051 ± 0.019	2	0.019 ± 0.113	1	0.009 ± 0.035	2	0.006 ± 0.02	2	0 ± 0.107	3	0 ± 0.375
Guaiacol	1	0.063 ± 0.194	2	0.049 ± 0.972	2	0.023 ± 0.367	2	0.03 ± 0.203	2	0 ± 1.105	3	0 ± 3.884
Iso-eugenol	1	0.922 ± 0.235		0.408 ± 0.885	1	0.314 ± 0.261	2	0.124 ± 0.144	2	0 ± 0.783	3	0 ± 2.754
Methylchrysene	4a	0.023 ± 0.004	2	0.038 ± 0.025	1	0.052 ± 0.007	2	0.029 ± 0.004	4a	0 ± 0.037		0.21 ± 0.059
Methylfluoranthene	4a	0.559 ± 0.056		0.264 ± 0.192	1	0.27 ± 0.028	2	0.236 ± 0.015	2	0.01 ± 0.012	3	0.005 ± 0.041
Methylguaiacol	1	0.031 ± 0.294	1	0.021 ± 1.476	1	0.011 ± 0.557	2	0.015 ± 0.309	4a	0 ± 1.678		0 ± 5.9
Ethylguaiacol	1	0.006 ± 0.304	2	0.006 ± 1.525	1	0 ± 0.576	2	0.003 ± 0.319	2	0 ± 1.734		0 ± 6.095
Propylguaiacol	1	0.002 ± 0.266	2	0.002 ± 1.331		0 ± 0.503	2	0 ± 0.279		0 ± 1.514		0 ± 5.322
Sinapic aldehyde	1	1.08 ± 0.401	2	33.86 ± 7.403	1	36.03 ± 1.931	2	26.975 ± 1.07		0 ± 0.839	4a	0 ± 2.951
Syringealdehyde		0 ± 0.314		14.55 ± 5.737	1	10.69 ± 1.423	2	12.95 ± 0.789	2	0.083 ± 1.788	3	0 ± 6.285
Vanillin	1	0.802 ± 0.496	2	0.507 ± 1.5	1	0.409 ± 0.207	2	0.202 ± 0.114	2	0 ± 0.619	3	0 ± 2.175
Caffeine											3	0 ± 0.582
Compound Name		**Meat Cooking**										
OC (g / kg biomass)		0.18										
EC (g / kg biomass)		0.0										
PAHs (ng / µg TC)												
Fluoranthene		0.090 ± 0.013										
Pyrene		0.057 ± 0.021										
Benzo(ghi)fluoranthene		0.000 ± 0.005										
Benzo(b)fluoranthene / Benzo(k)fluoranthene		0.036 ± 0.045										
Benzo(e)pyrene	1	0.000 ± 0.013										
Benzo(ghi)perylene	1	0.000 ± 0.014										
Phenanthrene		0.302 ± 0.029										
Other (ng / µg TC)												
Cholesterol	1	3.74 ± 0.171										

[a] OC and EC emissions from cigarettes have units of (mg / cigarette).

[b] Levoglucosan concentration not available because datafile became corrupted during final quantification.

12 SOURCE APPORTIONMENT OF ULTRAFINE (PM0.1) AND FINE (PM1.8) AIRBORNE PARTICULATE MATTER DURING A WINTER POLLUTION EPISODE (CRPAQS) IN CENTRAL CALIFORNIA

12.1 Introduction

Increasing evidence suggests that airborne ultrafine particles may pose a danger to human health [155]. There are two main hypotheses for the mechanism of injury associated with ultrafine particles. The shear number of ultrafine particles may overwhelm the ability of the alveolar macrophages that clear foreign objects from the lungs [5, 168, 169]. Alternatively, ultrafine particles may cross cell membranes where they can interfere with the internal cell functions [10]. If the latter hypothesis is true, then the mass concentration and chemical composition of particles in the ultrafine size fraction are important factors to consider.

All combustion sources emit ultrafine particles but the chemical composition of the particles released from different sources is not the same (see for example [58, 90, 103, 140, 159, 161, 162]). The relationship between ultrafine particle composition and health effects is not clearly understood at this time. It will therefore be necessary to determine the health effects associated with ultrafine particles emitted from different sources in order to design effective emissions control programs to protect public health. One method to study the health effects of ultrafine particles released from different sources is to directly test each source using cell cultures or inhalation exposure experiments. A second approach is to test ambient ultrafine particulate matter for health effects while at the same time calculating source contributions to that ambient ultrafine particulate matter. This latter approach properly accounts for important atmospheric transformations such as chemical reaction, condensation / evaporation, and coagulation. It can also simultaneously consider multiple sources, which may reveal interactions that influence health effects. The key to this approach is the accurate source apportionment of airborne ultrafine particulate matter.

Numerous studies have performed source apportionment calculations for coarse (Dp<10 μm) and fine (Dp<2.5μm) airborne particle fractions (see for example [19, 98, 167, 170, 171]), but very little is currently known about source contributions to airborne ultrafine particle mass. Ultrafine size thresholds of Dp < 0.1 μm (PM0.1) and Dp < 0.18 μm (PM0.18) have been suggested as relevant size fractions for health effects studies. The focus of the current paper is to quantify PM0.1 source contributions during a severe air quality episode in California's San Joaquin Valley (SJV). The San Joaquin Valley routinely experiences some of the highest particulate matter concentrations in the United States [65, 172] and the population in the region is growing rapidly suggesting that poor air quality will become an even more important public health problem in the future.

12.2 Methods

12.2.1 Ambient Sample Collection

Size-resolved airborne particulate matter was collected with Micro Orifice Uniform Deposit Impactors (MOUDIs) (MSP Corp, Shoreview MN) and Reference Ambient Air Samplers (RAAS) (Andersen Instruments, Smyra GA) during the California Regional Particulate Air Quality Study (CRPAQS) [65, 173]. The samples discussed in the current study were collected over 7 days during the period December 15 – 28, 2000 at Sacramento and over 11 days during the period December 15, 2000 – January 7, 2001 at Modesto, and Bakersfield. Two samples were collected at all locations on each day: 10am-6pm (daytime) and 8pm-8am (nighttime). The sample locations span a north-south transect of the San Joaquin Valley. PM1.8 concentrations during the study period exceeded 150 $\mu g\ m^{-3}$ [65]. PM0.1 concentrations during the study episode reached approximately 1 $\mu g\ m^{-3}$ [65] which is comparable to concentrations measured in Los Angeles [61, 160].

Two MOUDIs were used at each location to support a full range of chemical analysis for the collected particles. The first MOUDI was loaded with Teflon substrates (Teflo R2PJ47) to support elemental analysis by Inductively Coupled Plasma Mass Spectrometry (ICPMS) analysis [174]. Water-soluble ions were also measured using Ion Chromatography (IC). The second MOUDI was loaded with foil substrates that were then used to quantify carbon concentrations with thermal – optical carbon analysis [65]. RAAS samples were collected on Teflon filters (water-soluble ion and elemental analysis) and quartz filters (carbon analysis). A set of backup quartz filters were used to quantify the gas-phase adsorption artifact on the front quartz filter. All collection media used for carbon analysis was pre-baked at 500^{o}C for 48hrs to remove any carbon contamination.

All of the measurements used in the current chapter were made using extensive quality assurance protocols and the data was subjected to rigorous quality control checks to ensure precision and accuracy [65]. Samples were stored in Petri dishes sealed with Teflon tape at -18^{o}C before and after collection. Approximately 10% of the sampling media was retained as field blanks to characterize background levels. External standards were used during analytical procedures to verify accuracy, and duplicate measurements were used to verify precision. MOUDI measurements were summed to produce PM1.8 values that were then compared to collocated filter measurements.

12.2.2 Source Apportionment Methodology

Traditional molecular marker Chemical Mass Balance (CMB) studies employ “source profiles” that describe the concentration of elements and molecules normalized by the concentration of particulate organic carbon. Although numerous elements and molecules may be carried through this procedure, the majority of the source attribution information is contained in a set of “core” tracer compounds that are unique to individual source categories. These “core” tracer compounds are chosen for their specificity and for their stability in the particle phase once they are emitted to the atmosphere. Numerous semi-

volatile or reactive compounds are specific to certain sources but they are not conserved in the particle phase and so they do not carry useful source apportionment information. These elements and compounds are carried through the calculation primarily to corroborate the final CMB result with mass conservation checks.

The difficulties encountered during the collection of ultrafine particles (low pressure, bounce artifacts, adsorption / desorption artifacts) and the low concentration of ultrafine particles in the atmosphere make it difficult to obtain useful information about semi-volatile and/or reactive tracer compounds for ultrafine source apportionment calculations. The "core" tracer compounds specific to individual source categories were used as the basis for ultrafine source apportionment calculations in the current study. These compounds include levoglucosan (biomass combustion), hopanes and steranes (lubricating oil), and heavy PAHs (gasoline-fuel; may be confounded by coal combustions but this source is not present in California). The amount of elemental carbon and organic carbon associated with each unit of these tracers is discussed in Chapters 9 and 11. Cholesterol has been used historically as a tracer for meat cooking [143, 151] but recent evidence suggests that other "unknown" sources of cholesterol may be present in the atmosphere. The concentration of meat cooking particles in the atmosphere identified with cholesterol is considered tentative in the present study.

Diesel fuel contributions to HDDV particulate matter exhaust were quantified during the emissions source testing discussed in Chapters 4 and 9 using light PAHs fluoranthene and pyrene. These compounds are both semi-volatile and reactive in the atmosphere making their use for ambient source apportionment studies uncertain anywhere outside the immediate roadside environment. Traditional CMB calculations use elemental carbon (EC) as a tracer for diesel fuel contributions to ambient particulate matter by assuming that elemental carbon not associated with other sources is emitted from diesel engines. This methodology was also adopted in the current study to estimate diesel fuel contributions to ambient particulate matter.

The source apportionment algorithm devised for the current study prioritizes sources in order from most certain to least certain based the level of confidence in the tracer compounds. Conservation of mass constraints are employed separately for EC and OC so that uncertain sources do not apportion more carbon than the measured concentrations. The individual steps in the algorithm to predict source contributions to EC and OC are summared as follows:

1. Calculate biomass contributions to EC using levoglucosan as a tracer. Certainty = high.
2. Calculate motor oil contributions to EC using hopanes and steranes (expressed as equivalent concentration of 17α(H)-21β(H)-29-norhopane) as a tracer. Certainty = high.
3. Calculate gasoline-fuel contributions to EC using benzo[ghi]perylene and coronene (expressed as equivalent concentration of benzo[ghi]perylene) as a tracer. Certainty = high.

4. Calculate meat cooking contributions to EC using cholesterol as a tracer. Certainty = low.
5. Assign residual EC to diesel-fuel. Certainty = medium.
6. Calculate diesel-fuel contribution to OC using diesel-fuel EC as a tracer. Certainty = medium.
7. Calculate biomass contributions to OC using levoglucosan as a tracer. Certainty = high.
8. Calculate motor oil contributions to OC using hopanes and steranes (expressed as equivalent concentration of 17α(H)-21β(H)-29-norhopane) as a tracer. Certainty = high.
9. Calculate gasoline-fuel contributions to OC using benzo[ghi]perylene and coronene (expressed as equivalent concentration of benzo[ghi]perylene) as a tracer. Certainty = high.
10. Calculate meat cooking contributions to OC using cholesterol as a tracer. Certainty = low. Constrain meat cooking contributions to the amount of residual OC not already accounted for by other sources.

12.2.3 Source Apportionment Profiles

Table 12-1 summarizes the source profiles used in the current study. Cholesterol and levoglucosan were used as unique tracers for meat cooking and biomass combustion respectively, with ratios of tracer/OC and tracer/OC on MOUDI stages as discussed in Chapter 11 [175]. Benzo[ghi]perylene was used as a unique marker for gasoline-fuel PM and 17α(H)-21β(H)-29-norhopane was used as a unique marker for lubricating oil PM as discussed in Chapter 9 [176]. Lubricating oil and gasoline-fuel contributions to EC and OC depend on vehicle technology. Weighted-average lubricating oil profile and gasoline-fuel profiles were developed in the present study to quantify the contribution the on-road average gasoline fleet to particulate matter concentrations. The California Emissions Factor model (EMFAC) was used to estimate the distribution of particulate matter emissions from different classes of gasoline vehicles in the counties surrounding Sacramento, Modesto, and Bakersfield during December 2000 and January 2001. EMFAC estimated that 95-96% of the PM2.5 emissions from gasoline-powered motor vehicles were produced by vehicles equipped with three way catalysts (TWC). Non-catalyst equipped vehicles (NCAT) were assumed to account for 3-4% of the PM2.5 emissions from gasoline-powered vehicles with the remaining 1% of the on-road gasoline vehicle PM2.5 emissions attributed to vehicles emitting visible smoke (SMKR). All of the LDGV profiles are discussed in greater detail in Chapter 9 [176].

The amount of total carbon per unit of hopanes associated with lubricating oil emitted from heavy duty diesel vehicles (HDDVs) ranged from ~0-17 (μg C / ng hopane) (see Table 9-7). Different grades of lubricating oil and, to a certain extent, different operating conditions result in different amounts of hopanes and steranes per unit of carbon in the lubricating oil particle-phase emissions. The uncertainty range associated with lubricating oil profiles from HDDVs were relatively large because the size distributionsn of light PAHs used to identify diesel fuel contributions to exhaust PM were similar to the

size distributions of hopanes and steranes. Test HDDV-5 produced a lubricating oil profile that was consistent with LDGV tests within relatively tight uncertainty estimates. The lubricating oil profile developed for HDDV-5 will be used for all HDDVs in the current study. A complete description of the HDDV profiles is presented in Chapter 9.

Heavy PAHs such as benzo[ghi]perylene and coronene are good candidate tracers for gasoline-fuel contributions to particulate matter emissions from motor vehicles because these compounds are only emitted at trace levels from other sources and they are not destroyed or formed at significant rates by atmospheric chemical reaction. A similar tracer for diesel fuel contributions to carbonaceous particulate matter emissions was not found in the current study. Particle-phase emissions of light PAHs such as fluoranthene were measured at very high concentrations in diesel exhaust [103] but these compounds must be used with extreme care. Fluoranthene and light PAHs are semi-volatile which means that their particle-phase concentration decreases as the diesel exhaust plume is diluted with background air. This makes their use in regions outside the immediate roadside enrionment difficult. Changes to ambient temperature can also have a large effect on phase-partitioning for these compounds, complicating source apportionment analysis. Finally, fluoranthene and pyrene are produced by atmospheric reactions leading to higher concentrations that may confound source apportionment studies. Fluoranthene and pyrene were not used as tracers in the current study. The methodology for calculating diesel-fuel source contributions to airborne particulate matter using EC as a tracer is desribed in Section 12.2.2.

12.3 Results

12.3.1 Ambient Concentrations

Figure 12-1 shows the average size and composition distribution of airborne particulate matter collected at Sacramento, Modesto, and Bakersfield during the period December 2000 – January 2001 (11 sample days). Panels 1(a,c,e) show the daytime average (10am-6pm) while Panels 1(b,d,f) show the nighttime average (8pm-8am). The accumulation mode in the distribution has strong contributions from ammonium nitrate with a peak diameter below 1 μm. Daytime ammonium nitrate concentrations are generally larger than nighttime concentrations. The chemical composition of smaller particles is dominated by elemental carbon (EC) and organic carbon (OC). The higher nighttime concentration of these carbon particles reflects the dominance of primary emissions [173]. The carbonaceous fraction of the nighttime PM0.1 and PM0.18 mass is approximately 96% and 83%, respectively. The carbonaceous fraction of the daytime PM0.1 and PM0.18 mass is approximately 91% and 81%, respectively. The remainder of the PM0.1 and PM0.18 mass is composed of nitrate, ammonium ion, sulfate, and other material. A thorough discussion of the dominant mechanisms that produce the average profiles illustrated in Figure 12-1 is provided by Herner et al. [173].

Figure 12-2 illustrates the normalized size distribution of total carbon, benzo[ghi]perylene, 17α(H)-21β(H)-29-norhopane, levoglucosan, and cholesterol at Sacramento, Modesto, and Bakersfield. Concentrations in each size fraction were

normalized by dividing with the measured PM1.8 concentration to illustrate the relative size distribution of each species. Organic carbon and elemental carbon size distributions were highly correlated (R^2>0.9) and so only the total carbon size distribution is shown. Total carbon size distributions have larger mean diameter during the daytime than nighttime at Sacramento and Bakersfield. Mixing depths are larger during the daytime than during the nighttime, allowing carbonaceous particles from higher in the atmosphere to reach the ground-level monitor. Nighttime total carbon profiles are dominated by fresh combustion emissions while daytime total carbon profiles reflect more aged aerosol [173].

Each of the organic compounds illustrated in Figure 12-2 is characteristic of a single class of sources. Cholesterol is emitted by meat cooking operations, levoglucosan is emitted mainly from biomass combustion, 17α(H)-21β(H)-29-norhopane is contained in lubricating oil, and benzo[ghi]perylene is expected to be dominated by gasoline emissions. Benzo[ghi]perylene has a size distribution peak between 0.18-0.32 μm particle diameter at all locations in both the daytime and nighttime. Size distributions for other compounds show more variation with the peak diameter sometimes occurring between 0.18-0.32 μm particle diameter and sometimes at larger particle sizes. The geometric standard deviation of each size distribution also varies widely. Cholesterol generally has the broadest particle size distribution while benzo[ghi]perylene and 17α(H)-21β(H)-29-norhopane generally have sharper peaks. The differences between the size distributions of the various particle-phase organic compounds reflect the fact that these compounds exist in particles emitted from different sources. Each source releases particles to the atmosphere with a characteristic size distribution (see for example [58, 90, 103, 140, 159, 161, 162]). Coagulation gradually transforms the aerosol into an internal mixture but this process is not instantaneous and it does not necessarily result in uniform contributions from all sources to all size fractions of the particle distribution. A detailed understanding of the compound concentrations within each size fraction is needed before size-resolved source apportionment calculations can be carried out.

Tables 12-2 through 12-4 illustrate the measured concentrations of organic compounds, potassium, organic carbon, and elemental carbon in the PM0.1, PM0.18, and PM1.8 size fractions at Sacramento, Modesto, and Bakersfield, respectively. Daytime concentrations and nighttime concentrations are reported separately at each location. All nighttime concentrations were higher than daytime concentrations, reflecting the enhancement of primary emissions in the stagnant nighttime atmosphere [173]. Elemental carbon concentrations in the ultrafine size fraction (PM0.1) ranged from 29 – 71 μg m^{-3} during the day and 93 – 183 ng m^{-3} during the night. Organic carbon concentrations in the ultrafine size fraction ranged from 168 – 321 ng m^{-3} during the day and 393 – 825 ng m^{-3} during the night. The most abundant organic compound detected was levoglucosan with ultrafine concentrations ranging from 1 – 271 ng m^{-3}. The next most abundant species was cholesterol, with ultrafine concentrations ranging from 0.1 – 0.6 ng m^{-3}. Polycyclic aromatic hydrocarbons (PAHs) were measured in the ultrafine size fraction at concentrations ranging from 0 – 36 pg m^{-3} during the day and 0 – 227 pg m^{-3} at night. Hopane and sterane concentrations in the ultrafne size fraction ranged from 0 – 6.5 pg m^{-3}.

12.3.2 Quality Assurance Checks

Figure 12-3 illustrates agreement between co-located filter-based and MOUDI samplers as a quality assurance check for the species listed in Tables 12-2 – 12-4. Each data point in the sub-panels of Figure 12-3 represents a sampling period corresponding to the panels of Figure 12-1. Good agreement is observed between the co-located samples in all cases. Statistics for a linear regression analysis between the co-located filter-based and MOUDI samples are shown in Table 12-5. Except for a few of the lighter (semi-volatile) PAHs, $R^2 > 0.9$ for PAHs, $R^2 > 0.8$ for hopanes and steranes, and $R^2 > 0.99$ for levoglucosan and cholesterol. The slope of the regression line was greater than 0.7 in all cases, which is typical for comparisons between filter-based and MOUDI samplers. Based on the high level of correlation between co-located samples, the concentrations illustrated in Tables 12-2 – 12-4 are able to support accurate source apportionment calculations.

12.3.4 Size-Resolved Source Contributions

Figure 12-4 illustrates the size distribution of predicted source contributions to particulate organic carbon concentrations at Sacramento between December 15 – 28, 2000 and Modesto, and Bakersfield between December 15 and January 7, 2001 using the source profiles illustrated in Table 12-5 and the measured concentrations shown in Tables 12-1 – 12-3 (along with concentrations measured for all size fractions between 0.056 – 1.8 μm). Wood burning and meat cooking are predicted to dominate the organic carbon size distribution at all locations. Contributions to organic carbon concentrations from lubricating oil, gasoline fuel, and diesel fuel are predicted to be relatively minor at the sampling sites during the present study. This reflects the fact that the sites were located in residential and light commercial areas. Organic carbon concentrations are generally not over-predicted in any size fraction with the exception of over-predictions to ultrafine OC concentrations at Modesto at night. Postive residual organic carbon concentrations were detected during all daytime sampling periods and at Bakersfield during the nighttime. The residual organic carbon may be produced by some primary source such as natural gas combustion that was not included in the calculation. Extensive oil and gas refining operations in the vicinity of Bakersfield may be one example of such an unknown source. It is also possible that secondary organic aerosol formation occurs in the atmosphere, leading to the formation of additional organic carbon in the particle-phase that cannot be attributed to a primary source.

Figure 12-5 shows the size distribution of predicted source contributions to particulate elemental carbon concentrations at Sacramento between December 15 – 28, 2000 and Modesto, and Bakersfield between December 15, 2000 – January 7, 2001. Both predicted and measured elemental carbon concentrations are significantly lower than organic carbon concentrations. EC over-predictions are observed during the evening hours at Sacramento but are otherwise small. Gasoline-fuel is the single largest source of predicted EC concentrations at all locations and times, with a peak between 0.18 – 0.32 μm particle diameter and a tail extending into the ultrafine mode. Predicted contributions to EC concentrations from diesel engines are observed during the day but generally not at night. This trend is consistent with the increased use of diesel vehicles during working

hours and the increased transport of diesel exhaust to the sampling sites during the daytime when wind speeds and atmospheric mixing are greater than during the night. Lubricating oil contributions to EC are relatively small at all locations, with much of this material predicted to occur at sizes larger than 0.1 μm particle diameter. Predicted wood combustion and meat cooking contributions to EC concentrations are minor.

12.3.5 Fine and Ultrafine Source Contributions

Table 12-6 and Figure 12-6 illustrate predicted source contributions to particulate carbon (organic + elemental) concentrations in the PM1.8 size fraction at Sacramento, Modesto, and Bakersfield during the current study. Total carbonaceous PM1.8 concentrations ranged from 7.6 – 27.9 μg m^{-3}. Wood smoke accounted for ~50% of PM1.8 carbon during the nighttime at Sacramento and Modesto and ~15% of nighttime carbonaceous PM1.8 at Bakersfield. Gasoline fuel contributions to nighttime carbonaceous PM1.8 ranged from 27-41%. Diesel fuel made little contribution to nighttime PM1.8 concentrations, which is not surprising since the sampling sites were not located close to major highways and the majority of the diesel traffic on surface streets occurs during normal working hours during the day. Motor oil contributions to PM1.8 concentrations ranged from 4-8% during the nighttime hours. Predicted meat cooking contributions to PM1.8 concentrations were surprisingly large at Modesto and Bakersfield during the evening hours, ranging from 12-19%. This level of meat cooking is consistent with the cholesterol concentrations measured in the airborne particles while simultaneously considering carbon mass conservation constraints. Never-the-less, the quantification of meat cooking contributions to airborne particle concentrations using cholesterol as a tracer should be considered preliminary, since it is possible that some other source of cholesterol is present in the atmosphere.

Wood smoke contributions to PM1.8 concentrations are predicted to decrease during the daytime hours. This trend is consistent with increased temperatures during the day and the normal workday diurnal pattern. Predicted meat cooking contributions to PM1.8 are significantly enhanced during the day, ranging from 40-58%. Once again, this level of meat smoke contribution is consistent with the measured cholesterol concentrations in the airborne particle PM1.8 measurements, but it is higher than the level suggested by previous source apportionment studies for central California during winter stagnation events [167]. The quantification of meat cooking contributions to airborne particle mass should be considered preliminary at the present time. Predicted gasoline fuel contributions to PM1.8 concentrations ranged from 13-24%. Diesel fuel contributions to PM1.8 were predicted to be 13% at Sacramento during the day but were less than 1% at Modesto and Bakersfield. Lubricating oil (from either gasoline or diesel engines) was predicted to account for ~6-7% of the PM1.8 at Modesto and Bakersfield but could not be detected at Sacramento during the day.

Table 12-7 and Figure 12-7 illustrate predicted source contributions to ultrafine (PM0.1) total particulate carbon (organic + elemental) concentrations at Sacramento, Modesto, and Bakersfield. Total PM0.1 concentrations ranged from 0.4 μg m^{-3} at Modesto during

the daytime to 1.1 μg m^{-3} at Modsto during the nighttime. Wood combustion was the single largest source of ultrafine particles at the Sacramento, Modesto, and Bakersfield during the evening hours. Wood smoke contributions to ultrafine (PM0.1) particle concentrations during the nighttime ranged from 56% at Bakersfield to 81% at Modesto. Gasoline-fuel accounted for approximately 20-30% of the ultrafine (PM0.1) particle mass during the nighttime sampling periods at all locations. Diesel fuel contributions to PM0.1 mass were predicted to be 1-3% during the night.

Ultrafine particle concentrations during daytime sampling periods contained a greater amount of material from "unknown" sources. Wood smoke was still the single largest source of known ultrafine particle mass with contributions ranging from 3-43%. Estimated meat cooking contributions to ultrafine particle mass ranged from 11-37%. Given the surprisingly large predictions for meat cooking contributions to PM1.8, the meat cooking contribution to PM0.1 must also be viewed with caution. Diesel fuel contributions to PM0.1 mass were predicted to be 21% at Sacramento and 11% at Bakersfield during the day. Diesel fuel contributions to PM0.1 at Modesto were still predicted to be less than 1% during the day. Gasoline fuel was predicted to account for 2-10% of the PM0.1 mass, while motor oil was predicted to account for 3-5%. Unknown sources accounted for 58% of the PM0.1 mass at Modesto and 24% of the PM0.1 mass at Sacramento during the day.

12.4 Discussion

The results of the current study illustrate the capability to carry out source apportionment calculations in the ultrafine size range and present typical results during a severe winter pollution event in the San Joaquin Valley of California. Nighttime concentrations of carbon are generally more than double the daytime concentrations due to stagnant atmospheric conditions at night [173]. The relative change of the source contributions to PM0.1 and PM1.8 concentrations illustrated in the current study reflects the mix of sources around the sampling locations. Sites were generally located in light commercial (Modesto and Bakersfield) or residential (Sacramento) areas and so the relative contribution from transportation sources decreases at these sites during the evening hours. Identical sampling conducted adjacent to a major transportation corridor would likely reveal the opposite trend.

12.5 Conclusions

Size-resolved samples of airborne particulate matter collected at 3 sites in the San Joaquin Valley of California were extracted with organic solvents and analyzed for detailed organic compounds using GC-MS. The smallest size fraction analyzed was $0.056 < Dp < 0.1$ μm particle diameter which accounts for the majority of the mass in the ultrafine (PM0.1) size range. Source profiles for ultrafine particles developed during pervious studies were applied to the measurements at each sampling site to calculate source contributions to organic and elemental carbon concentrations. Ultrafine elemental carbon concentrations ranged from 0.03 μg m^{-3} during the daytime to 0.18 μg m^{-3} during

the nighttime. Gasoline fuel, diesel fuel, and lubricating oil accounted for the majority of the ultrafine elemental carbon concentrations, with relatively minor contributions from biomass combustion and meat cooking. Ultrafine organic carbon concentrations ranged from 0.2 μg m^{-3} during the daytime to 0.8 μg m^{-3} during the nighttime. Wood combustion was found to be the largest source of ultrafine organic carbon. Meat cooking was also identified as a significant potential source of PM0.1 mass but further study is required to verify the contributions from this sources. Gasoline fuel, diesel fuel, and lubricating oil made minor contributions to PM0.1 organic carbon mass. Total ultrafine particulate matter concentrations were dominated by contributions from wood combustion and meat cooking during the current study. Future inhalation exposure studies may wish to target these sources as potential causes of adverse health effects.

Table 12-1: Source profiles used for simple apportionment calculations.

Source	Tracer	Tracer / OC	Tracer / EC
Diesel Fuel	EC[1]	2.56	1
Gasoline	Benzo[ghi]perylene[2]	0.0009	0.0003
Lubricating Oil	17α(H)-21β(H)-29-norhopane	0.0004	0.0003
Wood Burning	Levoglucosan	0.15	5.0
Meat Cooking	Cholesterol	0.0015	0.15

[1]Residual EC not explained by other sources was used as a tracer for diesel-fuel contributions to OC. See text discussion for source apportionment algorithm.

[2]Gasoline engines were found to be the dominant source of benzo[ghi]perylene during source tests. Coal combustion may also release these compounds but this source is not present in significant quantitites in California. See text discussion for additional caveats.

Table 12-2: Concentration of organic compounds, potassium, organic carbon, and elemental carbon measured in the PM0.1, PM0.18, and PM1.8 size fractions at Sacramento between December 15, 2000 to January 7, 2001.

	Sacramento Day				Sacramento Night		
PAHs (pg / m3)	**PM0.1**	**PM0.18**	**PM1.8**		**PM0.1**	**PM0.18**	**PM1.8**
Fluoranthene	0 ± 0.24	0 ± 0.3	96.1 ± 0.2		0 ± 22.42	17.2 ± 35.98	670 ± 118.43
Pyrene	0 ± 0.13	0 ± 0.18	78.3 ± 0.37		0 ± 12.21	11.5 ± 14.04	906 ± 76.44
Retene	0 ± 0.18	5.5 ± 0.39	282 ± 1.39		42.4 ± 17.27	115 ± 39.67	3340 ± 587.72
Benzo[ghi]flouranthene	0 ± 0.1	0 ± 0.13	69.3 ± 0.34		12 ± 9.22	59.2 ± 11.94	1380 ± 112.08
Chrysene	0 ± 0.02	4 ± 0.18	55.1 ± 0.59		26.5 ± 2.86	96.2 ± 15.8	1690 ± 144.61
Benzo[b]fluoranthene	12.4 ± 0.29	30.4 ± 0.3	144 ± 0.27		93.3 ± 14.06	248 ± 16.39	3340 ± 134.28
Benzo[k]fluoranthene	0 ± 0.23	0 ± 0.25	20.8 ± 0.62		18.7 ± 10.55	18.7 ± 10.59	680 ± 20.56
Benzo[e]pyrene	6.88 ± 0.04	24.1 ± 0.06	72.5 ± 0.79		50.3 ± 2.35	130 ± 8.18	1670 ± 71.66
Benzo[a]pyrene	0 ± 0.12	0 ± 0.23	71.2 ± 0.33		54.8 ± 5.9	119 ± 9.11	3120 ± 36.92
Perylene	0 ± 0.2	0 ± 0.23	0 ± 0.34		9.88 ± 9.52	9.88 ± 10.37	0 ± 15.39
Indeno[1,2,3-cd]pyrene	0 ± 4.97	102 ± 6.08	374 ± 16.31		91.2 ± 231.77	355 ± 355.41	5750 ± 1023.02
Benzo[ghi]perylene	9.93 ± 4.05	64 ± 6.08	388 ± 15.58		96.2 ± 188.83	375 ± 279.44	4060 ± 776.43
Coronene	0 ± 1.09	63.8 ± 1.95	371 ± 4.64		50.9 ± 50.77	331 ± 94.08	3040 ± 299.74
MW302 PAHs	0 ± 0.38	0 ± 0.72	0 ± 1.47		131 ± 18.13	541 ± 38.68	8850 ± 203.83
Hopanes / Steranes (pg / m3)							
17B(H)-21A(H)-30-Norhopane	0 ± 0.03	0 ± 0.03	0 ± 0.04		0 ± 2.51	62.6 ± 3.61	922 ± 10.81
17A(H)-21B(H)-Hopane	0 ± 0.05	0 ± 0.07	0 ± 0.15		0 ± 4.91	48.6 ± 5.53	980 ± 13.87
ABB-20R-C29-Ethylcholestane	0 ± 0.01	0 ± 0.03	0 ± 0.09		0 ± 0.99	24.8 ± 1.68	443 ± 9.22
Other Organic Compounds (ng / m3)							
Levoglucosan	15.5 ± 0	35 ± 0	60.7 ± 0		103 ± 0	354 ± 0	2050 ± 0
Cholesterol	0.132 ± 0	0.213 ± 0	6.49 ± 0		0.394 ± 0	1.59 ± 0	20 ± 0.01
Other Species (ng / m3)							
Potassium	11.9 ± 10	21.4 ± 14.1	93.1 ± 20		19.4 ± 10	68 ± 14.14	345 ± 10
Organic Carbon	309 ± 110	801 ± 156	6100 ± 330		771 ± 70	2500 ± 98.99	18700 ± 220
Elemental Carbon	70.5 ± 110	218 ± 156	1430 ± 330		183 ± 70	596 ± 98.99	4450 ± 220

Table 12-3: Concentration of organic compounds, potassium, organic carbon, and elemental carbon measured in the PM0.1, PM0.18, and PM1.8 size fractions at Modesto between December 15, 2000 to January 7, 2001.

	Modesto Day				Modesto Night		
PAHs (pg / m3)	**PM0.1**	**PM0.18**	**PM1.8**		**PM0.1**	**PM0.18**	**PM1.8**
Fluoranthene	0 ± 1.53	3.99 ± 1.92	161 ± 1.61		7.66 ± 12.48	30.9 ± 20.06	449 ± 59.03
Pyrene	3.63 ± 0.83	7.9 ± 1.16	154 ± 2.21		11.4 ± 6.84	47.6 ± 8.22	577 ± 47.08
Retene	5.86 ± 1.16	13.7 ± 2.45	181 ± 7.13		120 ± 12.45	155 ± 23.36	1020 ± 149.93
Benzo[ghi]flouranthene	4 ± 0.63	12.5 ± 0.81	185 ± 2.26		16.6 ± 5.23	114 ± 9.21	1130 ± 89.75
Chrysene	7.17 ± 0.15	20.4 ± 1.13	212 ± 3.46		34.8 ± 2.69	176 ± 12.79	1590 ± 127.96
Benzo[b]fluoranthene	23.7 ± 1.88	76.2 ± 1.94	646 ± 5.25		103 ± 8.34	368 ± 12.68	2960 ± 117.31
Benzo[k]fluoranthene	4.28 ± 1.44	9.19 ± 1.59	97.4 ± 3.28		22.8 ± 5.9	64.8 ± 6.1	679 ± 15.39
Benzo[e]pyrene	12.1 ± 0.24	42.9 ± 0.46	316 ± 4.76		55.3 ± 2.05	185 ± 6.31	1390 ± 56.29
Benzo[a]pyrene	10.2 ± 0.77	39.3 ± 1.46	182 ± 2.19		81.2 ± 4.13	207 ± 6.95	2120 ± 42.54
Perylene	2.76 ± 1.3	2.76 ± 1.47	0 ± 1.73		13.6 ± 5.31	32.4 ± 5.82	331 ± 9.03
Indeno[1,2,3-cd]pyrene	23.2 ± 31.6	162 ± 38.72	1200 ± 83.45		143 ± 128.85	586 ± 197.88	4030 ± 462.33
Benzo[ghi]perylene	35.6 ± 25.75	152 ± 38.73	1040 ± 79.62		144 ± 104.98	488 ± 155.51	2700 ± 349.69
Coronene	29 ± 6.92	135 ± 12.44	813 ± 24.22		141 ± 28.53	333 ± 52.54	2540 ± 135.22
MW302 PAHs	0 ± 2.4	148 ± 4.56	1140 ± 10.34		227 ± 11.61	643 ± 24.72	3730 ± 76.74
Hopanes / Steranes (pg / m3)							
17B(H)-21A(H)-30-Norhopane	6.47 ± 0.19	15 ± 0.21	250 ± 1.07		0 ± 1.39	41.6 ± 2.16	361 ± 15.22
17A(H)-21B(H)-Hopane	0 ± 0.33	12.9 ± 0.43	330 ± 1.58		0 ± 2.73	51 ± 3.86	515 ± 21.72
ABB-20R-C29-Ethylcholestane	2.87 ± 0.08	6.75 ± 0.17	60.9 ± 0.53		0 ± 0.55	28.4 ± 1.28	183 ± 7.86
Other Organic Compounds (ng / m3)							
Levoglucosan	1.65 ± 0	3.61 ± 0	63.4 ± 0		271 ± 0	465 ± 0	2080 ± 0
Cholesterol	0.0631 ± 0	0.186 ± 0	7.1 ± 0		0.496 ± 0	5.25 ± 0	35.2 ± 0
Other Species (ng / m3)							
Potassium	2.46 ± 10	44 ± 14.14	47.2 ± 20		1.9 ± 10	46.6 ± 14.14	261 ± 10
Organic Carbon	321 ± 110	1230 ± 155.56	9210 ± 330		825 ± 70	3980 ± 98.99	22700 ± 220
Elemental Carbon	65.6 ± 110	285 ± 155.56	1690 ± 330		170 ± 70	822 ± 98.99	4550 ± 220

Table 12-4: Concentration of organic compounds, potassium, organic carbon, and elemental carbon measured in the PM0.1, PM0.18, and PM1.8 size fractions at Bakersfield between December 15, 2000 to January 7, 2001.

	Bakersfield Day				Bakersfield Night		
PAHs (pg / m3)	**PM0.1**	**PM0.18**	**PM1.8**		**PM0.1**	**PM0.18**	**PM1.8**
Fluoranthene	0 ± 1.53	2.83 ± 1.92	189 ± 1.79		2.28 ± 11.22	24.5 ± 18.05	338 ± 50.12
Pyrene	0 ± 0.83	0 ± 1.16	138 ± 2.15		0 ± 6.11	31.4 ± 7.34	439 ± 36.32
Retene	3.72 ± 1.16	7.09 ± 2.45	279 ± 7.34		30.2 ± 8.76	101 ± 20.22	1130 ± 130.37
Benzo[ghi]flouranthene	0.724 ± 0.63	5.09 ± 0.81	195 ± 2.32		5.43 ± 4.6	80.9 ± 7.66	618 ± 49.91
Chrysene	0.948 ± 0.14	7.43 ± 1.12	178 ± 3.33		11.6 ± 1.36	129 ± 10.89	902 ± 74.59
Benzo[b]fluoranthene	6.45 ± 1.87	36.6 ± 1.92	439 ± 3.69		43.1 ± 7.01	306 ± 11.69	2120 ± 84.11
Benzo[k]fluoranthene	1.43 ± 1.44	5.41 ± 1.59	90.9 ± 3.27		8.21 ± 5.27	57.8 ± 5.56	348 ± 13.9
Benzo[e]pyrene	3.46 ± 0.23	20.9 ± 0.42	207 ± 4.36		22.7 ± 1.12	155 ± 5.87	1210 ± 49.17
Benzo[a]pyrene	2.65 ± 0.76	17.5 ± 1.45	163 ± 2.1		24.8 ± 2.93	63.7 ± 4.6	1580 ± 63.1
Perylene	0 ± 1.3	0 ± 1.47	0 ± 1.73		5.64 ± 4.76	27.1 ± 5.19	240 ± 11.4
Indeno[1,2,3-cd]pyrene	0 ± 31.6	81 ± 38.71	1120 ± 83.41		37.4 ± 115.88	478 ± 178.11	4540 ± 438.09
Benzo[ghi]perylene	3.38 ± 25.74	73.7 ± 38.72	821 ± 79.52		36.2 ± 94.41	317 ± 139.87	2450 ± 334.57
Coronene	0 ± 6.91	67.1 ± 12.42	587 ± 23.95		24.6 ± 25.38	194 ± 47.12	1690 ± 165.36
MW302 PAHs	0 ± 2.4	166 ± 4.56	1590 ± 12.22		91.7 ± 9.25	320 ± 20.38	2930 ± 172.47
Hopanes / Steranes (pg / m3)							
17B(H)-21A(H)-30-Norhopane	4.72 ± 0.17	9.28 ± 0.19	220 ± 0.95		0 ± 1.25	96.9 ± 3.69	332 ± 13.97
17A(H)-21B(H)-Hopane	0 ± 0.33	5.84 ± 0.43	208 ± 1.17		0 ± 2.46	39.1 ± 2.97	344 ± 14.63
ABB-20R-C29-Ethylcholestane	4.17 ± 0.07	7.63 ± 0.17	161 ± 0.46		6.29 ± 0.55	39.5 ± 1.39	180 ± 7.67
Other Organic Compounds (ng / m3)							
Levoglucosan	12.4 ± 0	29.9 ± 0	233 ± 0		39.3 ± 0	132 ± 0	659 ± 0
Cholesterol	0.634 ± 0	1.56 ± 0	6.68 ± 0		0.564 ± 0	1.12 ± 0	4.04 ± 0
Other Species (ng / m3)							
Potassium	1.49 ± 10	5.24 ± 14.14	186 ± 20		6.09 ± 10	37.6 ± 14.14	314 ± 10
Organic Carbon	168 ± 110	864 ± 155.56	9610 ± 330		393 ± 70	2960 ± 98.99	17500 ± 220
Elemental Carbon	28.6 ± 110	162 ± 155.56	1480 ± 330		92.7 ± 70	670 ± 98.99	3600 ± 220

Table 12-5: Regression statistics between co-located filter-based samplers and MOUDI PM1.8 measurements of organic compounds, potassium, organic carbon, and elemental carbon.

	Regression Statistics	
PAHs	**Slope**	**R^2**
Fluoranthene	0.82	0.70
Pyrene	0.76	0.69
Retene	0.72	0.99
Benzo[ghi]flouranthene	0.81	0.96
Chrysene	0.84	0.98
Benzo[b]fluoranthene	0.87	0.99
Benzo[k]fluoranthene	0.96	0.96
Benzo[e]pyrene	0.91	0.98
Benzo[a]pyrene	0.72	0.95
Perylene	0.81	0.69
Indeno[1,2,3-cd]pyrene	0.84	0.93
Benzo[ghi]perylene	0.84	0.93
Coronene	0.77	0.95
MW302 PAHs	0.78	0.90
Hopanes / Steranes		
17B(H)-21A(H)-30-Norhopane	0.71	0.81
17A(H)-21B(H)-Hopane	0.74	0.80
ABB-20R-C29-Ethylcholestane	0.71	0.84
Other Organic Compounds		
Levoglucosan	0.98	1.00
Cholesterol	0.72	0.99
Other Species		
Potassium	0.95	0.97
Organic Carbon	0.91	1.00
Elemental Carbon	0.96	0.98

Table 12-6: Predicted source contributions to PM1.8 carbon concentrations at Sacramento, Modesto, and Bakersfield between December 15, 2000 and January 7, 2001.

PM1.8 (μ gm^{-3})	SAC DY	SAC NT	MOD DY	MOD NT	BFK DY	BFK NT
Diesel EC	0.703	0.000	0.000	0.000	0.000	0.000
Diesel OC	0.274	0.000	0.000	0.000	0.000	0.000
Gasoline EC	0.675	7.209	1.730	4.914	1.250	4.435
Gasoline OC	0.390	4.159	0.999	2.836	0.722	2.561
Lubricating Oil EC	0.000	0.965	0.305	0.492	0.289	0.441
Lubricating Oil OC	0.000	1.330	0.389	0.627	0.396	0.604
Wood Smoke EC	0.012	0.410	0.013	0.416	0.047	0.132
Wood smoke OC	0.405	13.680	0.423	13.877	1.556	4.392
Food Cooking EC	0.043	0.134	0.047	0.234	0.045	0.027
Food cooking OC	4.329	0.000	4.734	5.402	4.453	2.691
Unknown EC	0.000	-4.272	-0.409	-1.505	-0.153	-1.436
Unknown OC	0.700	-0.519	2.665	0.000	2.486	7.241
Total	7.532	23.096	10.896	27.294	11.090	21.088

Table 12-7: Predicted source contributions to PM0.1 carbon concentrations at Sacramento, Modesto, and Bakersfield between December 15, 2000 and January 7, 2001.

PM0.1 (μg m^{-3})	SAC DY	SAC NT	MOD DY	MOD NT	BFK DY	BFK NT
Diesel EC	0.058	0.016	0.000	0.000	0.016	0.011
Diesel OC	0.023	0.006	0.000	0.000	0.006	0.004
Gasoline EC	0.008	0.144	0.060	0.267	0.003	0.065
Gasoline OC	0.005	0.083	0.035	0.154	0.002	0.038
Lubricating Oil EC	0.000	0.000	0.005	0.000	0.004	0.005
Lubricating Oil OC	0.000	0.000	0.007	0.000	0.005	0.006
Wood Smoke EC	0.003	0.021	0.000	0.054	0.002	0.008
Wood smoke OC	0.104	0.684	0.011	1.810	0.083	0.262
Meat Cooking EC	0.001	0.003	0.000	0.003	0.004	0.004
Meat cooking OC	0.088	0.000	0.042	0.000	0.072	0.083
Unknown EC	0.000	0.000	-0.001	-0.154	0.000	0.000
Unknown OC	0.090	-0.003	0.227	-1.139	0.000	0.000
Total	0.379	0.954	0.387	0.995	0.196	0.486

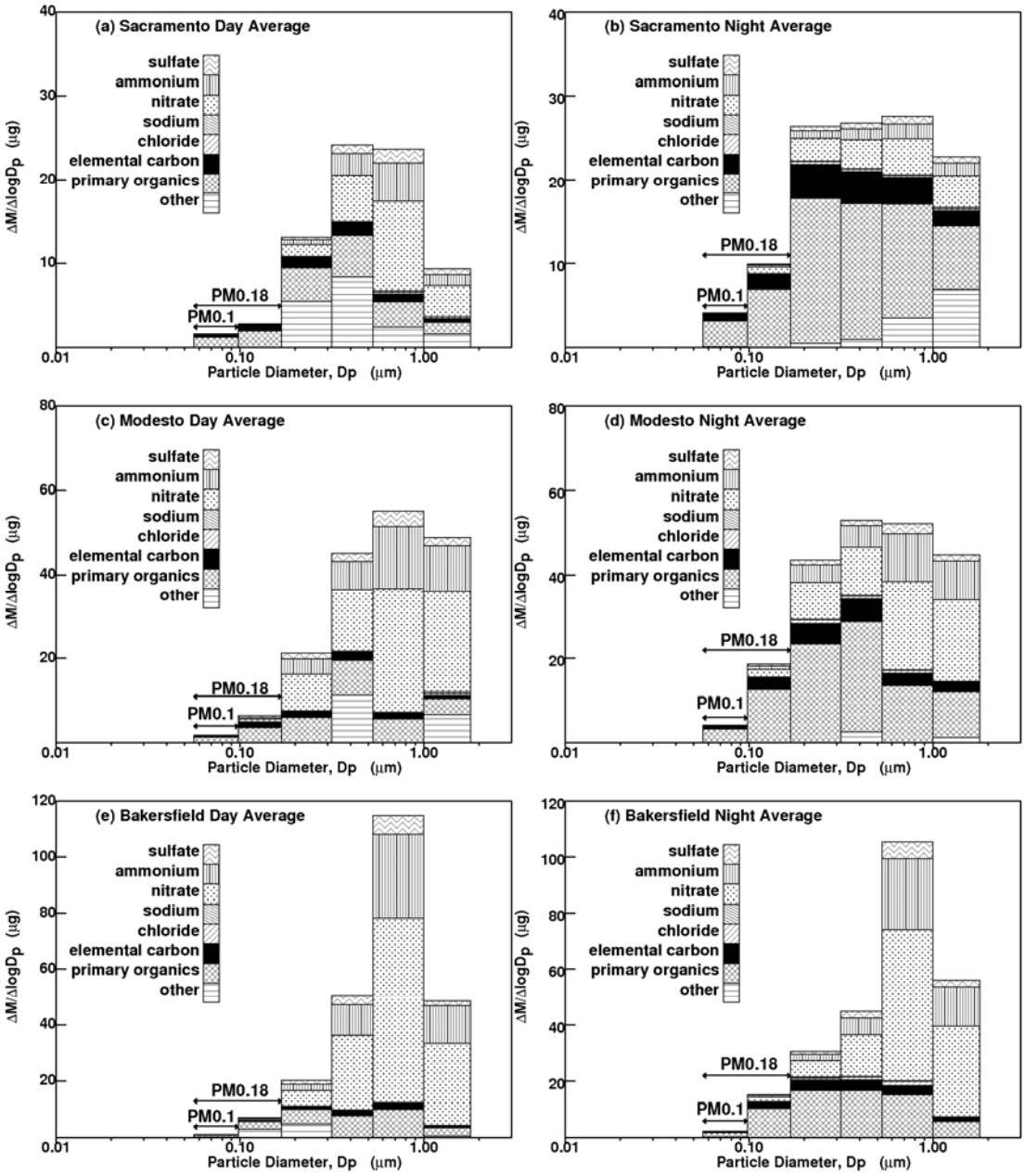

Figure 12-1: Size and composition distribution of airborne particulate matter collected at Sacramento, Modesto, and Bakersfield between December 15, 2000 – January 7, 2001. Day average samples were collected between 10-18 PST. Night average samples were collected between 20-8 PST.

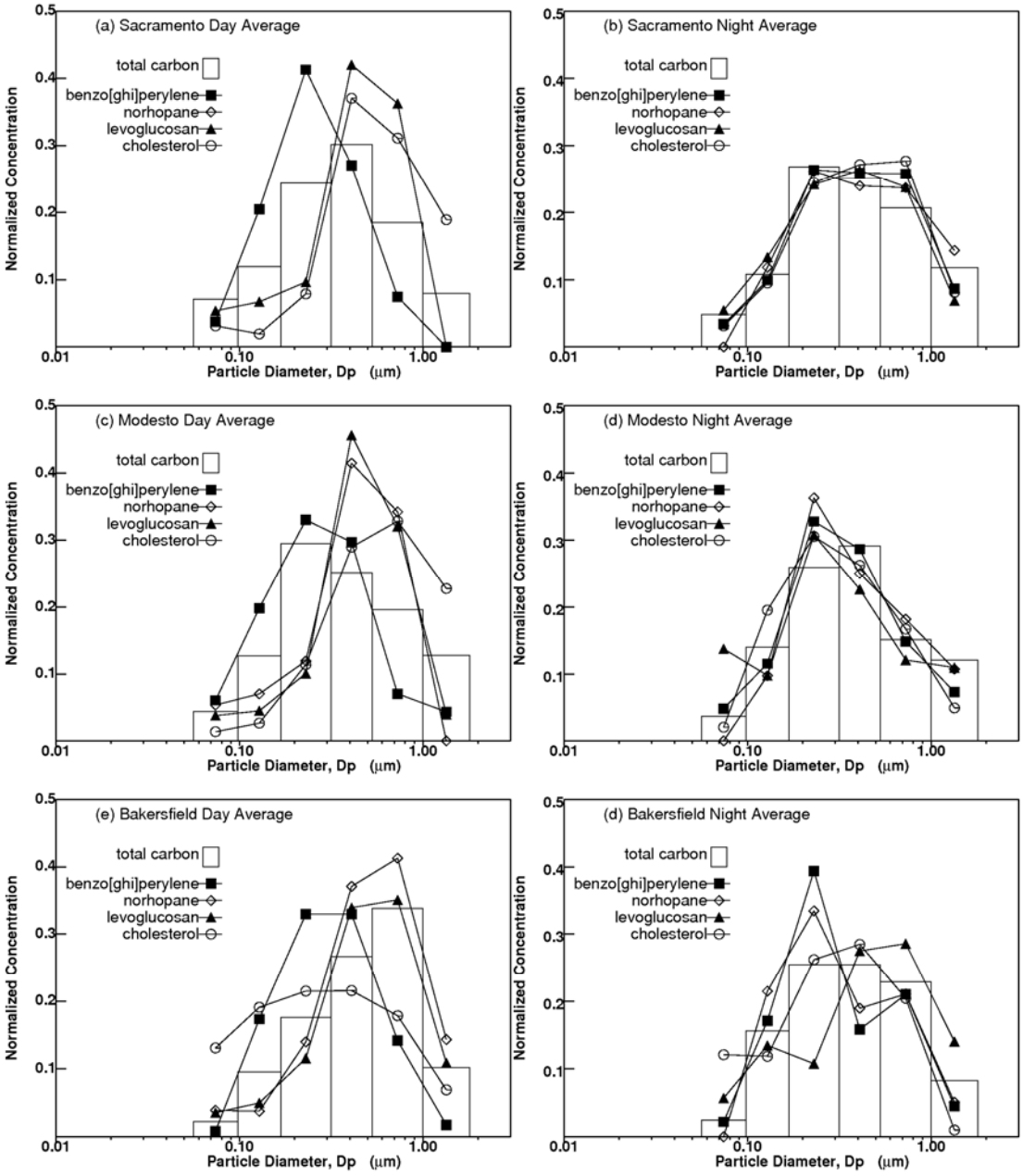

Figure 12-2: Normalized size distribution of particle-phase total carbon, benzo[ghi]perylene, 17α(H)-21β(H)-29-norhopane, levoglucosan, and cholesterol. Concentrations in each size fraction were normalized by the total PM1.8 concentration.

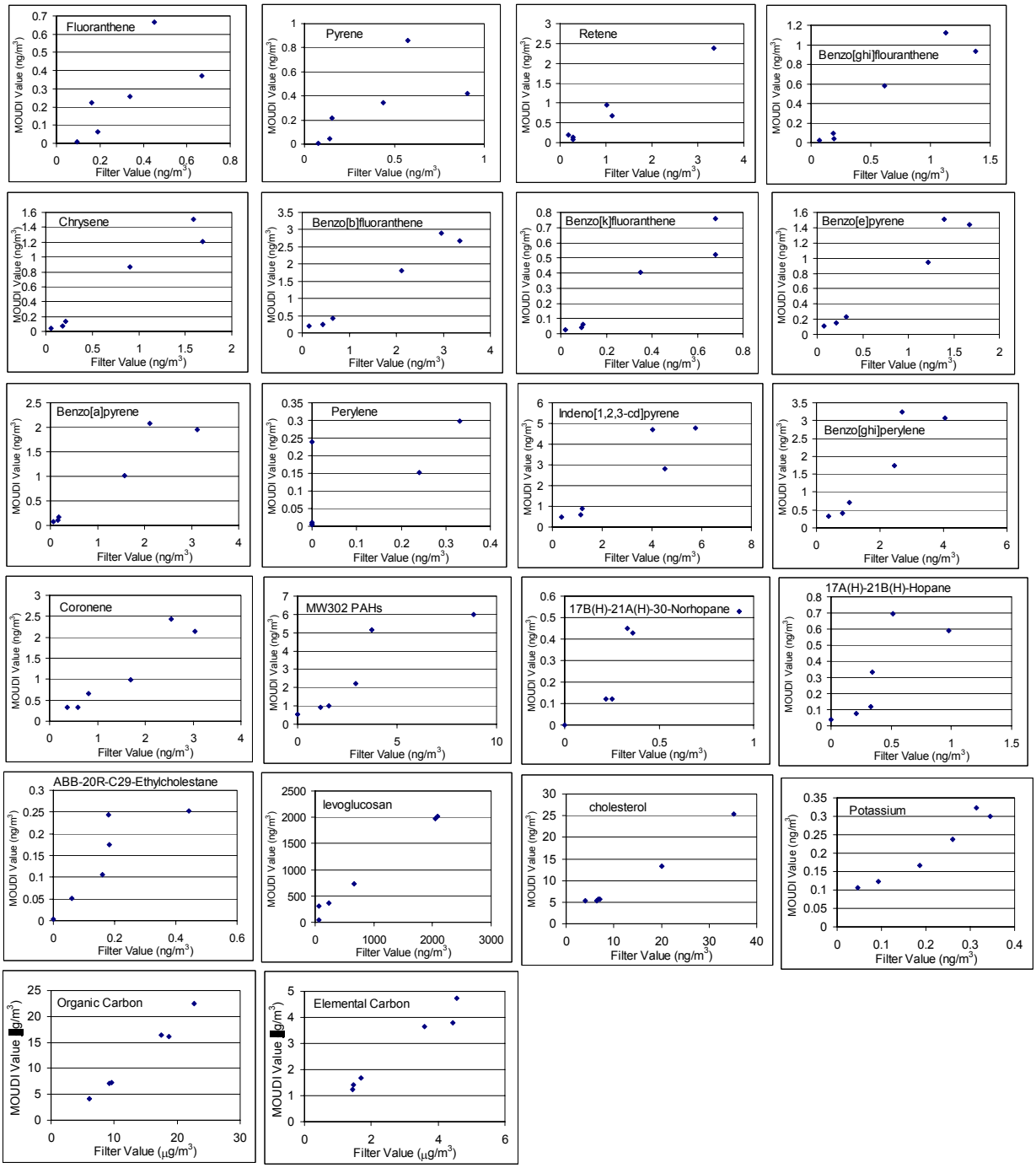

Figure 12-3: Agreement between measurements of particle-phase species made using co-located filter-based samplers and MOUDIs. Each datapoint corresponds to a panel of Figure 12-1. Regression statistics are summarized in 2.

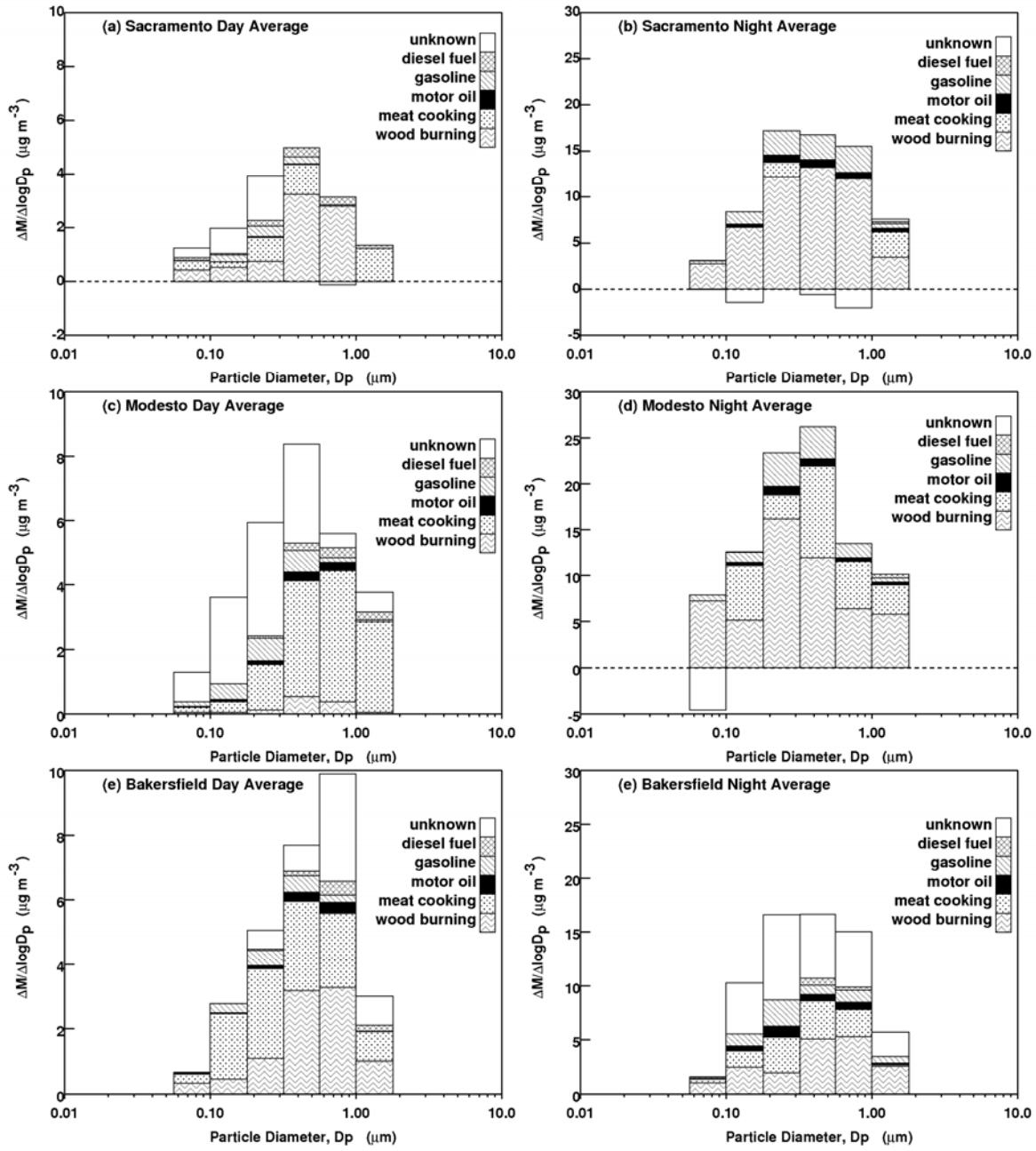

Figure 12-4: Predicted source contributions to size-resolved particulate organic carbon (OC) at Sacramento, Modesto, and Bakersfield between December 15, 2000 and January 7, 2001. Residual concentrations of OC (positive or negative) are illustrated as "unknown".

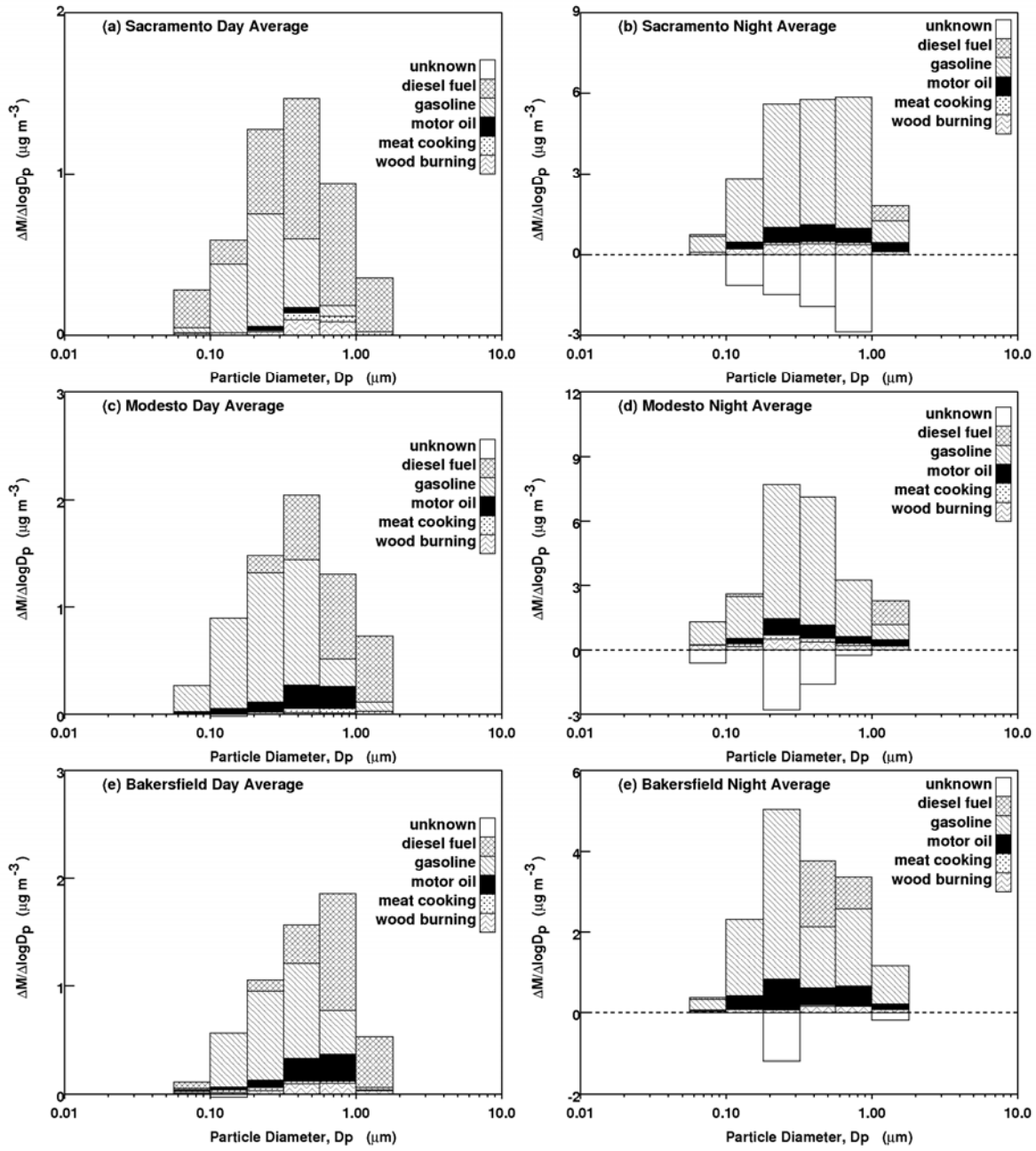

Figure 12-5: Predicted source contributions to size-resolved particulate elemental carbon (EC) at Sacramento, Modesto, and Bakersfield between December 15, 2000 and January 7, 2001. Residual concentrations of EC (positive or negative) are illustrated as "unknown".

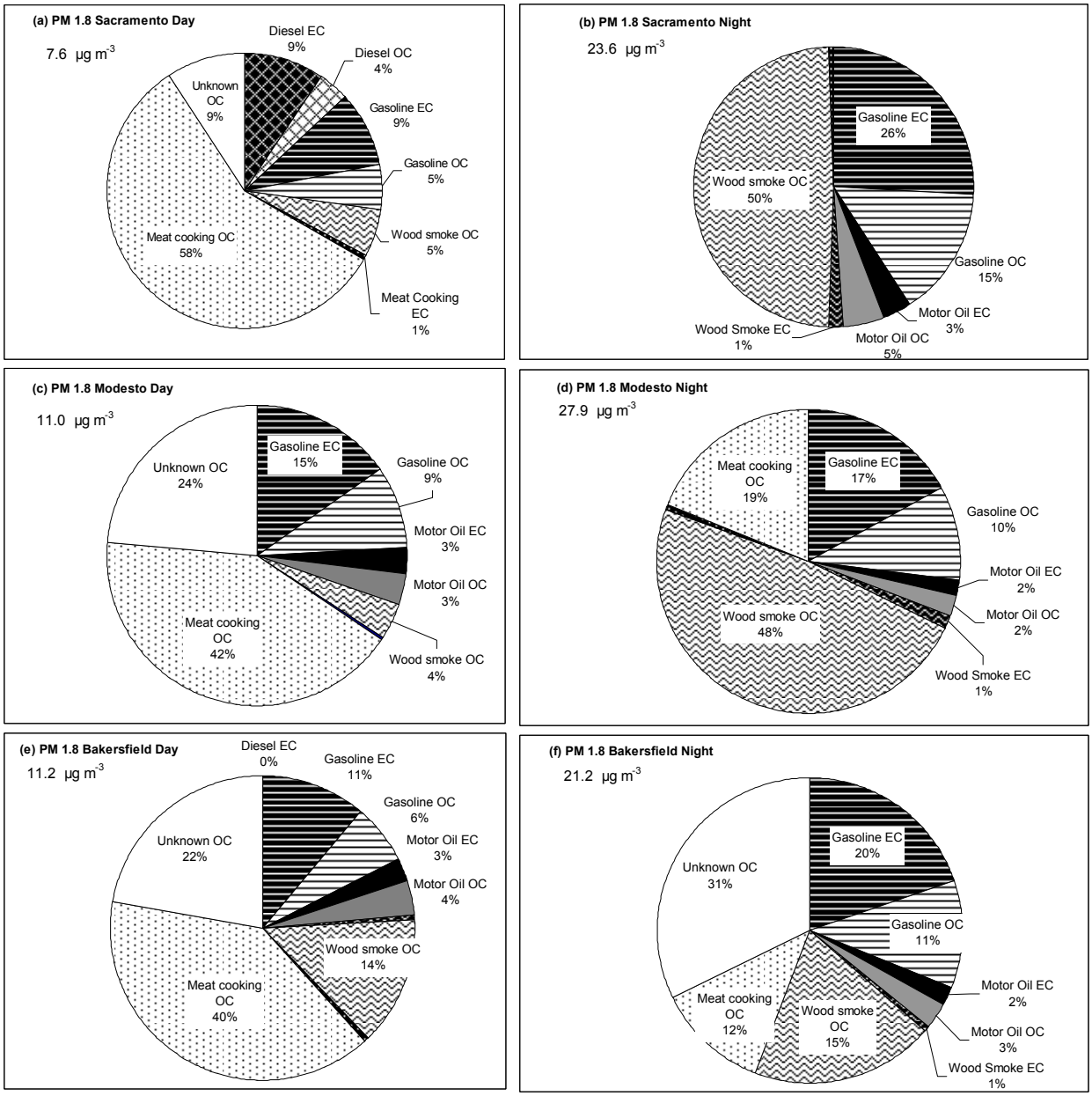

Figure 12-6: Predicted source contributions to PM1.8 concentrations at Sacramento, Modesto, and Bakersfield between December 15 2000 to January 7, 2001.

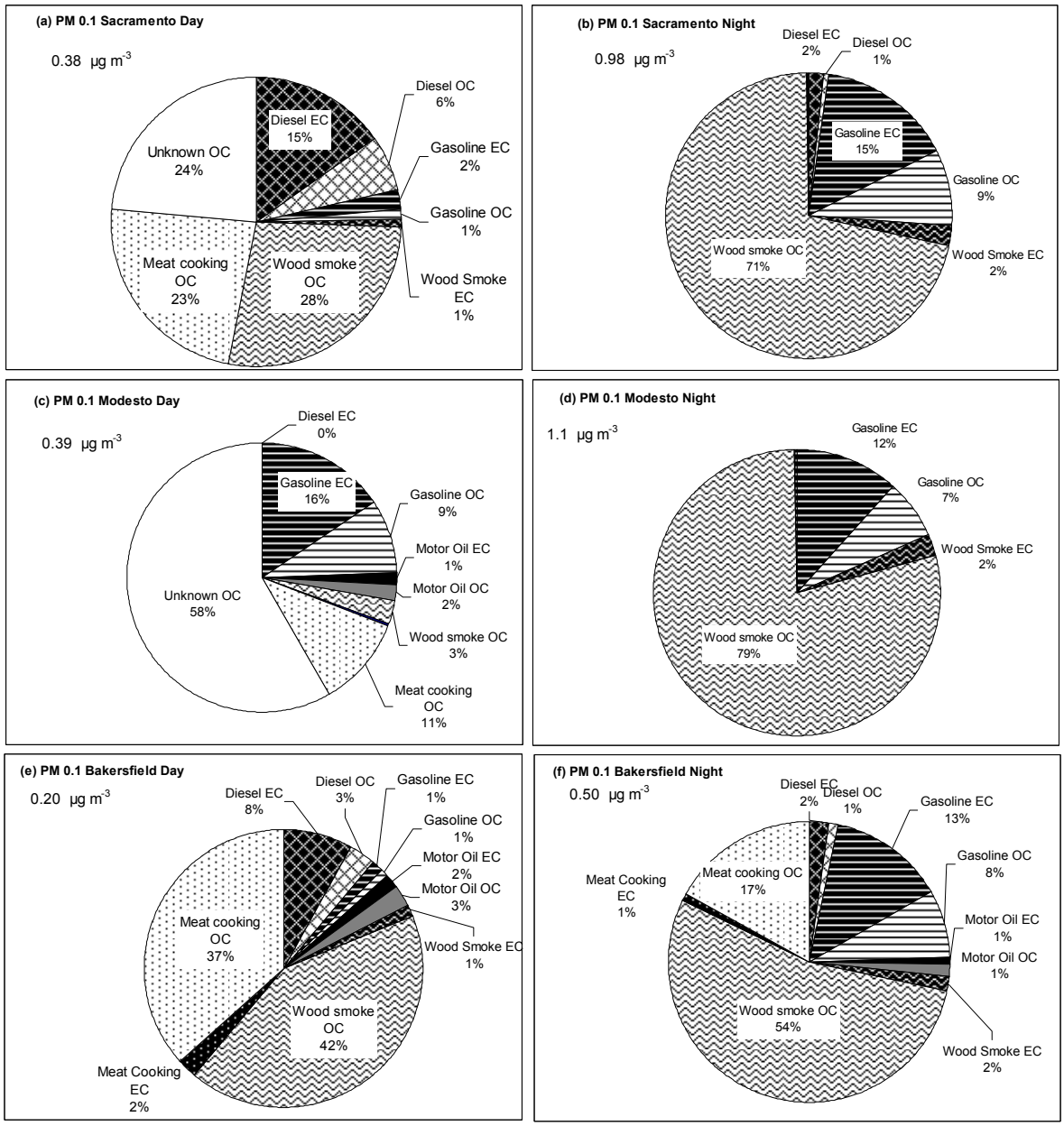

Figure 12-7: Predicted source contributions to PM0.1 concentrations at Sacramento, Modesto, and Bakersfield between December 15 2000 to January 7, 2001.

13 SOURCE APPORTIONMENT OF FINE PM DURING THE VEHICLE-ORIENTED TRAJECTORY STUDY (SCOS97)

13.1 Introduction

In the past decade, the EPA has undertaken the implementation of a $PM_{2.5}$ (airborne particulate matter with a diameter less than 2.5 μm) health-derived air pollution standard to regulate both acute (24-hr) and chronic (annual) exposure to $PM_{2.5}$. The genesis for this standard is an observed correlation between increased $PM_{2.5}$ concentrations (both short-term and chronic) and increased mortality and morbidity [177-179]. If a location is in violation of an air quality standard, then a plan needs to be developed and implemented to reduce that pollutant. The most cost effective method of pollutant abatement is typically source controls. Effective source controls require a detailed understanding of the relative strength of the pollutant source(s). As such, much regulatory and research effort has gone into determining the origin of $PM_{2.5}$.

The earliest source apportionment efforts were directed at determining the origin of the PM_{fine} in Southern California [19, 180, 181]. PM_{fine} is a more loosely defined PM size fraction than $PM_{2.5}$ and is typically used to describe the combination of the nucleation and accumulation size modes. These early studies did not necessarily focus on a sharp cut at 2.5 μm, which is also the case for the ambient samples analyzed here. These early PM_{fine} source apportionment studies all found the dominant sources to be meat cooking, wood burning, diesel vehicles, and gasoline vehicles. There are some differences between the results in these studies but in general these four source types are larger contributors than the other sources that were identified: tire wear, paved road dust, vegetative detritus, natural gas combustion, and cigarette smoke. In these early studies, 65-90% of the organic mass could be accounted for using the primary sources types mentioned above, with the other 10-35% attributed to some unknown source category. This amount of organic mass with unknown source-origin is larger at sampling sites further inland, suggesting that organic mass is created as the air moves from the coast over Los Angeles and then on to Riverside. This phenomenon is investigated in the current study.

A significant portion of the PM source apportionment effort has moved away from the CMB approach, as alternative source apportionment tools (for example, Positive Matrix Factorization, PMF) have been developed that do not require the detailed understanding of the source profiles [182, 183]. The disadvantage of these alternative approaches is the need for numerous receptor samples that must exhibit some relative source variability. To date, quantification of the organic components in numerous receptor samples has been prohibitively resource extensive and alternative source apportionment models have necessarily focused on the inorganic portion of the PM. In Southern California, where the organic portion of the PM_{fine} dominates, the inability to directly focus on organic mass limits the usefulness of these alternative approaches. The current study used EPA-CMB 8.2 to explore PM_{fine} origins.

A CMB source apportionment model requires high quality ambient chemical concentrations and equally high quality chemical signatures for relevant sources. Modern versions of CMB models typical use chemical measurement uncertainties to weight their linear regression fit, so high quality not only refers to accurate values but also knowledge of the associated uncertainty. Accurate chemical measurements, specifically for compounds that are helpful to source apportionment of PM_{fine}, are very difficult and expensive to obtain – nearly impossible in the past. Luckily, good CMB results can also be obtained with highly precise measurements, and an accurate understanding of the associated uncertainty. Therefore, consistency of methods for sampling and quantification are vital to accurate CMB analysis. The concept of consistency was explored in this work.

13.2 Methods

13.2.1 Chemical Mass Balance (CMB) Source Apportionment Model:

A CMB model uses knowledge of emission source characteristics along with the characteristics of the pollutants at the receptor to determine the contribution of each source to the pollutant level at the receptor. A CMB model assumes that the concentration of a given chemical species at a receptor is the sum of the contributions of that chemical species from each source. Mathematically this is shown below:

$$c_i = \sum_{j=1}^{m} f_{ij} a_{ij} s_j \qquad \text{for i = 1..n}$$

where c_i is the concentration of chemical species i, f_{ij} is the fraction of species i from source j that has been unaltered before that species reached the receptor, a_{ij} is the fraction of species i in the emissions of source j, and s_j is the concentration of pollutants from source j at the receptor. Successful application of a CMB model starts with a critical selection of chemical species. Only those chemical species that are not depleted via chemical reactions or via preferential removal mechanisms, and which are not created via atmospheric chemical reaction should be used (i.e., f_{ij} = 1). Second, since the model requires that the source profiles (a_{ij}) be linearly independent, chemical species must be chosen which are unique to specific source types. The selected chemical species are often termed 'fingerprints' because they are emitted from one specific source or emitted in a unique abundance by that source.

In other words, these fingerprints are the chemical signatures of the specific source emissions. All combustion sources (e.g., wood, gasoline, cigarettes, food) are organic, so their emission fingerprints consist primarily of organic compounds. Successful application of a CMB model to apportion PM_{fine} mass must involve organic emission fingerprints [184]. Several researchers have determined, qualitatively and/or quantitatively, source fingerprints for wood combustion [141, 185-187] vehicle emissions [14, 28, 75, 188] cigarette smoke [144, 189], and meat cooking [158, 163]. For example,

cholesterol is emitted during food cooking but cannot be found in the emissions from any other source type.

Schauer and colleagues [19] developed a CMB model that took advantage of the unique molecular markers emitted by each source type. This model has been successfully applied to PM2.5 collected in southern California during 1982 [19], southern California during 1993 [180],and the San Joaquin Valley during 1995 [167], and Atlanta [137].

CMB calculations will be performed using the EPA/DRI CMB8.0 software package.

13.2.2 Receptor Sample Collection:

The 1997 Southern California Ozone Study (SCOS97) was a large multi-investigator field campaign conducted from June 16 to October 15, 1997. This study was designed to collect meteorological and air quality measurements to support further development of photochemical modeling tools. Besides ozone, SCOS97 also focused on aerosol origins and evolutions. As part of the aerosol effort, a Vehicle-Oriented Trajectory Study was conducted by the Glen Cass and Kim Prather research groups. This study took place during August 16-31, 1997 and looked at looked at three sites that mapped a typical air trajectory path inland, from Central Los Angeles quickly out to Azusa where it might stagnate and slowly move on to Riverside [190]. The Cass group deployed filter samplers that collected particles with a diameter less than 1.9 μm at each of these sites. In order to have enough organic compound mass in an extract to be above the quantification limits, filter samples were composited into two sample periods at each site; therefore we are exploring a total of six PM_{fine} samples, or two air parcel trajectories.

13.2.3 Organic Compound Quantification for Receptor Samples:

Filter samples were composited and spiked with known amounts of deuterated internal standards (decane, D22; pentadecane, D32; tetracosane, D50; phenol, D5; benzaldehyde, D6; hexanoic acid, D11; decanoic acid, D19; benzoic acid, D5). These spiked samples were extracted twice with hexane, followed by three extractions of a 2:1 benzene:isopropanol mixture. All solvent extracts of a sample were combined and reduced in volume. Compounds were identified and quantified on a HP 5890 gas chromatograph (GC) coupled with an HP 5972 mass selective detector (MS). The GC was equipped with a 30 m HP-1701 capillary column. A co-injection standard, 1-phenyldodecane, was used to monitor the instrument response. Compounds were identified with authentic standards or NIST mass spectral library matching. Individual organic compounds were quantified by integrating compound peaks in the relevant ion chromatograms using the HP ChemStation Software. Ion counts are normalized by ions counts for a relevant internal standard, and then the relative ion counts are converted to mass ratios using response factors. Mass ratios are then converted from mass ratios to mass on the substrates by using the known internal spike concentration and spike volumes. Finally, these masses are converted to mass concentrations by dividing by the volume of air sampled by the collective substrates.

This quantification process is rigorous but prone to bias. Standards that are used to derive response factors inherently have error associated with them. Across all the chemical components in the standards that error is likely close to zero; however, for a single component that error can be several percent. In the end, one chemical species may end up several percent high and another may end up several percent low. The same standard is used thought out the quantification process resulting in excellent precision; but a consistent bias. A similar bias can result from the choice of normalizing internal standard. Again, if the same internal standard is always used for normalization, then excellent results are obtained; however, this is not always the case. Choice of internal standard is important beyond these bias considerations. Absolute GC-MS response factors vary significantly (by as much as 50%) even between consecutive analysis of the same sample. Luckily, the ratio of compound peak areas stays similar if those compounds have similar GC retention times and have similar functionality. Those two caveats are critical, and as such accurate quantification of organic compounds via GC-MS requires high quality internal standards. This fact is mentioned here to help highlight the compounds that are quantified that have the potential to be more precise than accurate; these would be the compounds that are normalized by internal standards that are not similar, in this case the PAH, oxy-PAH, and the hopanes.

13.2.4 Other Compound Quantification for Receptor Samples:

In addition to the quantification of the organic tracers via GC-MS, the receptor samples also underwent thermal optical transmissions analysis for elemental carbon and total organic carbon. Co-located samples collected on Teflon filters were analyzed for water-soluble ions using ion chromatography and trace metals using Neutron Activation Analysis.

13.2.5 Chemical Concentrations at the Receptors:

Table 13-1 shows the chemical concentrations for the three sites during the two sampling periods. Note the chemical species that were identified include alkanes, polycyclic aromatic hydrocarbons (PAH), oxygenated PAHs (oxy-PAH), hopanes, elemental carbon (EC), organic carbon (OC), and trace metals. Alkanes come from a variety of sources: heavy n-alkanes are relatively high in tire wear, mid-range n-alkanes are relatively high in motor vehicle emissions, odd numbered carbon n-alkanes are relatively high in vegetative debris, and iso- and anteiso-alkanes are relatively high in cigarette smoke. PAH and oxy-PAH originate from almost all combustion sources; although the heavier PAH are relatively high in gasoline and the lighter PAH are relatively high in diesel emissions. The hopanes originate solely from combustion of lubricating oil (both from diesel and gasoline powered vehicles). Levoglucosan, a tracer for biomass combustion, and cholesterol, a tracer for meat cooking, could not be quantified in these samples and as such those sources are likely to be difficult to extract in the CMB model.

Uncertainties shown in Table 13-1 for bulk carbon, ions, and elements were propagated from the analytical uncertainties for the sampling periods that are included in each event. The organics uncertainties were based on the accuracy and precision of known quantities

of different types of compounds after undergoing GC/MS analysis by Michael Hannigan's group at the University of Colorado. These uncertainties are 10% of the measured value for n-alkanes, 15% for PAHs, and 15% for hopanes.

Table 13-1: Receptor Concentrations (µg/m3). Sample codes correspond to Los Angeles (LA), Azusa (AZ), and Riverside (RV) during sampling period 1 (V11) and sampling period 2 (V21). Uncertainty estimates are shown in brackets.

	V11-LA	V11-AZ	V11-RV	V21-LA	V21-AZ	V21-RV
EC	2.32 (0.92)	2.72 (0.95)	1.58 (0.89)	2.11 (0.90)	1.91 (0.92)	0.80 (0.88)
OC	11.52 (1.29)	13.81 (1.40)	12.13 (1.29)	11.30 (1.27)	14.49 (1.45)	10.84 (1.28)
Cl-	4.23E-1 (9.20E-2)	9.46E-2 (9.71E-2)	2.06E-2 (9.43E-2)	3.18E-1 (8.91E-2)	6.62E-2 (9.46E-2)	6.77E-2 (1.03E-1)
Al	6.99E-2 (2.96E-2)	1.58E-1 (2.71E-2)	2.54E-1 (3.11E-2)	5.64E-2 (2.23E-2)	2.60E-1 (1.00E-1)	2.35E-1 (2.85E-2)
As	3.62E-4 (2.29E-4)	6.95E-4 (2.75E-4)	2.74E-4 (2.62E-4)	1.08E-4 (1.97E-4)	1.86E-4 (2.56E-4)	1.80E-4 (2.49E-4)
Ba	8.63E-3 (4.57E-3)	1.19E-2 (4.72E-3)	1.66E-2 (4.94E-3)	9.69E-3 (4.51E-3)	7.90E-3 (4.66E-3)	9.57E-3 (4.44E-3)
Cd	1.36E-5 (5.21E-4)	2.42E-4 (5.18E-4)	0.00E+0 (3.33E-4)	6.88E-5 (5.89E-4)	1.59E-4 (4.90E-4)	8.77E-5 (4.00E-4)
Fe	5.14E-1 (1.41E-1)	2.67E-1 (8.24E-2)	1.05E+0 (1.16E-1)	4.17E-1 (1.27E-1)	3.93E-1 (1.48E-1)	2.91E-1 (9.21E-2)
K	2.34E-2 (1.74E-2)	4.68E-2 (2.25E-2)	1.89E-1 (3.94E-2)	2.92E-2 (1.17E-2)	7.86E-2 (4.38E-2)	7.00E-2 (2.84E-2)
Mg	4.47E-2 (2.56E-2)	5.17E-2 (2.57E-2)	7.99E-2 (2.78E-2)	5.85E-2 (2.76E-2)	1.41E-2 (1.28E-2)	3.47E-1 (7.46E-2)
Mn	1.35E-2 (2.61E-4)	8.86E-3 (8.38E-4)	2.43E-2 (4.19E-4)	9.55E-3 (2.05E-4)	8.31E-3 (2.05E-4)	5.65E-3 (1.61E-4)
Mo	4.09E-3 (1.03E-3)	1.41E-3 (4.44E-4)	2.24E-4 (1.99E-4)	4.97E-3 (1.19E-3)	1.29E-3 (4.34E-4)	1.92E-5 (4.41E-5)
Na	2.41E-1 (1.86E-2)	2.58E-1 (1.90E-2)	1.86E-1 (1.48E-2)	3.66E-1 (2.52E-2)	3.40E-1 (2.38E-2)	3.27E-1 (2.30E-2)
Rb	7.06E-4 (1.49E-3)	0.00E+0 (1.49E-3)	2.16E-3 (3.07E-3)	0.00E+0 (1.49E-3)	2.44E-3 (2.57E-3)	0.00E+0 (3.34E-4)
Sr	1.07E-3 (1.22E-3)	5.68E-5 (2.03E-4)	5.71E-3 (2.12E-3)	2.37E-3 (1.03E-3)	7.49E-4 (1.12E-3)	1.63E-3 (9.40E-4)
Ti	6.54E-3 (4.43E-3)	6.31E-2 (1.11E-2)	3.66E-2 (7.69E-3)	1.25E-2 (8.45E-3)	6.38E-2 (1.65E-2)	2.13E-2 (8.45E-3)
V	3.34E-3 (1.80E-4)	6.02E-3 (4.02E-4)	4.10E-3 (2.23E-4)	3.29E-3 (1.95E-4)	9.90E-3 (1.89E-3)	2.63E-3 (1.82E-4)
Zn	6.08E-2 (1.75E-2)	4.26E-2 (2.09E-2)	4.43E-2 (1.67E-2)	8.94E-2 (1.99E-2)	4.51E-2 (1.72E-2)	2.50E-2 (1.76E-2)
n-tetracosane	1.23E-2 (1.23E-3)	8.67E-3 (8.67E-4)	1.01E-2 (1.01E-3)	1.19E-2 (1.19E-3)	2.02E-2 (2.02E-3)	4.93E-3 (4.93E-4)
n-pentacosane	2.37E-2 (2.37E-3)	1.18E-2 (1.18E-3)	2.10E-2 (2.10E-3)	1.83E-2 (1.83E-3)	2.47E-2 (2.47E-3)	9.56E-3 (9.56E-4)
n-hexacosane	3.05E-2 (3.05E-3)	1.21E-2 (1.21E-3)	2.27E-2 (2.27E-3)	1.86E-2 (1.86E-3)	1.82E-2 (1.82E-3)	1.28E-2 (1.28E-3)
n-heptacosane	2.73E-2 (2.73E-3)	1.02E-2 (1.02E-3)	2.11E-2 (2.11E-3)	1.51E-2 (1.51E-3)	1.35E-2 (1.35E-3)	1.18E-2 (1.18E-3)

n-octacosane	2.54E-2 (2.54E-3)	8.34E-3 (8.34E-4)	2.04E-2 (2.04E-3)	1.18E-2 (1.18E-3)	1.15E-2 (1.15E-3)	9.69E-3 (9.69E-4)
n-nonacosane	1.99E-2 (1.99E-3)	9.02E-3 (9.02E-4)	2.63E-2 (2.63E-3)	1.05E-2 (1.05E-3)	1.02E-2 (1.02E-3)	8.60E-3 (8.60E-4)
n-triacontane	1.55E-2 (1.55E-3)	4.99E-3 (4.99E-4)	1.34E-2 (1.34E-3)	6.96E-3 (6.96E-4)	5.99E-3 (5.99E-4)	4.72E-3 (4.72E-4)
n-hentriacontane	1.18E-2 (1.18E-3)	7.09E-3 (7.09E-4)	1.37E-2 (1.37E-3)	7.67E-3 (7.67E-4)	6.47E-3 (6.47E-4)	5.74E-3 (5.74E-4)
n-dotriacontane	1.26E-2 (1.26E-3)	5.87E-3 (5.87E-4)	1.39E-2 (1.39E-3)	8.66E-3 (8.66E-4)	9.25E-3 (9.25E-4)	4.71E-3 (4.71E-4)
n-tritriacontane	1.40E-2 (1.40E-3)	6.90E-3 (6.90E-4)	1.17E-2 (1.17E-3)	7.79E-3 (7.79E-4)	1.06E-2 (1.06E-3)	6.32E-3 (6.32E-4)
n-tetratriacontane	9.59E-3 (9.59E-4)	4.10E-3 (4.10E-4)	1.20E-2 (1.20E-3)	5.29E-3 (5.29E-4)	5.89E-3 (5.89E-4)	4.22E-3 (4.22E-4)
Fluoranthene	4.40E-4 (6.60E-5)	1.80E-4 (2.70E-5)	1.60E-4 (2.40E-5)	3.30E-4 (4.95E-5)	1.90E-4 (2.85E-5)	1.50E-4 (2.25E-5)
triphenylene-chrysene	5.10E-4 (7.65E-5)	2.00E-4 (3.00E-5)	1.50E-4 (2.25E-5)	3.20E-4 (4.80E-5)	2.40E-4 (3.60E-5)	1.40E-4 (2.10E-5)
benzo[e]pyrene	5.70E-4 (8.55E-5)	2.20E-4 (3.30E-5)	2.10E-4 (3.15E-5)	2.50E-4 (3.75E-5)	2.80E-4 (4.20E-5)	1.30E-4 (1.95E-5)
benzo[a]pyrene	5.50E-4 (8.25E-5)	1.00E-4 (1.50E-5)	1.00E-4 (1.50E-5)	2.90E-4 (4.35E-5)	1.30E-4 (1.95E-5)	5.00E-5 (7.50E-6)
benzo[ghi]perylene	3.01E-3 (4.52E-4)	6.70E-4 (1.01E-4)	6.60E-4 (9.90E-5)	1.68E-3 (2.52E-4)	1.18E-3 (1.77E-4)	3.40E-4 (5.10E-5)
coronene	1.35E-3 (2.03E-4)	3.40E-4 (5.10E-5)	3.00E-4 (4.50E-5)	7.70E-4 (1.16E-4)	7.80E-4 (1.17E-4)	1.50E-4 (3.00E-4)
18a(H)-22,29,30-trisnorneohopane	8.80E-4 (1.32E-4)	3.10E-4 (4.65E-5)	3.00E-4 (4.50E-5)	2.70E-4 (4.05E-5)	5.10E-4 (7.65E-5)	1.70E-4 (2.55E-5)
17a(H)-21b(H)-hopane	1.70E-3 (2.55E-4)	9.70E-4 (1.46E-4)	9.30E-4 (1.40E-4)	1.10E-3 (1.65E-4)	1.09E-3 (1.64E-4)	3.40E-4 (5.10E-5)
17a(H)-21b(H)-29-norhopane	1.26E-3 (1.89E-4)	6.40E-4 (9.60E-5)	5.40E-4 (8.10E-5)	9.20E-4 (1.38E-4)	8.10E-4 (1.22E-4)	2.60E-4 (3.90E-5)

13.2.6 Source Profiles:

As mentioned previously, high quality chemical signatures for sources are vital to CMB source apportionment. Early success with CMB source apportionment of PM_{fine} is the exception to this rule as early studies employed highly consistent methods to characterize both the receptors and sources. A main deficiency of these early studies was that very few individual sources were tested to develop a profile that was characteristic of the broad source type. For example, only two natural gas-fired appliances were tested and their profiles were used to represent the entire population of natural gas-fired appliances in Southern California. Over the past decade researchers have focused on developing source profiles that are more representative of a broad source type, specifically for motor vehicles and wood combustion. The disadvantage of these efforts is that the methods that they employed were not always consistent with the methods used to develop the original profile libraries. The old and new source profiles could only be successfully combined if both measurements were accurate (a more stringent requirement than consistency). As part of the current study, a database of these PM_{fine} source profiles has been compiled and investigated for consistency. Table 13-2 shows the chemical signatures for the relevant

sources that were used in this work. The relevancy of these source types to the PM_{fine} concentration in Southern California has been determined in previous work [79].

Table 13-2: Source profiles (g / g OC) for fine PM. Uncertainty estimates are shown in brackets.

	Gasoline	Smoker	Diesel	Brake	Tire
EC	0.30 (0.02)	0.01 (0.00)	2.56 (0.23)	0.39 (0.18)	0.01 (0.00)
OC	1.00 (0.06)	1.00 (0.06)	1.00 (0.09)	1.00 (0.56)	1.00 (0.05)
Cl-	1.79E-3 (1.52E-3)	1.79E-3 (1.52E-3)	0.00E+0 (2.52E-3)	2.53E-2 (4.65E-1)	9.48E-4 (2.69E-2)
Al	6.21E-4 (1.24E-4)	9.12E-5 (1.93E-5)	9.46E-4 (1.89E-4)	2.44E-2 (2.63E-2)	6.55E-5 (8.07E-5)
As	4.13E-5 (5.06E-5)	4.13E-5 (5.06E-5)	5.65E-4 (4.80E-4)	8.23E-4 (3.52E-3)	0.00E+0 (1.11E-5)
Ba	7.50E-6 (6.04E-6)	7.50E-6 (6.04E-6)	6.58E-6 (6.86E-6)	2.28E-1 (1.73E-2)	6.66E-5 (1.36E-5)
Cd	7.00E-8 (1.10E-7)	7.00E-8 (1.10E-7)	1.54E-5 (1.37E-5)	0.00E+0 (1.71E-4)	0.00E+0 (0.00E+0)
Fe	7.96E-4 (3.03E-4)	7.96E-4 (3.03E-4)	0.00E+0 (0.00E+0)	3.76E+0 (2.59E-1)	8.32E-4 (9.80E-5)
K	9.90E-5 (8.34E-5)	9.90E-5 (8.34E-5)	8.08E-4 (1.06E-3)	1.37E-2 (1.55E-2)	6.19E-5 (4.82E-5)
Mg	1.21E-3 (2.97E-4)	1.21E-3 (2.97E-4)	9.45E-4 (1.08E-3)	4.85E-2 (9.22E-3)	5.14E-5 (2.57E-5)
Mn	2.25E-5 (1.94E-5)	2.25E-5 (1.94E-5)	7.43E-5 (8.89E-5)	2.40E-2 (1.53E-3)	8.75E-6 (7.86E-7)
Mo	5.64E-5 (1.31E-5)	5.64E-5 (1.31E-5)	0.00E+0 (3.04E-5)	9.09E-4 (7.35E-5)	2.57E-6 (1.05E-7)
Na	3.27E-4 (3.29E-4)	3.27E-4 (3.29E-4)	6.62E-4 (1.15E-3)	5.04E-2 (2.19E-2)	1.06E-4 (6.71E-5)
Rb	1.37E-5 (1.68E-5)	1.37E-5 (1.68E-5)	4.74E-5 (5.04E-5)	7.86E-5 (1.38E-4)	5.24E-7 (6.29E-7)
Sr	1.25E-5 (1.02E-5)	1.25E-5 (1.02E-5)	0.00E+0 (0.00E+0)	3.09E-3 (3.19E-4)	1.10E-6 (6.29E-7)
Ti	4.23E-5 (8.46E-6)	0.00E+0 (1.00E-8)	7.68E-5 (1.54E-5)	3.17E-2 (2.98E-3)	2.36E-5 (4.19E-6)
V	1.88E-5 (2.36E-5)	1.88E-5 (2.36E-5)	4.28E-4 (3.25E-4)	8.63E-4 (1.93E-4)	1.10E-6 (6.29E-7)
Zn	4.95E-3 (2.27E-3)	4.95E-3 (2.27E-3)	2.97E-3 (3.75E-3)	7.27E-2 (3.53E-2)	1.99E-3 (1.10E-4)
n-tetracosane	0.00E+0 (1.00E-8)	0.00E+0 (1.00E-8)	0.00E+0 (1.00E-8)	1.78E-5 (1.78E-6)	3.17E-4 (3.17E-5)
n-pentacosane	1.70E-4 (3.40E-5)	5.04E-4 (1.03E-4)	4.36E-4 (8.72E-5)	5.33E-5 (5.33E-6)	4.86E-4 (4.86E-5)
n-hexacosane	0.00E+0 (1.00E-8)	1.97E-4 (5.56E-5)	2.51E-4 (5.02E-5)	3.08E-5 (3.08E-6)	5.16E-4 (5.16E-5)
n-heptacosane	0.00E+0 (1.00E-8)	0.00E+0 (1.00E-8)	1.13E-4 (2.26E-5)	1.96E-5 (1.96E-6)	6.31E-4 (6.31E-5)
n-octacosane	1.12E-5 (2.25E-6)	0.00E+0 (1.00E-8)	9.51E-5 (1.90E-5)	1.87E-5 (1.87E-6)	7.46E-4 (7.46E-5)
n-nonacosane	1.90E-4 (3.80E-5)	0.00E+0 (1.00E-8)	6.52E-5 (1.31E-5)	3.08E-5 (3.08E-6)	1.08E-3 (1.08E-4)
n-triacontane	0.00E+0	0.00E+0	0.00E+0	1.96E-5	1.52E-3

	(1.00E-8)	(1.00E-8)	(1.00E-8)	(1.96E-6)	(1.52E-4)
n-hentriacontane	3.79E-6 (7.65E-7)	0.00E+0 (1.00E-8)	1.52E-4 (3.04E-5)	2.15E-5 (2.15E-6)	2.06E-3 (2.06E-4)
n-dotriacontane	7.60E-6 (1.53E-6)	0.00E+0 (1.00E-8)	3.97E-5 (7.94E-6)	1.50E-5 (1.50E-6)	2.69E-3 (2.69E-4)
n-tritriacontane	2.44E-6 (4.93E-7)	0.00E+0 (1.00E-8)	8.27E-6 (1.66E-6)	1.50E-5 (1.50E-6)	3.42E-3 (3.42E-4)
n-tetratriacontane	2.40E-6 (4.85E-7)	0.00E+0 (1.00E-8)	0.00E+0 (1.00E-8)	7.48E-6 (7.48E-7)	4.32E-3 (4.32E-4)
fluoranthene	0.00E+0 (0.00E+0)	SO	1.12E-3 (2.25E-4)	0.00E+0 (0.00E+0)	SO
triphenylene-chrysene	2.08E-4 (4.17E-5)	1.57E-4 (3.93E-5)	1.43E-4 (2.85E-5)	1.59E-5 (2.38E-6)	2.28E-5 (3.42E-6)
benzo[e]pyrene	3.29E-4 (6.59E-5)	1.31E-4 (3.47E-5)	3.39E-5 (6.79E-6)	7.85E-6 (1.18E-6)	1.44E-5 (2.17E-6)
benzo[a]pyrene	1.93E-4 (3.85E-5)	1.22E-4 (3.23E-5)	4.95E-6 (9.94E-7)	6.92E-6 (1.04E-6)	1.08E-5 (1.63E-6)
benzo[ghi]perylene	6.94E-4 (1.39E-4)	3.22E-4 (8.73E-5)	0.00E+0 (0.00E+0)	0.00E+0 (0.00E+0)	0.00E+0 (0.00E+0)
coronene	7.43E-4 (1.49E-4)	SO	0.00E+0 (0.00E+0)	0.00E+0 (0.00E+0)	SO
18a(H)-22,29,30-trisnorneohopane	1.16E-5 (1.74E-6)	1.16E-5 (1.74E-6)	7.52E-5 (1.13E-5)	3.27E-6 (4.91E-7)	8.22E-5 (1.23E-5)
17a(H)-21b(H)-hopane	1.88E-4 (3.75E-5)	1.66E-4 (3.36E-5)	1.65E-5 (3.30E-6)	0.00E+0 (0.00E+0)	5.53E-4 (8.30E-5)
17a(H)-21b(H)-29-norhopane	1.57E-4 (3.14E-5)	SO	3.62E-5 (7.24E-6)	0.00E+0 (0.00E+0)	SO
references	[191, 192]	[191, 192]	[191, 192]	[148, 192]	[148, 192]

Table 13-2b – Source profiles (continued) (g / g OC) for fine PM. Uncertainty estimates are shown in brackets.

	Dust	Meat	Nat Gas	Veg Deb
EC	0.15 (0.10)	0.00 (0.01)	0.08 (0.06)	0.03 (0.01)
OC	1.00 (0.09)	1.00 (0.06)	1.00 (0.09)	1.00 (0.07)
Cl-	2.24E-2 (4.71E-3)	5.03E-3 (2.37E-3)	4.56E-2 (2.43E-2)	2.64E-3 (1.62E-3)
Al	2.83E-1 (1.67E-1)	1.15E-3 (5.62E-4)	2.64E-3 (2.61E-3)	7.94E-2 (7.06E-3)
As	5.00E-6 (0.00E+0)	0.00E+0 (2.96E-4)	0.00E+0 (0.00E+0)	6.49E-5 (1.55E-5)
Ba	3.95E-4 (2.50E-5)	5.92E-4 (9.76E-3)	0.00E+0 (1.52E-2)	9.66E-3 (3.77E-3)
Cd	2.50E-6 (0.00E+0)	0.00E+0 (1.48E-3)	1.07E-3 (4.29E-3)	6.06E-4 (2.29E-4)
Fe	2.08E-2 (1.64E-3)	2.96E-4 (2.96E-4)	1.03E-3 (4.81E-3)	8.55E-2 (1.12E-2)
K	7.88E-3 (6.45E-4)	1.01E-2 (8.88E-4)	2.04E-3 (1.09E-3)	5.17E-2 (7.40E-3)
Mg	5.83E-3 (6.18E-4)	0.00E+0 (1.78E-3)	1.05E-3 (1.28E-3)	8.35E-5 (4.33E-5)
Mn	3.73E-4 (2.75E-5)	0.00E+0 (2.96E-4)	2.19E-4 (4.24E-4)	1.88E-3 (1.82E-4)
Mo	0.00E+0	0.00E+0	2.09E-3	2.97E-4

	(5.00E-5)	(5.92E-4)	(4.30E-3)	(2.07E-4)
Na	5.09E-3 (6.40E-4)	1.09E-2 (3.25E-3)	2.51E-2 (1.66E-2)	1.48E-3 (2.12E-3)
Rb	2.75E-5 (0.00E+0)	0.00E+0 (2.96E-4)	1.95E-4 (8.04E-4)	2.38E-4 (3.40E-5)
Sr	1.18E-4 (7.50E-6)	0.00E+0 (2.96E-4)	0.00E+0 (3.35E-3)	8.22E-4 (7.11E-5)
Ti	6.34E-2 (4.49E-2)	0.00E+0 (3.55E-3)	1.14E-3 (5.78E-4)	8.25E-3 (4.51E-4)
V	4.50E-5 (1.00E-5)	0.00E+0 (1.48E-3)	2.07E-4 (2.81E-4)	5.44E-4 (1.27E-4)
Zn	1.02E-3 (1.38E-4)	0.00E+0 (2.96E-4)	0.00E+0 (1.16E-2)	4.15E-2 (4.23E-2)
n-tetracosane	6.31E-5 (1.26E-5)	4.09E-5 (4.09E-6)	2.89E-3 (2.89E-4)	1.18E-4 (1.18E-5)
n-pentacosane	7.35E-5 (1.47E-5)	5.98E-5 (5.98E-6)	1.42E-3 (1.42E-4)	6.64E-4 (6.64E-5)
n-hexacosane	9.21E-5 (1.84E-5)	4.09E-5 (4.09E-6)	6.12E-4 (6.12E-5)	3.46E-4 (3.46E-5)
n-heptacosane	1.01E-4 (2.01E-5)	1.02E-4 (1.02E-5)	8.28E-4 (8.28E-5)	2.93E-3 (2.93E-4)
n-octacosane	9.40E-5 (1.88E-5)	1.79E-4 (1.79E-5)	3.27E-4 (3.27E-5)	8.90E-4 (8.90E-5)
n-nonacosane	8.74E-5 (1.75E-5)	1.21E-4 (1.21E-5)	1.29E-3 (1.29E-4)	1.99E-2 (1.99E-3)
n-triacontane	7.15E-5 (1.43E-5)	0.00E+0 (0.00E+0)	1.70E-4 (1.70E-5)	1.39E-3 (1.39E-4)
n-hentriacontane	7.42E-5 (1.48E-5)	0.00E+0 (0.00E+0)	4.27E-4 (4.27E-5)	2.98E-2 (2.98E-3)
n-dotriacontane	5.96E-5 (1.19E-5)	0.00E+0 (0.00E+0)	2.83E-5 (2.83E-6)	2.59E-3 (2.59E-4)
n-tritriacontane	6.82E-5 (1.36E-5)	0.00E+0 (0.00E+0)	1.80E-5 (1.80E-6)	1.60E-2 (1.60E-3)
n-tetratriacontane	0.00E+0 (0.00E+0)	0.00E+0 (0.00E+0)	0.00E+0 (0.00E+0)	2.88E-4 (2.88E-5)
fluoranthene	SO	SO	SO	SO
triphenylene-chrysene	0.00E+0 (0.00E+0)	4.25E-5 (6.37E-6)	4.94E-2 (7.42E-3)	7.58E-6 (1.14E-6)
benzo[e]pyrene	0.00E+0 (0.00E+0)	1.02E-5 (1.53E-6)	2.98E-3 (4.47E-4)	0.00E+0 (0.00E+0)
benzo[a]pyrene	0.00E+0 (0.00E+0)	8.81E-6 (1.32E-6)	0.00E+0 (0.00E+0)	0.00E+0 (0.00E+0)
benzo[ghi]perylene	0.00E+0 (0.00E+0)	1.11E-5 (1.67E-6)	0.00E+0 (0.00E+0)	0.00E+0 (0.00E+0)
coronene	SO	SO	SO	SO
18a(H)-22,29,30-trisnorneohopane	7.48E-5 (1.12E-5)	0.00E+0 (0.00E+0)	0.00E+0 (0.00E+0)	0.00E+0 (0.00E+0)
17a(H)-21b(H)-hopane	2.84E-4 (4.26E-5)	0.00E+0 (0.00E+0)	0.00E+0 (0.00E+0)	0.00E+0 (0.00E+0)
17a(H)-21b(H)-29-norhopane	SO	SO	SO	SO
reference	[148]	[163]	[12, 151]	[12, 148]

13.3 Results

Four separate quality control efforts were undertaken in the current study: (1) check consistency of the CMB model between users, (2) investigation of the robustness of the model, (3) comparison of the results to previous work, and (4) comparison of the CMB model results for the different sites but the same air parcel. Each of these quality control efforts is described in detail below.

13.3.1 Consistency between Users:

As a first check, the CMB model was applied to the same dataset by different users. This simple check ensures that the model is being used properly. The ambient organics data shown in Table 13-1 was first presented in a report to the California Air Resources Board by Alexandrova and Allen [190]. In that report, CMB source apportionment modeling was also undertaken. Table 2.2 from the report by Alexandrova and Allen [190] describes the best CMB results, which were generated with the following sources: road dust, vegetative debris, two types of diesel vehicles, gasoline vehicles, and meat charbroiling. The first quality control objective of this work was to repeat this source apportionment analysis with additional species, EC, OC, and trace metals. The same sources and the receptor data was used in both sets of analysis, but the authors were unable to reproduce the CMB results described in Table 2.2 of the report by Alexandrova and Allen [190]. The references for the source profiles used by Alexandrova and Allen [190] are similar to those used in the current study, but the actual profiles used in the source apportionment work were not presented. Without this information, it is impossible to diagnose the source of error in the previous study. In summary, the authors do not believe that the results presented in Table 2.2 of Alexandrova and Allen [190] are correct.

13.3.2 Robustness of the Model:

The validity of a specific CMB source apportionment result can be explored by (1) comparing the compound concentrations predicted by CMB to the measured compound concentrations (especially for the compounds that are source specific tracers), (2) using the output modified pseudo-inverse (MPIN) matrix which can be an indicator for how influential a compound is in the fit of a specific source, and (3) repeating the CMB runs with systematic removal of source types and compounds. If CMB predictions respond strongly to the removal of a single compound then the model prediction is not robust. In the Appendix, Tables A1-A28 document the initial 25 iterations of the CMB source apportionment effort using the ambient measurements shown in Table 13-1 and the source profiles shown in Table 13-2. In addition to the typical measurement uncertainty weighted CMB runs, we did several CMB runs where the weighting was done by source profile variability rather than measurement uncertainty. For example, we used the standard deviation of the five published heavy duty diesel emissions profiles as an estimate of the uncertainty for that profile. This was done to eliminate quantification bias between the ambient samples and the source profiles.

In a final attempt to use the CMB software, we explored a simplied approach using the most dominant unique tracer for each source to directly calculate source contributions to airborne particulate matter concentrations. The key challenge to this approach is the selection of the appropriate unique tracer compound for each source. The selection process used in the current study involved checking for consistency in the ambient measurements between multiple compounds that could track the same source. In the six ambient samples shown in Table 13-1 the hopanes, which track motor vehicle emissions, are usually in the same relative ratio. Heavy PAHs are emitted from coal combustion, fuel oil combustion and gasoline combustion. Since only gasoline combustion sources are present in Southern California, heavy PAHs serve as useful tracers for gasoline engine emissions. The relative ratio of these compounds is constant in the ambient samples. Different n-alkanes originate from tire wear, vegetative debris, and motor vehicles; however, there was no consistent ratio among the n-alkanes. Several features of the n-alkane measurements in Table 13-1 failed quality control checks, casting doubt on their accuracy. Quantification of n-alkanes in a sample extract is relatively straightforward; and since the organics quantification procedures used to generate the ambient organics used here focused on n-alkane internal standards it is quite likely that the n-alkane quantification in the sample extracts was accurate. N-alkanes are a common source of contamination during organic analysis. Blank samples are typically used to quantify background n-alkane concentrations. In this work, we are unsure if n-alkane blank subtraction occurred and as such we repeated the CMB source apportionment work without n-alkanes.

Once the n-alkanes are removed, the ambient measurement dataset consists of only PAH, oxy-PAH, hopanes, EC, OC, and metals, which subsequently limits our source apportionment ability to motor vehicles and brake wear (because levoglucosan and cholesterol were not measured). The most basic CMB source apportionment model run is presented in Table 13-3. In this run 17a(H)-21b(H)-hopane and benzo[ghi]perylene are used as the dominant tracers for gasoline engine emissions, flouranthene is used as a dominant tracer to track diesel engine emissions, and Fe is used as a dominant tracer for brake wear. Small amounts of 17a(H)-21b(H)-hopane, benzo[ghi]perylene , fluoranthene, and Fe are present in sources other than those listed above. These concentrations were set to zero in source profiles other than the dominant source to simplify the calculation. EC was not used as a fitting component, so comparing the calculated to measured EC provides a useful check for the validity of this model run. In 5 of the 6 samples listed in Table 13-1, the amount of EC predicted by the simplified approach described above closely matches the measured EC concentration. In addition, the two central LA samples exhibited higher motor vehicle contributions than the downwind sites which would be expected based on increased traffic density at the central LA sampling location.

Table 13-3: Simplified CMB results for SCOS97 using 1 dominant tracer for each source.

	V11-LA	V11-AZ	V11-RV	V21-LA	V21-AZ	V21-RV
R2	0.93	0.70	0.80	0.86	0.82	0.78
Chi2	2.15	10.77	12.77	4.84	5.75	7.54
%OC_explained	58.3%	13.5%	16.9%	35.9%	21.5%	9.6%
N_Diesel	0.39 (0.10)	0.16 (0.04)	0.14 (0.04)	0.29 (0.07)	0.17 (0.04)	0.13 (0.03)
N_Gas5%	6.19 (1.12)	1.64 (0.33)	1.62 (0.33)	3.65 (0.67)	2.84 (0.54)	0.83 (0.16)
BrakeWea	0.14 (0.04)	0.07 (0.02)	0.28 (0.04)	0.12 (0.03)	0.11 (0.04)	0.08 (0.03)
EC calc:meas	1.21 (0.49)	0.33 (0.12)	0.59 (0.33)	0.87 (0.37)	0.67 (0.32)	0.76 (0.84)

To explore the robustness of this approach, we included an additional hopane (norhopane) an additional heavy PAH (coronene) and did not zero primary tracer concentrations in any of the profiles. Table 13-4 shows that the results from this analysis are similar to those illustrated in Table 13-3, indicating some robustness in this approach. In addition, the motor vehicle contribution to PM_{fine} concentrations at each site are similar in the two sample sets; again, this would be expected.

Table 13-4: Final CMB predictions for SCOS97.

	V11-LA	V11-AZ	V11-RV	V21-LA	V21-AZ	V21-RV
R2	0.80	0.56	0.68	0.73	0.71	0.77
Chi2	5.26	13.77	14.60	7.76	7.67	5.20
%OC_explained	44.4%	9.4%	11.9%	27.7%	17.6%	10.8%
N_Diesel	0.40 (0.10)	0.16 (0.04)	0.15 (0.04)	0.30 (0.07)	0.17 (0.04)	0.14 (0.03)
N_Gas5%	4.58 (0.61)	1.07 (0.16)	1.01 (0.15)	2.71 (0.37)	2.27 (0.31)	0.96 (0.15)
BrakeWea	0.14 (0.04)	0.07 (0.02)	0.28 (0.04)	0.12 (0.03)	0.11 (0.04)	0.08 (0.03)
EC calc:meas	1.02 (0.41)	0.27 (0.10)	0.49 (0.28)	0.75 (0.32)	0.59 (0.28)	0.82 (0.90)

The only compounds that were not included in the results illustrated in Table 13-4 were the mid MW-range PAH and the oxy-PAH. These species originate from source that were not included in the model: natural gas emissions, meat cooking, and wood combustion. Wood combustion is likely an insignificant source given the hot ambient temperatures and since the wood smoke marker, levoglucosan, was not found in the ambient samples. The inclusion of meat cooking and natural gas emission will be explored.

13.3.4 Previous Studies:

Table 13-5 documents the previous PM_{fine} source apportionment results for Southern California that were generated using a CMB model. For reference, Downtown LA would be similar to Central LA, Pasadena is close to Azusa, and Riverside is close to Rubidoux. The split between gasoline engine exhaust and diesel engine exhaust is driven by the choice of gasoline exhaust profile in that inclusion of smoker vehicles can displace the split [191]; and as such we have included the total motor vehicle contribution in this table as this is likely the most valid comparison. The total motor vehicle contributions determined in the SCOS97 samples is similar to the levels observed previously.

Table 13-5: Contribution (µg m-3) of motor vehicles to PMfine organic mass.

	Downtown	Pasadena	Rubidoux	LA Basin	Central	Azusa	Riverside
Sample Type	1982 annual average	1982 annual average	1982 annual average	1993 annual average	1997 August	1997 August	1997 August
Diesel Vehicles	2.72±0.28	1.24±0.17	1.26±0.12	0.84±0.20	0.36 to 0.48	0.19 to 0.20	0.17 to 0.18
Gasoline Vehicles	1.56±0.17	1.20±0.14	0.25±0.04	0.61±0.29	3.25 to 5.00	1.28 to 2.72	1.15 to 1.21
Total Motor Vehicles	4.28	2.44	1.51	1.45	3.61 to 5.48	1.47 to 2.92	1.32 to 1.49

Site-to-Site Comparison: As discussed previously, the goal of this study was to explore how an air parcel accumulated PM and how that PM aged as the parcel moved from Central Los Angeles to Azusa and then on to Riverside. In both the 1997 trajectory sets summarized in Table 13-5, the absolute concentration of motor vehicle PM_{fine} concentrations in the atmosphere is the highest in Central LA and decreases as the air parcels moves downwind. This is not simply a dilution effect because the fraction of the OC attributable to motor vehicles also decreases as the parcel moves inland. The results shown in Table 13-5 combined with the measurements shown in Table 13-1 demonstrate that motor vehicle exhaust accounts for 27 - 44% of PM_{fine} in Central LA and only 11 - 12% of PM_{fine} in Riverside. This decrease in OC contribution must be due to an increase in some other OC source as the air parcel moves inland. One possible source of additional OC is meat cooking operations which have been identified as a major source of organic aerosol in Los Angeles but could not be quantified in the current study due to missing cholesterol measurements. Another possible source of additional OC is atmospheric reactions forming new aerosol; this does not eliminate the motor vehicle fleet as the original source of this PM since gas-phase VOCs emitted by motor vehicles may be the dominant source of the secondary organic aerosol.

13.4 Conclusions

The ambient measurements made at Central Los Angeles, Azusa, and Riverside during the SCOS97 field study could not be used as in their entirety due to likely contamination of n-alkanes. Elimination of these species combined with missing measurements (levoglucosan and cholesterol) reduced the number of sources that could be tracked in CMB calculations to to motor vehicles and brake wear. The simplification of the model resulted in a more robust calculation that provided answers that are consistent with previous results and our understanding of source distributions in Southern California. Simplified CMB calculations were able to account for 49-102% of measured EC concentrations in 5 of the 6 samples collected during SCOS97. No consistent spatial trend was observed in the amount of EC that was explained by the model. The lack of spatial pattern is logical as we would expect that motor vehicles would be the dominant source of EC regardless of location. The motor vehicles accounted for 9 - 44% of the

measured OC concentrations indicating that other sources (meat cooking, natural gas combustion, dust, and secondary organic aerosol formation) account for 55 - 91 %.

14 CONCLUSIONS

14.1 Size and Composition of Particulate Matter Emitted From Heavy Duty Diesel Vehicles

Particulate matter emissions from heavy duty diesel vehicles (HDDVs) were collected using a chassis dynamometer / dilution sampling system that employed filter-based samplers, cascade impactors, and Scanning Mobility Particle Size (SMPS) measurements. Four diesel vehicles with different engine and emission control technologies were tested using the California Air Resources Board (CARB) Heavy Heavy-Duty Diesel Truck (HHDDT) 5 mode driving cycle. Vehicles were tested using a simulated inertial weight of either 56,000lbs or 66,000lbs. The exhaust particles were then analyzed for total carbon, elemental carbon (EC), organic matter (OM), and water-soluble ions.

HDDV fine (< 1.8 μm aerodynamic diameter) and ultrafine (56 – 100 nm aerodynamic diameter) PM emission rates ranged from 181 – 581 mg/km and 25 – 72 mg/km, respectively, with the highest emission rates in both size fractions associated with the oldest vehicle tested. The ratio of EC to OM in both fine and ultrafine HDDV exhaust particles was a strong function of driving cycle and vehicle age. Older diesel vehicles produced higher EC/OM ratios than newer vehicles. Transient modes produced very high EC/OM ratios while idle and creep modes produced very low EC/OM ratios. Calcium was the most abundant water-soluble ion with smaller amounts of magnesium, sodium, ammonium ion and sulfate also detected.

The mass distribution of diesel exhaust particles measured with cascade impactors and two SMPS instruments were in good agreement in the ultrafine size range. Particle mass distributions emitted during the full 5-mode HDDV tests peaked between 100 - 180 nm and their shapes were not a function of vehicle age. In contrast, particle mass distributions emitted during the idle and creep driving modes from the newest diesel vehicle had a peak diameter of ~70 nm while mass distributions emitted from older vehicles had a peak diameter larger than 100 nm for both the idle and creep modes. Increasing inertial loads reduced the OM emissions, causing the residual EC emissions to shift to smaller sizes. The same HDDV tested at 56,000 lbs and 66,000 lbs had higher PM0.1 elemental carbon emissions (+22%) and lower PM0.1 OM emissions (-38%) at the higher load condition.

14.2 Size and Composition of Particulate Matter Emitted From Light Duty Gasoline Vehicles

Size-resolved particulate matter emitted from light-duty gasoline vehicles (LDGVs) was characterized using filter-based samplers, cascade impactors, and Scanning Mobility Particle Size measurements in August and September of 2002. Thirty LDGVs, with different engine and emissions control technologies ranging in model year from 1965 to 2003 and with odometer readings from 1,264 to 207,104 miles, were tested on a chassis dynamometer using the Federal Test Procedure (FTP), the Unified Cycle (UC), and the Correction Cycle (CC).

LDGV particulate matter (PM) emission rates were strongly correlated with vehicle age and emissions control technology. The oldest vehicles had average fine PM (56 – 100 nm aerodynamic diameter) and ultrafine PM (< 1.8 μm aerodynamic diameter) emission rates of 213 mg/km and 9.6 mg/km, respectively. The newest vehicles had fine and ultrafine PM emission rates of 371 μg/km and 51 μg/km, respectively. Light duty trucks and sport utility vehicles had fine and ultrafine PM emission rates nearly double the corresponding PM emission rates from passenger cars. Higher particulate matter emission rates were associated with vehicle cold starts and hard accelerations. The Federal Test Procedure driving cycle produced the lowest vehicle emissions, followed by the Unified Cycle and the Correction Cycle.

PM mass distributions peaked between 100 and 180 nm particle diameter for all vehicles except those emitting visible smoke, which peaked between 180 and 320 nm. The majority of the PM was composed of carbonaceous material, with only trace amounts of sulfate, calcium, and ammonium ion detected. Elemental carbon (EC) and organic matter (OM) had similar size distribution, but the ratio of EC to OM in LDGV exhaust particles was a strong function of emissions control technology and vehicle maintenance. LDGV classes with lower PM emissions generally had a higher fraction of EC in their emissions. The composition of the PM emitted from newer LDGV technologies had the largest ratio of EC to OM, while OM dominated the composition of the PM emitted from older vehicles. Driving cycles with cold starts and hard accelerations tended to produce higher EC to OM ratios in ultrafine particles.

14.3 Size Distribution of Trace Organic Species Emitted From Heavy-Duty Diesel Vehicles

Size distributions of particulate hopanes, steranes, and polycyclic aromatic hydrocarbons (PAHs) were measured in the exhaust from four heavy duty diesel vehicles (HDDVs) operated under idle, creep, transient, and two high speed driving modes. Particulate matter was collected using a chassis dynamometer and a dilution sampling system equipped with cascade impactors and filter samplers. Samples were extracted using organic solvents and analyzed using GC-MS. Size distributions of hopanes and steranes were functions of engine load conditions and vehicle technology. Hopanes and steranes peaked in size ranges larger than 0.18 μm aerodynamic particle diameter under light load conditions and less than 0.10 μm aerodynamic particle diameter under heavier load conditions. The eight hopane size distributions emitted from newer technology (>1998) vehicles were unimodal while the four hopane size distributions emitted from older technology vehicles (<1992) were bimodal. Similar trends between older and newer vehicles were not observed for sterane size distributions. The PAH composition emitted from HDDVs was a function of driving cycle and vehicle technology. Light driving cycles produced quantifiable emissions of 3, 4, 5, and 6 ring PAHs (including coronene). Heavier driving cycles produced only the 3 and 4 ring PAHs in quantifiable amounts.

PM1.8 and PM0.1 source profiles constructed using the relative abundance of hopanes and steranes to total organic carbon were functions of vehicle load condition. Increasing

load reduced the relative abundance of lubricating oil tracers in the PM1.8 size fraction and increased the abundance of these tracers in the PM0.1 size fraction. The relative abundances of PAHs in the PM0.1 and PM1.8 size fractions emitted from the oldest vehicle tested (1985 HDDV) were significantly higher than for any other vehicle tested.

14.4 Size Distribution of Trace Organic Species Emitted From Light Duty Gasoline Vehicles.

Size distributions for particulate hopanes+steranes and nonvolatile PAHs emitted from five classes of light-duty gasoline-powered vehicles were measured using the Federal Test Procedure (FTP), Unified Cycle (UC), and Correction Cycle (CC) driving cycles. 17α(H)-21β(H)-29-norhopane, 17α(H)-21β(H)-hopane, αββ-20R-stigmastane and αββ-20S-stigmastane were highly correlated and behaved consistently across sampling methods. Coronene and benzo[ghi]perylene were the most ubiquitous heavy PAHs detected in the vehicle exhaust.

Hopane+sterane distributions emitted from vehicles without an operating catalyst (including "cold-start" emissions) were bimodal with one mode between 0.1-0.18 μm and the second mode > 0.32μm diameter. Hopane+sterane emissions released from vehicles with an operating catalyst had a single mode between 0.1-0.18 μm diameter. Hopane+sterane emissions from visibly smoking vehicles had a single mode between 0.18-0.32 μm diameter. Heavy PAH size distributions for all vehicle classes consistently had a single mode between 0.10-0.18 μm particle diameter (0.1-0.32 μm diameter for smoking vehicles). The geometric standard deviations for PAH size distributions were generally smaller than the corresponding hopane+sterane distributions.

PAH, hopane and sterane emissions shifted to smaller sizes during the more aggressive UC and CC driving cycles relative to the FTP. The fraction of PAH, hopane and sterane emissions in the ultrafine (D_p<0.1 μm) range more than doubled during "warm-start" UC and CC cycles vs. the FTP cycle. The enhancement of ultrafine PAHs during "cold-start" UC driving cycles was less pronounced. Source-profiles constructed using (analyte mass) / (organic carbon (OC) mass) in the fine and ultrafine size fractions were approximately equal during all FTP tests except for enhanced ultrafine (hopane+sterane) / OC concentrations emitted from passenger cars equipped with three way catalysts. The PAH / OC concentrations in the ultrafine size fraction decreased by an order of magnitude under the UC vs. FTP driving cycle. These trends suggest that hopanes+steranes and heavy PAHs act as tracers for separate processes of particulate organic carbon formation.

14.5 Elemental Composition of Gasoline, Diesel Fuel, and Lubricating Oil from Light Duty Gasoline and Heavy Duty Diesel Vehicles

Gasoline, diesel fuel, and lubricating oil samples, obtained from light-duty gasoline and heavy-duty diesel vehicles, were analyzed for their elemental composition using Inductively Coupled Plasma – Mass Spectrometry. Elemental composition was determined using multiple instrument octopole modes and including the introduction of

oxygen in the carrier gas. The most abundant elements observed in gasoline from light-duty gasoline vehicles (LDGVs) were S, Si, Ni, Fe, and Cu; in diesel fuel from heavy-duty diesel vehicles (HDDVs) the most abundant elements were S, Zn, Ca, P, Si, and Sr. Trends between the LGDV and HDDV lubricating oil data sets are consistent with Ca as the most abundant element followed by Zn, P, S and K. The primary source of these elements in gasoline is expected to come from within the vehicles sampled whereas the primary source of elements in diesel fuel and lubricating oils is likely from additive packages.

14.6 Elemental Composition of Particulate Matter Emissions From Light Duty Gasoline and Heavy Duty Diesel Vehicles

The size-resolved elemental composition of particulate matter emissions from light-duty gasoline and heavy-duty diesel vehicle chassis dynamometer studies were measured using Inductively Coupled Plasma – Mass Spectrometry methods. Zn was the most ubiquitous element detected throughout the data set, with $PM_{1.8}$ emission factors ranging from 36 – 6826 ng/km. Al, K, Ni, and Cu were also present in both LDGV and HDDV PM; however the LDGV data set contained unique elements of lower molecular weight than the HDDV data set. Elemental size distributions were either uni-modal peaking at small sizes (<320 nm), uni-modal peaking at larger sizes (>560 nm), or bi-modal. Ca and Fe were well correlated between the LDGV PM samples and previously reported LDGV gasoline concentrations, as were Mg, Cr, Mn, and Pb between PM samples and previously reported LDGV lubricating oil concentrations. For HDDVs, Ca, Cu, Zn, Se, Sr, Cd, and Pb were all well correlated between PM samples and previously reported HDDV diesel fuel concentrations, with no strong correlations between PM samples and previously reported HDDV lubricating oil concentrations.

14.7 Size and Composition Distributions of Particulate Matter Emissions From a Busy California Freeway

Size-resolved particulate matter (PM) samples were collected near a busy freeway in San Diego, CA over a 7 day period in the summer of 2004. Samples were collected at a site ~1000m upwind of the freeway, a site 18m downwind of the freeway, and a site 37 m downwind of the freeway during two discrete weekday and one weekend period. Samples were analyzed for organic carbon, elemental carbon, water-soluble ions, and elements. Comparisons were made to previously reported light-duty gasoline vehicle (LDGV) and heavy-duty diesel vehicle (HDDV) PM emissions measured using chassis dynamometers. All upwind and downwind fine PM mass distributions peaked between 560 nm and 1000 nm and were dominated by sulfate, with significant quantities of ammonium and various trace elements. The difference between upwind and downwind concentrations was small, but an effective emissions signature was still detected within the uncertainty limits of the measurements. The fine PM mass concentrations measured 18 m and 37 m downwind of the freeway were 5.4 μg m-3 and 3.1 μg m-3 greater, respectively, than the fine PM concentrations measured at the upwind location. These signals reflect both a freeway contribution to ambient PM as well as the effects of downwind dilution.

The freeway emissions signature for elemental carbon had a size distribution that peaked between 0.1 – 0.18 μm, analogous to both the LGDV and HDDV chassis dynamometer signatures. The organic carbon size distribution signature from the freeway was similar to the LDGV chassis dynamometer emissions with maxima between 0.18 – 0.32 μm. Freeway emissions of particulate Ca and Zn had size distributions that were bimodal and had similar shape to HDV dyanometer emissions between 0.1-0.18 μm and LDGV dynamometer emissions between 0.56-1.0 μm. Both Ca and Zn have been measured previously in gasoline, diesel fuel, and lubricating oil from LDGVs and HDDVs; these results illustrate plausible linkages between motor vehicle combustion components and fine PM contributions from a busy freeway. Concentrations of Cu, Fe, and Sr all had size distributions that peaked at sizes larger than 1 μm particle diameter, consistent with their presence in brake and / or road dust.

Elemental carbon and organic carbon emissions both exhibited weekday-weekend effect. Greater concentrations of elemental carbon were observed during the weekday sampling periods below 0.18 μm, with greater concentrations of organic carbon observed during the weekend period above 0.18 μm. These findings were consistent with the observed local traffic patterns with a higher number and percentage of HDDVs present during the weekday versus the weekend sampling periods.

14.8 Separating Lubricating Oil vs. Fuel Contributions To Particulate Matter Emissions From Light Duty Gasoline and Heavy Duty Diesel Vehicles

Size-resolved samples of particulate matter emitted from heavy duty diesel vehicles (HDDVs) and light duty gasoline vehicles (LDGVs) were analyzed for elemental carbon (EC), organic carbon (OC), and individual organic compounds. The size distribution of EC and OC was well correlated in all tests. Hopane and sterane size distributions did not match the total carbon size distribution, suggesting that emission of lubricating oil are not the dominant source of particulate carbon in the exhaust. Regression analysis using 17α(H)-21β(H)-29-norhopane as a tracer for lubricating oil and flouranthene as a tracer for diesel fuel was able to explain the size distribution of particulate EC and OC emissions from HDDVs. A similar regression analysis performed using 17α(H)-21β(H)-29-norhopane as a tracer for lubricating oil and benzo[ghi]perylene as a tracer for gasoline was able to explain the size distribution of particulate EC and OC emitted from LDGVs. Fuel contributions to particulate matter exhaust from both HDDVs and LDGVs were very significant. EC emissions from all diesel vehicles operated under relatively high load conditions were dominated by fuel contributions. OC emissions from diesel vehicles were more evenly apportioned between fuel and oil contributions. EC emissions from LDGVs operated under fuel-rich conditions were also dominated fuel contributions. Fuel contributions also accounted for the majority of the OC emissions from LDGVs except for vehicles emitted visible smoke for which oil contributions to OC were slightly greater than fuel contributions.

The results of the current study clearly illustrate that fuel and lubricating oil make separate and distinct contributions to particulate matter emissions from motor vehicles.

The regression between tracer concentrations and EC/OC provides source profile information that can be used in future ambient source apportionment studies.

14.9 Source Apportionment of Ultrafine (PM0.1) Airborne Particles in a Roadside Environment

Size distributions of particulate hopanes, steranes, and polycyclic aromatic hydrocarbons (PAHs) were measured at one site upwind (west) and two sites downwind (east) of the Interstate 5 (I5) freeway in San Diego, California. Particulate matter was collected with cascade impactors and filter samplers. Samples were extracted using organic solvents and analyzed using GC-MS. Size distributions of hopanes and steranes peaked in the 0.10 – 0.18 μm size range which corresponds with previous vehicular studies of lubricating oil size distributions. Light, particle-phase 4-ring PAHs have the same size distributions at the roadside and in heavy-duty diesel vehicle exhaust measurements while the heavy PAH size distribution matches that seen for gasoline powered vehicles.

Regression analysis was performed on motor vehicle hopane, sterane, and PAH emissions to apportion elemental carbon and organic carbon emissions to fuel and lubricating oil. EMFAC results for July 2004 were used to create weighted average lubricating oil and gasoline vehicle emissions profiles. The resulting equations were used to predict size distributions of EC and OC concentrations in the roadway environment using the measured organic tracer concentrations. The peak in both the measured and predicted EC size distribution occurred between 0.1 – 0.18 μm particle aerodynamic diameter. Lubricating oil, diesel fuel, and gasoline all contributed to EC concentrations across the full size range. Ultrafine OC concentrations measured 18 m downwind of the roadway were lower than the predicted values by 27-71%. Predictions of OC concentrations decrease by a factor of approximately 2 between 18 m – 37 m downwind of the roadway due to the effects of dilution. Ultrafine OC concentrations measured 37 m downwind of the roadway were in good agreement with predicted values from gasoline fuel, diesel fuel, and lubricating oil.

14.10 Size Distribution of Trace Organic Species Emitted From Biomass Combustion and Meat Cooking

Size-resolved particulate matter emissions from pine, California oak, east coast oak, eucalyptus, rice straw, cigarette smoke, and meat cooking were analyzed for trace organic species using solvent-extraction followed by GC-MS analysis. Six particle size fractions were studied between 0.056, 0.1, 0.18, 0.32, 0.56, 1.0, and 1.8 μm particle diameter. The smallest particle size fraction analyzed was in the ultrafine ($Dp < 0.1$ μm) range that has been implicated as a potential health concern. Fourteen PAHs were detected in the ultrafine size fraction of wood smoke with the most abundant species (benzo[ghi]fluoranthene) emitted at a rate of 0.2 – 0.4 (mg / kg wood burned). Nine PAHs were detected in the ultrafine size fraction of rice straw smoke with the most abundant compound (benzo(a)pyrene) emitted at 0.01 (mg / kg rice straw burned). The most abundant PAH measured in the ultrafine size fraction of cigarette smoke was

benzo(ghi)fluoranthene (0.07 mg / cigarette) followed closely by chrysene/triphenylene (0.06 mg / cigarette).

Besides PAHs, the most abundant compounds identified in the wood included levoglucosan (<MDL-150 mg / kg burned), acetovanillone (0.06-0.23 mg / kg burned), conferylaldehyde (2.7-13.21 mg / kg burned), iso-eugenol (0.07-0.53 mg / kg burned), and vanillin (0.12-0.46 mg / kg burned). The size distribution of each of these compounds was highly correlated (R^2>0.9) with the size distribution of particle-phase organic carbon (OC) and / or elemental carbon (EC). The only organic compounds besides PAHs detected in the ultrafine size fraction of rice straw and cigarette smoke were benz(de)anthracen-7-one (0.19 mg / kg rice straw burned) and 4-methylphenylacetone (2.64 mg / cigarette), respectively. Caffeine was measured in cigarette smoke size fractions greater than 0.1 μm with a total PM1.8 emissions rate of 1 (mg / cigarette). The most abundant organic species measured in meat cooking smoke was cholesterol with a size distribution that was highly correlated with both OC and EC. The concentration of each compound normalized by the concentration of total OC was relatively uniform for all particle sizes. Cholesterol and levoglucosan should prove to be useful tracers for meat cooking and wood smoke emissions in the ultrafine size range.

14.11 Source Apportionment of Ultrafine and Fine Airborne Particulate Matter During a Winter Pollution Episode (CRPAQS)

Size-resolved samples of airborne particulate matter collected at 3 sites in the San Joaquin Valley of California were extracted with organic solvents and analyzed for detailed organic compounds using GC-MS. The smallest size fraction analyzed was 0.056 < Dp < 0.1 μm particle diameter which accounts for the majority of the mass in the ultrafine (PM0.1) size range. Source profiles for ultrafine particles developed during pervious studies were applied to the measurements at each sampling site to calculate source contributions to organic and elemental carbon concentrations. Ultrafine elemental carbon concentrations ranged from 0.03 μg m^{-3} during the daytime to 0.18 μg m^{-3} during the nighttime. Gasoline fuel and lubricating oil accounted for the majority of the ultrafine elemental carbon concentrations, with relatively minor contributions from biomass combustion and meat cooking. Ultrafine organic carbon concentrations ranged from 0.2 μg m^{-3} during the daytime to 0.8 μg m^{-3} during the nighttime. Wood combustion and meat cooking were found to be the two largest sources of ultrafine organic carbon, with smaller contributions from diesel fuel, gasoline fuel, and lubricating oil. Total ultrafine particulate matter concentrations were dominated by contributions from wood combustion and meat cooking during the current study. Future inhalation exposure studies may wish to target these sources as potential causes of adverse health effects.

14.12 Source Apportionment of Fine PM During the Vehicle-Oriented Trajectory Study (SCOS97)

The ambient measurements made at Central Los Angeles, Azusa, and Riverside during the SCOS97 field study could not be used in their entirety due to likely contamination of n-alkanes. Elimination of n-alkanes from the data set combined with missing measurements (levoglucosan and cholesterol) reduced the number of sources that could be tracked in CMB calculations to motor vehicles and brake wear. The simplification of the model resulted in a more robust (stable) calculation, but with fewer source contributions determined. The results are consistent with findings from previous studies and our understanding of source distributions in Southern California.

Simplified CMB calculations were able to account for 49-102% of measured EC concentrations in 5 of the 6 samples collected during SCOS97. No consistent spatial trend was observed in the amount of EC that was explained by the model. The lack of spatial pattern is expected since motor vehicles should be the dominant source of EC regardless of location. Motor vehicles accounted for 9 - 44% of the measured OC concentrations indicating that other sources (meat cooking, natural gas combustion, dust, and secondary organic aerosol formation) account for 56 - 91 % of OC.

15 REFERENCES

1. Levy, J.I., J.K. Hammitt, and J.D. Spengler, *Estimating the mortality impacts of particulate matter: What can be learned from between-study variability?* Environmental Health Perspectives, 2000. **108**(2): p. 109-117.
2. Dockery, D.W., C.A. Pope, 3rd, X. Xu, J.D. Spengler, J.H. Ware, M.E. Fay, B.G. Ferris, Jr., and F.E. Speizer, *An association between air pollution and mortality in six U.S. cities.* New England journal of medicine, 1993. **329**(24): p. 1753-9.
3. Samet, J.M., F. Dominici, F.C. Curriero, I. Coursac, and S.L. Zeger, *Fine particulate air pollution and mortality in 20 US Cities, 1987-1994.* New England Journal of Medicine, 2000. **343**(24): p. 1742-1749.
4. Venkataraman, C. and A.S. Kao, *Comparison of particle lung doses from the fine and coarse fractions of urban PM-10 aerosols.* Inhalation Toxicology, 1999. **11**(2): p. 151-169.
5. Oberdorster, G., R.M. Gelein, J. Ferin, and B. Weiss, *Association of Particulate Air-Pollution and Acute Mortality - Involvement of Ultrafine Particles.* Inhalation Toxicology, 1995. **7**(1): p. 111-124.
6. Schwartz, J. and L.M. Neas, *Fine particles are more strongly associated than coarse particles with acute respiratory health effects in schoolchildren.* Epidemiology, 2000. **11**(1): p. 6-10.
7. Penttinen, P., K.L. Timonen, P. Tiittanen, A. Mirme, J. Ruuskanen, and J. Pekkanen, *Ultrafine particles in urban air and respiratory health among adult asthmatics.* European Respiratory Journal, 2001. **17**(3): p. 428-435.
8. Peters, A., H.E. Wichmann, T. Tuch, J. Heinrich, and J. Heyder, *Respiratory effects are associated with the number of ultrafine particles.* American Journal Of Respiratory And Critical Care Medicine, 1997. **155**(4): p. 1376-1383.
9. Wichmann, H.E.S., C.; Tuch, T.; Wolke, G.; Peters, A.; Heinrich, J.; Kreyling, G.; Heyder, J. , *Daily mortality and fine and ultrafine particles in Erfurt, Germany, Part I: Role of particule number and particle mass.* Health Effects Institute Research Report 98, 2000.
10. Li, N., C. Sioutas, A. Cho, D. Schmitz, C. Misra, J. Sempf, M.Y. Wang, T. Oberley, J. Froines, and A. Nel, *Ultrafine particulate pollutants induce oxidative stress and mitochondrial damage.* Environmental Health Perspectives, 2003. **111**(4): p. 455-460.
11. Lloyd, A.C. and T.A. Cackette, *Diesel engines: Environmental impact and control.* Journal of the Air & Waste Management Association, 2001. **51**(6): p. 809-847.
12. Hildemann, L.M., G.R. Markowski, and G.R. Cass, *Chemical composition of emissions from urban sources of fine organic aerosol.* Environmental Science and Technology, 1991. **25**(4): p. 744-59.
13. Rogge, W.F., L.M. Hildemann, M.A. Mazurek, G.R. Cass, and B.R.T. Simoneit, *Sources of fine organic aerosol. 2. Noncatalyst and catalyst-equipped automobiles and heavy-duty diesel trucks.* Environmental Science and Technology, 1993. **27**(4): p. 636-51.

14. Schauer, J.J., M.J. Kleeman, G.R. Cass, and B.R.T. Simoneit, *Measurement of emissions from air pollution sources. 2. C-1 through C-30 organic compounds from medium duty diesel trucks.* Environmental Science & Technology, 1999. **33**(10): p. 1578-1587.
15. Lowenthal, D.H., B. Zielinska, J.C. Chow, J.G. Watson, M. Gautam, D.H. Ferguson, G.R. Neuroth, and K.D. Stevens, *Characterization of Heavy-Duty Diesel Vehicle Emissions.* Atmospheric Environment, 1994. **28**(4): p. 731-743.
16. Shi, J.P., D. Mark, and R.M. Harrison, *Characterization of particles from a current technology heavy-duty diesel engine.* Environmental Science & Technology, 2000. **34**(5): p. 748-755.
17. (CalEPA), C.E.P.A., *Proposed Identification of Diesel Exhaust as a Toxic Air Contaminant*. 1998, Prepared by the Air Resources Board and Office of Environmental Health Hazard Assessment.
18. EPA, U.S., *Code of Federal Regulations 40 CFR Part 80*. 2001. p. 17230-17273.
19. Schauer, J.J., W.F. Rogge, L.M. Hildemann, M.A. Mazurek, G.R. Cass, and B.R.T. Simoneit, *Source apportionment of airborne particulate matter using organic compounds as tracers.* Atmospheric Environment, 1996. **30**(22): p. 3837-3855.
20. (USEPA), U.S.E.P.A., *Health Assessment Document for Diesel Engine Exhaust*. 2002, Prepared by the National Center for Environmental Assessment for the Office of Transportation and Air Quality.
21. Eldering, A. and G.R. Cass, *Source-oriented model for air pollutant effects on visibility.* Journal of Geophysical Research-Atmospheres, 1996. **101**(D14): p. 19343-19369.
22. Ackerman, A.S., O.B. Toon, J.P. Taylor, D.W. Johnson, P.V. Hobbs, and R.J. Ferek, *Effects of aerosols on cloud albedo: Evaluation of Twomey's parameterization of cloud susceptibility using measurements of ship tracks.* Journal of the Atmospheric Sciences, 2000. **57**(16): p. 2684-2695.
23. EPA, U.S., *Regulatory Announcement EPA420-F-00-055.* 2000.
24. Saitoh, K., K. Sera, T. Shirai, T. Sato, and M. Odaka, *Determination of elemental and ionic compositions for diesel exhaust particles by particle induced X-ray emission and ion chromatography analysis.* Analytical Sciences, 2003. **19**(4): p. 525-528.
25. Holmen, B.A. and A. Ayala, *Ultrafine PM emissions from natural gas, oxidation-catalyst diesel, and particle-trap diesel heavy-duty transit buses.* Environmental Science & Technology, 2002. **36**(23): p. 5041-5050.
26. Hildemann, L.M., G.R. Markowski, M.C. Jones, and G.R. Cass, *Submicrometer aerosol mass distributions of emissions from boilers, fireplaces, automobiles, diesel trucks, and meat-cooking operations.* Aerosol Science and Technology, 1991. **14**(1): p. 138-52.
27. Zanini, G., M. Berico, F. Monforti, L. Vitali, S. Zambonelli, S. Chiavarini, T. Georgiadis, and M. Nardino, *Concentration measurement in a road tunnel as a method to assess "real-world" vehicles exhaust emissions.* Atmospheric Environment, 2006. **40**(7): p. 1242-1254.
28. Miguel, A.H., T.W. Kirchstetter, R.A. Harley, and S.V. Hering, *On-road emissions of particulate polycyclic aromatic hydrocarbons and black carbon from*

gasoline and diesel vehicles. Environmental Science & Technology, 1998. **32**(4): p. 450-455.
29. Geller, V.D., S.B. Sardar, H. Phuleria, P.N. Fine, and C. Sioutas, *Measurements of particle number and mass concentrations and size distributions in a tunnel environment.* Environmental Science & Technology, 2005. **39**(22): p. 8653-8663.
30. He, L.Y., M. Hu, Y.H. Zhang, B.D. Yu, and D.Q. Liu, *Chemical characterization of fine particles from on-road vehicles in the Wutong tunnel in Shenzhen, China.* Chemosphere, 2006. **62**(10): p. 1565-1573.
31. Park, K., F. Cao, D.B. Kittelson, and P.H. McMurry, *Relationship between particle mass and mobility for diesel exhaust particles.* Environmental Science & Technology, 2003. **37**(3): p. 577-583.
32. Sharma, M., A.K. Agarwal, and K.V.L. Bharathi, *Characterization of exhaust particulates from diesel engine.* Atmospheric Environment, 2005. **39**(17): p. 3023-3028.
33. Gross, D.S., M.E. Galli, P.J. Silva, S.H. Wood, D.-Y. Liu, and K.A. Prather, *Single particle characterization of automobile and diesel truck emissions in the Caldecott Tunnel.* Aerosol Science and Technology, 2000. **32**(2): p. 152-163.
34. Suess, D.T. and K.A. Prather, *Reproducibility of single particle chemical composition during a heavy duty diesel truck dynamometer study.* Aerosol Science and Technology, 2002. **36**(12): p. 1139-1141.
35. John, W. and G. Reischl, *A Cyclone for Size-Selective Sampling of Ambient Air.* Journal of the Air Pollution Control Association, 1980. **30**(8): p. 872-876.
36. Hildemann, L.M., G.R. Cass, and G.R. Markowski, *A Dilution Stack Sampler for Collection of Organic Aerosol Emissions: Design, Characterization and Field Tests.* Aerosol Science and Technology, 1989. **10**: p. 193-204.
37. Shah, S.D., D.R. Cocker, J.W. Miller, and J.M. Norbeck, *Emission rates of particulate matter and elemental and organic carbon from in-use diesel engines.* Environmental Science & Technology, 2004. **38**(9): p. 2544-2550.
38. Maldonado, H., *California Air Resources Board, Sacramento, CA*. 2004.
39. Bukowiecki, N., D.B. Kittelson, W.F. Watts, H. Burtscher, E. Weingartner, and U. Baltensperger, *Real-time characterization of ultrafine and accumulation mode particles in ambient combustion aerosols.* Journal of Aerosol Science, 2002. **33**(8): p. 1139-1154.
40. Robert, M.A., C.A. Jakober, S. VanBergen, and M.J. Kleeman, *Size and Composition Distribution of Particulate Matter 1. Light-duty Gasoline Vehicles.* Journal of the Air and Waste Management Association, *in review* 2007.
41. NIOSH, *NIOSH Manual of Analytical Methods, 4th ed. (1st Supplement)*. 1996, National Institute for Occupational Safety and Health: Cincinnati, OH.
42. Birch, M.E. and R.A. Cary, *Elemental carbon-based method for monitoring occupational exposures to particulate diesel exhaust.* Aerosol Science and Technology, 1996. **25**(3): p. 221-241.
43. Gray, H.A., G.R. Cass, J.J. Huntzicker, E.K. Heyerdahl, and J.A. Rau, *Elemental and Organic-Carbon Particle Concentrations - a Long-Term Perspective.* Science of the Total Environment, 1984. **36**(JUN): p. 17-25.

44. Chung, A., J.D. Herner, and M.J. Kleeman, *Detection of alkaline ultrafine atmospheric particles at Bakersfield, California.* Environmental Science & Technology, 2001. **V35 N11**(JUN 1): p. 2184-2190.
45. Toner, S.M., D.A. Sodeman, and K.A. Prather, *Single particle characterization of ultrafine and accumulation mode particles from heavy duty diesel vehicles using aerosol time-of-flight mass spectrometry.* Environmental Science & Technology, 2006. **40**(12): p. 3912-3921.
46. Fraser, M.P., K. Lakshmanan, S.G. Fritz, and B. Ubanwa, *Variation in composition of fine particulate emissions from heavy-duty diesel vehicles.* Journal of Geophysical Research, [Atmospheres], 2002. **107**(D21): p. ICC8/1-ICC8/6.
47. Yanowitz, J., M.S. Graboski, and R.L. McCormick, *Prediction of in-use emissions of heavy-duty diesel vehicles from engine testing.* Environmental Science & Technology, 2002. **36**(2): p. 270-275.
48. Alander, T.J.A., A.P. Leskinen, T.M. Raunemaa, and L. Rantanen, *Characterization of diesel particles: Effects of fuel reformulation, exhaust aftertreatment, and engine operation on particle carbon composition and volatility.* Environmental Science & Technology, 2004. **38**(9): p. 2707-2714.
49. Cocker, D.R., S.D. Shah, K. Johnson, J.W. Miller, and J.M. Norbeck, *Development and application of a mobile laboratory for measuring emissions from diesel engines. 1. Regulated gaseous emissions.* Environmental Science & Technology, 2004. **38**(7): p. 2182-2189.
50. Larson, S.M., G.R. Cass, K.J. Hussey, and F. Luce, *Verification of Image-Processing Based Visibility Models.* Environmental Science & Technology, 1988. **22**(6): p. 629-637.
51. Park, K., D.B. Kittelson, and P.H. McMurry, *Structural properties of diesel exhaust particles measured by transmission electron microscopy (TEM): Relationships to particle mass and mobility.* Aerosol Science And Technology, 2004. **38**(9): p. 881-889.
52. Kasper, G., *Dynamics And Measurement Of Smokes .1. Size Characterization Of Non-Spherical Particles.* Aerosol Science And Technology, 1982. **1**(2): p. 187-199.
53. Ahlvik, P.N., Leonidas; Keskinen, Jorma; Virtanen, Anelle, *Real Time Measurements of Diesel Particle Size Distribution with an Electrical Low Pressure Impactor.* SAE Technical Paper Series, 1998(980410).
54. Maricq, M.M., D.H. Podsiadlik, and R.E. Chase, *Size distributions of motor vehicle exhaust PM: A comparison between ELPI and SMPS measurements.* Aerosol Science And Technology, 2000. **33**(3): p. 239-260.
55. Virtanen, A.R., Jyrki; Marjamäki, Marko; Vaaraslahti, Kati; Keskinen. Jorma; Lappi; Maiji, *Effective Density of Diesel Exhaust Particles as a Function of Size.* SAE Technical Paper Series, 2002(2002-01-0056).
56. McMurry, P.H., X. Wang, K. Park, and K. Ehara, *The relationship between mass and mobility for atmospheric particles: A new technique for measuring particle density.* Aerosol Science And Technology, 2002. **36**(2): p. 227-238.
57. (USDOE), U.S.D.o.E., *Documentation for Emissions of Greenhouse Gases in the United States 2002*. 2004, Office of Integrated Analysis and Forecasting, U.S. Department of Energy: Washington D.C.

58. Kleeman, M.J., J.J. Schauer, and G.R. Cass, *Size and Composition Distribution of Fine Particulate Matter Emitted from Motor Vehicles.* Environmental Science and Technology, 2000. **34**(7): p. 1132-1142.
59. Bagley, S.T., *Characterization of Fuel and Aftertreatment Device Effects on Diesel Emissions.* Health Effects Institute Technical Report 76, 1996.
60. Erkki, L.P.M.J., Ojanen; Kati, Vaaraslahti; Jorma, Keskinen, *Sampling and Engine After-Treatment Effect On Diesel Exhaust Particle Size Distributions.* SAE Technical Paper Series, 2005(2005-01-0192).
61. Cass, G.R., L.A. Hughes, P. Bhave, M.J. Kleeman, J.O. Allen, and L.G. Salmon, *The chemical composition of atmospheric ultrafine particles.* Philosophical Transactions of the Royal Society of London Series A-Mathematical Pysical and Engineering Sciences, 2000. **V358 N1775**(OCT 15): p. 2581-2592.
62. Sodeman, D.A., S.M. Toner, and K.A. Prather, *Determination of single particle mass spectral signatures from light-duty vehicle emissions.* Environmental Science & Technology, 2005. **39**(12): p. 4569-4580.
63. Maricq, M.M., R.E. Chase, N. Xu, and D.H. Podsiadlik, *The effects of the catalytic converter and fuel sulfur level on motor vehicle particulate matter emissions: Gasoline vehicles.* Environmental Science & Technology, 2002. **36**(2): p. 276-282.
64. *Ultrafine Particulate Matter Source Profile Measurement for Light-Duty Gasoline Vehicles in California*, in *California Environmental Protection Agency Project No. 2R0204*. 2003, California Air Resources Board Hagen-Smit-Laboratory.
65. Herner, J.D., J. Aw, O. Gao, D.P. Chang, and M.J. Kleeman, *Size and composition distribution of airborne particulate matter in northern California: I-particulate mass, carbon, and water-soluble ions.* Journal of the Air & Waste Management Association, 2005. **55**(1): p. 30-51.
66. Slowik, J.G., K. Stainken, P. Davidovits, L.R. Williams, J.T. Jayne, C.E. Kolb, D.R. Worsnop, Y. Rudich, P.F. DeCarlo, and J.L. Jimenez, *Particle morphology and density characterization by combined mobility and aerodynamic diameter measurements. Part 2: Application to combustion-generated soot aerosols as a function of fuel equivalence ratio.* Aerosol Science And Technology, 2004. **38**(12): p. 1206-1222.
67. Chan, T.L. and D.R. Lawson, *Characteristics Of Cascade Impactors In Size Determination Of Diesel Particles.* Atmospheric Environment, 1981. **15**(7): p. 1273-1279.
68. Board, C.A.R., *Ultrafine Particulate Matter Source Profile Measurement for Light-Duty Gasoline Vehicles in California, HSL Project Number 2R0204*

2006.

.
69. Maricq, M.M., D.H. Podsiadlik, and R.E. Chase, *Gasoline vehicle particle size distributions: Comparison of steady state, FTP, and US06 measurements.* Environmental Science & Technology, 1999. **33**(12): p. 2007-2015.
70. Cadle, S.H., P. Mulawa, E.C. Hunsanger, K. Nelson, R.A. Ragazzi, R. Barrett, G.L. Gallagher, D.R. Lawson, K.T. Knapp, and R. Snow, *Light-duty motor vehicle exhaust particulate matter measurement in the Denver, Colorado, area.*

Journal of the Air & Waste Management Association, 1999. **49**(Special Issue SI): p. 164-174.
71. Mohr, M.L., U. and Margaria, G., *ACEA Programme on the Emissions of Fine Particulates from Passenger Cars (2) Part I : Particle Characterisation of a Wide Range of Vehicle Technologies, SAE Technical Paper Series 2003-01-1889.* 2003.
72. Chase, R.E., G.J. Duszkiewicz, T.E. Jensen, D. Lewis, E.J. Schlaps, A.T. Weibel, S. Cadle, and P. Mulawa, *Particle mass emission rates from current-technology, light-duty gasoline vehicles.* Journal Of The Air & Waste Management Association, 2000. **50**(6): p. 930-935.
73. Durbin, T.D., J.M. Norbeck, M.R. Smith, and T.J. Truex, *Particulate emission rates from light-duty vehicles in the South Coast air quality management district.* Environmental Science & Technology, 1999. **33**(24): p. 4401-4406.
74. Durbin, T.D., M.R. Smith, J.M. Norbeck, and T.J. Truex, *Population density, particulate emission characterization, and impact on the particulate inventory of smoking vehicles in the South Coast Air Quality Management District.* Journal Of The Air & Waste Management Association, 1999. **49**(1): p. 28-38.
75. Schauer, J.J., M.J. Kleeman, G.R. Cass, and B.R.T. Simoneit, *Measurement of emissions from air pollution sources. 5. C-1-C-32 organic compounds from gasoline-powered motor vehicles.* Environmental Science & Technology, 2002. **36**(6): p. 1169-1180.
76. Maricq, M.M. and X. Ning, *The effective density and fractal dimension of soot particles from premixed flames and motor vehicle exhaust.* Journal Of Aerosol Science, 2004. **35**(10): p. 1251-1274.
77. Maricq, M.M., D.H. Podsiadlik, and R.E. Chase, *Examination of the size-resolved and transient nature of motor vehicle particle emissions.* Environmental Science & Technology, 1999. **33**(10): p. 1618-1626.
78. Maricq, M.M.P.D.H.B., D.D. and Haghgooie, M., *Particulate Emissions from a Direct-Injection Spark-Ignition (DISI) Engine, SAE Technical Paper Series 1999-01-1530.* 1999.
79. Schauer, J.J., W.F. Rogge, L.M. Hildemann, M.A. Mazurek, and G.R. Cass, *Source apportionment of airborne particulate matter using organic compounds as tracers.* Atmospheric Environment, 1996. **30**(22): p. 3837-3855.
80. Gertler, A.W., J.A. Gillies, and W.R. Pierson, *An assessment of the mobile source contribution to PM10 and PM2.5 in the United States.* Water, Air, and Soil Pollution, 2000. **123**(1-4): p. 203-214.
81. Fraser, M.P., Z.W. Yue, and B. Buzcu, *Source apportionment of fine particulate matter in Houston, TX, using organic molecular markers.* Atmospheric Environment, 2003. **37**(15): p. 2117-2123.
82. Kleeman, M.J. and G.R. Cass, *Source contributions to the size and composition distribution of urban particulate air pollution.* Atmospheric Environment, 1998. **32**(16): p. 2803-2816.
83. Daigle, C.C., D.C. Chalupa, F.R. Gibb, P.E. Morrow, G. Oberdorster, M.J. Utell, and M.W. Frampton, *Ultrafine particle deposition in humans during rest and exercise.* Inhalation Toxicology, 2003. **15**(6): p. 539-552.

84. Ibald-Mulli, A., H.E. Wichmann, W. Kreyling, and A. Peters, *Epidemiological evidence on health effects of ultrafine particles.* Journal of Aerosol Medicine-Deposition Clearance and Effects in the Lung, 2002. **15**(2): p. 189-201.
85. Tsai, F.C., M.G. Apte, and J.M. Daisey, *An exploratory analysis of the relationship between mortality and the chemical composition of airborne particulate matter.* Inhalation Toxicology, 2000. **12**(Suppl. 2): p. 121-135.
86. Adonis, M.I., R.M. Riquelme, V.D. Martinez, L. Gil, C. Rios, L. Rodriguez, and E.M. Rodriguez, *PAHs and Mutagenicity of Inhalable and Respirable Diesel Particulate Matter in Santiago, Chile.* Polycyclic Aromatic Compounds, 2003. **23**(5): p. 495-514.
87. Bostrom, E., S. Engen, and I. Eide, *Mutagenicity testing of organic extracts of diesel exhaust particles after spiking with polycyclic aromatic hydrocarbons (PAH).* Archives of Toxicology, 1998. **72**(10): p. 645-649.
88. Flowers, L., S.H. Rieth, V.J. Cogliano, G.L. Foureman, R. Hertzberg, E.L. Hofmann, D.L. Murphy, S. Nesnow, and R.S. Schoeny, *Health assessment of polycyclic aromatic hydrocarbon mixtures: current practices and future directions.* Polycyclic Aromatic Compounds, 2002. **22**(3-4): p. 811-821.
89. Rogge, W.F., L.M. Hildemann, M.A. Mazurek, G.R. Cass, and B.R.T. Simoneit, *Mathematical modeling of atmospheric fine particle-associated primary organic compound concentrations.* Journal of Geophysical Research, 1996. **101**(D14): p. 19379-19394.
90. Zielinska, B., J.C. Sagebiel, W.P. Arnott, C.F. Rogers, K.E. Kelly, D.A. Wagner, J.S. Lighty, A.F. Sarofim, and G. Palmer, *Phase and Size Distribution of Polycyclic Aromatic Hydrocarbons in Diesel and Gasoline Vehicle Emissions.* Environmental Science & Technology, 2004. **38**: p. 2557-2567.
91. Chow, J.C., *Diesel engines: Environmental impact and control.* Journal of the Air & Waste Management Association, 2001. **51**(9): p. 1258-1270.
92. Watson, J.G., J.C. Chow, and J.E. Houck, *PM2.5 chemical source profiles for vehicle exhaust, vegetative burning, geological material, and coal burning in Northwestern Colorado during 1995.* Chemosphere, 2001. **43**(8): p. 1141-1151.
93. Robert, M.A., C.A. Jakober, S. VanBergen, and M.J. Kleeman, *Size and composition distribution of particulate matter 2. Heavy-duty diesel vehicles.* Journal of the Air & Waste Management Association, *in review* 2007.
94. Cass, G.R., *Organic molecular tracers for particulate air pollution sources.* TrAC, Trends in Analytical Chemistry, 1998. **17**(6): p. 356-366.
95. Kweon, C.-B., S. Okada, D.E. Foster, M.-S. Bae, and J.J. Schauer, *Effect of engine operating conditions on particle-phase organic compounds in engine exhaust of a heavy-duty direct-injection (D.I.) diesel engine.* Society of Automotive Engineers, [Special Publication] SP, 2003. **SP-1738**(In-Cylinder Diesel Particulate and NOx Control 2003): p. 73-89.
96. Phuleria, H.C., M.D. Geller, P.M. Fine, and C. Sioutas, *Size-resolved emissions of organic tracers from light- and heavy-duty vehicles measured in a California roadway tunnel.* Environmental Science and Technology, 2006. **40**: p. 4109-4118.
97. Watson, J.G., E. Fujita, J.C. Chow, B. Zielinska, L.W. Richards, W.D. Neff, and D. Dietrich, *Northern Front Range Air Quality Study Final Report*. 1998, DRI: Reno.

98. Schauer, J.J., M.P. Fraser, G.R. Cass, and B.R.T. Simoneit, *Source Reconciliation of Atmospheric Gas-Phase and Particle-Phase Pollutants during a Severe Photochemical Smog Episode.* Environmental Science and Technology, 2002. **36**(17): p. 3806-3814.
99. Seagrave, J., J.D. McDonald, E. Bedrick, E.S. Edgerton, A.P. Gigliotti, J.J. Jansen, L. Ke, L.P. Naeher, S.K. Seilkop, M. Zheng, and J.L. Mauderly, *Lung toxicity of ambient particulate matter from southeastern US sites with different contributing sources: Relationships between composition and effects.* Environmental Health Perspectives, 2006. **114**(9): p. 1387-1393.
100. Cadle, S.H., P.A. Mulawa, E.C. Hunsanger, K. Nelson, R.A. Ragazzi, R. Barrett, G.L. Gallagher, D.R. Lawson, K.T. Knapp, and R. Snow, *Composition of Light-Duty Motor Vehicle Exhaust Particulate Matter in the Denver, Colorado Area.* Environmental Science and Technology, 1999. **33**(14): p. 2328-2339.
101. Fine, P.M., B. Chakrabarti, M. Krudysz, J.J. Schauer, and C. Sioutas, *Diurnal Variations of Individual Organic Compound Constituents of Ultrafine and Accumulation Mode Particulate Matter in the Los Angeles Basin.* Environmental Science and Technology, 2004. **38**(5): p. 1296-1304.
102. Hagen-Smit-Laboratory, *Ultrafine Particulate Matter Source Profile Measurement for Light-Duty Gasoline Vehicles in California*, in *California Environmental Protection Agency Project No. 2R0204*. 2003.
103. Riddle, S., M.A. Robert, C.A. Jakober, M.P. Hannigan, and M.J. Kleeman, *Size Distribution of Trace Organic Species Emitted From Heavy-Duty Diesel Vehicles.* Environmental Science & Technology, 2007. **41**(6): p. 1962-1969.
104. Philip, R.P., *Fossil Fuel Biomarkers Applications and Spectra*. 1985, New York: Elsevier Science Publishers.
105. Marr, L.C., T.W. Kirchstetter, R.A. Harley, A.H. Miguel, S.V. Hering, and S.K. Hammond, *Characterization of Polycyclic Aromatic Hydrocarbons in Motor Vehicle Fuels and Exhaust Emissions.* Environmental Science and Technology, 1999. **33**(18): p. 3091-3099.
106. Westerholm, R.N., T.E. Alsberg, A.B. Frommelin, M.E. Strandell, U. Rannug, L. Winquist, V. Grigorladis, and K.-E. Egeback, *Effect of fuel polycyclic aromatic hydrocarbon content on the emissions of polycyclic aromatic hydrocarbons and other mutagenic substances from a gasoline-fueled automobile.* Environmental Science & Technology, 1988. **22**: p. 925-930.
107. Brandenberger, S., M. Mohr, K. Grob, and H.P. Neukom, *Contribution of unburned lubricating oil and diesel fuel to particulate emission from passenger cars.* Atmospheric Environment, 2005. **39**: p. 6985-6994.
108. Finlayson-Pitts, B.J. and J.N. Pitts, *Chemistry of the Upper and Lower Atmosphere*. 2000, San Diego: Academic Press.
109. Lin, C.C., S.J. Chen, K.L. Huang, W.I. Hwang, G.P. Chang-Chien, and W.Y. Lin, *Characteristics of metals in nano/ultrafine/fine/coarse particles collected beside a heavily trafficked road.* Environmental Science & Technology, 2005. **39**(21): p. 8113-8122.
110. Kim, J.J., S. Smorodinsky, M. Lipsett, B.C. Singer, A.T. Hodgson, and B. Ostro, *Traffic-related air pollution near busy roads - The East Bay children's respiratory*

health study. American Journal of Respiratory and Critical Care Medicine, 2004. **170**(5): p. 520-526.
111. Kittelson, D.B., W.F. Watts, J.P. Johnson, M.L. Remerowki, E.E. Ische, G. Oberdorster, R.A. Gelein, A. Elder, P.K. Hopke, E. Kim, W. Zhao, L. Zhou, and C.H. Jeong, *On-road exposure to highway aerosols. 1. Aerosol and gas measurements.* Inhalation Toxicology, 2004. **16**: p. 31-39.
112. Janssen, N.A.H., P.H.N. van Vliet, F. Aarts, H. Harssema, and B. Brunekreef, *Assessment of exposure to traffic related air pollution of children attending schools near motorways.* Atmospheric Environment, 2001. **35**(22): p. 3875-3884.
113. Zhou, L.M., P.K. Hopke, P. Paatero, J.M. Ondov, J.P. Pancras, N.J. Pekney, and C.I. Davidson, *Advanced factor analysis for multiple time resolution aerosol composition data.* Atmospheric Environment, 2004. **38**(29): p. 4909-4920.
114. Zhao, W.X. and P.K. Hopke, *Source apportionment for ambient particles in the San Gorgonio wilderness.* Atmospheric Environment, 2004. **38**(35): p. 5901-5910.
115. Woods, G., *Direct Elemental Analysis of Gasoline by Agilent 7500ce ORS ICP-MS.* Agilent Technologies, Inc., 2005.
116. Yvon, J., *Analysis of Major Elements in Glass Samples with a Sequential ICP-OES.* ICP Optical Emission Spectroscopy Application Note 42.
117. Popova, O.V., S.T. Bashkatova, E.N. Vasileva, and E.B. Kotin, *Additives for Increasing the Completeness of Combustion of Diesel Fuels.* Chemistry and Technology of Fuels and Oils, 1995. **31**(1-2): p. 88-94.
118. Wang, Y.F., K.L. Huang, C.T. Li, H.H. Mi, J.H. Luo, and P.J. Tsai, *Emissions of fuel metals content from a diesel vehicle engine.* Atmospheric Environment, 2003. **37**: p. 4637-4643.
119. Stohs, S.J. and D. Bagchi, *Oxidative Mechanisms in the Toxicity of Metal-Ions.* Free Radical Biology and Medicine, 1995. **18**(2): p. 321-336.
120. Harrison, R.M., R. Tilling, M.S.C. Romero, S. Harrad, and K. Jarvis, *A study of trace metals and polycyclic aromatic hydrocarbons in the roadside environment.* Atmospheric Environment, 2003. **37**(17): p. 2391-2402.
121. Lough, G.C., J.J. Schauer, J.S. Park, M.M. Shafer, J.T. Deminter, and J.P. Weinstein, *Emissions of metals associated with motor vehicle roadways.* Environmental Science & Technology, 2005. **39**(3): p. 826-836.
122. Robert, M.A., P.G. Green, M.A. Gras, and M.J. Kleeman, *Elemantal Composition of Gasoline, Diesel Fuel, and Motor Oil from Light-Duty Gasoline Vehicles and Heavy-Duty Diesel Vehicles* drafted.
123. Huggins, F.E., G.P. Huffman, and J.D. Robertson, *Speciation of elements in NIST particulate matter SRMs 1648 and 1650.* Journal Of Hazardous Materials, 2000. **74**(1-2): p. 1-23.
124. Green, R.S., S. Smorodinsky, J.J. Kim, R. McLaughlin, and B. Ostro, *Proximity of California public schools to busy roads.* Environmental Health Perspectives, 2004. **112**(1): p. 61-66.
125. Vliet, P.H.N., F.J.H. Aarts, N.A.H. Jansen, H. Harssema, and B. Brunekreef, *Traffic related air pollution and its effect on respiratory health of primary school children living near motorways.* Epidemiology, 1999. **10**(4): p. S171-S171.

126. Robert, M.A., C.A. Jakober, S. VanBergen, and M.J. Kleeman, *Size and composition distribution of particulate matter 1. Light-duty gasoline vehicles.* Journal of the Air & Waste Management Association, *in review* 2007.
127. Robert, M.A., C.A. Jakober, and M.J. Kleeman, *Size and composition distribution of particulate matter 2. Heavy-duty diesel vehicles.* Journal Of The Air & Waste Management Association, *in review* 2007.
128. Robert, M.A., C.A. Jakober, P.G. Green, M.A. Gras, and M.J. Kleeman, *Elemental Composition of Particulate Matter Emissions from Light-Duty Gasoline and Heavy-Duty Diesel Vehicles.* drafted.
129. Davis, A.P., M. Shokouhian, and S.B. Ni, *Loading estimates of lead, copper, cadmium, and zinc in urban runoff from specific sources.* Chemosphere, 2001. **44**(5): p. 997-1009.
130. Riddle, S., M.A. Robert, C.A. Jakober, M.P. Hannigan, and M.J. Kleeman, *Size distribution of trace organic species emitted from light-duty gasoline vehicles.* Environmental Science & Technology, in review 2007.
131. Riddle, S., M.A. Robert, C.A. Jakober, M.P. Hannigan, and M.J. Kleeman, *Size distribution of trace organic species emitted from heavy-duty diesel vehicles.* Environmental Science & Technology, 2007(accepted for publication).
132. Robert, M.A., C.A. Jakober, and M.J. Kleeman, *Size and composition distribution of particulate matter 1. Light-duty gasoline vehicles.* Journal of the Air & Waste Management Association, *in review* 2007.
133. Watson, J.G., J.C. Chow, Z. Lu, E.M. Fujita, D.H. Lowenthal, and D.R. Lawson, *Chemical mass balance source apportionment of PM10 during the Southern California Air Quality Study.* Aerosol Science and Technology, 1994. **21**(1): p. 1-36.
134. Motallebi, N., *Wintertime PM2.5 and PM10 source apportionment at Sacramento, California.* Journal of the Air & Waste Management Association, 1999. **49**(Spec. Issue): p. PM/25-PM/34.
135. Chow, J.C., J.G. Watson, D.H. Lowenthal, P.A. Solomon, K.L. Magliano, S.D. Ziman, and L.W. Richards, *Pm10 Source Apportionment in California San-Joaquin Valley.* Atmospheric Environment Part a-General Topics, 1992. **26**(18): p. 3335-3354.
136. Querol, X., A. Alastuey, S. Rodriguez, F. Plana, C.R. Ruiz, N. Cots, G. Massague, and O. Puig, *PM10 and PM2.5 source apportionment in the Barcelona Metropolitan area, Catalonia, Spain.* Atmospheric Environment, 2001. **35**(36): p. 6407-6419.
137. Zheng, M., G.R. Cass, J.J. Schauer, and E.S. Edgerton, *Source Apportionment of PM2.5 in the Southeastern United States Using Solvent-Extractable Organic Compounds as Tracers.* Environmental Science and Technology, 2002. **36**(11): p. 2361-2371.
138. Maykut, N.N., J. Lewtas, E. Kim, and T.V. Larson, *Source Apportionment of PM2.5 at an Urban IMPROVE Site in Seattle, Washington.* Environmental Science and Technology, 2003. **37**(22): p. 5135-5142.
139. Park, S.S., M.S. Bae, and Y.J. Kim, *Chemical composition and source apportionment of PM2.5 particles in the Sihwa area, Korea.* Journal of the Air & Waste Management Association, 2001. **51**(3): p. 393-405.

140. Kleeman, M.J., J.J. Schauer, and G.R. Cass, *Size and composition distribution of fine particulate matter emitted from wood burning, meat charbroiling, and cigarettes.* Environmental Science & Technology, 1999. **33**(20): p. 3516-3523.
141. Schauer, J.J., M.J. Kleeman, G.R. Cass, and B.R.T. Simoneit, *Measurement of emissions from air pollution sources. 3. C-1-C-29 organic compounds from fireplace combustion of wood.* Environmental Science & Technology, 2001. **35**(MAY 1): p. 1716-1728.
142. Schauer, J.J., M.J. Kleeman, G.R. Cass, and B.R.T. Simoneit, *Measurement of emissions from air pollution sources. 4. C-1-C-27 organic compounds from cooking with seed oils.* Environmental Science & Technology, 2002. **36**(FEB 15): p. 567-575.
143. Schauer, J.J., M.J. Kleeman, G.R. Cass, and B.R.T. Simoneit, *Measurement of emissions from air pollution sources 1. C1 through C29 organic compounds from meat charbroiling.* Environmental Science & Technology, 1999. **33**(10): p. 1566-1577.
144. Rogge, W.F., L.M. Hildemann, M.A. Mazurek, and G.R. Cass, *Sources Of Fine Organic Aerosol .6. Cigarette-Smoke In The Urban Atmosphere.* Environmental Science & Technology, 1994. **28**(7): p. 1375-1388.
145. Rogge, W.F., L.M. Hildemann, M.A. Mazurek, G.R. Cass, and B.R.T. Simoneit, *Sources of fine organic aerosol. 9. Pine, oak and synthetic log combustion in residential fireplaces.* Environmental Science & Technology, 1998. **32**(1): p. 13-22.
146. Rogge, W.F., L.M. Hildemann, M.A. Mazurek, G.R. Cass, and B.R.T. Simoneit, *Sources of fine organic aerosol .7. Hot asphalt roofing tar pot fumes.* Environmental Science & Technology, 1997. **31**(10): p. 2726-2730.
147. Rogge, W.F., L.M. Hildemann, M.A. Mazurek, G.R. Cass, and B.R.T. Simoneit, *Sources of fine organic aerosol .8. Boilers burning No. 2 distillate fuel oil.* Environmental Science & Technology, 1997. **31**(10): p. 2731-2737.
148. Rogge, W.F., L.M. Hildemann, M.A. Mazurek, G.R. Cass, and B.R.T. Simoneit, *Sources Of Fine Organic Aerosol .4. Particulate Abrasion Products From Leaf Surfaces Of Urban Plants.* Environmental Science & Technology, 1993. **27**(13): p. 2700-2711.
149. Rogge, W.F., L.M. Hildemann, M.A. Mazurek, G.R. Cass, and B.R.T. Simoneit, *Sources Of Fine Organic Aerosol .5. Natural-Gas Home Appliances.* Environmental Science & Technology, 1993. **27**(13): p. 2736-2744.
150. Rogge, W.F., L.M. Hildemann, M.A. Mazurek, G.R. Cass, and B.R.T. Simoneit, *Sources Of Fine Organic Aerosol .3. Road Dust, Tire Debris, And Organometallic Brake Lining Dust - Roads As Sources And Sinks.* Environmental Science & Technology, 1993. **27**(9): p. 1892-1904.
151. Rogge, W.F., L.M. Hildemann, M.A. Mazurek, G.R. Cass, and B.R.T. Simonelt, *Sources of Fine Organic Aerosol .1. Charbroilers and Meat Cooking Operations.* Environmental Science & Technology, 1991. **25**(6): p. 1112-1125.
152. Robert, M.A., C.A. Jakober, and M.J. Kleeman, *Carbon and metal size distributions in a roadside environment.* Atmospheric Environment, in preparation 2007.

153. Seinfeld, J.H. and S. Pandis, *Atmospheric Chemistry and Physics: From Air Pollution to Climate Change*. 1998, New York: John Wiley and Sons.
154. Hildemann, L.M., M.A. Mazurek, G.R. Cass, and B.R.T. Simoneit, *Quantitative characterization of urban sources of organic aerosol by high-resolution gas chromatography.* Environmental Science and Technology, 1991. **25**(7): p. 1311-25.
155. Pope, C.A., *Review: Epidemiological basis for particulate air pollution health standards.* Aerosol Science and Technology, 2000. **32**(1): p. 4-14.
156. Labban, R., J.M. Veranth, J.C. Chow, J.L.P. Engelbrecht, and J.G. Watson, *Size and geographical variation in PM1, PM2.5 and PM10: Source profiles from soils in the western United States.* Water Air and Soil Pollution, 2004. **157**(1-4): p. 13-31.
157. Fraser, M.P., G.R. Cass, and B.R.T. Simoneit, *Gas-Phase and Particle-Phase Organic Compounds Emitted from Motor Vehicle Traffic in a Los Angeles Roadway Tunnel.* Environmental Science and Technology, 1998. **32**(14): p. 2051-2060.
158. McDonald, J.D., B. Zielinska, E.M. Fujita, J.C. Sagebiel, J.C. Chow, and J.G. Watson, *Emissions from charbroiling and grilling of chicken and beef.* Journal of the Air & Waste Management Association, 2003. **53**(2): p. 185-194.
159. Phuleria, H.C., M.D. Geller, P.M. Fine, and C. Sioutas, *Size-resolved emissions of organic tracers from light-and heavy-duty vehicles measured in a California roadway tunnel.* Environmental Science and Technology, 2006. **40**(13): p. 4109-4118.
160. Hughes, L.S., G.R. Cass, J. Gone, M. Ames, and I. Olmez, *Physical and chemical characterization of atmospheric ultrafine particles in the Los Angeles area.* Environmental Science & Technology, 1998. **32**(9): p. 1153-1161.
161. Riddle, S., M.A. Robert, C.A. Jakober, M.P. Hannigan, and M.J. Kleeman, *Size Distribution of Trace Organic Species Emitted from Light-Duty Gasoline Vehicles.* Environmental Science & Technology, 2007. **submitted for publication**.
162. Hays, M.D., N.D. Smith, J. Kinsey, Y.J. Dong, and P. Kariher, *Polycyclic aromatic hydrocarbon size distributions in aerosols from appliances of residential wood combustion as determined by direct thermal desorption - GC/MS.* Journal of Aerosol Science, 2003. **34**(8): p. 1061-1084.
163. Schauer, J.J., M.J. Kleeman, G.R. Cass, and B.R.T. Simoneit, *Measurement of emissions from air pollution sources. 1. C-1 through C-29 organic compounds from meat charbroiling.* Environmental Science & Technology, 1999. **33**(MAY 15): p. 1566-1577.
164. Schauer, J.J., *Source Contributions to Atmospheric Organic Compound Concentrations: Emissions Measurements and Model Predictions*, in *Environmental Engineering Science*. 1998, California Institute of Technology: Pasadena CA. p. 400.
165. Hays, M.D., P.M. Fine, C.D. Geron, M.J. Kleeman, and B.K. Gullett, *Open burning of agricultural biomass: Physical and chemical properties of particle-phase emissions.* Atmospheric Environment, 2005. **39**(36): p. 6747-6764.

166. Nolte, C.G., J.J. Schauer, G.R. Cass, and B.R.T. Simoneit, *Highly polar organic compounds present in meat smoke.* Environmental Science & Technology, 1999. **33**(19): p. 3313-3316.
167. Schauer, J.J. and G.R. Cass, *Source Apportionment of Wintertime Gas-Phase and Particle-Phase Air Pollutants Using Organic Compounds as Tracers.* Environmental Science and Technology, 2000. **34**(9): p. 1821-1832.
168. Oberdorster, G., J. Ferin, R. Gelein, S.C. Soderholm, and J. Finkelstein, *Role of the Alveolar Macrophage in Lung Injury - Studies with Ultrafine Particles.* Environmental Health Perspectives, 1992. **97**: p. 193-199.
169. Oberdorster, G., J. Ferin, and B.E. Lehnert, *Correlation between Particle-Size, in-Vivo Particle Persistence, and Lung Injury.* Environmental Health Perspectives, 1994. **102**: p. 173-179.
170. Subramanian, R., N.M. Donahue, A. Bernardo-Bricker, W.F. Rogge, and A.L. Robinson, *Contribution of motor vehicle emissions to organic carbon and fine particle mass in Pittsburgh, Pennsylvania: Effects of varying source profiles and seasonal trends in ambient marker concentrations.* Atmospheric Environment, 2006. **40**(40): p. 8002-8019.
171. Cao, J.J., F. Wu, J.C. Chow, S.C. Lee, Y. Li, S.W. Chen, Z.S. An, K.K. Fung, J.G. Watson, C.S. Zhu, and S.X. Liu, *Characterization and source apportionment of atmospheric organic and elemental carbon during fall and winter of 2003 in Xi'an, China.* Atmospheric Chemistry and Physics, 2005. **5**: p. 3127-3137.
172. Chow, J.C., L.W.A. Chen, J.G. Watson, D.H. Lowenthal, K.A. Magliano, K. Turkiewicz, and D.E. Lehrman, *PM2.5 chemical composition and spatiotemporal variability during the California Regional PM10/PM2.5 Air Quality Study (CRPAQS).* Journal of Geophysical Research, 2006. **111**(D10).
173. Herner, J.D., Q. Ying, J. Aw, O.H. Gao, D.P. Chang, and M.J. Kleeman, *Dominant Mechanisms that Shape the Airborne Particle Size and Composition Distribution.* Aerosol Science and Technology, 2006. **40**: p. 827-844.
174. Herner, J.D., P.G. Green, and M.J. Kleeman, *Measuring the trace elemental composition of size-resolved airborne particles.* Environmental Science & Technology, 2006. **40**(6): p. 1925-1933.
175. Kleeman, M.J., M.A. Robert, S.G. Riddle, P.M. Fine, M.D. Hays, J.J. Schauer, and M.P. Hannigan, *Size Distributions of Trace Organic Compounds Emitted from Biomass Combstion and Meat Charbroiling.* Environmental Science & Technology, 2007. **submitted for publcation**.
176. Riddle, S.G., M.A. Robert, C.A. Jakober, M. Hannigan, and M.J. Kleeman, *Size-Resolved Source Apportionment of Airborne Particles in a Roadside Environment.* Environmental Science & Technology, 2007. **submitted for publication**.
177. Bell, M.L., J.M. Samet, and F. Dominici, *Time-series studies of particulate matter.* Annual Review of Public Health, 2004. **25**: p. 247-280.
178. Pope, C.A., R.T. Burnett, M.J. Thun, E.E. Calle, D. Krewski, K. Ito, and G.D. Thurston, *Lung cancer, cardiopulmonary mortality, and long-term exposure to fine particulate air pollution.* Jama-Journal of the American Medical Association, 2002. **287**(9): p. 1132-1141.

179. Schwarze, P.E., J. Ovrevik, M. Lag, M. Refsnes, P. Nafstad, R.B. Hetland, and E. Dybing, *Particulate matter properties and health effects: consistency of epidemiological and toxicological studies.* Human & Experimental Toxicology, 2006. **25**(10): p. 559-579.
180. Hannigan, M.P., W.F. Busby, and G.R. Cass, *Source contributions to the mutagenicity of urban particulate air pollution.* Journal of the Air & Waste Management Association, 2005. **55**(4): p. 399-410.
181. Manchester-Neesvig, J.B., J.J. Schauer, and G.R. Cass, *The distribution of particle-phase organic compounds in the atmosphere and their use for source apportionment during the Southern California Children's Health Study.* Journal of the Air & Waste Management Association, 2003. **53**(9): p. 1065-1079.
182. Kim, E., P.K. Hopke, T.V. Larson, N.N. Maykut, and J. Lewtas, *Factor analysis of Seattle fine particles.* Aerosol Science and Technology, 2004. **38**(7): p. 724-738.
183. Lee, P.K.H., J.R. Brook, E. Dabek-Zlotorzynska, and S.A. Mabury, *Identification of the major sources contributing to PM2.5 observed in Toronto.* Environmental Science & Technology, 2003. **37**(21): p. 4831-4840.
184. Daisey, J.M., J.L. Cheney, and P.J. Lioy, *Profiles of Organic Particulate-Emissions from Air-Pollution Sources - Status and Needs for Receptor Source Apportionment Modeling.* Journal of the Air Pollution Control Association, 1986. **36**(1): p. 17-33.
185. Simoneit, B.R.T., W.F. Rogge, M.A. Mazurek, L.J. Standley, L.M. Hildemann, and G.R. Cass, *Lignin Pyrolysis Products, Lignans, And Resin Acids As Specific Tracers Of Plant Classes In Emissions From Biomass Combustion.* Environmental Science & Technology, 1993. **27**(12): p. 2533-2541.
186. Fine, P.M., G.R. Cass, and B.R.T. Simoneit, *Organic compounds in biomass smoke from residential wood combustion: Emissions characterization at a continental scale.* Journal of Geophysical Research-Atmospheres, 2002. **107**(D21): p. -.
187. Hays, M.D., C.D. Geron, K.J. Linna, N.D. Smith, and J.J. Schauer, *Speciation of gas-phase and fine particle emissions from burning of foliar fuels.* Environmental Science & Technology, 2002. **36**(11): p. 2281-2295.
188. Cadle, S.H., P.A. Mulawa, E.C. Hunsanger, K. Nelson, R.A. Ragazzi, R. Barrett, G.L. Gallagher, D.R. Lawson, K.T. Knapp, and R. Snow, *Composition of light-duty motor vehicle exhaust particulate matter in the Denver, Colorado area.* Environmental Science & Technology, 1999. **33**(14): p. 2328-2339.
189. Kavouras, I.G., N. Stratigakis, and E.G. Stephanou, *Iso- and anteiso-alkanes: Specific tracers of environmental tobacco smoke in indoor and outdoor particle-size distributed urban aerosols.* Environmental Science & Technology, 1998. **32**(10): p. 1369-1377.
190. Alexandrova, O.A. and J.O. Allen, *Fine and Ultrafine Particle in California*. 2005, California Air Resources Board: Sacramento, CA.
191. Schauer, J.J. and G.C. Lough, *Gasoline/Diesel PM Split Study*. 2006, National Renewable Energy Laboratory: Golden, CO.

192. Schauer, J.J., G.C. Lough, M.M. Shafer, C.C. Christensen, M.F. Arndt, J.T. DeMinter, and J.S. Park, *Characterization of Metals Emitted from Motor Vehicles*. 2006, Health Effects Institute: Boston, MA. p. 88.